TECHNICAL REPORT STANDARD TITLE PAGE

1. Report No.	2. Government Accession No.	3. Recipient's Catalog No.
FHWA/TX-79/01+114-6		

4. Title and Subtitle	5. Report Date
BEHAVIOR OF POST-TENSIONED POLYMER-IMPREGNATED CONCRETE BEAMS	June 1978
	6. Performing Organization Code

7. Author(s)	8. Performing Organization Report No.
Ekasit Limsuwan, David W. Fowler, Ned H. Burns, and Donald R. Paul	Research Report 114-6

9. Performing Organization Name and Address	10. Work Unit No.
Center for Highway Research The University of Texas at Austin Austin, Texas 78712	11. Contract or Grant No. Research Study 3-9-71-114
	13. Type of Report and Period Covered
12. Sponsoring Agency Name and Address Texas State Department of Highways and Public Transportation; Transportation Planning Division P. O. Box 5051 Austin, Texas 78763	Interim
	14. Sponsoring Agency Code

15. Supplementary Notes

Study conducted in cooperation with the U. S. Department of Transportation, Federal Highway Administration

Research Study Title: "Polymer-Impregnated Concrete for Highway Application"

16. Abstract

This study was conducted to investigate the behavior of post-tensioned polymer-impregnated concrete (PIC) beams. Three major areas of behavior were studied by experimental and theoretical analyses: flexure, shear, and time-dependent deflections. Test results were compared to values calculated according to ACI Standard 318-71 and to results from numerical analyses for inclined cracking and ultimate shears, moment capacity, and tendon stress increase.

The beams were dried to remove the moisture from the concrete voids, impregnated with the monomer system, and polymerized by thermal-catalytic methods. The tendons were stressed to about 70 percent of the ultimate strength prior to the testing.

Nineteen simply-supported beams with I-shaped cross sections were tested using two symmetrically placed concentrated loads. For flexure, the major variables were the prestressing steel percentage, the monomer system, the impregnation depth of PIC, and tendon bonding. For shear, the number of wires per tendon and the amount of web reinforcement were the major variables. Three control beams were tested, one for flexure and two for shear. For time-dependent deflection tests, the number of wires and the magnitude and duration of sustained loads were selected as variables. In all beams, bonded reinforcing bars were used to supplement longitudinal reinforcement to prevent cracking from the drying process.

17. Key Words	18. Distribution Statement
polymer-impregnated concrete, PIC, post-tensioned, beams, flexure, shear, time-dependent deflections, experimental, theoretical	No restrictions. This document is available to the public through the National Technical Information Service, Springfield, Virginia 22161.

19. Security Classif. (of this report)	20. Security Classif. (of this page)	21. No. of Pages	22. Price
Unclassified	Unclassified	314	

Form DOT F 1700.7 (8-69)

BEHAVIOR OF POST-TENSIONED POLYMER-IMPREGNATED CONCRETE BEAMS

by

Ekasit Limsuwan, David W. Fowler,
Ned H. Burns, and Donald R. Paul

Research Report Number 114-6

Polymer-Impregnated Concrete for Highway Application

Research Project 3-9-71-114

conducted for

State Department of Highways and Public Transportation

in cooperation with the

U.S. Department of Transportation
Federal Highway Administration

by the

CENTER FOR HIGHWAY RESEARCH
THE UNIVERSITY OF TEXAS AT AUSTIN

June 1978

The contents of this report reflect the views of the authors, who are responsible for the facts and the accuracy of the data presented herein. The contents do not necessarily reflect the official views or policies of the Federal Highway Administration. This report does not constitute a standard, specification, or regulation.

PREFACE

This report summarizes research on the structural properties of post-tensioned polymer-impregnated concrete beams. These tests are the first to be reported for post-tensioned members.

The authors are extremely appreciative of the support of personnel of the State Department of Highways and Public Transportation. John Nixon, Donald O'Connor, Andy Seely, Ralph Banks, and H.D. Butler have been particularly helpful with suggestions and encouragement. John Nichols of the Federal Highway Administration has also been very supportative and helpful in this study.

Thanks are also due to all of the research assistants who have contributed to this study. They include Prajya Phinyawat, Bancha Suparinayok, Andy Knysh, Robert Fry, Ron Webster, and John McIntyre.

June 1978

Ekasit Limsuwan
David W. Fowler
Ned H. Burns
Donald R. Paul

ABSTRACT

This study was conducted to investigate the behavior of post-tensioned polymer-impregnated concrete (PIC) beams. Three major areas of behavior were studied by experimental and theoretical analyses: flexure, shear, and time-dependent deflections. Test results were compared to values calculated according to ACI Standard 318-71 and to results from numerical analyses for inclined cracking and ultimate shears, moment capacity, and tendon stress increase.

The beams were dried to remove the moisture from the concrete voids, impregnated with the monomer system, and polymerized by thermal-catalytic methods. The tendons were stressed to about 70 percent of the ultimate strength prior to the testing.

Nineteen simply-supported beams with I-shaped cross sections were tested using two symmetrically placed concentrated loads. For flexure, the major variables were the prestressing steel percentage, the monomer system, the impregnation depth of PIC, and tendon bonding. For shear, the number of wires per tendon and the amount of web reinforcement were the major variables. Three control beams were tested, one for flexure and two for shear. For time-dependent deflection tests, the number of wires and the magnitude and duration of sustained loads were selected as the variables. In all beams, bonded reinforcing bars were used to supplement longitudinal reinforcement to prevent cracking from the drying process.

The maximum number of wires for polymer-impregnated concrete beams was four times greater than that for unimpregnated concrete beams. For equal percentages of steel, the PIC developed significantly more deflection and inelastic rotation capacity and slightly greater flexural strength than control beams. PIC beams, with four times more tendons than the control, developed bending moments three times greater than the control beam did but with about the same maximum deflections.

Crack patterns and modes of failure were similar to those of ordinary post-tensioned concrete beams; the beams containing bonded tendons were significantly improved in strength and deflection compared to unbonded beams.

Friction loss and friction coefficients for PIC beams containing unbonded tendons were found to be slightly higher than for the control beam containing the same percentage of steel; the wobble and friction coefficients were determined to be about 0.005 and 0.50, respectively. The equivalent rectangular stress block for 100 percent MMA-PIC was determined. The test results for flexure indicate reserve strength beyond values predicted by the ACI equation. A numerical iteration procedure was developed to predict load-deflection response and yielded good agreement with the test results.

Beams tested for shear strength were found to develop shear-compression failure. Empirical equations to predict inclined cracking shear and ultimate shear for PIC beams were developed from the test results.

Creep of PIC was determined from time-dependent deflection tests to be one-tenth to one-thirteenth of the creep for unimpregnated concrete. Creep ceased almost entirely after a period of 4 months. Relaxation of the wire tendons was found to be 2.9 percent.

Proposed design criteria for post-tensioned PIC beams are presented on the basis of the test results and in conjunction with the theoretical analyses.

SUMMARY

This investigation was performed to determine the behavior of post-tensioned polymer-impregnated concrete (PIC) beams. Beams with I-shaped cross sections were dried, impregnated with monomer under pressure and polymerized by thermal-catalytic methods. Tendons were stressed to about 70 percent of the ultimate strength after impregnation and prior to testing.

For flexure, up to 4 times the number of wires could be used for PIC beams as for unimpregnated beams. Ultimate moments were about 3 times greater than for control beams, and maximum deflections were about the same. For equal percentages of steel, PIC beams developed significantly greater deflections and inelastic rotation and slightly greater flexural strength.

Wobble and friction coefficients were determined, and the parameters for an equivalent rectangular stress block to predict ultimate moment were found.

Beams tested for shear strength were found to develop shear compression failures. Empirical equations were developed to predict inclined cracking shear and ultimate shear.

Creep of PIC beams was determined from long-term loading tests to be one-tenth to one-thirteenth of the creep for unimpregnated concrete. Creep ceased almost entirely after 4 months.

Proposed design criteria for post-tensioned PIC beams are presented.

IMPLEMENTATION STATEMENT

The results of this investigation establish the strength, stiffness, and behavior of polymer-impregnated concrete post-tensioned beams. Suggested design procedures are recommended. These structural members have significant potential for use in highway structures where increased strength, reduced size, reduced creep, and increased durability are required. In particular, PIC post-tensioned slabs and beams appear feasible in coastal areas where corrosion of reinforcing steel is a serious problem.

TABLE OF CONTENTS

	Page
PREFACE	iii
LIST OF FIGURES	xiv
LIST OF TABLES	xxi
SUMMARY	vi
IMPLEMENTATION STATEMENT	vii
Chapter	
I. INTRODUCTION	1
1.1 Background	1
1.2 Structural Properties of Polymer-Impregnated Concrete	2
1.2.1 Compressive Stress-Strain Relationship	2
1.2.2 Tensile Strength	6
1.2.3 Shear Strength	6
1.2.4 Creep	6
1.2.5 Durability	8
1.3 Prestressed Concrete Beam	10
1.3.1 Tensile Stress-Strain Relationship for Steel Types	10
1.3.2 Prestressing Method	11
1.3.3 Bonded or Unbonded Tendons	13
1.3.4 Loss of Prestress	14
1.4 Research Objectives and Scope	15
1.4.1 Flexural Strength	15
1.4.2 Shear Strength	16
1.4.3 Time-Dependent Behavior	16
II. THEORETICAL ANALYSIS OF PRESTRESSED CONCRETE BEAMS	17
2.1 Analysis for Flexure	17
2.1.1 Strain Profile and Stress Distribution	17
2.1.2 Stress in Concrete Due to Prestress and Loads	18

Chapter Page

2.1.3 Friction Consideration for Unbonded Tendon 21
2.1.4 Response of Prestressing Steel under Loads 24
2.1.5 Moment Curvature Relationship and Load-Deflection Response 27
2.2 Analysis for Shear 29
2.2.1 Principal Tensile Stress 30
2.2.2 Inclined Cracking Shear 32
2.2.3 Tendon Shear Resistance 34
2.2.4 Ultimate Shear 34
2.2.5 Web Reinforcement 35
2.3 Computer Program PICB 37
III. MATERIAL PROPERTIES AND PREPARATION OF TEST SPECIMENS 41
3.1 Materials 41
3.1.1 Concrete and Polymer-Impregnated Concrete 41
3.1.2 Monomer System 41
3.1.3 Prestressing Steel 43
3.1.4 Reinforcing Steel 43
3.2 Fabrication of Test Specimens 46
3.2.1 Description of Test Beams 46
3.2.2 Forms 46
3.2.3 Placing of Tendons and Reinforcing Steel 49
3.2.4 Casting and Curing 49
3.3 Impregnation Techniques 49
3.3.1 Drying 50
3.3.2 Evacuation 53
3.3.3 Soaking 53
3.3.4 Pressurizing 53
3.3.5 Curing 57
3.4 Post-Tensioning Procedure 57
3.4.1 Stressing Equipment 59
3.4.2 Post-Tensioning Method 61
3.4.3 Grouting 61

Chapter		Page
IV.	INSTRUMENTATION AND TEST PROCEDURE	65
	4.1 Test for Flexural and Shear Strength	65
	4.1.1 Loading System	65
	4.1.2 Load Measurement	65
	4.1.3 Deflection Reading	69
	4.1.4 Strain Measurement	69
	4.1.5 Crack Marking	71
	4.2 Test for Time-Effect on Flexural Behavior	71
	4.2.1 Loading System	71
	4.2.2 Loading Measurement	74
	4.2.3 Deflection Readings	74
	4.2.4 Strain Measurement	74
V.	TESTS FOR FLEXURAL STRENGTH	79
	5.1 Description of Test Series	79
	5.1.1 Fully-Impregnated Beams	79
	5.1.2 Partially-Impregnated Beams	80
	5.1.3 Control Beam	80
	5.2 Test Results	80
	5.2.1 Initial Prestressing Forces	83
	5.2.2 Load-Deflection Responses	83
	5.2.3 Tendon Stress	97
	5.2.4 Crack Patterns and Mode of Failure	102
	5.2.5 Strain Distributions	108
	5.2.6 Deflection Curves	115
	5.3 Evaluation of Test Results	119
	5.3.1 Friction Loss	119
	5.3.2 Useful Limit of Strain for Polymer-Impregnated Concrete	122
	5.3.3 Moment-Curvature Relationship	126
	5.3.4 Structural Properties of Polymer-Impregnated Concrete for Flexural Members	131
	5.3.5 Stress Distribution of Polymer-Impregnated Concrete for Flexural Members	138

Chapter Page

5.3.6 Stress Distribution of Polymer-Impregnated Concrete Generated from Strain Readings 140
5.3.7 Equivalent Rectangular Stress Distribution 147
5.3.8 Comparison of Test Results to Theoretical Analysis 150
5.4 Effect of Independent Variables on Flexural Behavior 167
5.4.1 Provision for Maximum Number of Wires in Tendon . . . 167
5.4.2 Effect of Percentage of Steel 170
5.4.3 Effect on Monomer System 173
5.4.4 Effect of Polymer Depth 177
5.4.5 Comparison of Bonded and Unbonded Tendon Members 180
VI. TESTS FOR SHEAR STRENGTH 185
6.1 Description of Test Program 185
6.1.1 Fully-Impregnated Beams 185
6.1.2 Control Beams 185
6.2 Test Results 187
6.2.1 Load-Deflection Responses 187
6.2.2 Crack Patterns and Mode of Failure 187
6.2.3 Tendon Stress Responses 191
6.2.4 Useful Limit of Strains 198
6.3 Evaluation of Test Results 198
6.3.1 Shear at Inclined Cracking 200
6.3.2 Ultimate Shear 205
6.4 Comparison of Test Results with Theoretical Analysis 206
6.4.1 Cracking Moments 206
6.4.2 Tendon Stress Increase 209
6.4.3 Ultimate Moments 209
6.4.4 Shear Strength 212
6.5 Effects of Independent Variables on Shear Strength 212
6.5.1 Web Reinforcement 212
6.5.2 Percentage of Prestressing Steel 218

Chapter		Page
VII.	TIME EFFECT ON FLEXURAL BEHAVIOR	221
	7.1 Description of Test Program	221
	7.1.1 Beam PBT-4	221
	7.1.2 Beam PBT-8	222
	7.2 Test Results	222
	7.2.1 Time-Dependent Deflections	222
	7.2.2 Tendon Stress	225
	7.2.3 Strain Distributions	228
	7.3 Evaluation of Test Results	228
	7.3.1 Calculated Creep of Polymer-Impregnated Concrete	228
	7.3.2 Comparison of Creep in Polymer-Impregnated Concrete and Unimpregnated Concrete	232
	7.3.3 Comparison of Measured with Computed Tendon Forces	234
	7.3.4 Relaxation of Prestressing Steel	234
VIII.	DESIGN CRITERIA FOR POST-TENSIONED PIC BEAMS	241
	8.1 Structural Properties of Polymer Impregnated Concrete	241
	8.1.1 Compressive Strength	241
	8.1.2 Modulus of Elasticity	242
	8.1.3 Tensile Strength	242
	8.1.4 Modulus of Rupture	242
	8.2 Loss of Prestress	242
	8.2.1 Friction Losses	243
	8.2.2 Creep of Polymer-Impregnated Concrete	243
	8.2.3 Relaxation of Prestressing Steel	244
	8.3 Flexural Strength	244
	8.3.1 Stress Distribution of Polymer-Impregnated Concrete	244
	8.3.2 Tendon Stress	245
	8.3.3 Cracking Moment	245
	8.3.4 Ultimate Moment	245
	8.4 Shear Strength	246
	8.4.1 Web Shear	246

Chapter Page

8.4.2 Flexural Shear 246
8.4.3 Ultimate Shear 247
IX. CONCLUSIONS AND RECOMMENDATIONS 249
9.1 Conclusions 249
9.1.1 Flexural Strength 249
9.1.2 Shear Strength 252
9.1.3 Time Dependent Behavior 252
9.2 Recommendations 253

APPENDIX A Comparison of Load Data from Load Cell and Hydraulic Jack 255
APPENDIX B Concrete Mix Data 259
APPENDIX C Cylinder Strengths of Polymer-Impregnated Concrete and Unimpregnated Control 263
APPENDIX D Proportion of Grouting Materials 271
APPENDIX E Calibration Curve of Spring 275
APPENDIX F Comparison of Electrical and Mechanical Strain Gages for Concrete Cylinder 279

BIBLIOGRAPHY 283

LIST OF TABLES

Table		Page
1.1	Summary of Properties of Concrete Polymer Material	3
1.2	Tensile Strength of PIC	7
1.3	Shear Strength of PIC	7
1.4	Creep of MMA-Impregnated Concrete	9
3.1	Modulus and Strengths of Polymer-Impregnated Concrete and Unimpregnated Controls	42
5.1	Summary of the Fully Impregnated Beams	81
5.2	Summary of the Partially Impregnated Beams	82
5.3	Summary of Initial Tendon Forces and Midspan Camber	84
5.4	Loads, Moments and Deflections at Initial Cracking and Ultimate for Flexural Beams	91
5.5	Friction Losses for Each Test Beam	120
5.6	Friction Coefficients Calculated From Test Results	123
5.7	Average Measured Values of Concrete Strain at Failure	124
5.8	Moments and Curvatures at Initial Cracking and Ultimate for Flexural Test Beams	130
5.9	Tensile and Compressive Strengths for Different Monomer Systems	137
5.10	Rupture Modulus for Different Monomer Systems	139
5.11	Development of Equivalent Rectangular Stress Block	151
5.12	Increased Tendon Stress	164
5.13	Comparison of Cracking Moments	165
5.14	Comparison of Ultimate Moments	168
6.1	Description of Beams for Shear Tests	186

Table		Page
6.2	Loads, Moments and Deflections at Cracking and Ultimate for Shear Test Beams	190
6.3	Useful Limit of Strain for Beams Tested for Shear	199
6.4	Shear to Form Flexural Cracks at Critical Section	201
6.5	Measured Shear at Inclined Cracking	203
6.6	Computed and Measured Shear Capacities	207
6.7	Comparison of Cracking Moments	208
6.8	Comparison of Tendon Stress Increase	210
6.9	Comparison of Ultimate Moments	211
6.10	Predicted Diagonal Shear Strength	213
6.11	Observed and Predicted Flexural-Shear Strength	214
7.1	Comparison of Unit Creep of PIC and Unimpregnated Concrete	235

LIST OF FIGURES

Figure		Page
1.1	Compressive Stress-Strain Curve for Polymer-Impregnated Concrete	4
1.2	Typical Stress-Strain Curves for Prestressing and Reinforcing Steel	12
2.1	Conversion of an Imposed Strain Gradient to Forces	19
2.2	Cross Section Strain and Forces	19
2.3	Concentric and Eccentric Prestress on a Section	20
2.4	Friction Consideration for Unbonded Tendon	22
2.5	Variation of Steel Stress with Load	25
2.6	Typical Moment-Curvature Relationship and Load-Deflection Curve of Prestressed Concrete Beam	28
2.7	Typical Stress Block at a Point of a Prestressed Concrete Beam	31
2.8	Ultimate Design for Flexural Shear	36
2.9	General Flow Diagram	38
3.1	Stress-Strain Curve for Prestressing Steel	44
3.2	Stress-Strain Curves of Reinforcing Steel	45
3.3	Description of Test Beams	47
3.4	Details of Formwork	48
3.5	Drying Enclosure and Infrared Heater	51
3.6	Typical Weight Loss of the Specimen During Drying Process	52
3.7	Impregnation Chamber	54
3.8	Pressurizing System	55
3.9	Soaking Apparatus	56

Figure		Page
3.10	Curing Tank, Gas Burners, and Electric Heater in Polymerization Process	58
3.11	Stressing Equipment	60
3.12	Conventional Grouting System	62
3.13	Polymer Grouting System	64
4.1	Loading System for Flexural and Shear Tests	66
4.2	Hydraulic Ram and Load Cell in Loading System	67
4.3	Location of Dial Indicators for Measuring Deflections	68
4.4	Strain Gauge Locations on Beam Section	70
4.5	Loading System for Time-Dependent Deflection Tests	72
4.6	Screw Jack and Spring Loading System for Sustained Load Tests	73
4.7	Dial Indicator Arrangement for Sustained Load Tests	75
4.8	Strain Measurement in Sustained Load Beams Using Berry Gauge	76
5.1	Observed Load-Deflection Responses for PBF-Series Beams	86
5.2	Observed Load-Deflection Responses for PBM-Series Beams	87
5.3	Observed Load-Deflection Responses for PBB-Series Beams	88
5.4	Observed Load-Deflection Responses for PBP-Series Beams	89
5.5	Observed Load-Deflection Response for Control Beam	90
5.6	Observed Tendon Stress Response Under Loads for PBF-Series Beams	97
5.7	Observed Tendon Stress Response Under Loads for PBM-Series Beams	98

Figure		Page
5.8	Observed Tendon Stress Responses Under Loads for PBP-Series Beams	99
5.9	Observed Tendon Stress Response Under Loads for Control Beam	100
5.10	Crack Patterns for PBF-Series Beams	103
5.11	Crack Patterns for PBM-Series Beams	104
5.12	Crack Patterns for PBB-Series Beams	104
5.13	Crack Patterns for PBP-Series Beams	105
5.14	Crack Patterns for Control Beam	105
5.15	PBF-2 and PBF-8 After Failure	107
5.16	Bonded and Unbonded Beams After Failure	109
5.17	Beams with Different Monomer Systems After Failure	110
5.18	Control Beam and Partially Impregnated Beams After Failure	111
5.19	Measured Strain Distributions for PBF-Series Beams	112
5.20	Measured Strain Distributions for PBM and PBB Series Beams	113
5.21	Measured Strain Distributions for PBP and PBC Series Beams	114
5.22	Deflection Curves for PBF-Series Beams	116
5.23	Deflection Curves for PBM and PBB Series Beams	117
5.24	Deflection Curves for PBP and PBC Series Beams	118
5.25	Measured Values of Concrete Strain at Failure	125
5.26	Moment-Curvature Relationships for PBF-Series Beams	127
5.27	Moment-Curvature Relationships for PBB and PBM-Series Beams	128

Figure		Page
5.28	Moment-Curvature Relationships for PBP and PBC-Series Beams	129
5.29	Stress-Strain Relationship of Cylinders Subjected to Repeated High-Intensity Loading	133
5.30	Relationship Between Modulus of Elasticity and Cylinder Strength of Polymer-Impregnated Concrete	134
5.31	Relationship Between Compressive Strength and Polymer Loading of 100% MMA Polymer-Impregnated Concrete	135
5.32	Modified Stress Distributions in Compressive Zone of Polymer-Impregnated Concrete Beams	141
5.33	Load-Deflection Responses for PBF-2 Generated from Modified Stress Distributions	143
5.34	Load-Deflection Responses for PBF-4 Generated from Modified Stress Distributions	144
5.35	Load-Deflection Responses for PBF-6 Generated from Modified Stress Distributions	145
5.36	Load-Deflection Responses for PBF-8 Generated from Modified Stress Distributions	146
5.37	Stress Distributions for Polymer-Impregnated Concrete Generated from Strain Readings	148
5.38	Equivalent Rectangular Stress Distribution for Polymer-Impregnated Concrete Beams	149
5.39	Comparison of Load-Deflection Responses for PBF-2 and PBF-6	153
5.40	Comparison of Load-Deflection Responses for PBF-4 and PBF-8	154
5.41	Comparison of Load-Deflection Responses for PBM-50 and PBM-75	155
5.42	Comparison of Load-Deflection Responses for PBP-2 and PBP-4	156

Figure		Page
5.43	Comparison of Load-Deflection Responses for PBC-2	157
5.44	Comparison of Tendon Stress Responses Under Load for PBF-2 and PBF-6	158
5.45	Comparison of Tendon Stress Responses Under Loads for PBF-4 and PBF-8	159
5.46	Comparison of Tendon Stress Responses Under Loads for PBM-50 and PBM-75	160
5.47	Comparison of Tendon Stress Responses Under Loads for PBP-2 and PBP-4	161
5.48	Comparison of Tendon Stress Responses Under Loads for Control Beam	162
5.49	Relationship Between Toughness and Percentage of Prestressing Steel	171
5.50	Effect of Percentage of Steel on Inelastic Rotation Capacity for Polymer-Impregnated Concrete Beams	172
5.51	Effect of Percentage of Steel on Tendon Stress Increase . . .	174
5.52	Load-Deflection Responses for Beams with Different Monomer Systems	175
5.53	Tendon Stress Responses for Beams with Different Monomer Systems	176
5.54	Effect of Percentage of BA in Monomer System on Tendon Stress Increase	178
5.55	Load-Deflection Responses for Beams with Different Polymer Depths	179
5.56	Tendon Stress Responses for Beams with Different Polymer Depths	181
5.57	Load-Deflection Responses for Beams Containing Bonded and Unbonded Tendons	182
6.1	Observed Load-Deflection Responses for S-Series Beams	188
6.2	Observed Load-Deflection Responses for C-Series Beams	189

Figure		Page
6.3	Crack Patterns for S-Series Beams	192
6.4	Crack Patterns for C-Series Beams	193
6.5	PBS-6S and PBS-8S After Failure	194
6.6	PBC-2C and PBS-6S After Failure	195
6.7	Observed Tendon Stress Response Under Loads for S-Series Beams	196
6.8	Observed Tendon Stress Responses Under Loads for C-Series Beams	197
6.9	Flexural Shear for Polymer-Impregnated Concrete Beams	204
6.10	Comparison of Load-Deflection Responses for PBF-4 and PBS-4S	215
6.11	Comparison of Load-Deflection Responses for PBF-8 and PBS-8S	216
6.12	Comparison of Load-Deflection Responses for PBF-6, PBS-6S, and PBS-6C	217
6.13	Effect of Percentage of Steel on Shear Strength	219
7.1	Time Dependent Deflections Under Deadweight of the Beams	223
7.2	Time Dependent Deflections Under Sustained Loads	224
7.3	Time Effect on Tendon Forces Under Deadweight of the Beams	226
7.4	Time Effect on Tendon Forces Under Sustained Loads	227
7.5	Strain Distribution over Beam Depth	229
7.6	Initial Stress Distribution at Midspan	231
7.7	Calculated Unit Creep of Polymer-Impregnated Concrete	233
7.8	Comparison of Measured and Computed Change in Tendon Force	236

Figure Page

7.9 Time-Dependent Relaxation of Prestressing Steel 238

CHAPTER I. INTRODUCTION

1.1 Background

Polymer-impregnated concrete (PIC), which consists of precast portland cement concrete impregnated with a liquid monomer system that is subsequently polymerized or converted to a solid plastic in situ, is receiving considerable attention in the U.S. because of its remarkable strength and durability properties. The first polymer-impregnated concrete was produced at Brookhaven National Laboratory (BNL) at the request of the U.S. Bureau of Reclamation (USBR) in 1965. Since then many extensive research programs have been conducted by various other institutes to develop impregnation techniques for various types of application. It is fortunate that many mechanical and physical properties of polymer-impregnated concrete have been investigated, along with its applications.

Initial developmental work in the U.S. has been directed toward applications in which the durability properties would be an advantage, such as partial-depth impregnation of bridge decks (6,7,14), bridge deck panels (16), tunnel support and lining systems (8), concrete pipes (9), desalting plants (9), brick masonry (10), and concrete tiles (13). However, little attention has been directed toward structural applications in which the high strength and stiffness of PIC could be utilized.

A research effort was initiated at The University of Texas at Austin to develop a practical process for partial-depth impregnation for concrete bridge slabs (6,7,10,11,12,14,15). The partial-depth impregnation technique has been used in the U.S. for treatment of bridge decks (10,14), dam outlet walls, and stilling basin floors (15). The increased strength, stiffness, and creep of polymer-impregnated concrete indicated good potential for prestressed beams. Significantly less creep than for ordinary concrete, and in some cases no creep or even negative creep (1,2,5), was observed for this material. In recent years, the use of PIC for prestressed members has been considered in order to improve their strength and ductility characteristics (16). However, the research reported here was performed only for pretensioned members which were

impregnated after the concrete had been prestressed. The additional strength increase of PIC was not considered in the design of the pretensioned members.

This report describes the research conducted on post-tensioned PIC beams. The beams were impregnated and then post-tensioned. The investigation included the following as major considerations: flexural strength, shear strength, time-dependent deflection, and differences between beams with bonded and unbonded tendons.

1.2 Structural Properties of Polymer-Impregnated Concrete

The first measurements of structural and physical properties of PIC were made in 1966 by the U.S. Bureau of Reclamation (USBR) at Brookhaven National Laboratory (BNL), where the first PIC that was produced with methyl methacrylate (MMA) developed very high strength properties. A summary of the properties of PIC is shown in Table 1.1. The test specimens had an average polymer loading of 6.7 percent, polymerized by Cobalt 60 gamma radiation (1-5).

In general, the improvement in strength of PIC is a function of polymer loading and type of monomer system (3) while the improvement in durability seems to be a function of polymer loading and the degree of success in sealing the surface of concrete (5). The polymer loading, which is defined as percent of polymer in concrete by weight, depends primarily on the impregnation technique and the percentage of voids in the concrete. Radiation polymerization gives slightly better strength properties than thermal catalytic polymerization (2). Low strength concrete generally has more voids and can absorb more monomer than high strength concrete (3.11).

It should be indicated that Poisson's ratio and the coefficient of thermal expansion of PIC are higher than for unimpregnated concrete (4). The other properties are significantly improved, as discussed below.

1.2.1 Compressive Stress-Strain Relationship

The compressive stress-strain relationship for MMA-impregnated concrete was measured for the first time by the USBR (3). The stress-strain curves for PIC and for unimpregnated concrete are shown in Fig. 1.1. It should be noted that the modulus of elasticity for PIC is significantly higher than for unimpregnated concrete. The reported modulus of elasticity for each curve in the figure as evaluated by the USBR method (3) is rather low in comparison to the

Table 1.1

Summary of Properties of

Concrete Polymer Material (1,5)

Description of Properties	Control	PIC
Compressive strength ,psi	5267	20,255
Tensile strength, psi	416	1,627
Modulus of elasticity, psi	3.5×10^{6}	6.3×10^{6}
Poisson's ratio, in/in	0.16	0.20
Flexural modulus of elasticity, psi	4.3×10^{6}	6.2×10^{6}
Coefficient of expansion, in/in ^{o}F	4.02×10^{-6}	5.36×10^{-6}
Water permeability, ft/yr	6.2×10^{-4}	0
Water absorption, %	5.3	0.29
Freeze-thaw durability		
Number of cycles	590	2420
% wt. loss	26.5	0.5
Hardness-impact ("L" hammer)	32.0	55.3

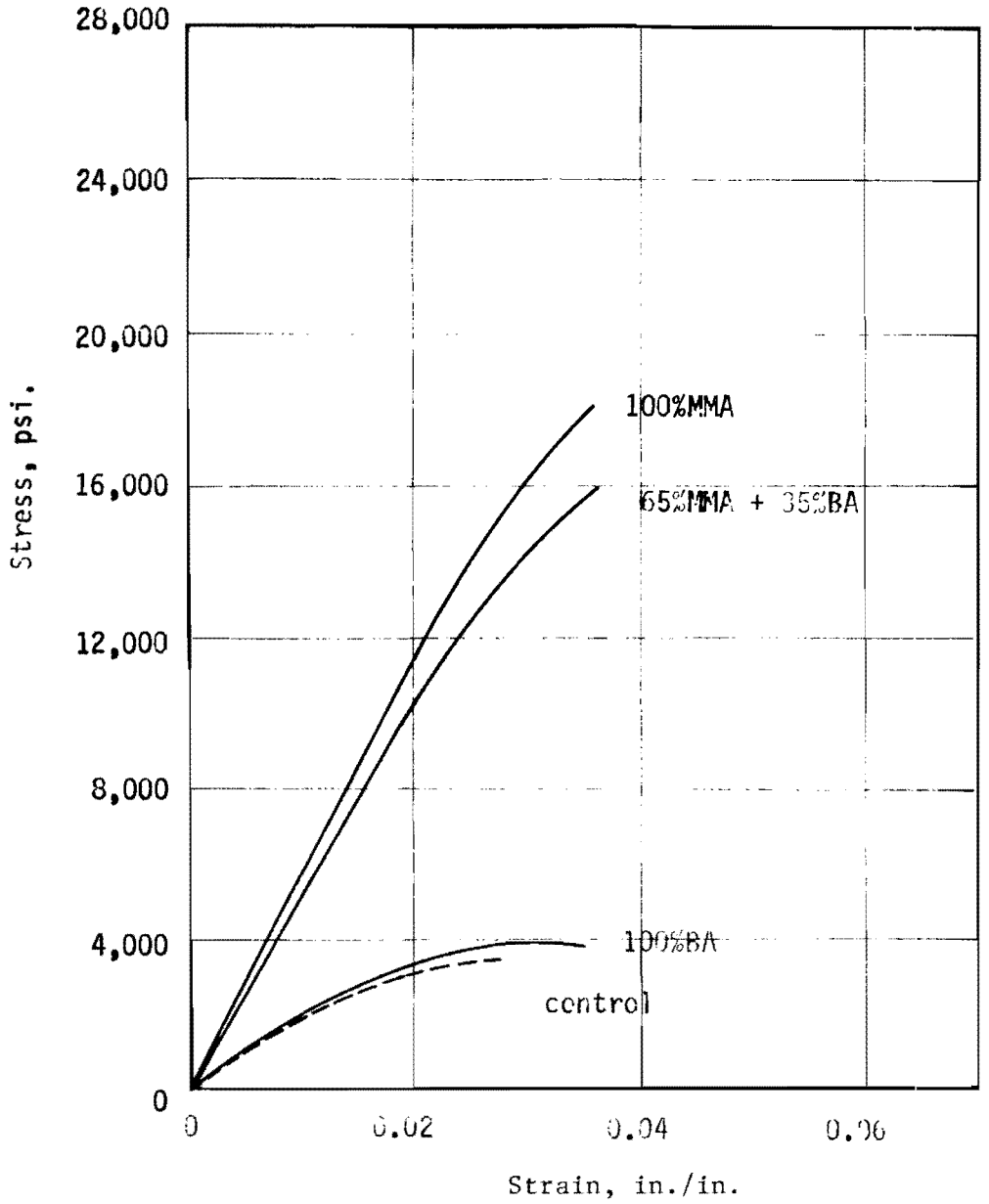

Fig. 1.1 Compressive Stress-Strain Curve for Polymer-Impregnated Concrete (3,5).

ASTM method (50), which was used for the unimpregnated concrete. However, the testing technique does not allow measurement after the maximum load has been attained. The ultimate compressive strength of PIC is about 2 to 5 times higher than that of unimpregnated concrete. The most significant fact about these curves is that, while the deformation of the unimpregnated concrete sample is continuously nonlinear and irreversible, the deformation of MMA-impregnated concrete is completely linear up to more than 75 percent of ultimate load and at failure the departure from linearity is less than 7.5 percent (3). The compressive stress-strain properties of MMA-impregnated concrete indicate that the composite is a hard, brittle material. The brittleness of the composite can be reduced by adding plasticizers to the monomer system (5).

It was found that the monomer system would affect the shape of the curve, thus influencing both the modulus of elasticity and the ultimate compressive strength (1,11), as shown in Fig. 1.1. Polymer-impregnated concrete (PIC) made from glassy polymers such as methyl methacrylate (MMA) or isobutyl methacrylate (IBMA) generally produced the highest modulus of elasticity and ultimate compressive strength. PIC made with butyl acrylate (BA), which was the most rubbery polymer in the study, developed the smallest increase in stiffness and ultimate compressive strength (10). The ultimate compressive strain of MMA-impregnated concrete is about 20 percent higher than that of unimpregnated concrete. The strength and stiffness of PIC produced with other monomers, such as isobutyl acrylate (IBA), butyl methacrylate (BMA), or styrene (S), were less than those produced with MMA (1).

It has been found that the original concrete strength only slightly affects the ultimate compressive strength of PIC. Tests at BNL on PIC made with concrete with strengths of 1670 psi to 4300 psi showed that the weakest concrete increased in strength by a factor of 9 while the strongest concrete increased by a factor of 4. Ultimate strengths were almost the same (3,4).

Recently, the compressive stress-strain curves of PIC up to the maximum stress have been shown to be similar to the ones in Fig. 1.1. The complete stress-strain curves of PIC have been found by means of flexural tests on reinforced PIC beams and repeated load tests of cylinders (11).

1.2.2 Tensile Strength

Tensile strength of PIC has been determined at USBR using direct tensile strength and splitting tensile strength tests (1,5). The direct tensile strength of a specimen is generally about 85 percent of the value obtained in the splitting tensile strength test (1). However, the strengths vary with monomer systems and polymer loading. The tensile strength improvement for PIC is about the same as the improvement of compressive strength. The values shown in Table 1.2 for the different monomer systems, glass-like (MMA), intermediate (BMA), and rubbery (IBA) materials, are from Ref. 10. The monomer systems included one percent (wt) of benzoyl peroxide (BP) and 10 percent trimethylolpropane trimethacrylate (TMPTMA). The control specimens had an average compressive strength of 4000 psi and a water-cement ratio of 7.5 gal per sack. It should be noted that the stiffness, or modulus of elasticity, and Poisson's ratio of PIC are relatively the same for both compression and tension (5). The tensile stress-strain relationship of PIC appears to be much more linear than that of plain concrete. The average tensile strain of MMA-impregnated concrete is about 20 percent higher than that of unimpregnated concrete (5).

1.2.3 Shear Strength

Shear strength of MMA-impregnated concrete is about 3700 psi, 2 to 3 times greater than of unimpregnated concrete (5). As can be seen in Table 1.3, the shear strength of PIC is a function of the monomer system. It should be noted that the values shown in the table were obtained from tests reported in Ref. 5, which were performed in accordance with the USBR standard, in which the specimen were 2-in. diameter by 7-in. long cylinders. The specimens were oven-dried at 177^{o}C prior to impregnation, evacuated, soaked, and pressurized and then polymerized by thermal-catalytic means. MMA-impregnated concrete is currently considered to exhibit the best improvement in shear strength among well known PIC materials. This significant increase in shear strength could allow some reduction of stirrups in flexural members.

1.2.4 Creep

The creep of PIC is one of the most interesting of all its mechanical properties. Negative creep has been observed in PIC specimens under both low

Table 1.2

Tensile Strength of PIC (Ref. 10)

Monomer	Polymer Loading (%)	Tensile Strength (psi)
Control	-	476
MMA	5.75	1037
IBA	5.58	878
BMA	5.68	726

Table 1.3

Shear Strength of PIC (Ref. 5)

Type of PIC	Polymer Loading (%)	Test Method	Shear Strength (psi)
Control	-	Single shear	1140
	-	Double shear	1730
MMA	8.0	Single shear	3760
	8.2	Double shear	3670
Styrene-TMPTMA(a)	7.7	Single shear	2880
MMA-TMPTMA(b)	7.1	Single shear	2510

(a) 60 % wt styrene + 40 % wt TMPTMA

(b) 70 % wt MMA + 30 % wt TMPTMA

tensile and compressive stresses, but it may prove to be insignificant in the design of a structure (1,4,5). The creep of PIC under compressive stress does not equal the creep under tensile stress but both increase with the stress. Comparing MMA-impregnated concrete specimens with unimpregnated ones under the same loads shows that the PIC specimens experience about one-fifth as much creep at 690 psi and about one-seventh as much creep at 2313 psi. At a load of 7000 psi, which is about 30 percent of the ultimate strength, the PIC specimens have about 10 percent of the creep deformation per unit stress of unimpregnated concrete at 2313 psi (5). The PIC specimens with different monomer systems have different creep; the PIC impregnated with MMA or chlorostyrene shows a smaller creep than styrene specimens or other types of PIC (1,5). Table 1.4 illustrates the creep of MMA-impregnated concrete under low and high compressive stresses and high tensile stress as a function of time (5).

1.2.5 Durability

Polymer-impregnated concrete has been shown to have greatly improved physical and mechanical properties related to durability performance. It was found that partial-depth polymer impregnation provided excellent protection against freeze-thaw resistance and water penetration. It was also found that abrasion and skid resistance were not reduced and were in some cases improved (6). Durability tests of PIC, including resistance to freezing and thawing, acids, sulfates, sodium chloride, and weathering, were conducted at BNL and The University of Texas at Austin (1-5,10,18).

The freeze-thaw test as reported in References 1 and 3 indicated that an MMA-impregnated specimen had only a 0.5 percent weight loss after 12,010 cycles, an improvement of more than 900 percent over the control specimens. The unimpregnated concrete generally fails at less than 740 cycles and has a 25 percent weight loss.

In accelerated sulfate attack tests, PIC specimens have shown moderately to greatly improved resistance as compared with unimpregnated concrete. It was shown that PIC specimens expanded from 0.016 to 0.032 percent after 1436 cycles whereas the controls failed at 480 cycles with 0.500 percent expansion.

PIC specimens showed no loss in weight and no visible signs of deterioration when exposed to a 5 percent solution of sodium chloride for more than one year. Acid resistance tests indicate significant improvement. PIC specimens

Table 1.4

Creep of MMA-Impregnated Concrete (Ref. 5)

Creep Type	Stress (psi)	Monomer System	Polymer Loading (%)	Unit Creep (micro in./in.) Time (days) 8	31	70	261	562
	178	Control	-	0.051	0.191	0.258	0.331	0.257
Tension	178	MMA	4.6	-0.230	-0.051	-0.185	-0.191	-0.398
	345	MMA	4.6	-0.049	-0.023	-0.069	-0.049	-0.181
	690	Control	-	0.091	0.139	0.168	0.271	0.368
	690	MMA	5.4	0.006	0.011	0.039	0.029	0.066
Compression	2313	Control	-	0.131	0.198	0.239	0.336	0.336
	2313	MMA	5.4	0.015	0.023	0.036	0.038	0.049
	7000	MMA	5.4	0.019	0.025	0.035	0.041	0.049

(MMA) immersed in 15 percent hydrochloric acid (HCl) lost from 10 to 12 percent in weight after 1395 days of exposure while unimpregnated concrete specimens failed with a 25 percent weight loss after 105 days.

Tests conducted at The University of Texas at Austin showed that the corrosion of the reinforcing bars in fully-impregnated piles under seawater exposure ranged from 0.25 percent to 1 percent of surface area as compared to 8.5 percent for bars in plain concrete with a water-cement ratio of 6.4 gal/sack and to 45 percent for bars in concrete with a water-cement ratio of 8.5 gal/sack (10,18). The application of PIC for structural members should also provide remarkable durability as well as improved mechanical properties.

1.3 Prestressed Concrete Beam

Prestressed concrete first appeared in 1886, when P.H. Jackson, an engineer in San Francisco, California, obtained patents for tightening steel tie rods in artificial stones and concrete arches to serve as floor slabs (19). These applications were based on the concept that concrete, though strong in compression, was quite weak in tension and prestressing the steel against the concrete would put the concrete under compressive stress which could be utilized to counterbalance tensile forces due to dead or live loads. After its beginning in the United States, the significant growth in use and the development of prestressed concrete shifted to Europe. Leonhardt (20) has prepared an extensive historical resume of prestressed concrete in its many forms and applications. The use of prestressed concrete in this country grew rapidly after 1950 and now is very common for long-span structures, including buildings and bridges.

The development of new materials and methods for use in prestressed concrete is continually being pursued to enhance its economy relative to reinforced concrete. The use of PIC in prestressed members would appear to offer considerable potential because of the excellent compressive and tensile strengths, high modulus, and lower creep.

1.3.1 Tensile Stress-Strain Relationship for Steel Types

High tensile strength steel is almost the universal material used for prestressing tendons for prestressed concrete. Three forms of reinforcement are most widely used at the present time: wires, strands, and bars. In

general, the ultimate tensile strength of wires varies from 200,000 psi to 330,000 psi, depending on the diameter and production process. Seven-wire strands have strengths from 230,000 psi to 270,000 psi while steel bar strengths are between 140,000 psi and 170,000 psi. Typical stress-strain curves for a high-strength wire, bar, and strand are shown in Fig. 1.2. The modulus of elasticity for the steel can be accurately computed by those curves. The average ultimate elongation is about 4 percent for wires and 5 percent for bars.

In general, ASTM grade 40 or 60 reinforcing steel is used as shear reinforcement and may also be used as longitudinal reinforcement to control overstressing at transfer or in service. A typical stress-strain curve for steel is also presented in Fig. 1.2. It is noted that the moduli of elasticity of both types of steel are not significantly different but the ultimate tensile strength of high strength wire is about 4 to 5 times that of regular reinforcing steel.

1.3.2 Prestressing Method

Several techniques are available for imposing the designed compression force on the concrete. The two major schemes of prestressing are distinguished by the condition of the concrete surrounding the tendon at the time of stressing.

Pretensioning is the method of prestressing in which the tendons are tensioned before the concrete is placed. The tendons must be temporarily anchored against abutments at the ends of the bed when tensioned and the prestress force is transferred to the concrete after it has set. The procedure is employed in precasting plants or laboratories, where permanent prestressing beds can be provided.

Post-tensioning is the technique of prestressing in which the tendon is tensioned after the concrete has hardened. This scheme stresses the tendons by imposing the reaction directly against the hardened concrete. When the desired amount of prestressing force in the steel tendon has been obtained, some procedure, such as inserting steel shims between the stressing apparatus and the end of the beam, must be used to maintain the desired level of prestressing force. This post-tensioning method can be applied to either precast or cast-in-place members.

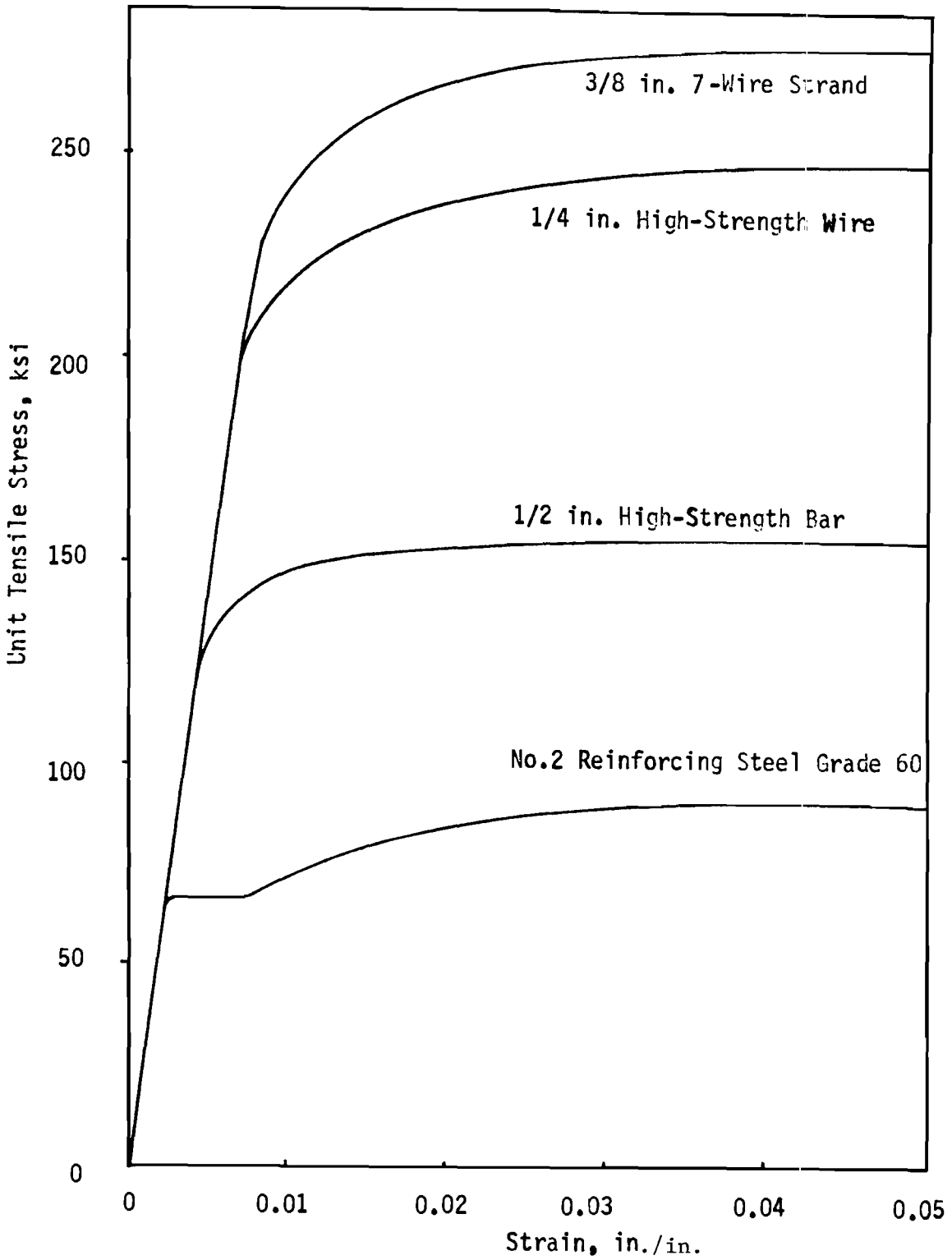

Fig. 1.2 Typical Stress-Strain Curves for Prestressing and Reinforcing Steel (19).

The pretensioning technique usually permits the fresh concrete to bond directly to the tensioned tendons. Post-tensioned tendons can be either bonded to the concrete or unbonded, depending upon the application.

The possible combinations of stressing type and subsequent bond condition illustrate the versatility available in prestressing concrete. Additional techniques, such as stressing in stages or combining pretensioning and post-tensioning can also be employed, but the fundamental goal of any prestressing operation is to impose a desired initial compressive strain on the concrete to offset the inherent weakness of the material in tension.

1.3.3 Bonded or Unbonded Tendons

Bonded tendons are those which are bonded along their length to the surrounding concrete. In general, the bonding of post-tensioned tendons is accomplished by subsequent grouting. If unbonded tendons are desired, the tendons are usually greased and wrapped with paper tape or plastic tubes. In prestressing, concrete will bond directly to the tendon right after the concrete has been placed.

There is a fundamental difference in the response to load of a structure containing bonded prestressed tendons compared to one having unbonded tendons. The strain at any point in a bonded tendon will equal the change in strain in the surrounding concrete at the level of the tendon plus the initial strain in the concrete due to prestressing. Bonding insures compatibility of strain such that the change in steel strain will vary according to the strain gradient existing at each point along the length of the beam. Tendon stress will be maximum at the point of maximum bending moment. With complete bond, any tension cracks that may develop in the concrete will tend to be small and spaced closely together and these cracks will normally close after the load causing the cracks is removed.

Unbonded tendons are free to slip with respect to the adjacent concrete, and any relative movement destroys local compatibility of strain. The freedom to slip allows all change in strain to be distributed along the length of the tendons. The tendon length, the curvature of the unbonded tendons, the coefficient of friction, and the variation of the strain distribution normally affect the amount of slip between concrete and tendon. The strain in the unbonded tendon at the point of maximum bending moment is not as large as the

corresponding strain might be in a bonded tendon. In general, the ultimate strength of a beam containing unbonded tendons is less than that of an identical beam with bonded tendons. Cracks in unbonded beams are large and spaced relatively far apart because slip of the tendon permits large strains to be accumulated at a few locations rather than being distributed along the length of the tendon, thus reducing the ultimate flexural resistance of the section. Because of this we require some bonded reinforcing along with unbonded tendons.

1.3.4 Loss of Prestress

Loss of prestress is primarily due to elastic shortening of concrete, creep and shrinkage of concrete, relaxation of prestressing reinforcement, anchorage take-up, friction between tendon and surrounding materials, and bending of the member.

For pretensioned beams, as the prestress is transferred to the concrete, the member shortens and the prestressed steel shortens with it. This elastic shortening results in the loss of prestressing. For post-tensioning, the problem is different. If there is only a single tendon in a member, the concrete shortens as the tendon is jacked against the concrete. Since the force in the cable is measured after the elastic shortening of the concrete has taken place, no loss of prestress due to that shortening needs to be accounted for. On the other hand, if there are more than one tendon and the tendons are stressed in succession, loss will occur. The first tendon to be tensioned would suffer the maximum loss, due to shortening of the concrete by subsequent application of prestressing from all other tendons.

Prestressed concrete members undergo time-dependent deformation primarily as a result of the dimensional instability of concrete, which is ascribed classically to two different phenomena, creep and shrinkage. In addition, the relaxation of the prestressing reinforcement, the time-dependent loss of stress at constant strain which occurs when steel is subjected to a high sustained stress, results in an inelastic change in the deformation. Relaxation for most steel commercially available is considered to be in the range of 1 to 5 percent of initial stress (19).

Friction loss occurs between the post-tensioned tendon and its surrounding material, either concrete or sheathing, whether lubricated or not. This friction loss can be conveniently considered as the length effect and the curvature

effect. Other loss, due to anchorage or slippage of the gripping systems, can be eliminated by stressing procedures and workmanship.

It is difficult to generalize the amount of loss of prestress because it is dependent on so many factors: the properties of concrete and steel, curing conditions, magnitude and time of application of prestress, and process of prestressing. The prediction can be made fairly accurately for concrete members prestressed as usual, based on the data in Refs. 19, 21, 22. With pretensioned beams of normal weight concrete the total loss of prestress from all sources is approximately 20 percent to 24 percent of the initial pretensioned stress in the tendon. For post-tensioned beams, the total losses are approximately 15 percent to 20 percent of the initial tension in the tendon.

1.4 Research Objectives and Scope

Mechanical and durability properties of polymer-impregnated concrete have been widely investigated for the past several years (1-5,10). The significant improvement of PIC in compressive strength, tensile strength, modulus of elasticity, shear strength, creep, and durability directed the research toward prestressed polymer-impregnated concrete, where higher strength of PIC and high strength steel can be compatible. However, no experimental data on prestressed beams of this material have been published to date. To survey the reliability of the techniques of design and analysis which will be used in practice, some experimental information is needed.

The primary objective of this series of investigations was to determine the behavior of post-tensioned PIC beams over the total range of loading up to the point of collapse. The phases of the investigations can be classified into several categories: flexural strength, shear strength, and time-dependent behavior.

Another objective was to develop a theoretical analysis to accurately predict strengths and behavior and a practical methodology for design purposes.

1.4.1 Flexural Strength

There were three primary objectives to the flexural strength study. The first was to determine the flexural behavior from the laboratory tests conducted on actual post-tensioned PIC beams. The second objective was to provide the analytical tools required to model in the computer a beam or beam-column

containing prestressed unbonded tendons. The third objective was to compare the calculated results of the theoretical analysis with the observed values.

The scope of the flexural behavior concerns load-deflection and tendon stress responses, friction losses, cracking and ultimate moments and mode of failure. The investigation explored the effects of percentages of steel, impregnation depths, bonded and unbonded tendons and monomer systems.

The scope of the proposed numerical analysis is limited in the following ways: the failure mode for any beam is assumed to be flexure; no provisions for shear, bond, or anchorage failure have been included; all applied loads are assumed to be short-term and statically applied.

1.4.2 Shear Strength

The primary objective of the shear test series is to determine the normal permissible shear stress for prestressed PIC beams by means of the laboratory tests and to compare the results with the calculated values based on the ACI Building Code and some theoretical analyses.

The scope of the shear strength computation for the fully-impregnated PIC beams was limited to the 100 percent MMA monomer system only. The investigation included effects of the web reinforcement and the percentage of prestressing steel.

1.4.3 Time-Dependent Behavior

The primary objective of this phase of the investigation was to determine the prestressing losses of post-tensioned PIC beams from the time-dependent deflection tests.

The scope of the prestressing losses is limited to the creep of PIC and relaxation of the prestressing steel. The shrinkage of PIC is assumed to be very small and negligible.

The creep and relaxation functions are to be determined and may be used for future design consideration.

CHAPTER II. THEORETICAL ANALYSIS OF PRESTRESS CONCRETE BEAMS

2.1 Analysis for Flexure

Making a precise analysis for flexural strength of a prestressed concrete section is a complicated problem, especially for the inelastic range, because concrete is generally not an elastic material after microcracking has occurred. Many tests have been performed and many assumptions have been made for stress distribution (23-27). The numerical iteration procedure developed by Pierce (30) to analyze a post-tensioned concrete beam containing unbonded tendons will be adapted in this study to analyze a post-tensioned PIC beam with unbonded tendons.

The analysis based on the rectangular stress block allowed by ACI 318-71 (27) will also be made in this study for purposes of comparison to the numerical procedure and the test results.

2.1.1 Strain Profile and Stress Distribution

The numerical analysis procedure for flexure, presented in Section 2.3 requires input data for stress-strain curves for concrete and various steel types to convert a given strain condition to an appropriate set of forces. The common assumption used in previous studies (25,28) is that the strain varies linearly over the depth of the cross section. This is equivalent to assuming that each cross section of the structure satisfied Bernoulli's hypothesis that sections plane before bending remain plane after bending.

Figure 2.1 schematically illustrates the conversion of strain to forces. The cross section is subdivided into horizontal elements and an average strain is imposed over the assumed individual concrete elements. Each element strain is converted to a stress and then the stress is multiplied by the segment area to obtain a force. Tension in the concrete equal to the indirect tensile strength is assumed. The resisting moment of each section is the summation of the product of the forces and moment arms.

Fortunately the ultimate strength of prestressed concrete beams can be predicted or calculated using rectangular stress block and tendon stress suggested by the ACI Building Code (27). By this procedure, the stress distribution can be replaced adequately by an equivalent rectangle of stress (Whitney stress block) with an intensity of $0.85\ f'_c$ and a depth, a, as shown in Fig. 2.2, where f'_c is the concrete compressive strength and a is the depth of the rectangular stress block. The distance c is from the top fiber to the neutral axis. It should be noted that tensile stress in the concrete is not considered in this method.

2.1.2 Stress in Concrete Due to Prestress and Loads

According to present practice, stresses in concrete due to prestress are computed by elastic theory. For a prestress force, F, applied at the centroid of the concrete section (Fig. 2.3a), the unit stress in the concrete is uniform across the section and is given by

$$f = \frac{F}{A} \tag{2.1}$$

where A is the area of the concrete section.

On the other hand, if the prestress force, F, is applied to the concrete section with an eccentricity e (Fig. 2.3b), then it is possible to resolve the prestress into two components: a concentric load, F, and a moment, Fe. By elasticity theory, Eq. 2.1 becomes

$$f = \frac{F}{A} \pm \frac{Fe\ y}{I} \tag{2.2}$$

where y is the distance from the neutral axis and I is the moment of inertia of the cross section. In this study tensile stress is assumed positive.

For an exact theoretical solution, the values of the cross-sectional area, A, and the moment of inertia, I, should be calculated on the basis of a transformed section, transforming the area of the steel for beams containing bonded tendons or bonded reinforcing bars. However, in cases where the beams have unbonded tendons, the net concrete section is used instead because unbonded tendons do not affect stiffness.

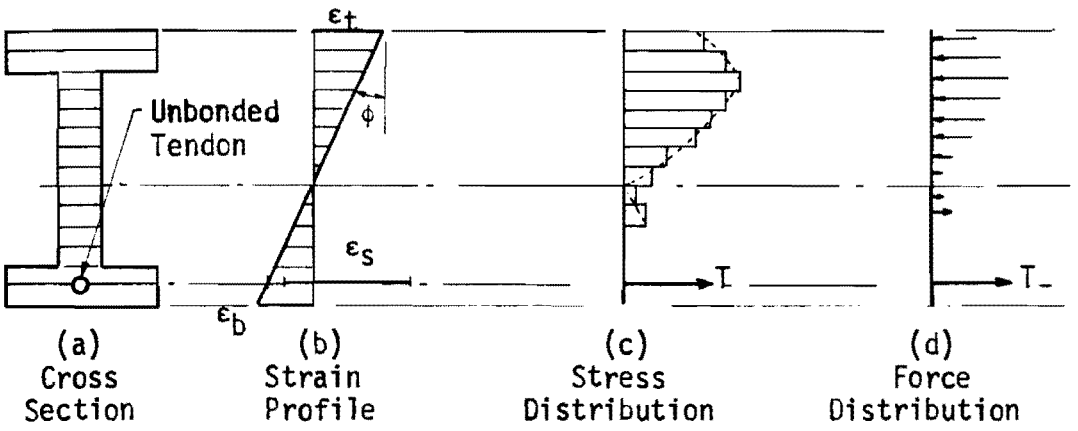

Fig. 2.1 Conversion of an Imposed Strain Gradient to Forces.

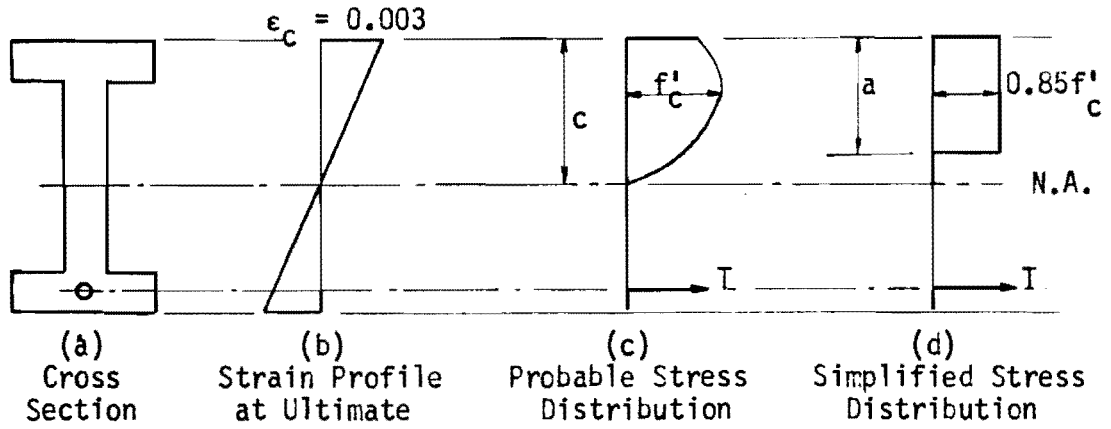

Fig. 2.2 Cross Section Strain and Forces.

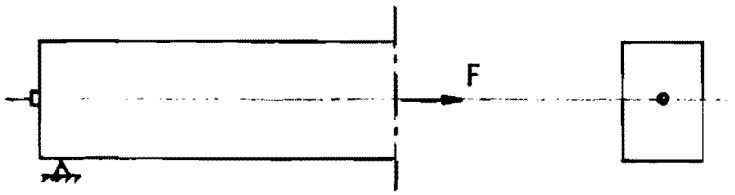

(a) Concentric Prestress.

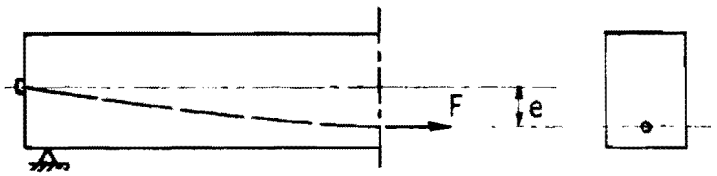

(b) Eccentric Prestress.

Fig. 2.3 Concentric and Eccentric Prestress on a Section .

It should be noted that, for a pretensioned member, the prestress force in the steel is reduced due to elastic shortening immediately after transfer. For a post-tensioned member with several tendons, the tensioning of any subsequent tendon would reduce the stress in previously tensioned tendons.

Stresses produced by external bending moment, due to externally applied loads or to the beam weight, are computed by usual elastic theory:

$$f = \pm \frac{My}{I} \tag{2.3}$$

where M is the bending moment at the section.

The resulting stresses in concrete due to both prestress and external loads are given by the sum of Eqs. 2.2 and 2.3:

$$f = \frac{F}{A} \pm (Fe \pm M) \frac{y}{I} \tag{2.4}$$

2.1.3 Friction Consideration for Unbonded Tendons

Post-tensioning unbonded tendons creates some stress loss due to friction between the tendons and the surrounding material. This friction loss can be conveniently considered in two different categories, the length effect and the curvature effect. The length effect considers the amount of friction that would be encountered if the tendons were straight, that is, not purposely bent or curved. In practice, the duct for the tendon cannot be perfectly straight, so some friction will exist between the tendon and the surrounding material.

The curvature effect represents the recognized loss in force resulting from known tendon curvature. This loss is again dependent on the coefficient of friction between the contact material and the pressure exerted by the tendon on the concrete. The coefficient of friction is a function of the smoothness of the potential sliding surface between unbonded tendons and surrounding concrete or duct material. The pressure between the tendon and concrete is dependent on the stress in the tendon and the total change in angle.

Some suggested ranges of values of wobble coefficients, K, and friction coefficients, μ, are given in Refs. 29 and 27. The numerical procedure developed by Pierce (30) can predict the stress distribution along the tendon from tendon geometry input data, prestressing force, and appropriate friction coefficients or wobble coefficients. Figure 2.4 shows schematically some of

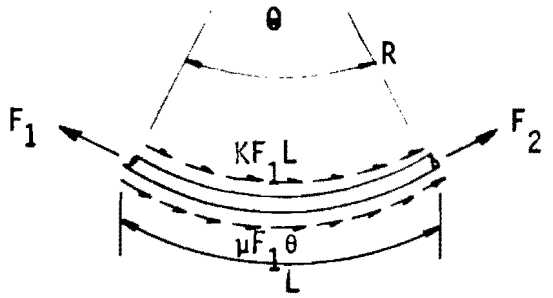

(a) Approximate Friction Loss along Circular Curve.

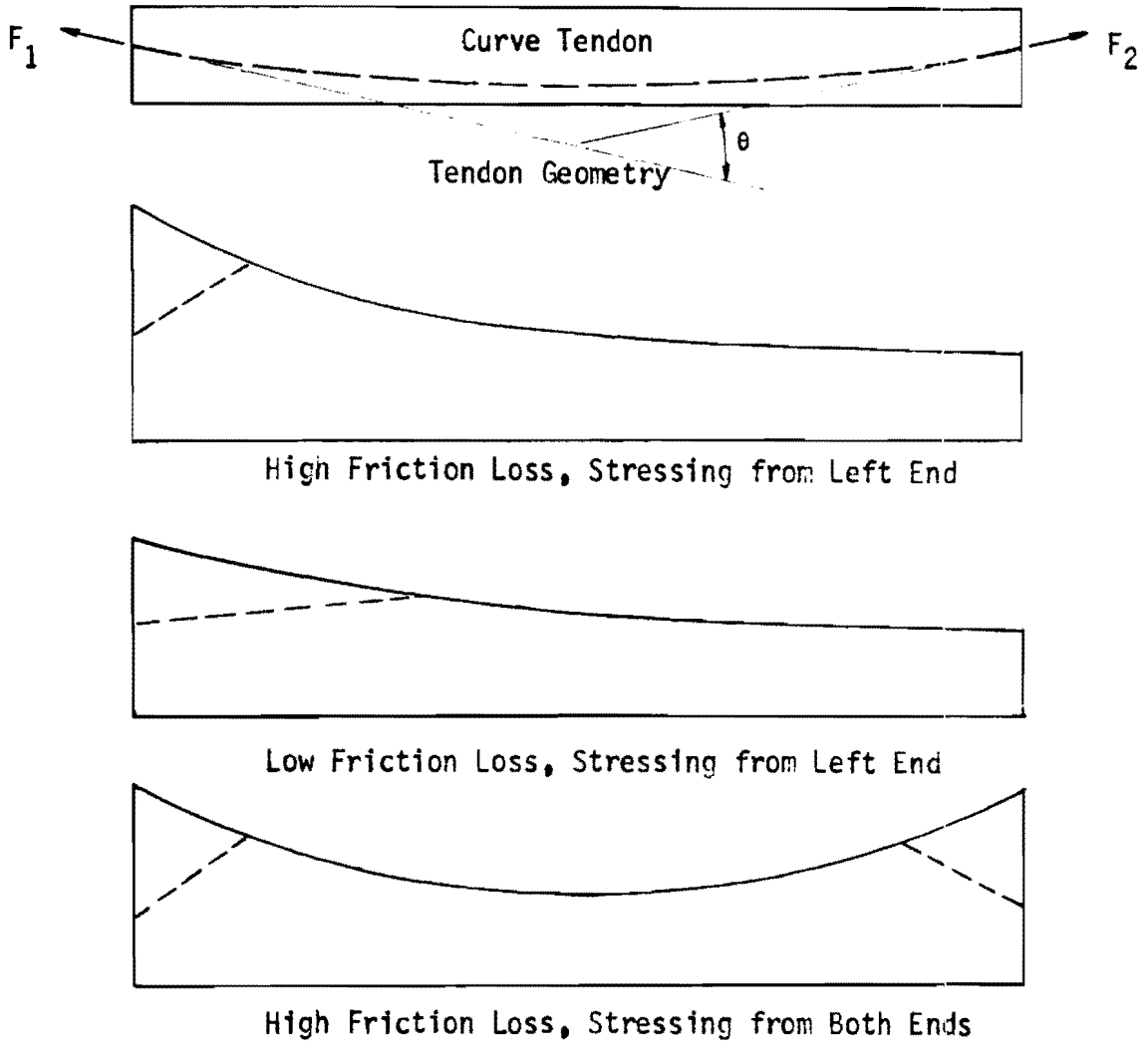

(b) Tendon Stress Variation due to Friction Loss.

Fig. 2.4 Friction Consideration for Unbonded Tendon.

the possible tendon stress variations measured along the length of the tendons that may be obtained by overstressing followed by subsequent release. The figure also illustrates the different stress variations between high friction loss and low friction loss and also between stressing at one end and at two ends. Perhaps the most common method of controlling loss due to friction is to slightly overstress the tendons during the stressing operation. The process of overstressing and releasing may be repeated as many times as necessary in order to approximate the desired final prestress condition.

The basic theoretical formula to compute friction loss has been derived in Ref. 19. The total friction loss due to length and curvature effects can be written as

$$F_2 = F_1 e^{-\mu\theta - KL} \tag{2.5}$$

where F_1 = tension at the jacking end

F_2 = tension at the section to be considered

μ = curvature friction coefficient

K = wobble friction coefficient

θ = angle change of tendon profile in radians from jacking end to point considered

L = tendon length from jacking end to point considered.

However, the difference in tension at the jacking end and at the other end of the curve is not excessive. An approximate formula may be written as

$$F_2 = F_1(1 - KL - \mu\theta) \tag{2.6a}$$

or

$$\frac{F_1 - F_2}{F_1} = L(K + \frac{\mu}{R}) \tag{2.6b}$$

where R = radius of tendon curvature.

An equilibrium model for this expression is illustrated in Fig. 2.4a and it is employed for computer analysis in program PICB, discussed in Section 2.3.

2.1.4 Response of Prestressing Steel Under Loads

Steel stresses in a prestressed concrete beam that are due to externally applied loads are completely different from those stresses in a reinforced concrete beam. In reinforced concrete, steel stresses are assumed to be directly proportional to the external moment. An increasing resistance to the external moment of a prestressed concrete beam is caused by the lengthening of the lever arm between the resisting compressive force, C, in the concrete and the tension, T, in the steel, which remains relatively unchanged in magnitude.

The variation of steel stress with external load on a simple beam is shown in Fig. 2.5. Initial prestress, f_o, indicates the stress in the steel after losses due to anchorage and elastic shortening have taken place. As the formwork is removed, the beam carries its own weight and deflects downward slightly and the stress in the steel increases from B to C. However, when the dead weight of the beam is relatively low, it can deflect upward and the beam may actually begin to carry load when prestress in the steel is at B'. As the beam soffit suddenly breaks loose from its formwork, the weight of the beam is at once transferred to the beam itself and the stress in the steel will increase from B' to C'. The stress at C' is slightly lower than the initial stress, f_o, by virtue of loss of prestress in the steel caused by the upward bending of the beam. If it is assumed that total loss of prestress occurs, the stress in the steel drops from C or C' to D, representing the effective prestress, f_c, for the beam.

When external load is applied to the beam, the beam will deflect downward so that stress in the steel will increase. For a beam with bonded tendons, such increase is linear from D to F, where the section cracks, and that can be completed by the elastic theory,

$$\Delta f_s = n f_c = n\frac{My}{I} \tag{2.7}$$

where y and I correspond to the transformed section and n is the modulus ratio of steel to concrete. When the section cracks, there is a

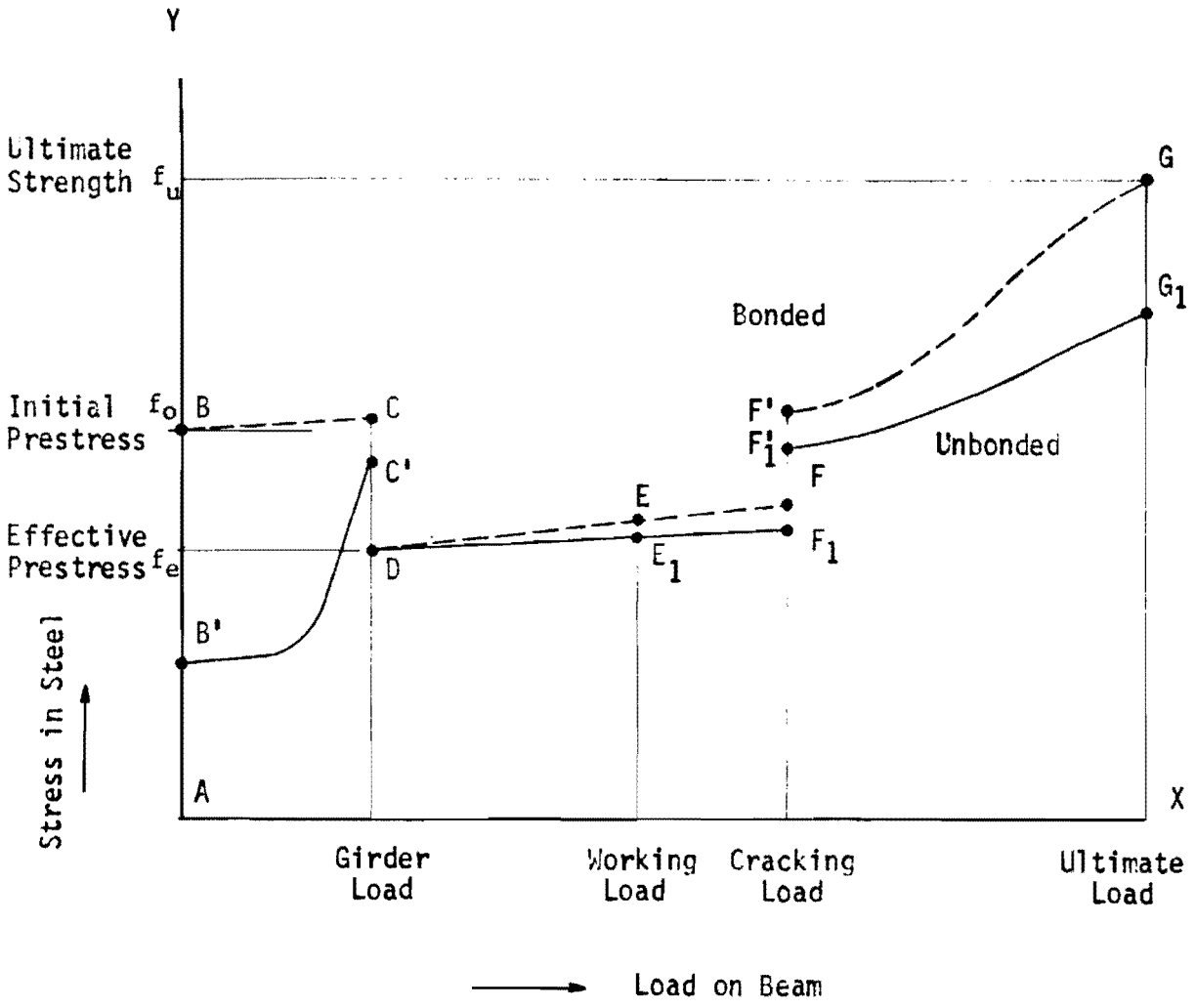

Fig. 2.5 Variation of Steel Stress with Load (19).

sudden increase of stress in the steel from F to F' . After the cracking, the stress in the steel will increase nonlinearly with the load and gradually approach its ultimate strength, G . The computation of steel stress beyond cracking to the ultimate load is a complicated problem for which an approximate solution is available. In this study, the steel stress will be computed from the steel stress-strain relationship and the moment curvature of the beam.

If the beam is unbonded and load is added to the beam, the steel slips with respect to the concrete. The stress in an unbonded tendon will increase more slowly than that in a bonded tendon because strain in an unbonded tendon will be distributed throughout its entire length. The average steel stress can be computed by usual elastic theory:

$$f_s = E_s \frac{\Delta}{L} = \frac{E_s}{L} \quad \frac{My\ dx}{E_c I} = \frac{n}{L} \quad \frac{My\ dx}{I} \tag{2.8}$$

where Δ = beam deflection

$n = E_s/E_c$

= ratio of steel modulus to the concrete modulus.

However, this expression disregards the effect of friction loss along the tendon. If y and I in Eq. 2.8 are constant and M is an integrable function of x , the solution can be found. On the other hand, if the tendon profile is not straight and if the tendon friction is considered, the solution is more difficult.

Pierce (30) derived the expression for determining the change in length as well as the radius of tendon curvature. The effects due to friction are also taken into account, as expressed in Eq. 2.9:

$$\Delta S \left(\frac{2AE}{S} + KT_1 + \frac{\mu T_1}{R} \right) = \Delta T_1 \left(2 - KS + \mu\theta\right) + \frac{\mu T \theta \Delta R}{R} \tag{2.9}$$

where $S, \Delta S$ = tendon length and change in tendon length

$T_1, \Delta T_1$ = tendon force and change in tendon force

$R, \Delta R$ = radius of tendon curvature and its change

θ = angle change of tendon profile

K = wobble friction coefficient

μ = curvature friction coefficient

A = area of prestressing steel

E = modulus of elasticity of prestressing steel.

The numerical analysis method is appropriate for solving this equation. However, the increase of tendon force from D to E_1 and F_1, as shown in Fig. 2.5, is considered to be linear but is not as fast as that in a beam with bonded tendons. When cracks develop in the unbonded beam, stress in the steel increases suddenly from F_1 to F'_1, and, after cracking, the relationship between tendon stress and load becomes nonlinear from F'_1 to G_1. The ultimate stress in unbonded tendons is generally less than that in a corresponding bonded beam.

2.1.5 Moment-Curvature Relationship and Load-Deflection Response

The behavior of a prestressed concrete beam can be represented by a moment-curvature relationship or a load-deflection curve. They are related to each other based on the structural characteristics; for a simple beam they are very similar in shape, as shown in Fig. 2.6.

In general, the curvature of a beam is changed due to its deflected shape, which is caused by externally applied loads, its own weight, and the prestress forces. The resisting moment is developed over the cross section of the beam to balance the loads and this moment varies directly with the strain gradient over the section. It should be noted that the strain can be converted into forces, and products of those forces and the distances to the neutral axis yield the moment, as described in Section 2.11. The curves are linear in the elastic range and become nonlinear after cracking occurs. The area under the load-deflection curve directly represents the toughness of the beam.

There are three stages of load required to represent the behavior of the prestressed concrete beam. The first stage is at transfer, when no external load is applied. The second stage is when cracks have developed and the final stage is at ultimate load, when the beam collapses. Immediately after transfer, most beams will camber upward due to the prestressing forces; both deflection and curvature are considered to be negative at this point and there is no external load or external moment except due to the beam weight.

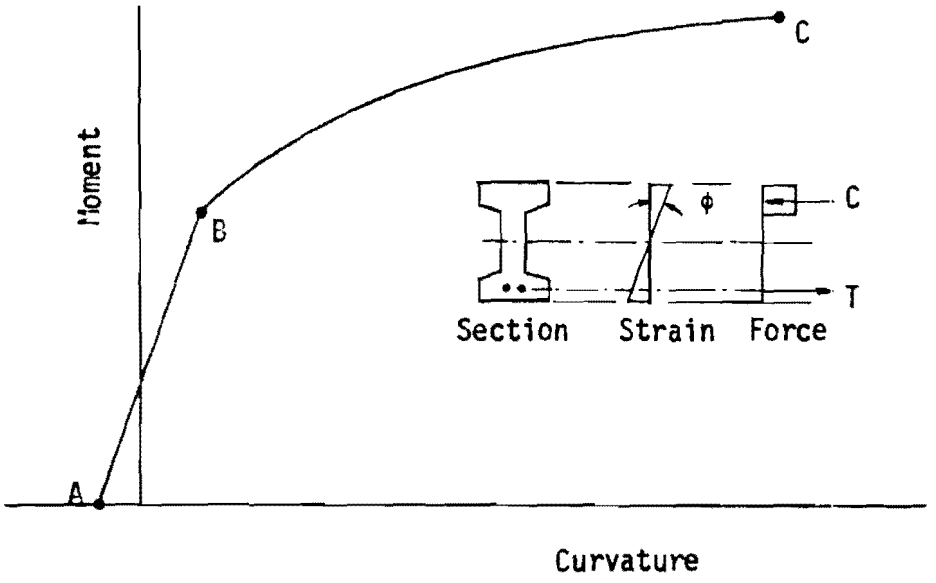

(a) Moment-Curvature Relationship.

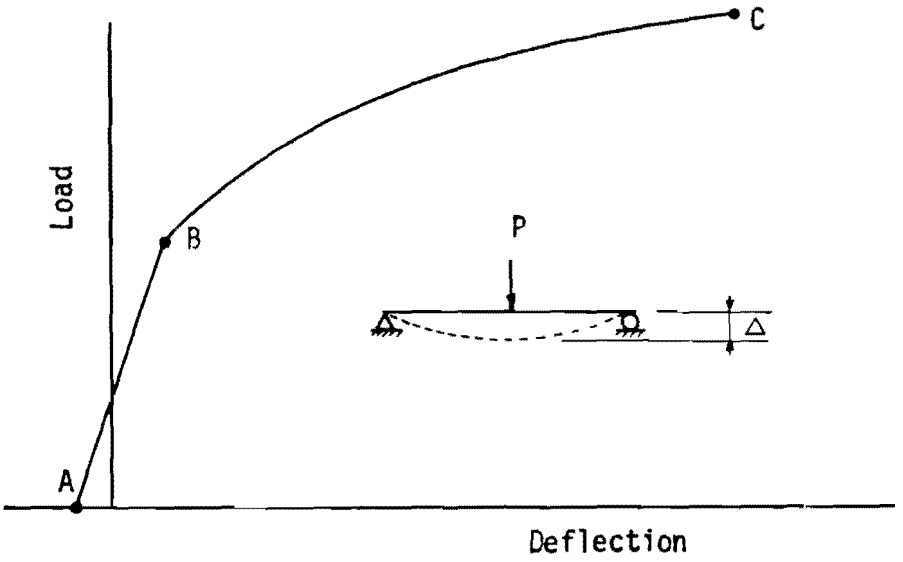

(b) Load-Deflection Curve.

Fig. 2.6 Typical Moment-Curvature Relationship and Load-Deflection Curve of Prestressed Concrete Beam.

The moment producing first cracking in a prestressed concrete beam is computed by the elastic theory, assuming that cracking starts when the tensile stress in the extreme fiber of the concrete reaches its modulus of rupture. It should be indicated that the first microcracking is often invisible to the naked eye but the stiffness of the beam decreases very fast beyond that stage.

At ultimate load, the beams may fail either by tension in prestressing steel or by compression in concrete. However, an exact analysis for the ultimate strength of a prestressed concrete section under flexure is a complicated theoretical problem because both steel and concrete are generally stressed beyond their elastic ranges. The ACI Code (27) assumes the ultimate strength of prestressed concrete beams corresponds to the compressive strain at the extreme fiber of 0.003 in./in. This study will utilize the numerical procedure presented in Section 2.3 to compute ultimate strength.

2.2 Analysis for Shear

The strength of the prestressed concrete beams in resisting shear or the contribution of shear and flexure cannot be predicted with a high degree of accuracy; most prestressed concrete beams have been designed and built on the basis of assumed theories for shear resistance. It is generally believed that prestressed beams, similarly to reinforced ones, practically never fail under direct shear or punching shear. They fail as a result of tensile stresses produced by flexure and shear, known as principal tension in prestressed concrete and as diagonal tension in reinforced concrete. Fracture occurs with excess principal tension. For prestressed concrete beams, prestressing forces the fracture angle to be more vertical than for reinforced concrete beams. In fact, prestressed concrete beams possess greater reliability in shear resistance than reinforced concrete beams, because prestressing will usually prevent the occurrence of shrinkage cracks which could conceivably destroy the shear resistance of the reinforced concrete beams, especially near the point of contraflexure. In general, shear resistance of prestressed concrete beams can be categorized as follows: the shear resistance of the inclined tendons, and the shear resistance of the web reinforcement. Tests on prestressed concrete beams seem to indicate that, when a shear failure occurs at a section, not only the shear but also the bending moment at that section influences the ultimate strength of the beams (31,32). There are essentially two types of shear failures: one, in which the cracking

starts in the web as a result of high principal tension, and the other, in which vertical flexural cracks occur first in the flange and gradually develop into inclined shear cracks in the web. The analysis for each type is presented in the following section.

2.2.1 Principal Tensile Stress

Prestressed concrete beams can fail as a result of principal tensile stresses, with the cracking initiating in the web of the shear span. Before cracking, the beam can be considered to be composed of a homogeneous material; the principal tensile stress can thus be computed by the methods usually used for strength of materials. After the cracking of concrete, whether produced by flexural or principal tension, this method of analysis is no longer applicable because there is evidence to show that the resistance of concrete to such principal tension is not a constant value but varies with the magnitude of the axial compression (33).

Computation of principal tensile stress in a prestressed concrete beam section is based on the elastic theory and on the classical method of determining the state of stress at a point. Figure 2.7b shows a typical stress block at a point of a prestressed concrete beam. The unit shear stress, v, is obtained by

$$v = \frac{VQ}{Ib} \tag{2.10}$$

where V = shearing force carried by concrete

Q = statical moment of the cross-sectional area above (or below) the level at which the stress is sought

I = static moment of inertia of the cross section

b = width of section at that level.

It should be noted that the values of the unit shearing stress, v, and the direct stress, f, vary as shown in Fig. 2.7c.

The maximum principal tensile stress, S_t, corresponding to the above v and f can be computed by the formula

$$S_t = \sqrt{v^2 + \left(\frac{f}{2}\right)^2} - \left(\frac{f}{2}\right) \tag{2.11}$$

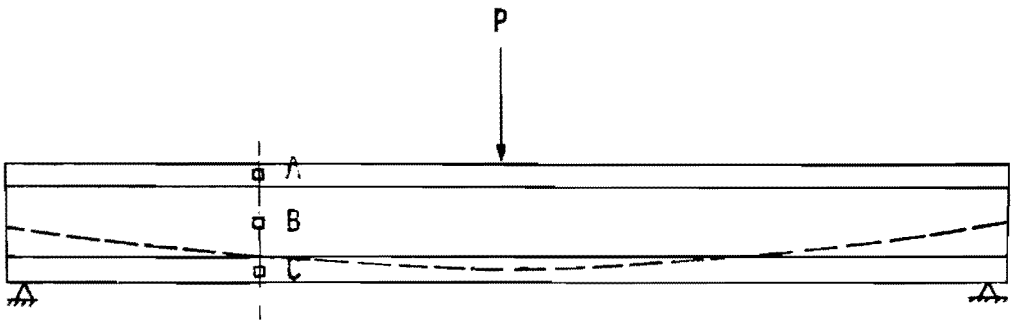

(a) Beam Subjected to Load.

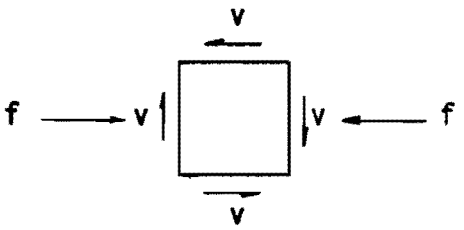

(b) Stress Block.

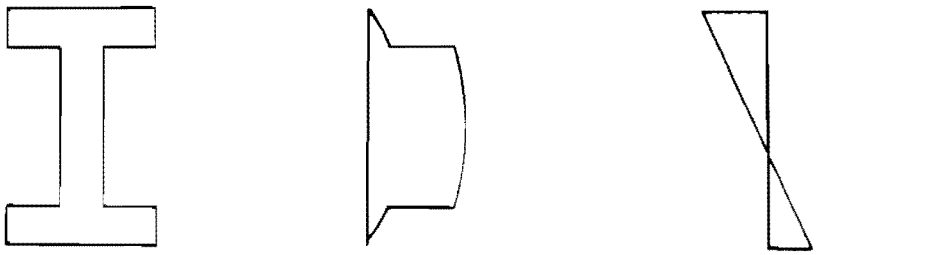

(c) Section and Stress Distributions.

Fig. 2.7 Typical Stress Block at a Point of a prestressed Concrete Beam.

or it can be solved graphically by use of Mohr's circle. If the value or principal tensile stress, S_t, exceeds the concrete tensile stress, shear cracks will initiate at that point. The direction of maximum principal tension is given by the relationship

$$\tan 2\theta = \frac{2v}{f} \tag{2.12}$$

where θ is the angle between S_t and the stress, f, in this case between S_t and the horizontal plane.

2.2.2 Inclined Cracking Shear

Two distinct potential modes of inclined cracking are associated with shear strength of prestressed concrete beams. The inclined crack may develop either as a pure shear crack originating in the web while the adjacent portion of the tension flange is still uncracked or as a flexural shear crack initiated by a flexure crack at some critical sections. The equations for prediction of the inclined cracking shear were presented by Olesen (46) and the ACI Building Code (42).

(a) Pure Shear Cracks: The cracks may originate in an uncracked portion as a result of principal tensile stress in the concrete. These cracks, commonly referred to as diagonal tension web cracks, occur in regions of high shear and low moment. The equation was derived by Olesen (46), based on the theories as presented in Section 2.2.1. It can be written as

$$V_{cs} = \frac{I\, b'}{Q}\, f_t \sqrt{1 + \frac{F_{se}}{A_c f_t}} \tag{2.13}$$

where V_{cs} = shear at pure shear cracking
I = moment of inertia
b' = web thickness
A_c = gross area of cross section
Q = first moment of area below centroid of a section
f_t = tensile strength of concrete determined as the splitting tensile strength
F_{se} = effective prestressing force.

The shear at which the shear crack develops may also be calculated by the ACI Eq. 11.12.

(b) Flexural Shear Cracks: The cracks which initially develop because of flexural stress occurring in regions of moderate flexure and moderate shear may become inclined and produce premature shear failure. The initial flexural crack is usually vertical. As additional load is applied, the vertical cracks progress upward and diagonally due to shear stress in the concrete. The cracks incline toward the load point for simple beams with concentrated loads. The failure occurs when this diagonal crack extends far enough into the top flange to cause destruction of the compression zone. This flexural shear can be predicted by ACI Eq. 11.11 or by the equation developed in Ref. 46:

$$V_{cf} = \frac{M_{cr}}{\frac{M}{V} - \frac{d}{2}} + b'd\sqrt{f'_c} \qquad (2.14)$$

where V_{cf} = shear at flexural shear cracking
M_{cr} = flexural cracking moment
M = moment at a section
V = shear at a section
d = effective depth
b' = web thickness
f'_c = compressive strength of concrete.

The flexural cracking moment, M_{cr}, can be determined by the equation

$$M_{cr} = \frac{I}{y_t}(f_r + f_{pc} - f_d) \qquad (2.15)$$

where f_r = modulus of rupture of concrete
f_{pc} = effective prestress
f_d = stress due to dead load.

Equations 2.13 and 2.14 do not necessarily yield the shear which will result in failure of the member. Tests have shown that some reserve strength

remains after the potential failure cracks form but no reliable estimate of the percentage has been determined (45,46). It should be noted that the smaller of the shears, V_{cs} or V_{cf}, is considered as the shear at inclined cracking for the beams.

2.2.3 Tendon Shear Resistance

The shear in prestressed concrete beams is generally considered to be carried by the concrete or web reinforcement, but, in some cases, the tendon may also assist in carrying shear. If the beam is prestressed with an inclined tendon, then the transverse component of the tendon will carry part of the shear, leaving only a portion to be carried by concrete cross section and web reinforcement.

Total shear carried by tendons can be expressed as follows:

$$V_p = F_{se} \sin \alpha \tag{2.16}$$

where V_p = tendon stress resistance
F_{se} = effective prestress force
α = inclined angle between slope of the tendon to horizontal plane (or axis).

The apparent shearing stress carried by the inclined tendon fundamentally depends on the tendon geometry and its effective prestress force.

2.2.4 Ultimate Shear

After the formation of the inclined cracking, the prestressed concrete beam is still able to carry some increased load but the shear strength cannot be easily predicted because many factors are involved. Tests conducted at the University of Illinois (31,45) have shown that the shear strength of prestressed concrete beams is a function of several variables, such as the section shape, cross-sectional area, strength of concrete, effective prestress, effective depth, shear span, and percentage of steel. The analysis of the ultimate shear may be developed on the basis of the observed failure mechanism. The design procedure was recommended on the basis of experimental work (46), as follows.

For beams failing in shear, the total ultimate shear on a section can be assigned to the concrete, the vertical stirrups, and the draped tendons. The ultimate shear is considered as the sum of the inclined cracking shear, V_{cs}, and the shear carried by vertical stirrups, V_{st}, and the shear carried by draped tendons, V_p. On the other hand, if the beams fail in flexure, the ultimate shear could be taken as the maximum shear corresponding to the loading which produces a flexural failure.

In this study all variables will be held constant except for prestress forces and web reinforcement. The prediction of ultimate shear will be discussed, based on test results for post-tensioned PIC beams tested in this study.

2.2.5 Web Reinforcement

The behavior of concrete before cracking is practically independent of the amount of web reinforcement, although the web reinforcement will play an important role after cracking. Web reinforcement is provided to limit cracking to minimize the distortion of adjacent sections, which may cause failure. The principal tension or inclined flexural cracking shear in concrete is computed as described in Section 2.22. Then when the concrete cracks, the tensile force is transferred to the stirrups. Shear is carried by both the stirrups and the concrete, as shown in Fig. 2.8.

The design for combined moment and shear can be based on the ultimate strength behavior, as shown in Fig. 2.8. The web stirrups, each supplying a force of $A_v f'_v$, will be called into action as the crack progresses. At the ultimate load, the inclined crack will likely extend over a projected distance of at least d, and the number of stirrups intercepted by the crack will be d/s. Thus, static equilibrium requires that

$$V_{st} = A_v f'_v \, d/s \tag{2.17}$$

where V_{st} = shear carried by vertical stirrups
A_v = area of each stirrup
f'_v = yield strength of the stirrups
d = effective depth of the section
s = spacing of stirrups.

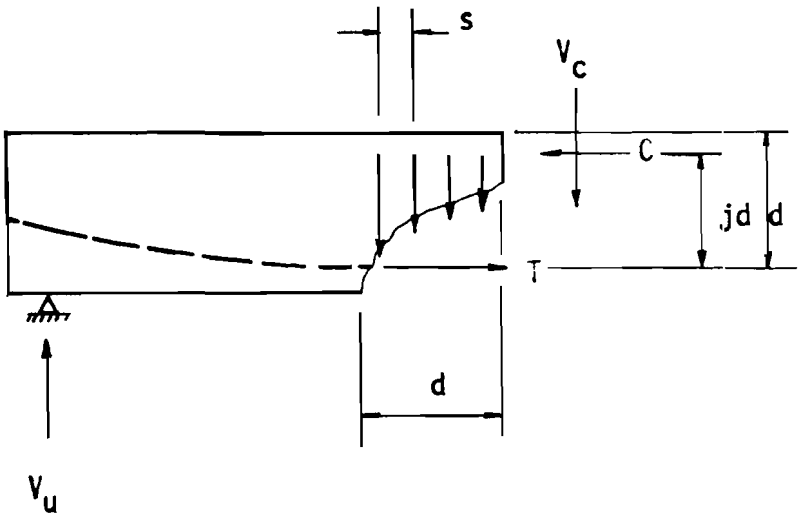

Fig. 2.8 Ultimate Design for Flexural Shear .

An empirical method for stirrup design was introduced by the 1963 ACI Code, based on the results of tests at the University of Illinois (32). For general cases, shear assigned to the web reinforcement, V_{st}, can be written as

$$V_{st} = V_u - V_c \tag{2.18}$$

where V_u = ultimate external shear, excluding the effect of prestress
V_c = inclined cracking shear; the smaller of web-shear cracking force or flexural shear cracking force is used.

2.3 Computer Program PICB

A computer program, PICB, has been developed to predict strength and behavior of post-tensioned polymer-impregnated concrete beams. In general, this program is adapted from program "PRESS 1" of Ref. 30 in order to relate the prestressed unbonded tendon problem to polymer-impregnated concrete beams. The primary numerical analysis program employs the basic theory of finite difference known as the discrete element method. The solution is obtained by an iterative procedure. The theoretical approach and the computation technique used in this computer program are similar to those presented in Refs. 30, 35, and 36. The discrete element beam-column model as presented by Matlock and Haliburton (36) has been modified for prestressed concrete beams by Atkins (35) and Pierce (30).

The computer program PICB was adapted to increase the applied load automatically until the final failure occurred. The program can be used for unimpregnated concrete beams, PIC beams, or composite beams made of both concrete and PIC. Stress-strain properties for PIC, unimpregnated concrete, and steel are input by successive points.

The computer program PICB is written in FORTRAN IV language for the CDC 6600 computer. The storage requirements of PICB are 177,000 octal locations. This permits the analysis of a 100-increment beam-column model containing a maximum of 10 unbonded tendons, 10 bonded reinforcing bars, and 10 bonded tendons, with 10 different cross sections to be solved. The general flowchart is presented in Fig. 2.9.

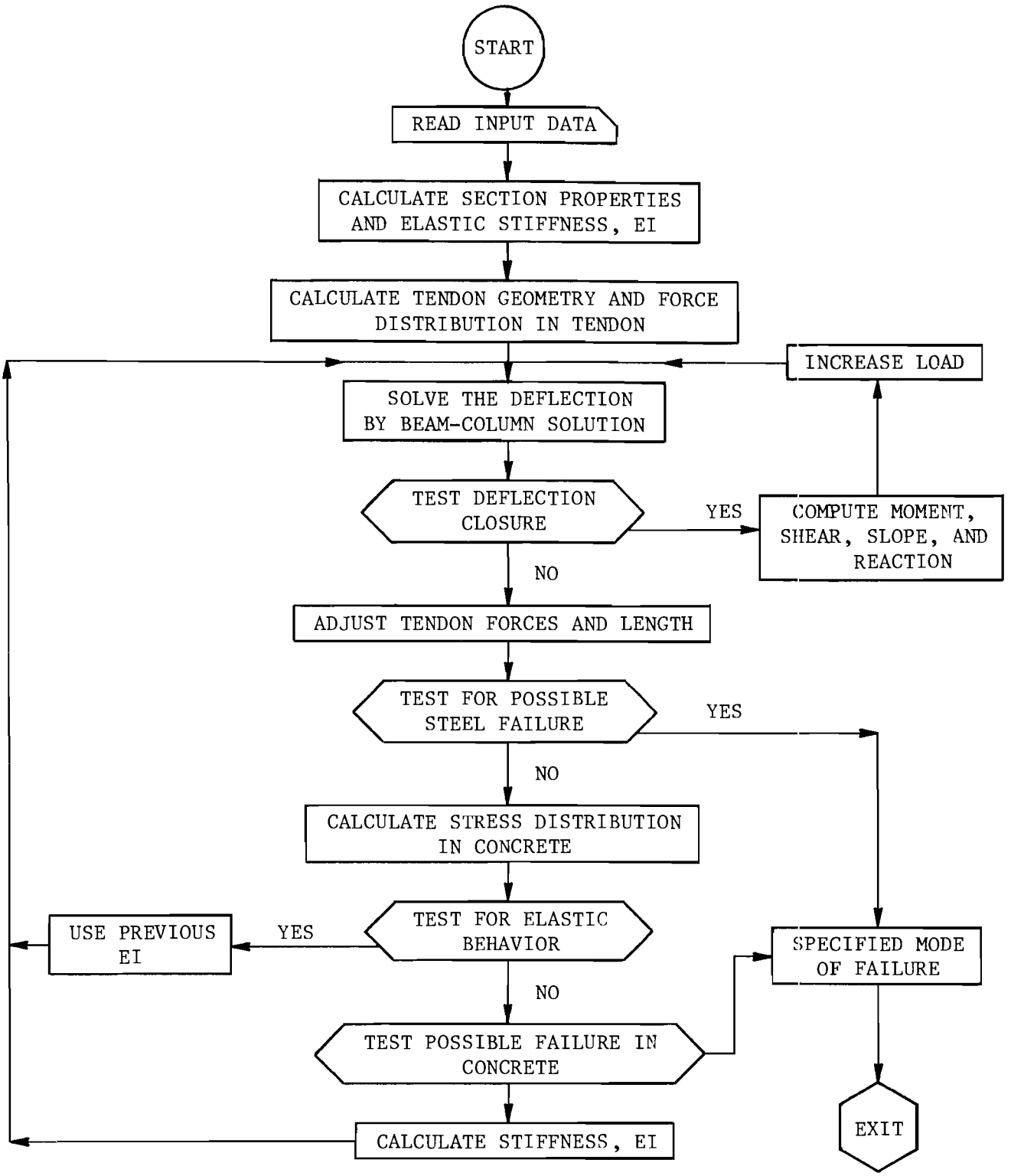

Fig. 2.9 General Flow Diagram.

The primary iteration loop consists of calculating deflections from the recursive solution, using the deflection values to find revised tensions in the unbonded tendons, and, finally, applying the deflections and tensions to calculate the new flexural stiffness. The new stiffness values are returned to the recursive solution and the cycle is continued until a satisfactory solution is obtained.

The input data are read into the computer first and then the computation effort proceeds. The input information includes control data, beam cross section and span, stress-strain relationship of concrete and steel, tendon geometry, bonded reinforcing prestressing history, applied loads, beam restraints, and support information. The first major computation concerns the evaluation of the section properties for each different cross section along the length of the beam column. If the total cross section area, the moment of inertia, and the geometric centroid of the cross section are known, the flexural elastic stiffness (EI) for each particular cross section can be established by multiplying the moment of inertia and the concrete modulus of elasticity. The next calculation package has to consider the unbonded tendons related to the profile locations and forces at individual increments. The primary prestressing moment at each discrete station can be evaluated by multiplying the prestressing force and the eccentricity from the geometric centroid.

Two quantities, the elastic flexural stiffness and the primary prestressing moments, in addition to the known loads and restraints, are necessary input requirements for the recursive technique mentioned in Section 2.3.2. The primary iteration loop is continued until an acceptable solution is obtained or 100 cycles per iteration are exhausted. The solution scheme usually closes in a few cycles for reasonable values of specified deflection tolerance. When the iterative deflections are satisfied, the computation of moments, shears, slopes and reactions will be completed and the values will be printed out. The external applied load can be increased for another solution, as specified in the control card. However, if the test for deflection fails, the lengths of the tendon and its tension force must be adjusted by the method described in Section 2.1.4. The new flexural stiffness will also be recalculated, as indicated in Section 2.3.4, and the new iteration of deflection calculation will be made until the deflections are satisfied.

The tests for possible failure in concrete or steel are checked in each iteration. The program will be terminated whenever the failure occurs.

The program output consists of five tables of computed results. The first output table represents the deflections, slopes, moments, shears, and support reactions at each discrete station. The station number and the distance along the beam from the left end of the member are labeled. The second table represents information pertaining primarily to the unbonded tendons. The initial and final tendon stresses as well as the tendon profile at each discrete station are represented. The primary prestressing moments as calculated prior to entering the primary iteration loop and the beam stiffness are also printed in the second table. The last three tables show the section properties, the record of failure, and the extreme fiber strain at each discrete station.

CHAPTER III. MATERIAL PROPERTIES AND PREPARATION OF TEST SPECIMENS.

3.1 Materials

3.1.1 Concrete and Polymer-Impregnated Concrete

Concrete used in this test program contained Colorado River sand and coarse aggregate graded to 3/8 in. maximum size, and type III cement. The mix consisted of 6 sacks per cubic yard of cement and 7 gallons per sack, water-cement ratio.

Design strength and slump were 4000 psi and 4 in., respectively. Eight test cylinders, 6 x 12-in., from each batch were used to measure the compressive and splitting tensile strength of the concrete at 28 days of age. The first batch was for control beams, shear beams, and partially impregnated beams. The second batch was for both bonded and unbonded beams in flexural series and for time-dependent beams.

In addition, 3 x 6-in. cylinders were prepared for impregnation with the same monomer systems and impregnation techniques as used for the beams. The compressive and splitting tensile strengths as well as the moduli of elasticity for these PIC cylinders were evaluated.

Table 3.1 shows the average strength and tangent modulus of elasticity for PIC and unimpregnated concrete cylinders. The mix design and strength of each individual batch are summarized in Appendices B and C, respectively.

3.1.2 Monomer System

The liquid monomers, methyl methacrylate (MMA) and butyl acrylate (BA), were selected for this test program on the basis of the structural properties of the resultant polymer-impregnated concrete. Most beams were impregnated with 100% MMA but two of these were impregnated with 75% MMA + 25% BA and 50% MMA + 50% BA, respectively.

Table 3.1

Modulus and Strengths of Polymer-Impregnated Concrete

and Unimpregnated Controls

Specimen Number	Batch Number	Monomer System	Avg. Polymer Loading(%wt)	Type of Test	Modulus of Elasticity(psi)	Ultimate Strength(psi)
PBF-2,PBF-4,PBF-6 PBF-8,PBT-4,PBT-8 PBB-4C,PBB-4P	2	100%MMA	6.07	Comp	6.50×10^6	15,100
			6.18	Tens	-	1,520
PBP-2,PBP-4, PBS-4S,PBS-6C, PBS-6S,PBS-8S	1	100%MMA	4.78	Comp	6.32×10^6	13,100
			4.97	Tens	-	1,280
PBM-75	1	75%MMA+25%BA	5.15	Comp	5.95×10^6	12,300
			5.12	Tens	-	1,200
PBM-50	1	50%MMA+50%BA	5.00	Comp	5.41×10^6	11,200
			5.05	Tens	-	1,100
PBC-2S,PBC-2C	1	Control	-	Comp	3.63×10^6	5,400
			-	Tens	-	506
PBC-2	2	Control	-	Comp	3.74×10^6	5,580
			-	Tens	-	512

Trimethylolpropane trimethacrylate (TMPTMA) was used as the cross-linking agent, and it was mixed by the proportion of 5% (wt) of the monomer. In addition, 0.5% (wt) of 2,2'-azobis isobutyronitrile (AIBN) was added to the monomer as the initiator in order to produce polymerization. The three components had been premixed before being introduced into the soaking chamber. The monomer solution was drained after soaking and stored in a 55-gallon drum at a temperature of 40^{o}F. It was recycled for about 2 weeks after mixing.

Thermal-catalytic polymerization methods were employed in this impregnation process, using hot water.

3.1.3 Prestressing Steel

Prestressing tendons for this study consisted of high strength 1/4-in.-diameter wires which conform to ASTM specification A-421-74 Grade 240. A typical stress-strain curve for this stress-relieved wire as tested by the manufacturer is shown in Fig. 3.1. The tendon yield strength was 219.8 ksi while its breaking strength was 250.6 ksi. The modulus of elasticity was 28.9×10^{6} psi.

The tendons were cut to the specified length and mechanical anchorages were provided at both ends utilizing the button head anchorage at the end of the wire typical of the Prescon system. They were coated with mastic and wrapped with waterproof paper to prevent concrete bonding, to reduce friction, and to protect the tendons during shipment or placing of the concrete.

3.1.4 Reinforcing Steel

Reinforcing steel was used for the supplementary longitudinal bonded reinforcement and for the vertical stirrups. The longitudinal bars were ASTM Grade 60 while the stirrups were ASTM Grade 40 and both grades satisfied ASTM-A 615-71. Typical stress-strain curves for these materials are shown in Fig. 3.2. The grade 40 bars have a yield strength of 48.69 ksi and an ultimate strength of 59.08 ksi. The yield strength of the grade 60 bars was 65.20 ksi while their ultimate strength was 87.43 ksi. However, both the 40 and the 60 bars had the same modulus of elasticity, 29×10^{6} psi.

It should be noted that only No. 2 undeformed bars were used for these beam tests. The supplementary longitudinal reinforcing bars were straight; no hooks or mechanical anchorages were provided. Otherwise, the web

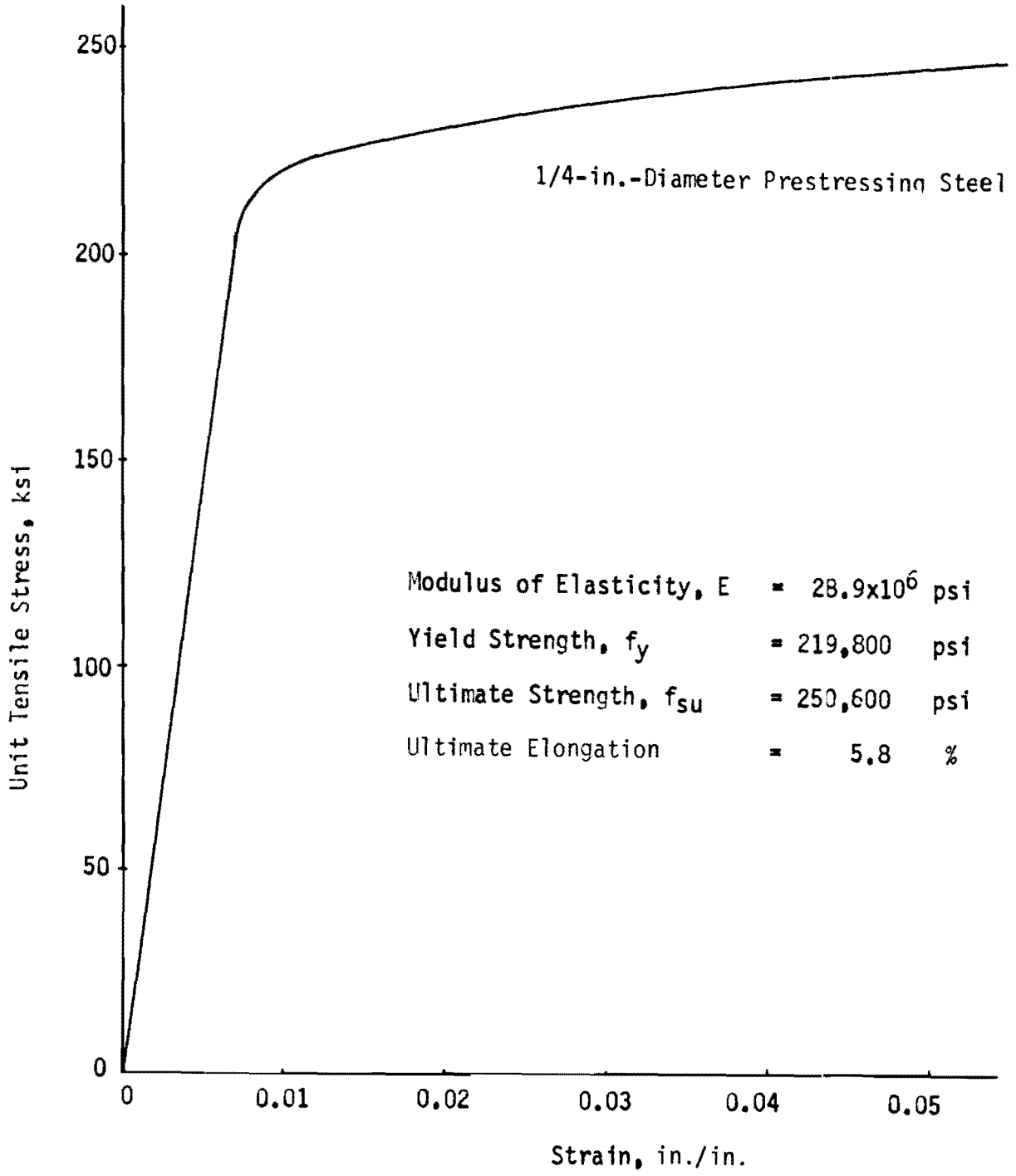

Fig. 3.1 Stress-Strain Curve for Prestressing Steel.

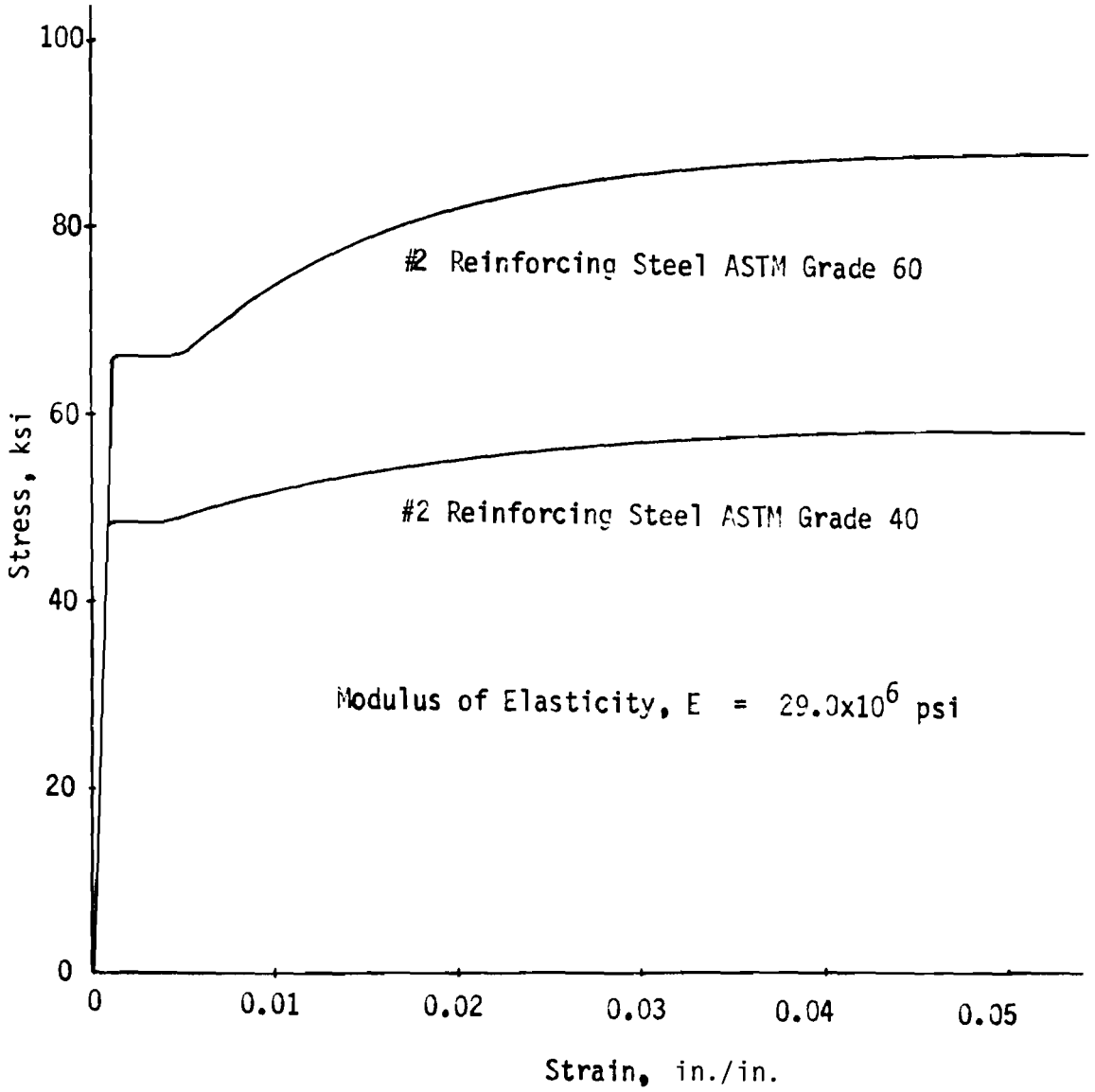

Fig. 3.2 Stress-Strain Curves of Reinforcing Steel.

reinforcing stirrups were C-shaped and tied to the longitudinal steel vertically, as shown in Fig. 3.3. The tendons were then tied to the stirrups to satisfy the required profile.

Two reinforcing steel bars were provided in the bottom flange, located 1-1/2 in. from the beam soffit, and one bar was provided in the center of the top flange, located 1 in. from the top fiber. The amount of bonded reinforcing steel was designed to resist the temperature-induced stresses during drying and impact stresses in lifting or moving. The design also complied with the ACI Building Code 318-71 Sect. 18.9.

3.2 Fabrication of Test Specimens

3.2.1 Description of Test Beams

All test beams were symmetrical I-sections, as shown in Fig. 3.3. Two sizes were used, 4 in. x 8 in. for most of the test specimens and 5 in. x 8 in. for two beams which contained bonded tendons. The total length of the beams was 8 ft., with the span length 7.5 ft. Typical web and flange thicknesses were 2 in. except for the two bonded tendon beams, which had flange thicknesses of 2 in. and web thicknesses of 3 in. Both ends of the beams were solid for a distance of approximately 9 in. to provide adequate bearing area and to cover the tendons. Bearing plates were slightly inclined to the vertical plane of the cross section so that the post-tensioning force was perpendicular to the bearing plate at each end of the beam.

The centroid of the draped, grouped tendons was 4 in. from the top fiber at both ends and 6.5 in. from the top fiber at midspan. Straight bonded reinforcing steel bars were provided as shown in Fig. 3.3, two at the bottom flange, 6.5 in. from top fiber, and one at the top flange, 1 in. from the top fiber.

3.2.2 Forms

Nine to ten beams were cast at one time in forms made of plywood and 2 x 4-in. lumber. Figure 3.4a shows the cross section of the assembled forms, and Fig. 3.4b shows a longitudinal section. Side panels consisted of 3/4-in. and 1/2-in. plywood nailed and glued together. End bearing plates of the beams were attached to the forms by two 3/8-in. bolts on each end. The forms

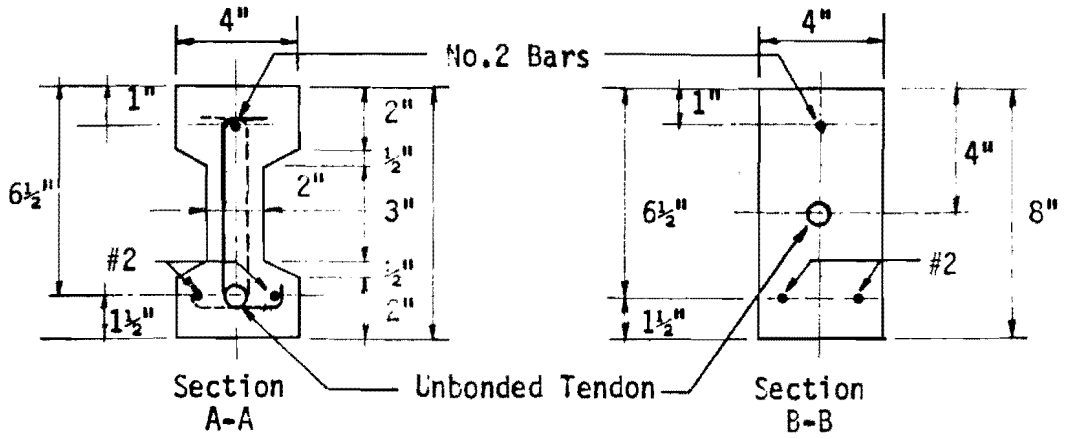

(a) Typical Cross Section of Beams with Unbonded Tendons.

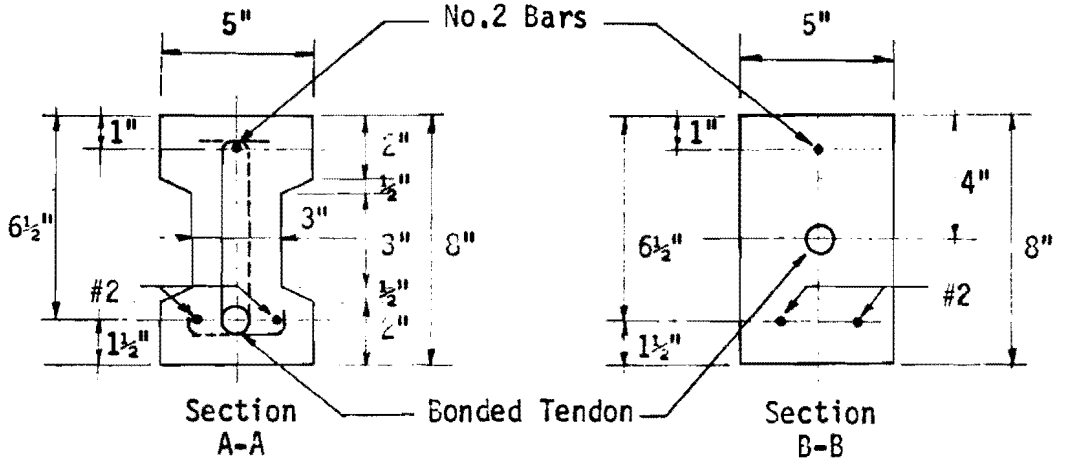

(b) Typical Cross Section of Beams with Bonded Tendons.

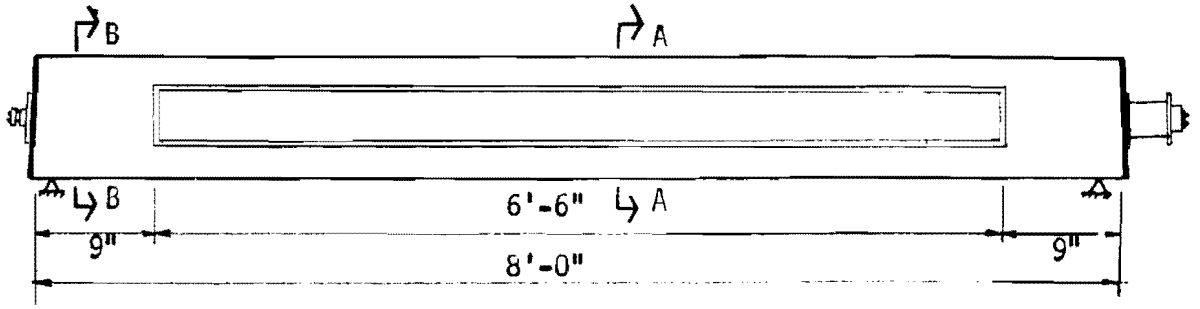

(c) Beam Elevation.

Fig.3.3 Description of Test Beams.

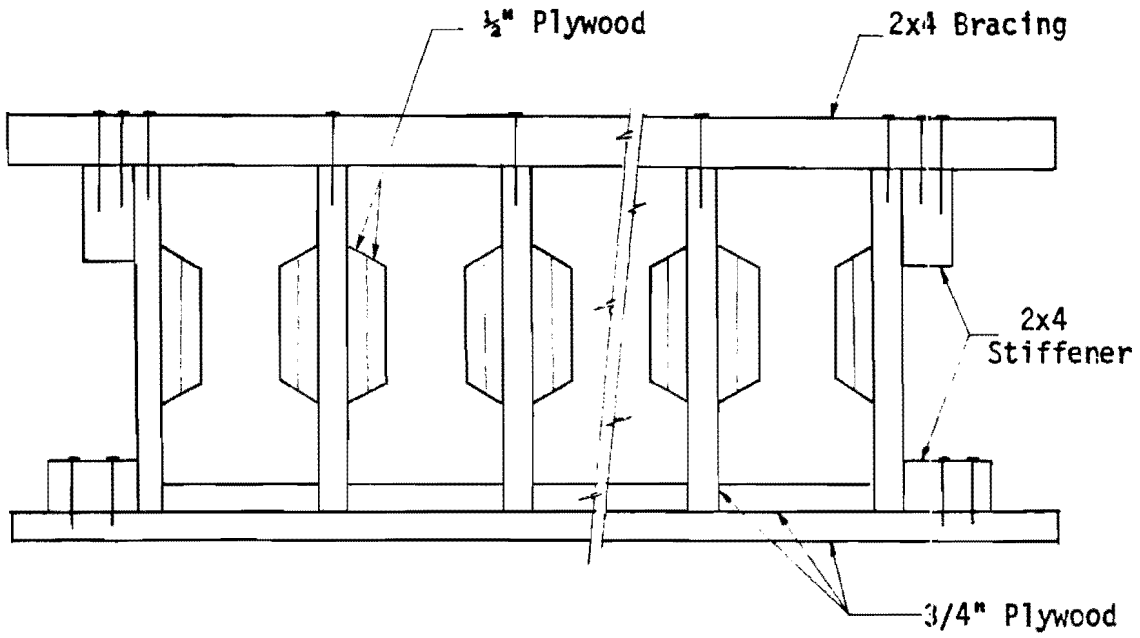

(a) Transverse Cross Section of Formwork.

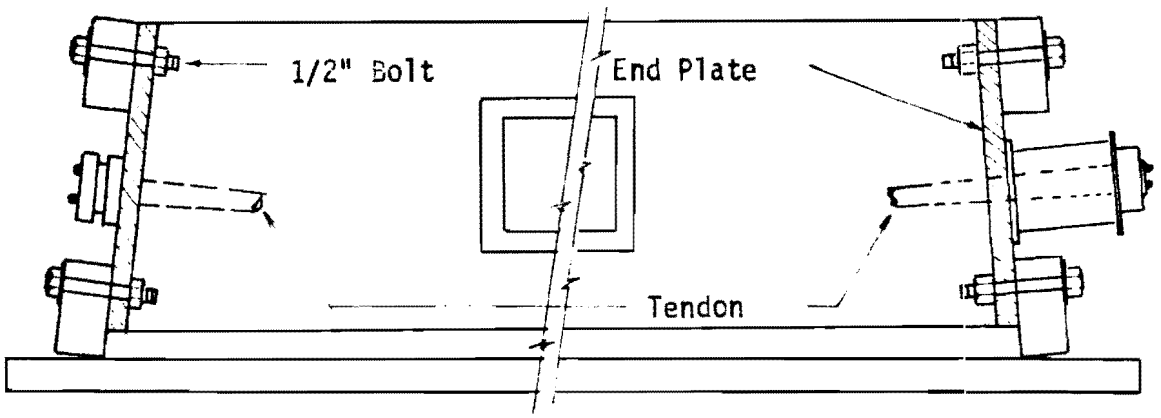

(b) Longitudinal Cross Section of Formwork.

Fig. 3.4 Details of Formwork.

were braced horizontally at two points between the ends to control the width.

Forms were sealed with two coats of lacquer, and joints were filled with caulking compound for watertightness. The forms were also oiled thoroughly on the inside faces before the tendons and reinforcing bars were placed.

3.2.3 Placing of Tendons and Reinforcing Steel Bars

Tendons were cut and the mechanical anchorages were assembled to both ends by the manufacturer. The additional No. 2 bars and stirrups were tied together before being placed into the forms. Strain gages were attached to each longitudinal reinforcing bar.

Bar chairs were placed at about 24-in. spacings and nailed securely to the forms. The tendon profiles were measured from the bottom of the forms and the tendons were wired to the stirrups to prevent movement during concrete placement.

3.2.4 Casting and Curing

Concrete was mixed and placed in the laboratory. The concrete was transported from the mixer to the forms in a wheelbarrow, placed into the forms with shovels, and vibrated with a high frequency vibrator. The top surfaces of the beams were given a trowel finish. The entire operation of mixing, placing, and finishing required about 2 hours for one pour of 9 to 10 beams.

When the concrete started to set, the beams were covered with wet burlap and polyethylene membrane to minimize the loss of moisture from the concrete. The burlap was kept moist for seven days. On the eighth day, the forms were removed and the beams were allowed to air cure at room temperature. Drying at elevated temperature for the impregnation process was not begun until the beams were at least 28 days old.

3.3 Impregnation Techniques

In general, polymer impregnation techniques for fully impregnated specimens require several steps: drying, evacuating the air, monomer application, pressurizing, removal from monomer, and curing. Since the beams were larger than any members impregnated thus far at The University of Texas,

special impregnation chambers and apparatus were designed for the tests. Thermal-catalytic polymerization was employed in this program.

3.3.1 Drying

Normally the water comprises only a small percentage of the total weight of concrete since the pore volume of the concrete is generally in the range of 10 to 15 percent. The water in the concrete is from the free water remaining during the hydration cycle, absorption of moisture during curing, or exposure to the environment. The amount of monomer that can be imbibed by a concrete specimen is limited by the amount of free water occupying the total void space.

To dry the water out of the concrete voids, test specimens were put in a rectangular box enclosure and dried by two infrared heaters. The enclosure sides and bottom were made of 2-in. fiberglas insulation covered with heavy duty aluminum foil. The enclosure was 15 in. wide, 18 in. high, and 9 ft. long; two beams and several 3 x 6-in. cylinders were dried at a time. The heaters were placed over the top surface of the beam as shown in Fig. 3.5, and the temperature inside the enclosure was controlled by moving the heater up and down. Thermocouples were attached to the top surface of the flange and to the soffits of the beam. The air temperature was also measured. A piece of sheet metal was placed over the concrete surface as shown in Fig. 3.5 to deflect the direct infrared rays to prevent overheating the top of the beam. Temperature readings were periodically taken and air temperature inside the enclosure was maintained in the range of 210 to 275°F (100-135°C). The surface temperatures of the beam were slightly lower than air temperature, and the temperatures of the upper beam surfaces were higher than those of the bottom surfaces.

The weights of the specimens were measured daily, and a drying time of about 120 hours was required to reach the equilibrium weight. The average total loss of weight during drying process was 2.12 percent for the first concrete batch and was 3.22 percent for the second batch. Figure 3.6 shows shows the typical weight loss of beams made from the second batch. The percent weight loss was calculated as

$$\% \text{ weight loss} = \frac{(\text{initial weight} - \text{dry weight}) \times 100}{\text{dry weight}}$$

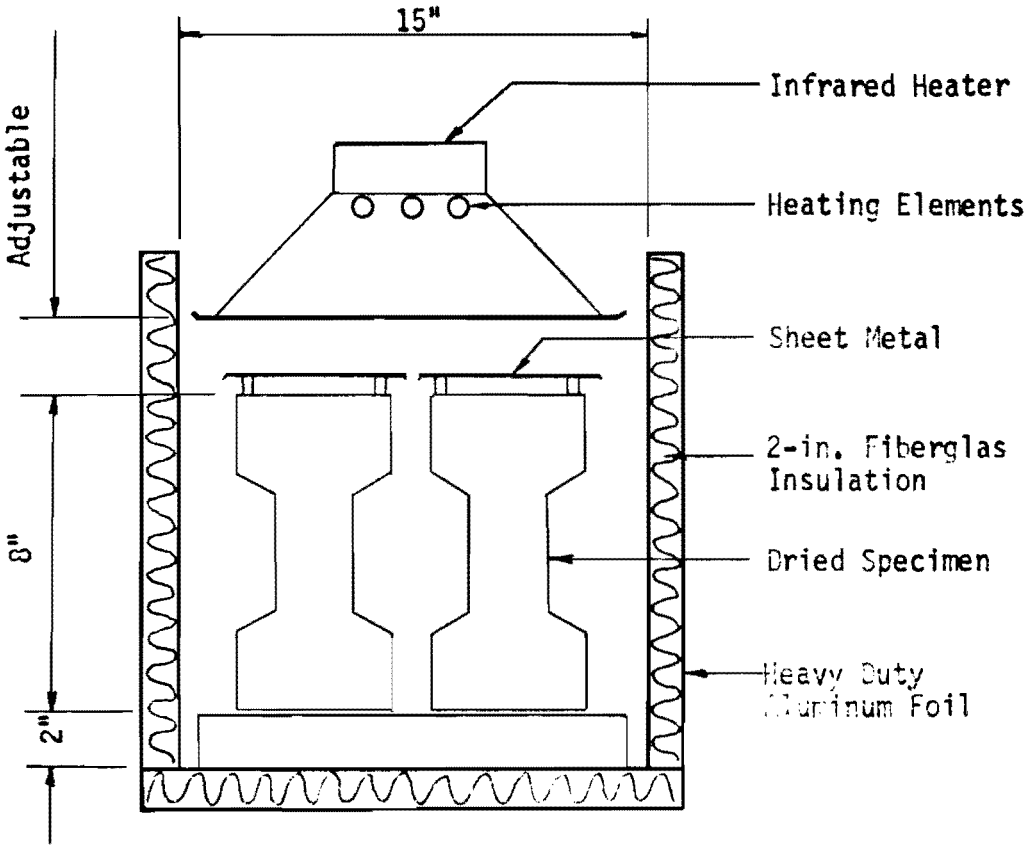

Fig. 3.5 Drying Enclosure and Infrared Heater.

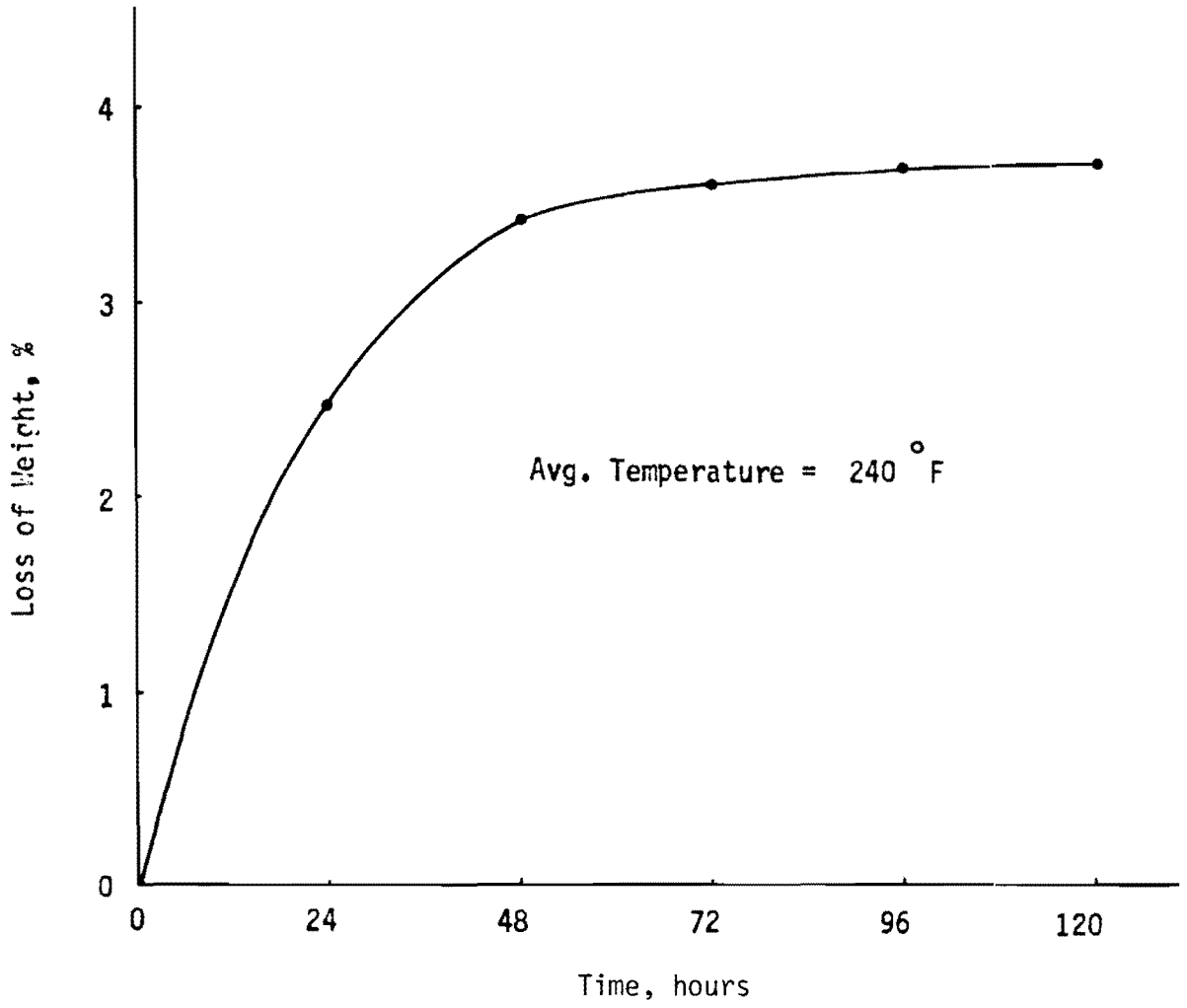

Fig. 3.6 Typical Weight Loss of the Specimen During Drying Process.

3.3.2 Evacuation

To obtain maximum monomer loading in the shortest time, evacuation of the air from the specimen prior to monomer soaking is required. The beam specimens were placed in an impregnation chamber, as shown in Fig. 3.7. The chamber was designed for evacuating, soaking, and pressurizing. The chamber was 9 in. high, 6.5 in. wide, and 10.0 ft long. The cover plate was bolted to the chamber with 3/8-in.-diameter high strength bolts at 3-in. spacings. A rubber gasket was used to seal the cover plate and the chamber. A two-way pressure gage was attached to the cover plate for monitoring pressure and vacuum. Similarly, three flexible hose fittings with valves were attached to the chamber for evacuation of air, application of monomer, and pressurizing with nitrogen gas.

For evacuation, a vacuum pump and its accessories were connected to the chamber, as shown in Fig. 3.8. The dried beam was placed in the chamber and the cover plate was bolted very tightly onto it. A check for leaking along the gasket was made before the vacuum pump was turned on. The evacuation pressure was maintained at 30 in. of Hg for 18 hours before soaking began. It should be noted that it took about 20 minutes to build up the required evacuation pressure.

3.3.3 Soaking

The monomer which had been pre-mixed and stored at 40^{o}F was injected into the chamber by flexible hose, as shown in Fig. 3.9. The flow rate was controlled by a valve so that the monomer level was maintained at about 1/4 to 1/2 in. above the top of the beam.

Total soaking time was 4 hours and pressure was applied during this period. After the soaking, the monomer was drained and restored in the cool room. It was recycled during a 2-week period.

3.3.4 Pressurizing

In an attempt to reduce the time for monomer soaking in a concrete specimen, pressure was applied as the last step in the procedure. After the concrete specimen was soaked with monomer for about 30 minutes, a pressure of 50 psi was applied and maintained in the chamber for 3 hours. Nitrogen was used to supply the pressure. Figure 3.8 shows the pressurizing system.

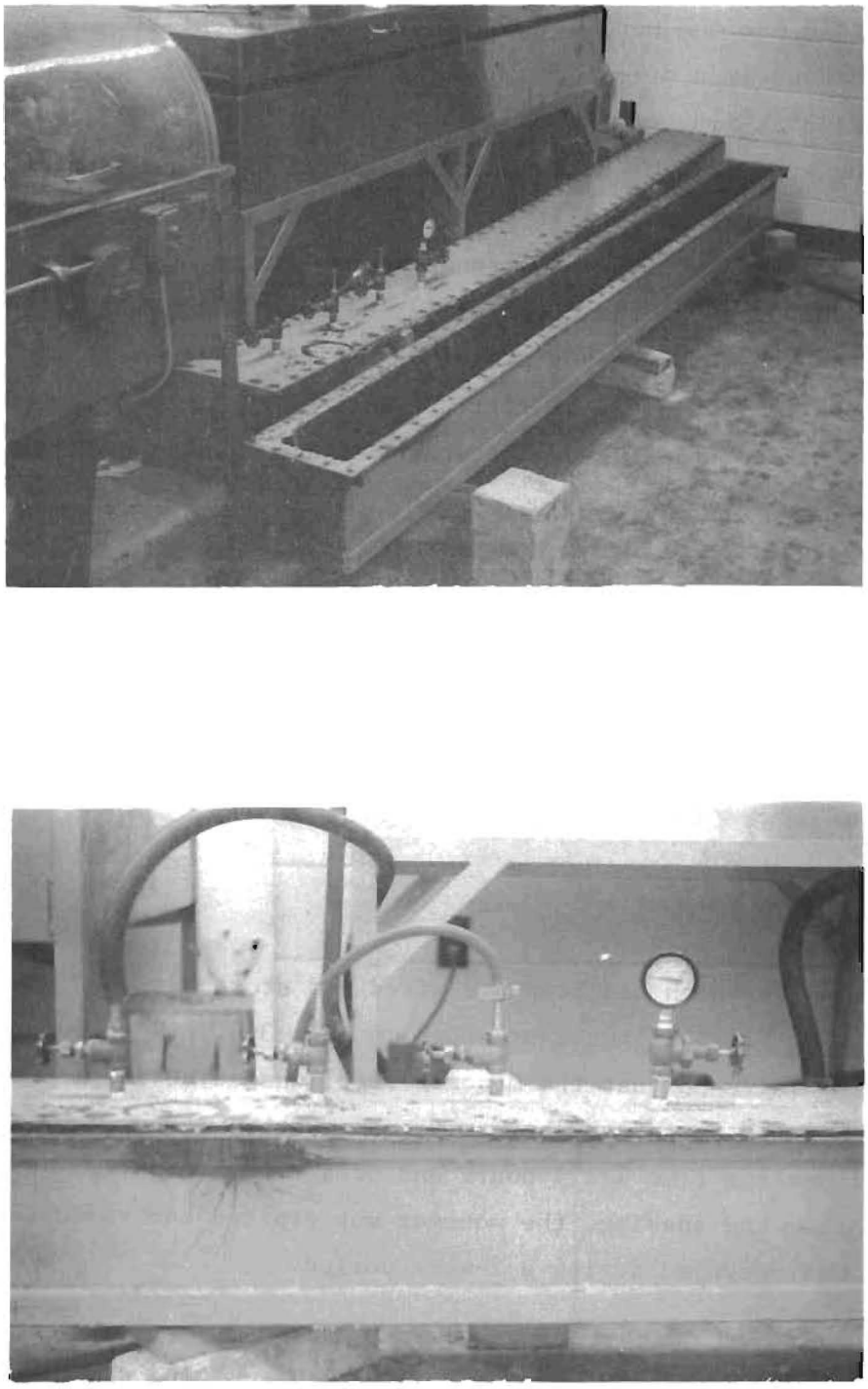

Fig. 3.7 Impregnation Chamber.

Fig. 3.8 Pressurizing System.

Fig. 3.9 Soaking Apparatus.

After the pressurizing, the pressure was released and the chamber was opened. The specimen was soaked in the chamber for another 30 minutes, and then it was moved to the curing vessel in preparation for the thermal-catalytic polymerization.

3.3.5 Curing

Hot water was used to provide the temperature required for the curing process. Water was preheated in a tank, with three gas burners and an electric heater, to a temperature of 176°F (80°C) before the soaking was completed. The beam was placed in the tank of hot water, and a small pump which is a part of the electric heater provided circulation. The water temperature was maintained at 176°F for 4.5 hours to complete the polymerization process. Figure 3.10 is a schematic showing the curing tank, gas burners, and the electric heater. The tank was made of steel plate and was 7 in. wide, 12 in. high, and 10 ft. long.

In the case of the beams containing bonded tendons, the excess monomer in the tendon conduit had to be blown out with air to the grout fittings. A piece of flexible hose was extended from the grout fitting at each end of the conduit; the end of one was connected to an air hose and the end of the other was elevated above water level. Air flowed through the conduit from one end to the other end. The blowing operation was continued throughout the curing process.

For the beams containing unbonded tendons, the excess monomer could not be forced out by the air-blowing operation because the fitting was not provided and the spaces between the tendons and the conduit were small. Some of the excess monomer drained out by gravity through the holes in the steel bearing plate at the beam ends, but some was left. The remaining monomer may have polymerized inside the paper conduit wrapped around the wire tendons.

3.4 Post-Tensioning Procedure

Both bonded and unbonded tendons were used in this study. There were 17 beams with unbonded tendons and only 2 beams contained bonded tendons. However, the prestressing method was essentially the same, except that those with bonded tendons required the additional step of grouting. The post-tensioning procedure and instrumentation will be detailed in this section.

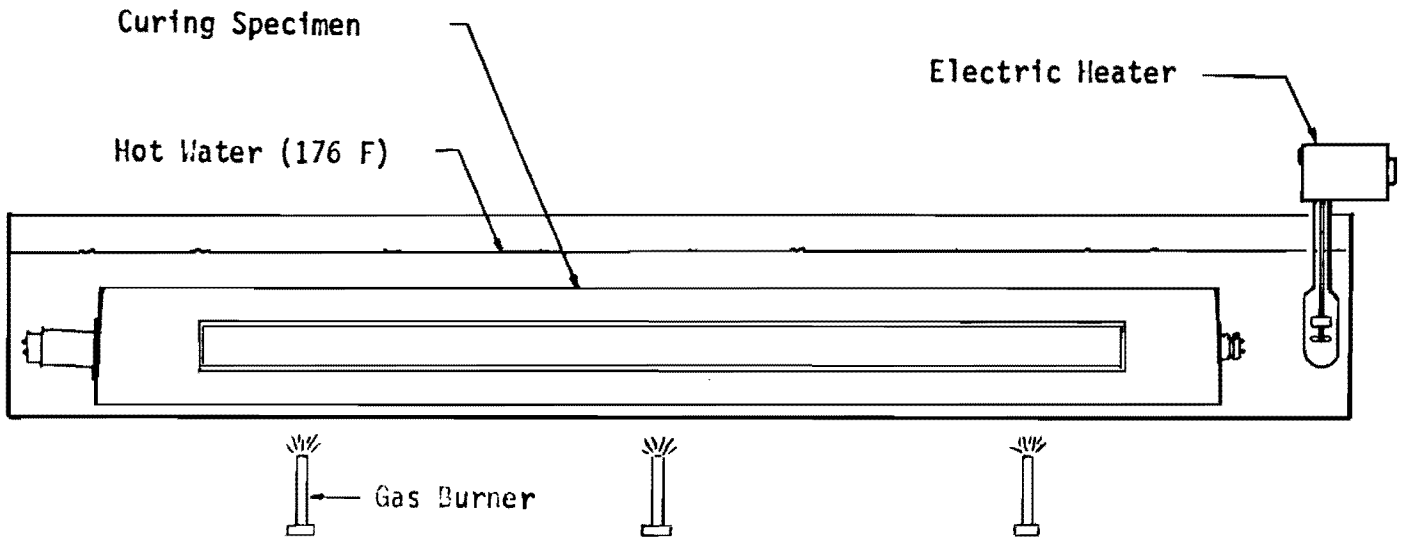

Fig. 3.10 Curing Tank, Gas Burners, and Electric Heater in Polymerization Process.

3.4.1 Stressing Equipment

Hydraulic jack. In post-tensioning, the most common method for stressing the tendon is jacking. A manually operated hydraulic ram and pump unit was connected with a control valve and pressure gauge in a circuit, as shown in Fig. 3.11. The post-tensioning forces were detected by the pressure gauge. The jack capacity was 60 tons but the maximum force for the tensioning was only 60 percent of the capacity.

Pulling rod. The pulling rod was essentially designed to fit the Prescon anchorage system. The rod consisted of a coupling at one end and a large nut at the other end. The hydraulic ram and the jacking chair were placed between the coupling and the nut. For stressing, the coupling was used to grip the tendon anchorage and pull it out with the pulling rod and ram. Two diameters of pulling rods were used, 1-in. and 1-1/2-in. The smaller, with a 2-in. coupling, was used for beams containing 2 or 4 wire tendons, while the larger one, attached to a 4-in. coupling, was used for beams containing 6 or 8 wire tendons. However, both rods were operated with the same hydraulic ram.

Jacking chair. The chair was used in post-tensioning to transfer force from the hydraulic ram to the end bearing plate. The chair had four legs made of steel bars which were welded to a 3/4-in. steel plate. The legs of the jacking chair were placed against the bearing plate of the beam. There was a hole at the center of the plate for a pulling rod to pass through. The legs were arranged to provide sufficient space under the chair so that the coupling could move during tensioning. They were long enough to accommodate the travel of the pulling head until the designed stress in the tendon was reached and shims could be installed. The hydraulic ram was passed over the pulling rod and placed against the jacking chair. The large nut was screwed onto the pulling rod to push the ram and the chair toward the bearing plate prior to stressing.

Figure 3.11 shows the pulling rod, jacking chair, and hydraulic ram assembled together prior to tensioning.

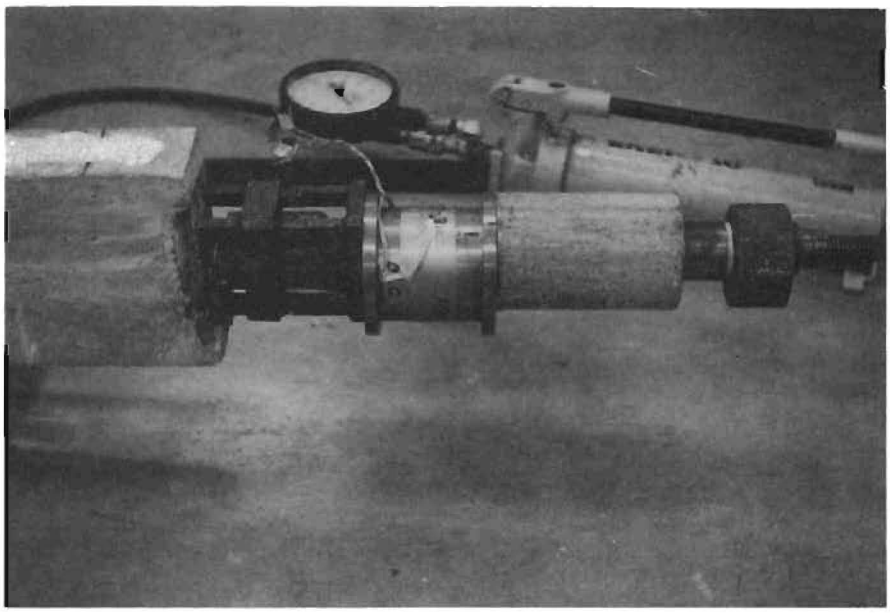

Fig 3.11 Stressing Equipment.

3.4.2 Post-Tensioning Method

A local cell was attached to the anchorage end of the tendons in order to determine the friction loss along the tendons. The jacking end was arranged as shown in Fig. 3.11, the coupling was fitted to the pulling head, the pulling rod was connected to the coupling, the jacking chair was passed through the pulling rod, and the legs of the chair were placed against the bearing plate. The ram, also, passed over the pulling rod and the nut was screwed onto the other end of the pulling rod until all the parts contacted each other.

To stress the beam, the hydraulic jack was pumped gradually; the ram pulled the group tendons by pushing against the jacking chair, which directly transferred the force to the bearing plate. The stressing force was determined by the pressure gage which was connected to the pump. Camber at the midspan of the beam and the force at the anchorage end, which corresponded to the stressing forces, were recorded. The tendons were stressed up to about 70 percent of their specified ultimate tensile strength, and pre-measured steel shims were inserted before the jacking force was released. Finally, the hydraulic ram and the stressing system were removed and the beam was ready for testing.

3.4.3 Grouting

Grout was injected into the tendon conduit to bond the tendons to the concrete after tensioning. The grout also served to protect the steel against corrosion. Corrugated sheet metal tubing was used for the tendon conduit in this investigation. Special pipe connections were welded to both ends of the conduit, and they were extended about 3 in. outside the concrete surface. A gate valve was also connected to each end of the pipe.

Since two types of grouping materials were used in this program, two grouting methods were employed:

Conventional grouting. A mixture of cement and water was injected into the conduit by a grouting pump, as shown in Fig. 3.12. A flexible hose was connected from the pump to one end of the conduit. The gate valve at that end was opened and the valve at the far end remained closed. When the injection started, the valve at the far end was opened to allow air and water in

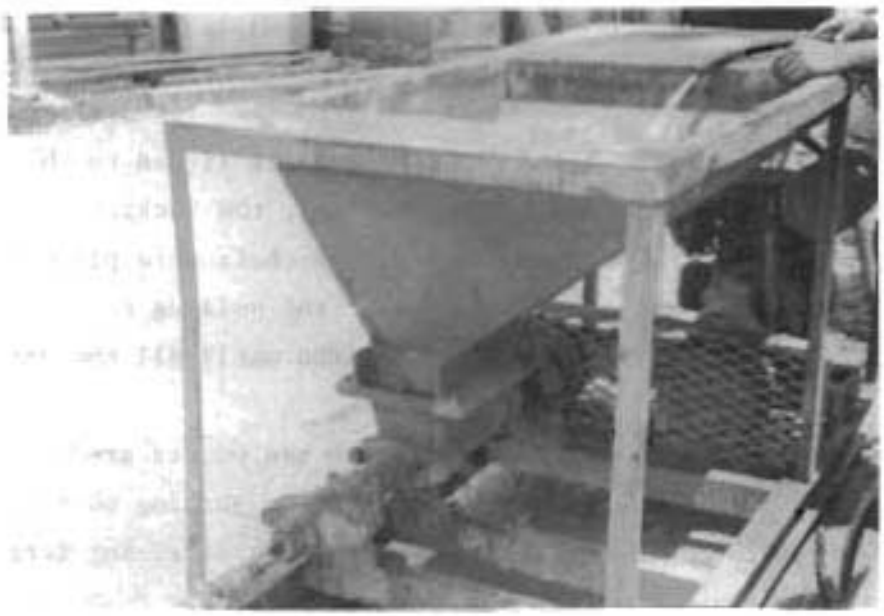

(a) Grouting Pump.

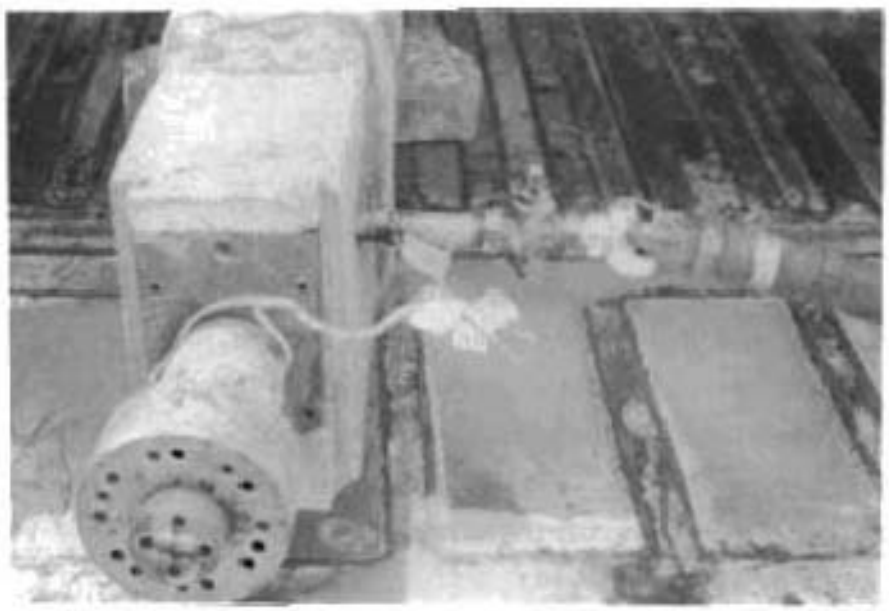

(b) Grouting Hose and Connections.

Fig 3.12 Conventional Grouting System.

the conduit to be forced out. The pressure was applied until the grouting material was forced out at the far end, when the valve at that end was closed. The valve at the inlet end was closed after the grouting materials filled up the conduit.

Polymer grouting. The liquid monomers, methyl methacrylate (MMA) and butyl acrylate (BA), were used for polymer grouting in a proportion of 75 percent (wt) to 25 percent (wt). Lauroyl peroxide (LP), 4 percent (wt) of monomer, was used as the initiator. In addition, N,N,-Dimethyl-para-toluidine (DMPT), 2 percent (wt), was added to the monomer as the promoter in order to increase the polymerization rate.

The mixed monomer was introduced into the conduit by gravity. First, the conduit was cleaned out with air pressure of about 60 psi. A clear plastic hose was connected to each side of the conduit and elevated above the beam, as shown in Fig. 3.13. A funnel was attached to one end of the hose for pouring the liquid monomer. Both valves were opened initially. The monomer was added until the level at each end was about 1 foot higher than the top of the beam and then the valve at the far end was closed. Holes in the end plates through which the tendon passed were sealed with silicon adhesive to prevent leaking. The monomer level was kept constant for about one hour and twenty minutes, until polymerization was completed. Appendix D summarizes the conventional and polymer materials used for grouting.

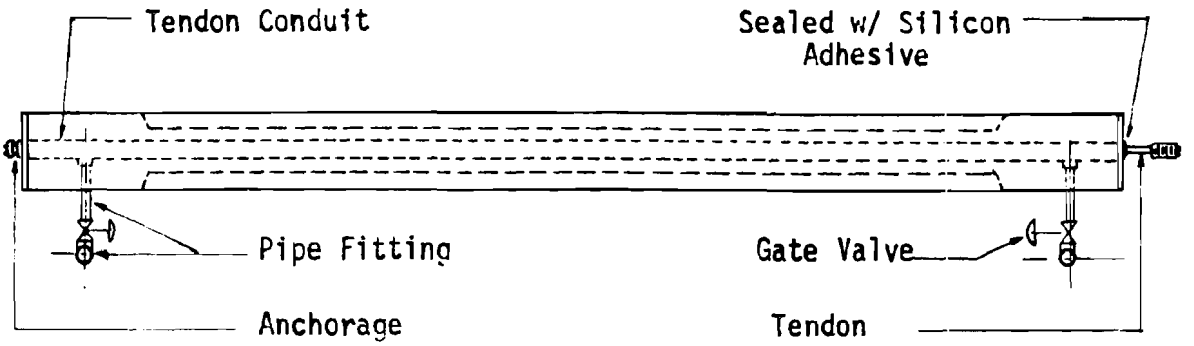

(a) Top View.

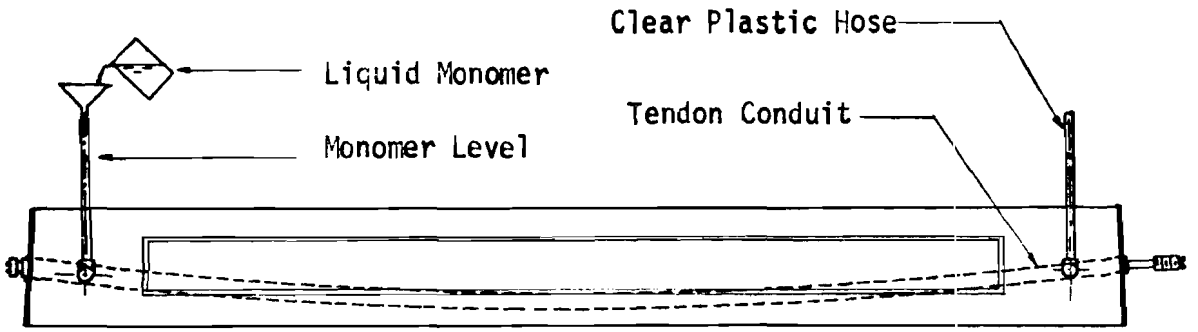

(b) Side View.

Fig. 3.13 Polymer Grouting System.

CHAPTER IV. INSTRUMENTATION AND TEST PROCEDURE.

4.1 Test for Flexural and Shear Strength

Test procedures for both shear and flexural behavior were identical. The beams were placed in the loading frame and then the tendons were tensioned to about 70 percent of their ultimate strength. External loads were applied to the beams within half an hour after stressing was completed. Deflections, strains, and tendon stresses corresponding to each load level were recorded. Cracks were observed and marked.

4.1.1 Loading System

Each test beam was simply supported by a bearing support at one end and a roller support at the other end as shown in Fig. 4.1. The span length was 7 ft., 6 in. while the shear span was 2 ft., 9 in.

The load was applied by a hydraulic ram at midspan to a W 10x25 beam which was simply supported on the prestressed beam. The ram was supported by a steel framing system. Bearing plates were used at the interface between the beam and each loading point to increase the bearing area of the contact surface. The load cell had been used in the loading system to check the applied load with the hydraulic pressure. It was placed underneath the hydraulic ram as shown in Fig. 4.1.

4.1.2 Load Measurement

The external load was applied by a hydraulic ram operated by a hand pump, as shown in Fig. 4.2. The applied loads were primarily measured by a pressure gauge connected to the hydraulic system. The hydraulic pressure was converted into load or force by a calibration curve. The forces from the pressure gage were used in the analysis.

An electric load cell was also placed under the hydraulic ram and the load cell wires were connected to a strain indicator for rechecking the applied loads. Upon completion of the test program, it was found that the

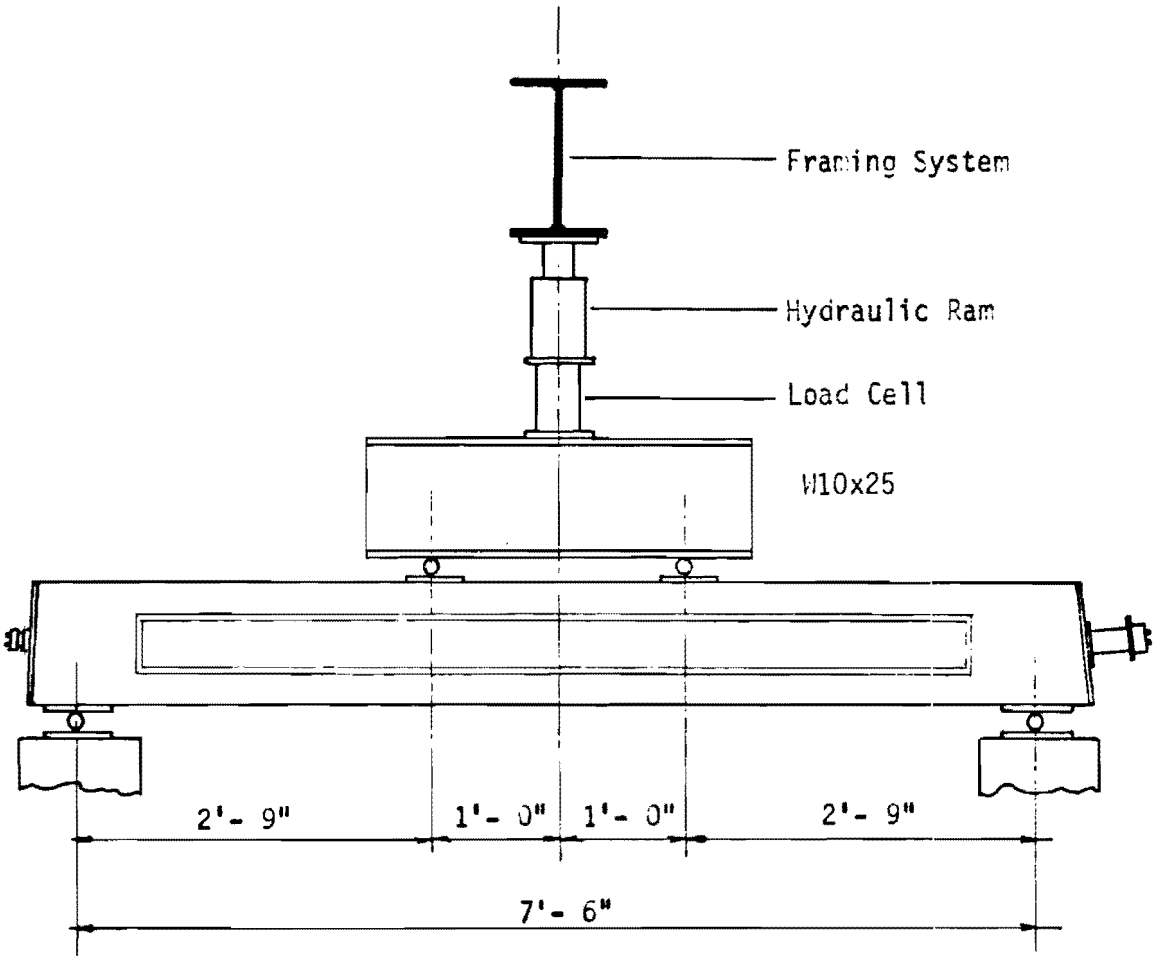

Fig. 4.1 Loading System for Flexural and Shear Tests.

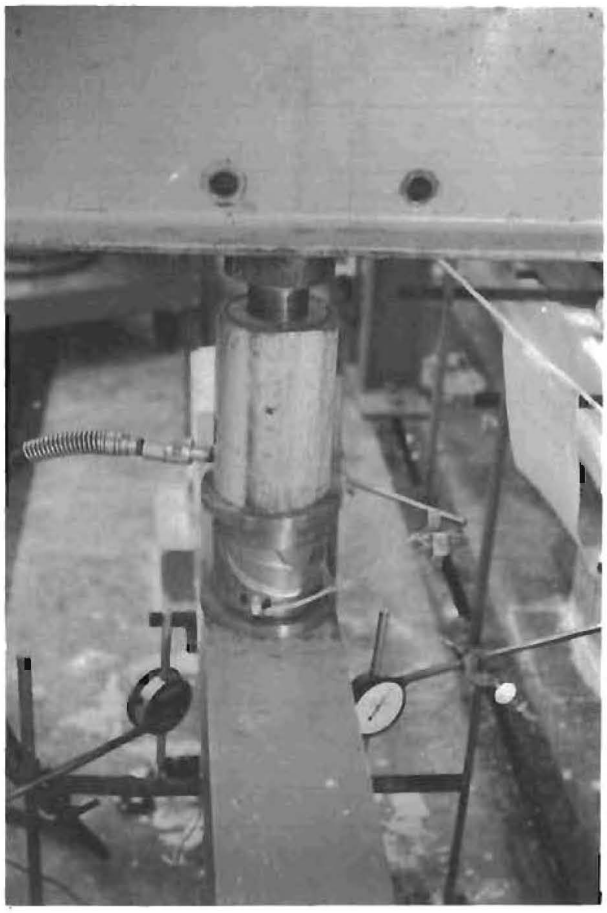

Fig. 4.2 Hydraulic Ram and Load Cell in Loading System.

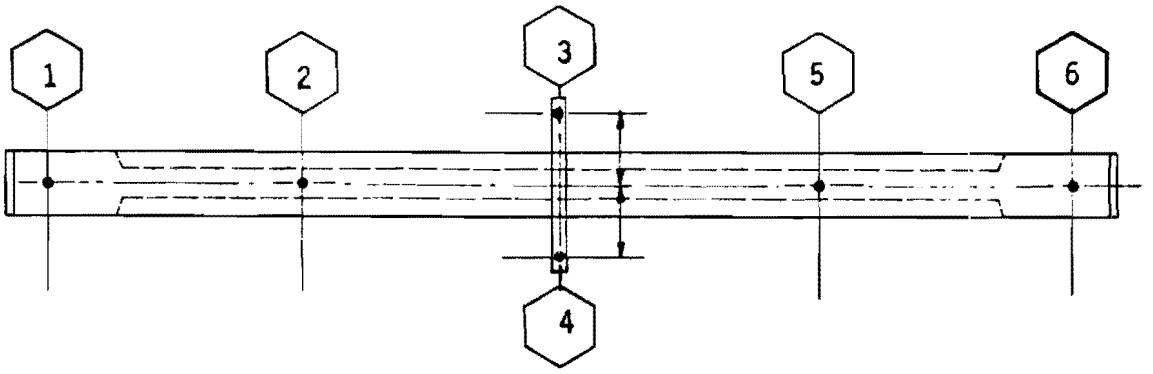

(a) Top View.

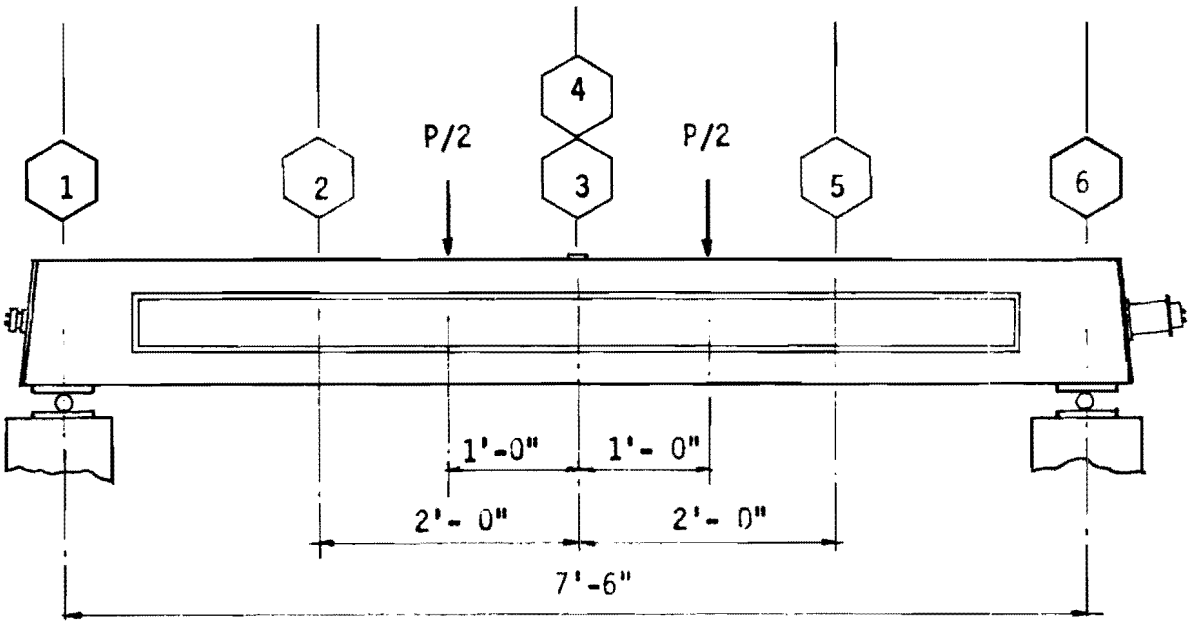

(b) Side View.

Fig. 4.3 Location of Dial Indicators for Measuring Deflections.

loads from the load cells which recorded the applied forces were in good agreement with the loads measured by the pressure gages (Appendix A).

In the early stages of each test, the loads were applied in increments of about one kip until the first crack appeared; then smaller increments of 250 to 500 pounds were used, due to nonlinear behavior of the beams. However, when the applied load exceeded 90 percent of the predicted ultimate load, a load increment corresponding to a midspan deflection of about 0.100 in. was applied until the final failure occurred.

4.1.3 Deflection Reading

Dial indicators were used for the deflection measurements along the beam, as shown in Fig. 4.3. Dial gages no. 1 and no. 6 were used to check the settlement of the supports while the other gages were used to determine the deflected shape of the beam under loads. Gages no. 3 and no. 4 were located at right angles to the midspan of the beam at equal distances from the beam center line. Gages nos. 2 and 5 were 2 feet from the midspan of the beam and they were located at the center line of the beam. The dial indicators could be read in 0.001-in. increments.

4.1.4 Strain Measurement

The strain distribution over the cross section of the beam was monitored by means of electrical strain gages. The strains were measured in both concrete and reinforcing steel bars.

For concrete, 2.4-in. paper backed strain gages were attached to the surface of the beam, as shown in Fig. 4.4. Gage no. 4 was at the centerline of the beam on the top surface, and nos. 5, 6, 7, and 8 were attached to the side of the top flange, as shown in Fig. 4.4. The strains measured by the electrical strain gages were checked to be sure they were in good agreement with the strains measured by means of dial indicators (Appendix F).

For the reinforcing steel, Teflon-backed strain gages (EA-06-230 DS-120 Micro-Measurement) were used and were sealed with waterproofing cement to prevent the entrance of moisture from the wet concrete. The location of each bonded reinforcing steel bar is indicated in Fig. 4.4.

It should be noted that all strain gages were located at the midspan of the beam and they were connected to the switch and balance units and strain

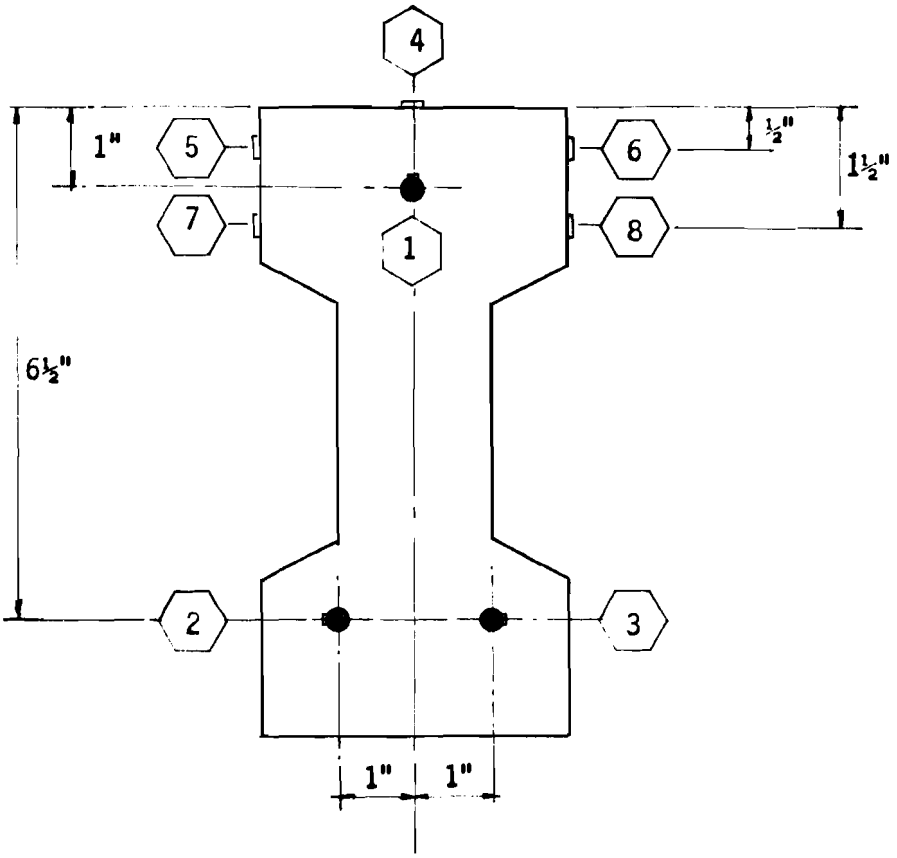

Fig. 4.4 Strain Gauge Locations on Beam Section.

indicator by a quater bridge circuit. The strains were read at each load increment.

4.1.5 Crack Marking

Crack patterns and some crack widths corresponding to each load reading were recorded. Prior to beginning the tests, grid lines were drawn on both sides of each beam to facilitate the mapping of crack propagation during the test. The reference lines for the load location and the support reactions were also marked on the beam in order to relate the crack patterns with the loading system.

The cracks were observed from the beginning of the test up to about 90 percent of the predicted ultimate load. In general, cracks at a particular loading were marked on the sides of the beam to study the behavior. Initial crack widths were not measured due to the difficulty of measuring very fine crack widths; however, some of the larger cracks were measured after they began to open.

4.2 Test for Time Effect on Flexural Behavior

Two PIC beams containing unbonded tendons were tested to determine the time effects on flexural behavior. After the beams were stressed, both tendon relaxation and beam deflections were observed for a few weeks. Two external point loads were then applied and sustained for several months. Time-dependent deflections and loss of prestress due to creep were measured periodically. The loading system is shown in Fig. 4.5.

4.2.1 Loading System

The loading system in this test was similar to the one for determining flexural and shear strengths. The beam was simply supported and loaded symmetrically with two loads provided by a screw jack, as shown in Fig. 4.6. The span length and placement of the loads were identical, as described in Sect. 4.1.1. The beams were subjected to a constant load by means of calibrated springs. The strains, deflections, and tendon forces were measured periodically during the test program.

The structural steel reaction frame was designed to accommodate two beams at a time. The legs of the frame were anchored to the floor system and

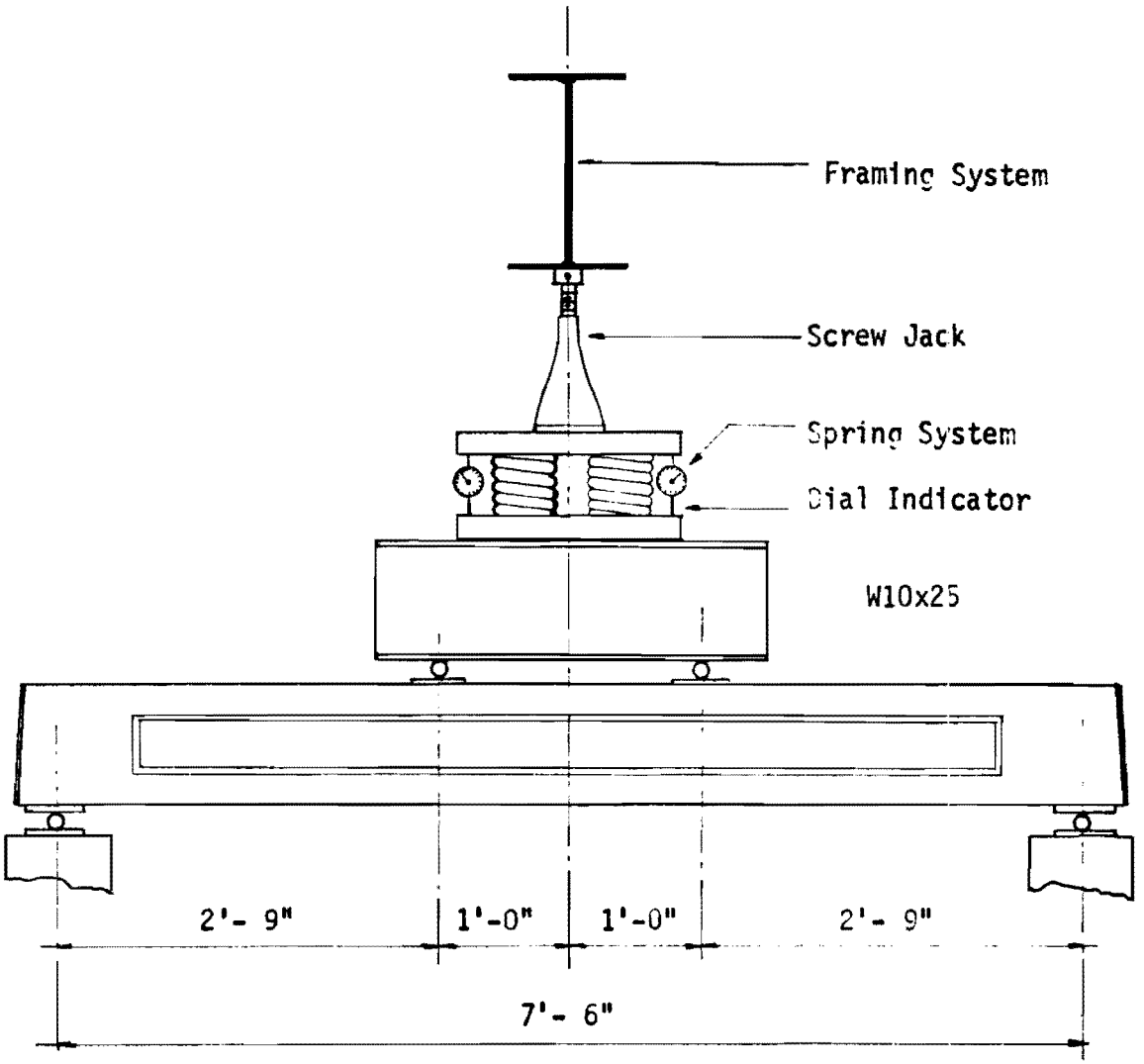

Fig. 4.5 Loading System for Time-Dependent Deflection Tests.

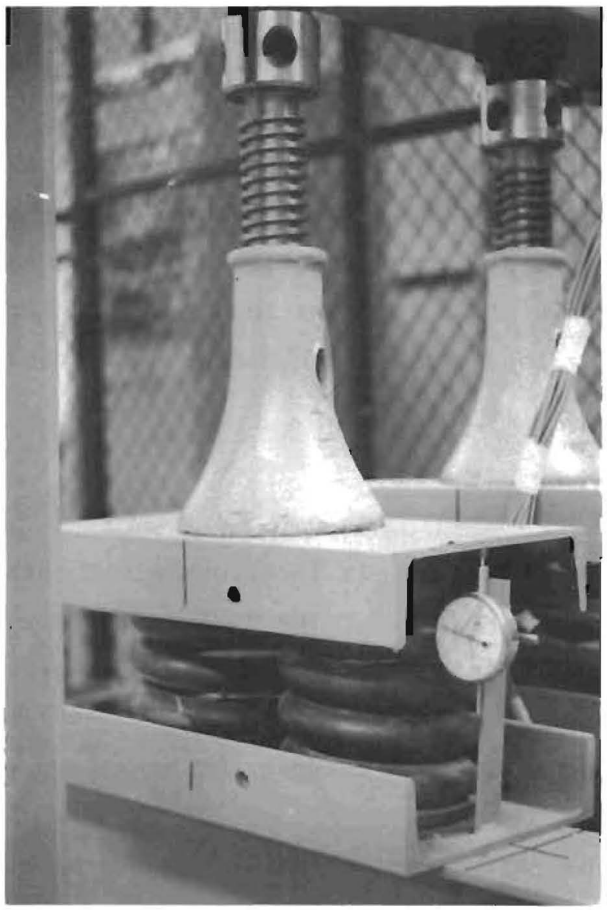

Fig. 4.6 Screw Jack and Spring Loading System for Sustained Load Tests.

the beam reactions were placed on the floor. Bearing plates were generally used at each load point.

4.2.2 Loading Measurement

The constant load on each beam was applied by the springs and a screw jack. The springs themselves were mounted in a spring jacket, as shown in Fig. 4.6, and two dial indicators were attached to read the deformation of the spring. The calibration curves for the spring systems are shown in Appendix E. The load-displacement relationship was linear. The screw jack was adjusted to maintain a constant load. Tendon forces and changes in forces were measured by load cells which had been attached to the tendons before stressing.

4.2.3 Deflection Readings

Deflections were measured at six locations along each beam, arranged similarly to that shown in Fig. 4.3. The dial indicators could be read in 0.0001-in. increments with an accuracy of about $\pm$ 0.1 percent. The gauges were attached to a small frame which was bolted to the floor. The metal plates were used at the interfaces between the beams and each contact point of the dial indicators.

Fig. 4.7 shows the arrangement of dial indicators for both beams during the sustained load tests.

4.2.4 Strain Measurement

Both mechanical and electrical gauges were used for measuring the strains. Eight electrical strain gauges, as shown in Fig. 4.4, were attached for each beam, three for steel and five for concrete. The strain gauges on the concrete, used only in the compression zone, were placed on the top fiber surface, 1/2 in. and 1-1/2 in., respectively, from the top fiber, as shown in Fig. 4.4. The gauges were coated with waterproofing cement to protect the gauges from moisture; a quarter bridge circuit was used for instrumentation.

A Berry gauge was also used to read the change in length of the fibers in the constant moment portion of the beams. Two metal buttons, each with an indentation in the center, were attached to the surface of the beam by epoxy at 8-in. intervals horizontally. Fig. 4.8 shows the reading of a

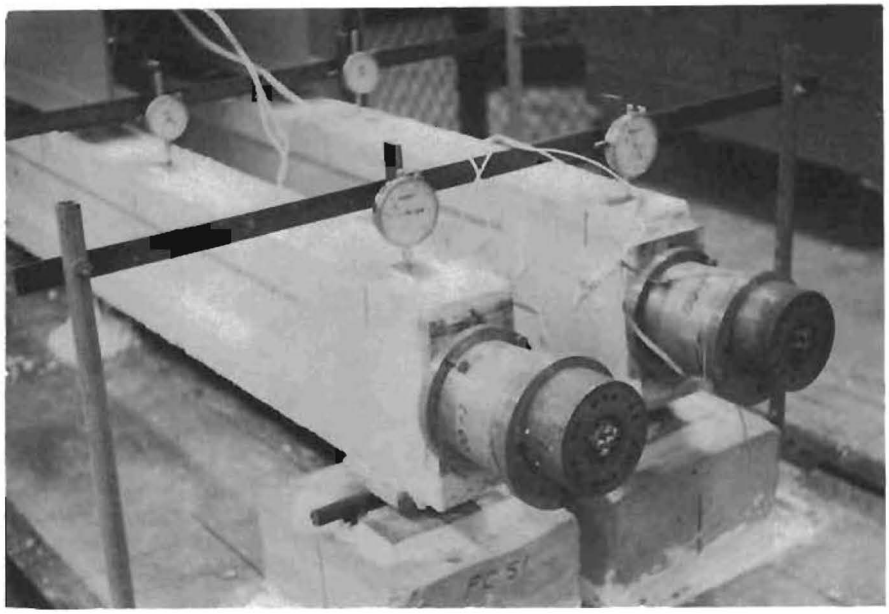

Fig. 4.7 Dial Indicator Arrangement for Sustained Load Tests.

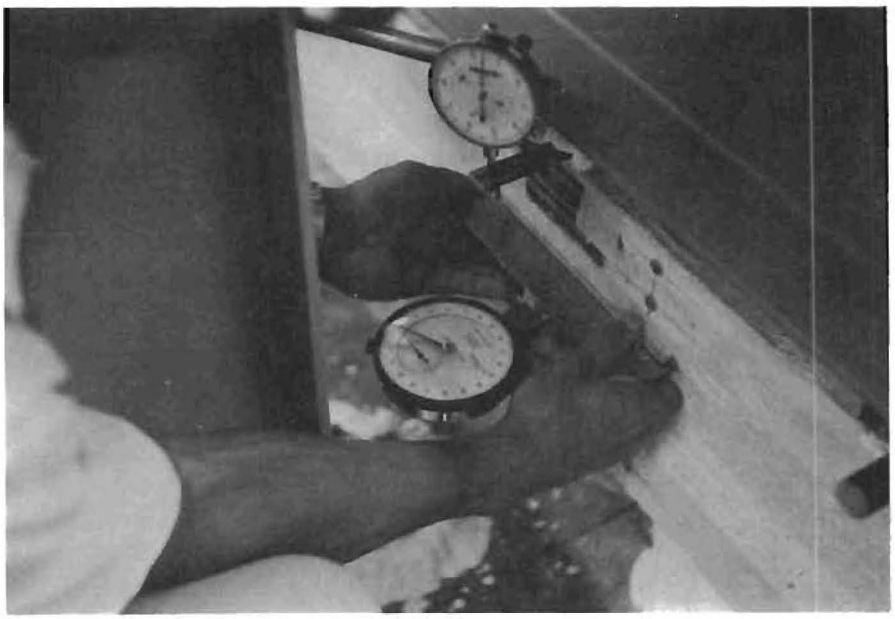

Fig. 4.8 Strain Measurement in Sustained Load Beams Using Berry Gauge.

Berry gauge for the beam. For each beam, strains were measured at four different levels from the top fiber, 1/2, 1, 4, and 7-in., respectively. The Berry gauge can read a strain increment of 0.0001 in.

CHAPTER V. TESTS FOR FLEXURAL STRENGTH

5.1 Description of Test Series

Eleven beams were tested for flexural behavior. All beams had the same symmetrical I-beam cross section and contained unbonded tendons, except for two beams which were one inch wider and contained bonded tendons. The beams can be classified into three different categories: fully-impregnated beams, partially-impregnated beams, and unimpregnated control beams. The fully-impregnated beams were impregnated throughout the cross section while the partially-impregnated beams were impregnated only through the top flange. One unimpregnated control beam was tested.

The 100 percent MMA monomer system was used for every test series except the PBM series, which used other systems. Adequate stirrups were provided in each beam to insure flexural failure.

5.1.1 Fully-Impregnated Beams

Many parameters were considered to affect the flexural behavior of the post-tensioned polymer-impregnated concrete beams, such as number of tendons, monomer systems, and types of tendons. The test specimens may be categoriezed as follows:

(a) PBF Series: The beams in this series contained different numbers of tendons. There were four beams, PBF-2, PBF-4, PBF-6, and PBF-8, which had 2, 4, 6, and 8-wire tendons, respectively. Each wire of the tendon was 0.25 in. in diameter and was unbonded.

(b) PBM Series: Different monomer systems were used for these beams. PBM-75 was impregnated with a monomer system consisting of 75 percent MMA and 25 percent BA while PBM-50 was impregnated with a monomer system consisting of 50 percent MMA and 50 percent BA. Both beams contained 2-wire unbonded tendons.

(c) PBB Series: Two beams were tested for flexural behavior with bonded tendons. Both beams contained 4-wire tendons and were grouted after they were post-tensioned. Two kinds of grouting materials were used. PBB-4C was grouted by conventional cement grouting material while PBB-4P was grouted with a material composed of liquid monomer, initiator, and promoter. The monomer solution was introduced while it was liquid, and it polymerized at room temperature within an hour after mixing. The proportions of both grouting materials are shown in Appendix D. Table 5.1 summarizes the fully-impregnated beams.

5.1.2 Partially-Impregnated Beams

PBP Series: In this series, only the nominal compression zone of each beam was impregnated by a 100 percent MMA-monomer system. The only variable in this test series was the number of tendons. The beams were designated PBP-2 and PBP-4, containing 2 and 4-wire unbonded tendons, respectively. Table 5.2 summarizes the partially impregnated beams and the control one.

5.1.3 Control Beam

PBC-2: This beam was tested as an unimpregnated control and contained a 2-wire unbonded tendon. It was cast at the same time and with the same mix as the PBF series. It should be mentioned that the beam was identical to PBF-2 except that it was not polymer impregnated.

5.2 Test Results

Test beams that comprise the series for flexural behavior were all subjected to essentially the same stressing and testing procedures as those described in Chapters 3 and 4. The tendons for all beams were stressed from one end and the strain at the opposite end was monitored by a load cell placed between the beam and the tendon anchoring nut. The tendons were first overstressed to permit insertion of the steel shims that held the tendons in the required stressed condition. Camber at midspan of each test beam was recorded during and after the post-tensioning process.

Soon after stressing was completed, the load beam was lowered onto the test specimen and initial readings on the dial gages were taken. The load cell measuring the tendon force and the deflection dial gages were read

Table 5.1

Summary of the Fully Impregnated Beams.

Test Series	Specimen No.	No. of Wires	$\rho_p = \frac{A_s}{bd}$	$\omega_p = \frac{\rho_p f_{ps}}{f'_{cp}}$	Monomer System	Tendon Type, Grouting Materials.
PBF	PBF-2	2	0.0038	0.053	100%MMA	Unbonded
	PBF-4	4	0.0076	0.098	100%MMA	Unbonded
	PBF-6	6	0.0113	0.142	100%MMA	Unbonded
	PBF-8	8	0.0151	0.186	100%MMA	Unbonded
PBM	PBM-75	2	0.0038	0.063	75%MMA +25%BA	Unbonded
	PBM-50	2	0.0038	0.069	50%MMA +50%BA	Unbonded
PBB	PBB-4C	4	0.0061	0.083	100%MMA	Bonded, Conventional
	PBB-4P	4	0.0061	0.083	100%MMA	Bonded, Polymer

Table 5.2

Summary of the Partially Impregnated Beams

Test Series	Specimen No.	No. of Wires	$\rho_p = \frac{A_s}{bd}$	$\omega_p = \frac{\rho_p f_{ps}}{f'_{cp}}$	Monomer System	Impregnation Depth
PBP	PBP-2	2	0.0038	0.053	100%MMA	2-1/2 in.
	PBP-4	4	0.0076	0.110	100%MMA	2-1/2 in.
Control	PBC-2	2	0.0038	0.142	None	-

after each increment of load was applied. The crack pattern and crack widths were observed during testing until failure was imminent. Strain readings of concrete and steel at midspan of the beams were taken at each increment of load.

5.2.1 Initial Prestressing Forces

Prestressing of forces at both ends of the tendons was measured by means of a pressure gauge at the stressing end and by means of a load cell at the anchorage end. The prestressing forces generally were varied due to the number of wires in the tendons. The objective was to apply the prestress at about 70 percent of the specified ultimate strength of the tendon, but in actual practice the initial prestress cannot be measured at the stressing end after the jacking pressure is released just after insertion of the steel shims. However, the maximum tendon forces at the stressing end were measured. The tendon forces at the holding end were measured both before and after the jacking force was released. Table 5.3 summarizes the tendon forces at both ends of the beam at various stages of stressing and the beam camber at midspan corresponding to each stage of stressing procedures.

5.2.2 Load-Deflection Responses

Plots of load versus midspan deflection for each test series are presented in Figs. 5.1 to 5.5. In the elastic range, the responses are typically linear and tend to deviate from linearity when the first crack occurs. Beyond the elastic range, the curves are not quite smooth, due to continued cracking, and the beams responded nonlinearly because the tendon stress was in the nonlinear portion of the stress-strain curve.

Cracking could usually be detected because the needle on the loading pressure gage would fall off or hesitate momentarily. This was especially true during the development of the first few cracks in the beam. In general, there was little noise when the new cracks originated in the PIC beams. The ultimate loads and the final deflections for individual beams were different due to the independent variables for each test series. Table 5.4 summarizes the loads and deflections at initial cracking and at ultimate loads. It should be noted that the deflections shown in the figures are based on a cambered position. The load-deflection response for each beam can be

Table 5.3

Summary of Initial Tendon Forces and Midspan Camber

Test Series	Specimen No.	Tendon Force at Stressing End Before Release (lb.)	Tendon Force at Anchoring End (lb.)		Camber at Midspan (in.)	
			Before Release	After Release	Before Release	After Release
PBF	PBF-2	17,500	15,000	15,000	0.041	0.038
	PBF-4	34,600	29,100	29,100	0.075	0.070
	PBF-6	51,400	44,600	44,600	0.142	0.111
	PBF-8	69,700	60,700	60,700	0.131	0.126
PBM	PBM-50	16,550	14,200	14,000	0.042	0.040
	PBM-75	16,550	14,000	14,000	0.045	0.042

(Continued)

Table 5.3

Summary of Initial Forces and Midspan Camber (cont.)

Test Series	Specimen No.	Tendon Force at Stressing End Before Release (lb.)	Tendon Force at Anchoring End (lb.)		Camber at Midspan (in.)	
			Before Release	After Release	Before Release	After Release
PBB	PBB-4C	35,900	35,020	34,950	0.064	0.062
	PBB-4P	35,900	34,840	34,700	0.053	0.052
PBP	PBP-2	16,550	14,200	13,800	0.082	0.074
	PBP-4	35,250	31,000	30,900	0.123	0.118
Control	PBC-2	16,200	14,500	14,500	0.050	0.048

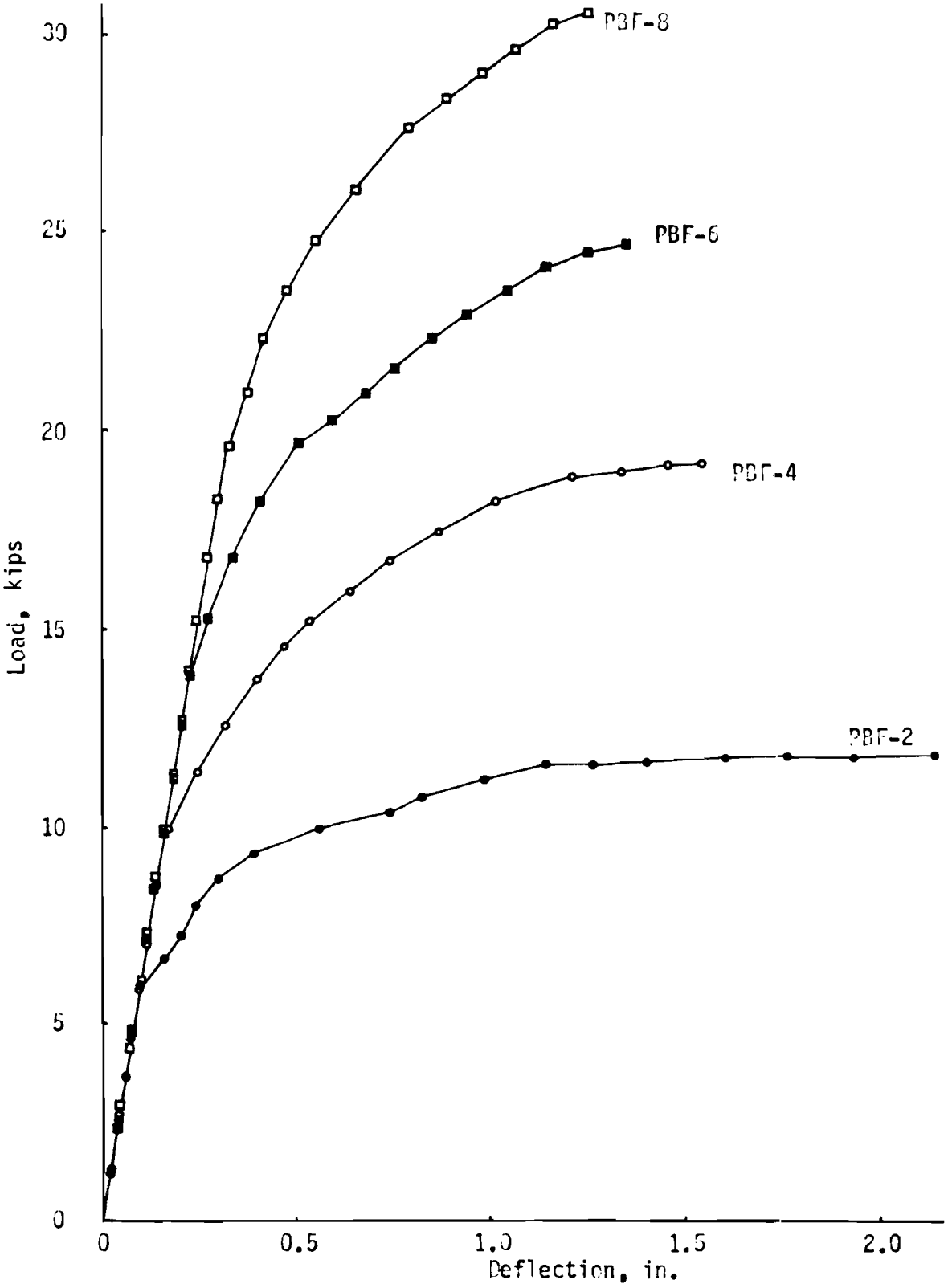

Fig. 5.1 Observed Load-Deflection Responses for PBF-Series Beams.

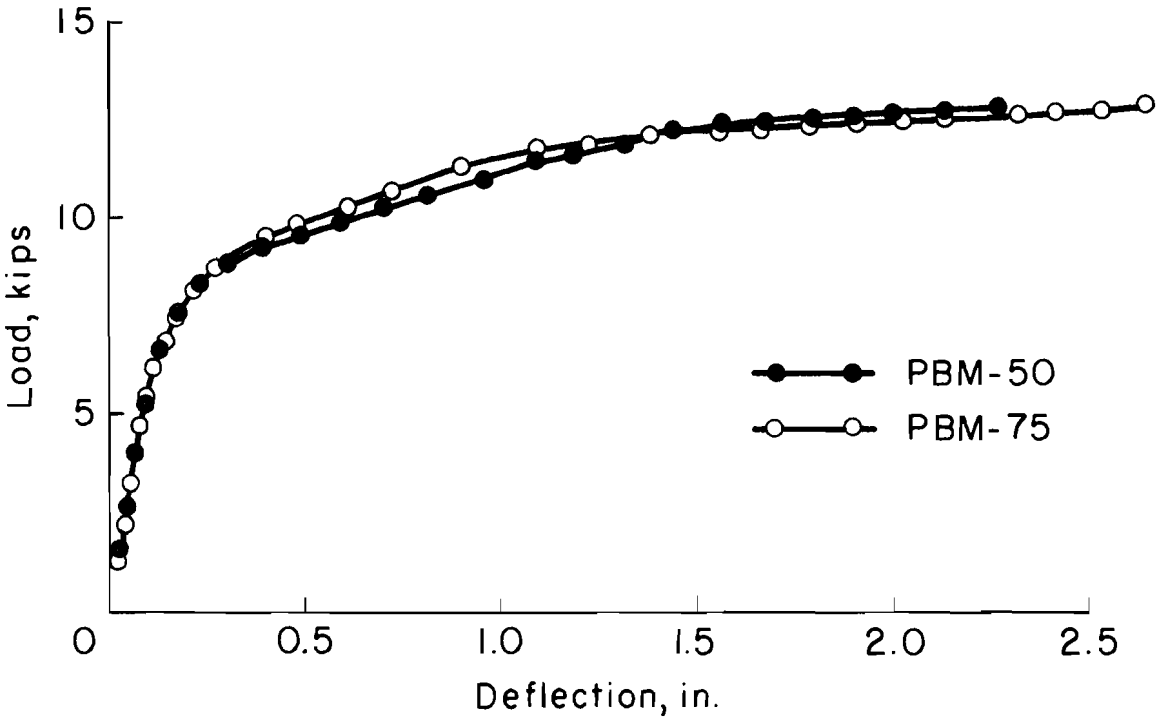

Fig. 5.2. Observed Load-Deflection Responses for PBM-Series Beams.

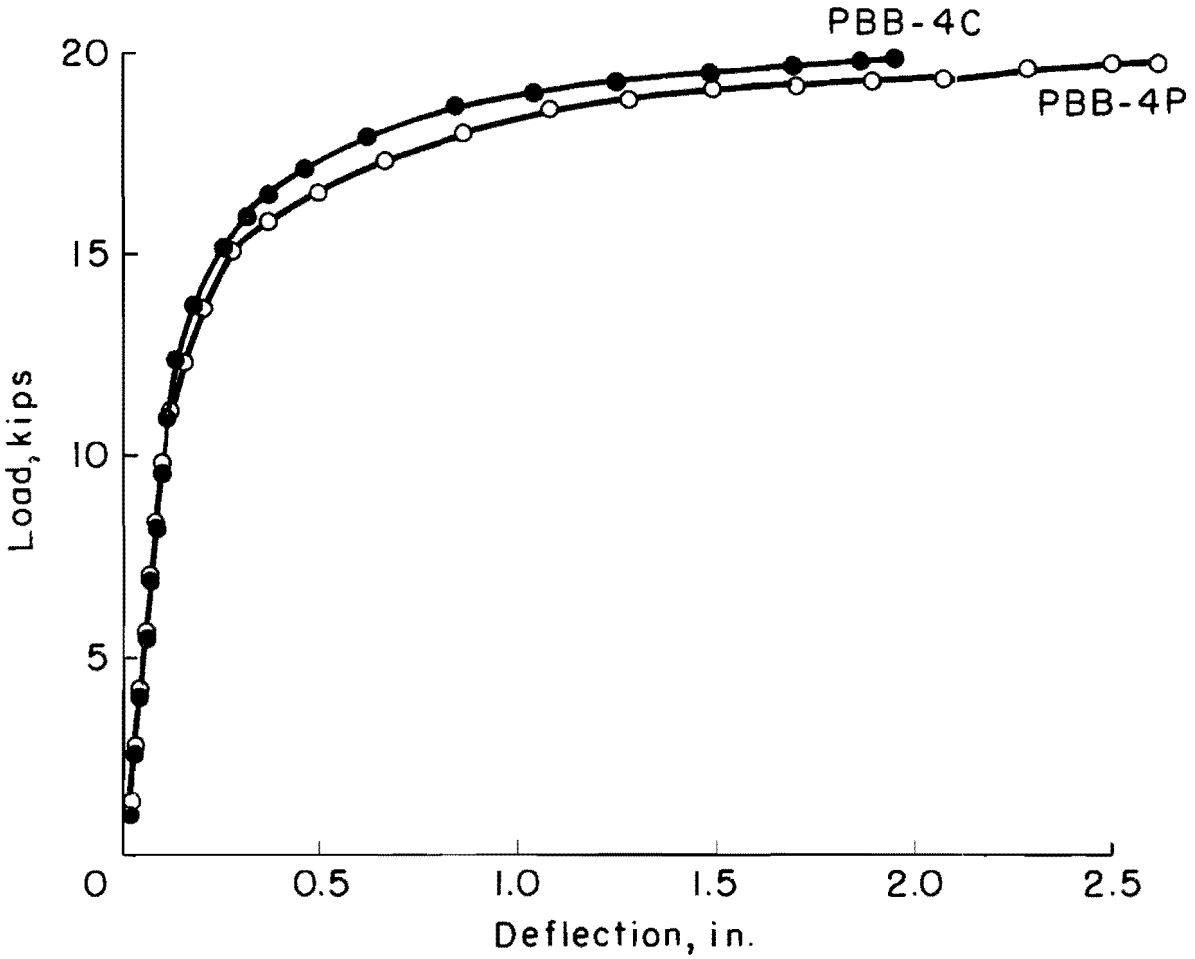

Fig. 5.3. Observed Load-Deflection Responses for PBB-Series Beams.

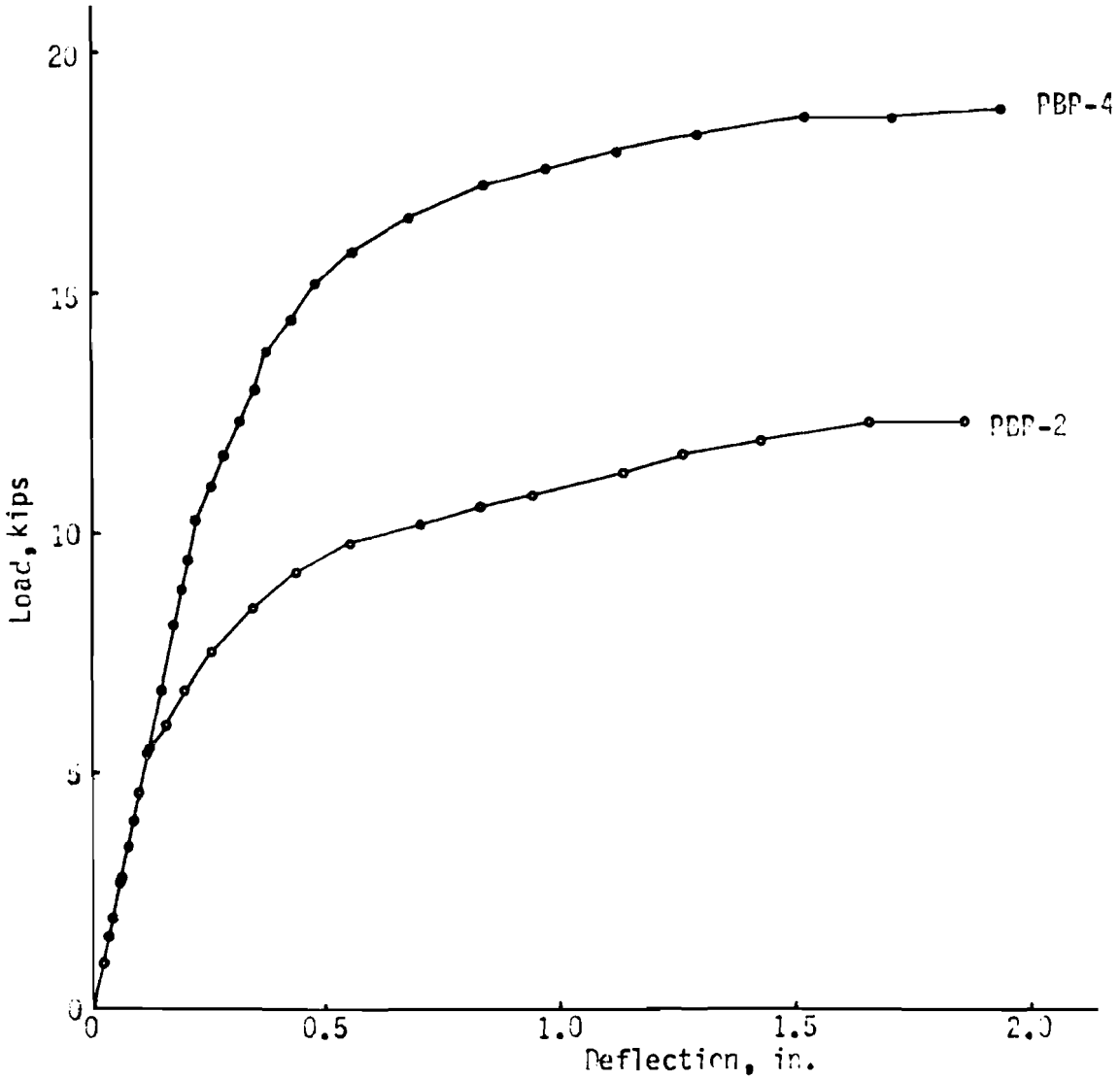

Fig. 5.4 Observed Load-Deflection Responses for PBP-Series Beams.

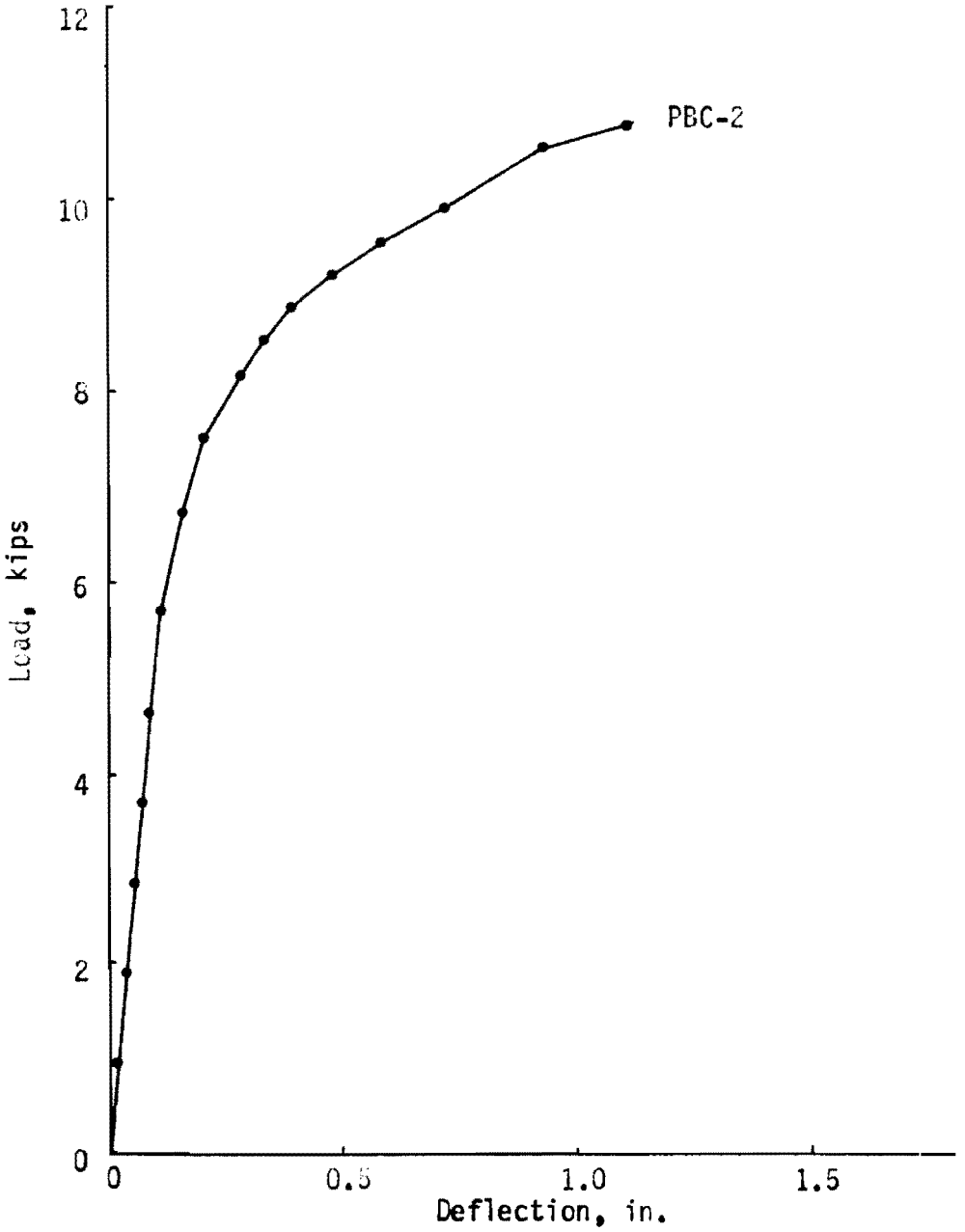

Fig. 5.5 Observed Load-Deflection Response for Control Beam.

Table 5.4

Loads, Moments and Deflections at Initial Cracking

and Ultimate for Flexural Beams

Test Series	Specimen No.	Cracking			Ultimate			
		Load P_{cr} (lb.)	Deflection, Δ_{cr} (in.)	Ratio, Δ_{cr}/L	Load, P_u (lb.)	Deflection, Δ_u (in.)	Ratio, Δ_u/L	Ratio, Δ_u/Δ_{cr}
PBF	PBF-2	6,000	0.115	1/783	11,900	2.422	1/37	21.06
	PBF-4	10,000	0.180	1/500	19,300	1.526	1/59	8.48
	PBF-6	13,800	0.209	1/430	24,700	1.340	1/67	6.41
	PBF-8	18,200	0.290	1/310	30.500	1.200	1/75	4.14
PBM	PBM-50	6,050	0.129	1/698	12,700	2.275	1/40	17.64
	PBM-75	6,050	0.118	1/763	12,780	2.869	1/31	24.31

(Continued)

Table 5.4

Loads, Moments and Deflections at Initial Cracking

and Ultimat for Flexural Beams (cont.)

Test Series	Specimen No.	Cracking			Ultimate			Ratio, Δ_u/Δ_{cr}
		Load, P_{cr} (lb.)	Deflection, Δ_{cr} (in.)	Ratio, Δ_{cr}/L	Load, P_u (lb.)	Deflection, Δ_u (in.)	Ratio, Δ_u/L	
PBB	PBB-4C	10,950	0.120	1/750	19,870	1.953	1/46	16.28
	PBB-4P	10,950	0.130	1/692	19,700	2.614	1/34	20.11
PBP	PBP-2	5,350	0.136	1/662	12,350	1.785	1/48	13.79
	PBP-4	9,550	0.210	1/428	18,860	1.924	1/47	9.16
Control	PBC-2	5,700	0.119	1/756	10,800	1.100	1/82	9.24

described as follows:

(a) PBF Series: Load-deflection response in this test series indicated that all beams had the same initial elastic stiffness, as shown in Fig. 5.1, but, after the first crack originated, each of the beams behaved differently. The number of wires in the tendon, which is the only variable in this series, totally affected the flexural behavior. Cracking load increased with the number of wires, corresponding to more prestress forces. The higher the number of wires in the tendons, the lower were the final deflections and the higher the ultimate loads. The toughness, which is represented by the area under the load-deflection curve, was slightly different for each beam and seemed to be a function of the number of wires in the tendons. The final deflections varied from 1.20 in. for PBF-8 to 2.42 in. for PBF-2. It should be noted that ultimate load did not increase in proportion to the number of wires in the tendons.

Beam PBF-2. The beam camber was 0.38 in. at midspan after post-tensioning, with a force of 15 kips at the anchorage end. The load-deflection response was linear until the first cracks occurred in the flexure span, at a load of 6 kips and a deflection of 0.115 in. From that point, the deflection increased at a faster rate than the load, especially when the applied load approached the ultimate load. The beam failed at the ultimate load, 11.9 kips, with the final deflection 2.42 in. The midspan deflection to span ratio at ultimate load was 1/37. The ultimate deflection was about 21 times higher than the cracking deflection.

Beam PBF-4. The initial post-tensioned force at the anchorage end was 29.10 kips. The tension force produced a camber of 0.070 in. at midspan of the beam. The first noticeable crack appeared at a load of 10 kips and a deflection of 0.180 in. The deflection-to-span ratio at the cracking load was 1/500. The load-deflection response was nonlinear after the first cracks. The ultimate load was 19.30 kips and the ultimate deflection was 1.530 in. The deflection-to-span ratio at ultimate load was 1/59.

Beam PBF-6. After a prestress force of 44.60 kips, the beam camber was 0.111 in. at midspan prior to the external load application. The load-

deflection response for PBF-6, as shown in Fig. 5.1, was linear up to the load of 13.80 kips, at which the first cracks occurred. After the cracking the deflection increased at a faster rate than the applied load. The beam failed at 24.70 kips. The cracking deflection was 0.209 in. while the ultimate deflection was 1.340 in. The maximum deflection was about 1/67th of the span length.

Beam PBF-8. This beam developed the largest camber in the PBF series, due to the highest post-tensioned force, 69.70 kips. The midspan camber was 0.126 in., at which the tendon force at the anchorage end was 60.70 kips. The cracking load was 18.20 kips, corresponding to a deflection of 0.290 in., while the ultimate load was 30.50 kips, corresponding to a deflection of 1.20 in. The ultimate deflection was about 10 times larger than the cracking deflection and it was about 1/75 of the span length.

(b) PBM Series: The load deflection responses for the PIC beams impregnated with different monomer systems are shown in Fig. 5.2. Both beams contained 2-wire unbonded tendons and the load-deflection responses were almost identical. The ultimate loads were about the same but the beam impregnated with the 75 percent MMA + 25 percent BA monomer system (PBM-75) developed a slightly larger deflection than that impregnated with the 50 percent MMA + 50 percent BA monomer system (PBM-50). The comparison of these responses to that for the PIC beam with the 100 percent MMA monomer system and the unimpregnated control beam is made later in this chapter.

Beam PBM-75. The camber of the beam was 0.42 in., due to the tendon force of 14.00 kips at the anchorage end. The midspan deflection was 0.118 in. when the first cracks occurred. The cracking load was 6.05 kips. The beam failed at a load of 12.78 kips and the deflection was 2.867 in. The ultimate deflection was about 24 times higher than the deflection at the first cracking. The midspan deflection to span ratio at ultimate load was 1/31.

Beam PBM-50. The load-deflection response of PBM-50 was similar to the one of PBM-75. The camber was 0.40 in., which was slightly less than that for PBM-75 even though the tendon forces were about the same. The cracking load was 6.05 kips, corresponding to a deflection of 0.129 in. The ultimate

load was 12.70 kips and the deflection was 2.275 in. The deflection at ultimate was about 18 times higher than the one at cracking load and was about 1/40 of the span length. The ultimate load was slightly higher than twice the cracking load.

(c) PBB Series: The tendons for the specimens in this test had been grouted with cement paste for PBB-4C and with polymer material for PBB-4P. Both of them responded to the applied external load with the same stiffness before cracking but there was a slight difference in stiffness after cracking. Fig. 5.3 indicates that PBB-4C had a bit higher stiffness than PBB-4P after cracking but the ultimate loads were about equal. PBB-4P had more ductility than PBB-4C since the ultimate deflection for PBB-4P was about 30 percent larger than that for PBB-4C.

Beam PBB-4C. The beam was grouted about 3 days after post-tensioning and it was tested about 4 weeks after grouting. The cement paste was allowed to set and adequately develop bond strength between the tendon and surrounding materials. The load-deflection was linear to the first cracking at 10.95 kips, corresponding to a deflection of 0.120 in. The ultimate load was 19.78 kips at which the deflection was 1.953 in. The ultimate deflection was about 16 times the deflection at the cracking load and was about 1/46 of the span length.

Beam PBB-4P. The beam was grouted by mixed liquid monomer, which could be polymerized and developed bond strength between tendon and surrounding materials within a couple hours. The cracking loads and ultimate loads of PBB-4P were about the same as those of PBB-4C. They were 10.95 kips and 19.70 kips, respectively. The deflection was 0.130 in. at cracking and 2.614 in. at ultimate. The ultimate deflection was about 20 times higher than that at cracking load. The maximum deflection-to-span ratio was 1/34.

(d) PBP Series: The load-deflection curves shown in Fig. 5.4 represent the response to static loads for partially impregnated beams containing 2-wire, unbonded tendons (PBP-2) and 4-wire, unbonded tendons (PBP-4). Both beams were impregnated to only a part of the depth of the top flange. The impregnation depth was 2.50 in., which was about 40 percent of the effective depth or about 31 percent of the total depth. The midspan camber after post-tensioning for a partially impregnated beam was slightly higher than

that for a fully impregnated one. The stiffnesses and deflections were about the same. The ultimate loads for those two were different due to the number of tendons, as follows:

Beam PBP-2. The beam was post-tensioned to about 13.80 kips at the anchorage end and produced a midspan camber of 0.074 in. Noticeable cracks appeared at a load of 5.35 kips and a deflection of 0.136 in. The deflection increased at a faster rate than the applied load after the first cracks. The beam failed at a load of 12.35 kips, corresponding to a deflection of 1.875 in. The ultimate deflection was about 14 times the cracking deflection and was about 1/48 of the span length.

Beam PBP-4. The camber at midspan was 0.118 in. due to the post-tensioning force of 30.90 kips at the anchorage end. The first cracks occurred at a load of 9.55 kips, and the deflection was 0.210 in. The ultimate load was 18.86 kips, with a maximum deflection of 1.924 in. The ultimate load was about twice the cracking load but the ultimate deflection was about 9 times higher than the deflection at cracking load. The maximum deflection to span ratio was about 1/47.

(e) PBC Series: Only one beam (PBC-2) was tested as a control beam and it contained a 2-wire, unbonded tendon. Fig. 5.5 shows the load-deflection response of the control beam; the maximum deflection was 1.10 in. and the ultimate load was 10.80 kips. The cracks originated at a load of 5.70 kips and the deflection was about 0.110 in. The ultimate deflection was about 10 times higher than the deflection at the cracking load. The maximum deflection to span ratio was 1/82. This ratio was very small in comparison to the corresponding PIC beam with partial or full impregnation.

5.2.3 Tendon Stress

Tendon stress during testing can be measured only at the holding end, as mentioned previously. Plots of load versus change in tendon stress for each test series are shown in Fig. 5.6 to Fig. 5.9. The typical responses of the tendon stresses under the external applied loads were linear until initial cracking occurred. The response was nonlinear and the rate of change in tendon stress was not consistent due to the development of new cracks.

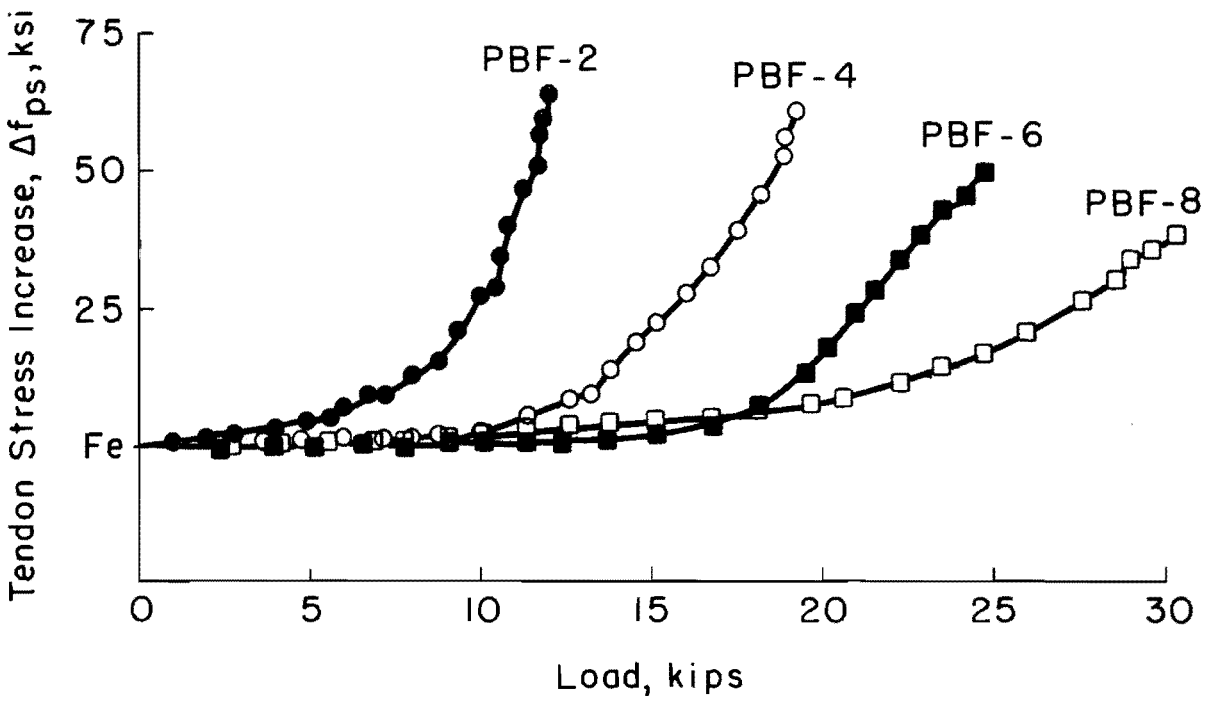

Fig. 5.6. Observed Tendon Stress Response Under Loads for PBF-Series Beams.

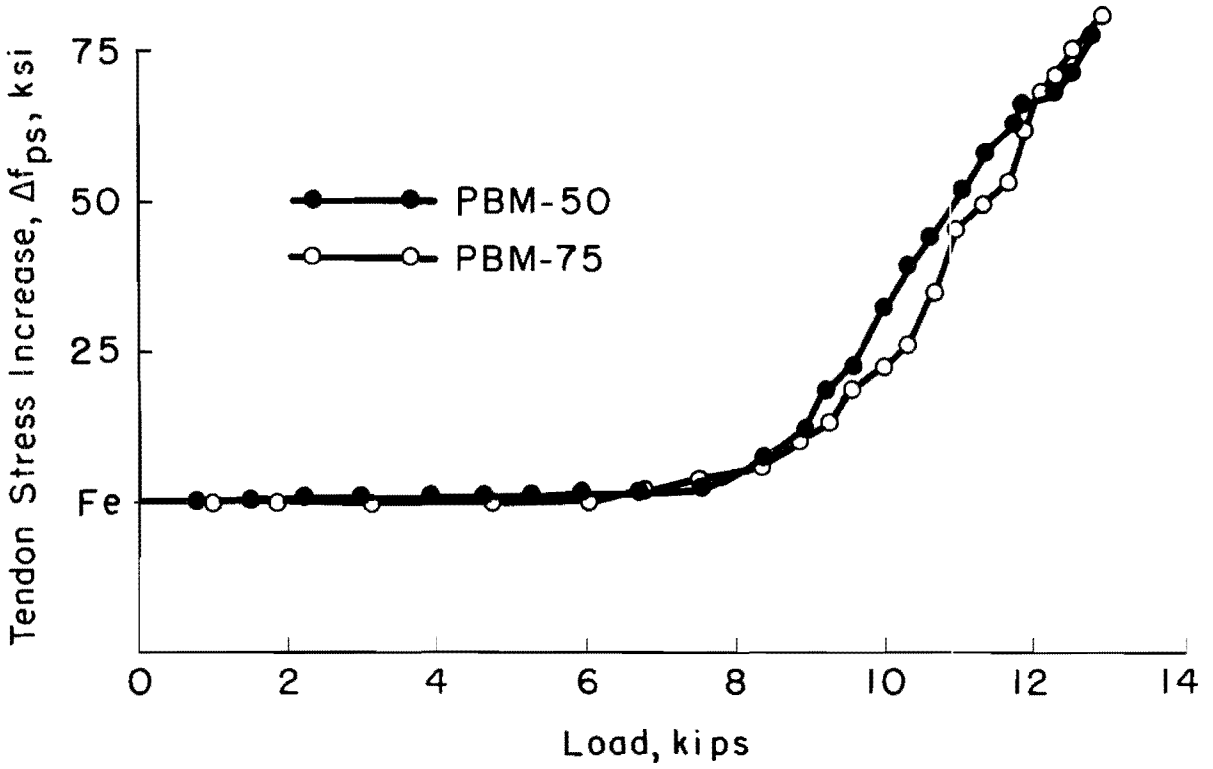

Fig. 5.7. Observed Tendon Stress Response Under Loads for PBM-Series Beams.

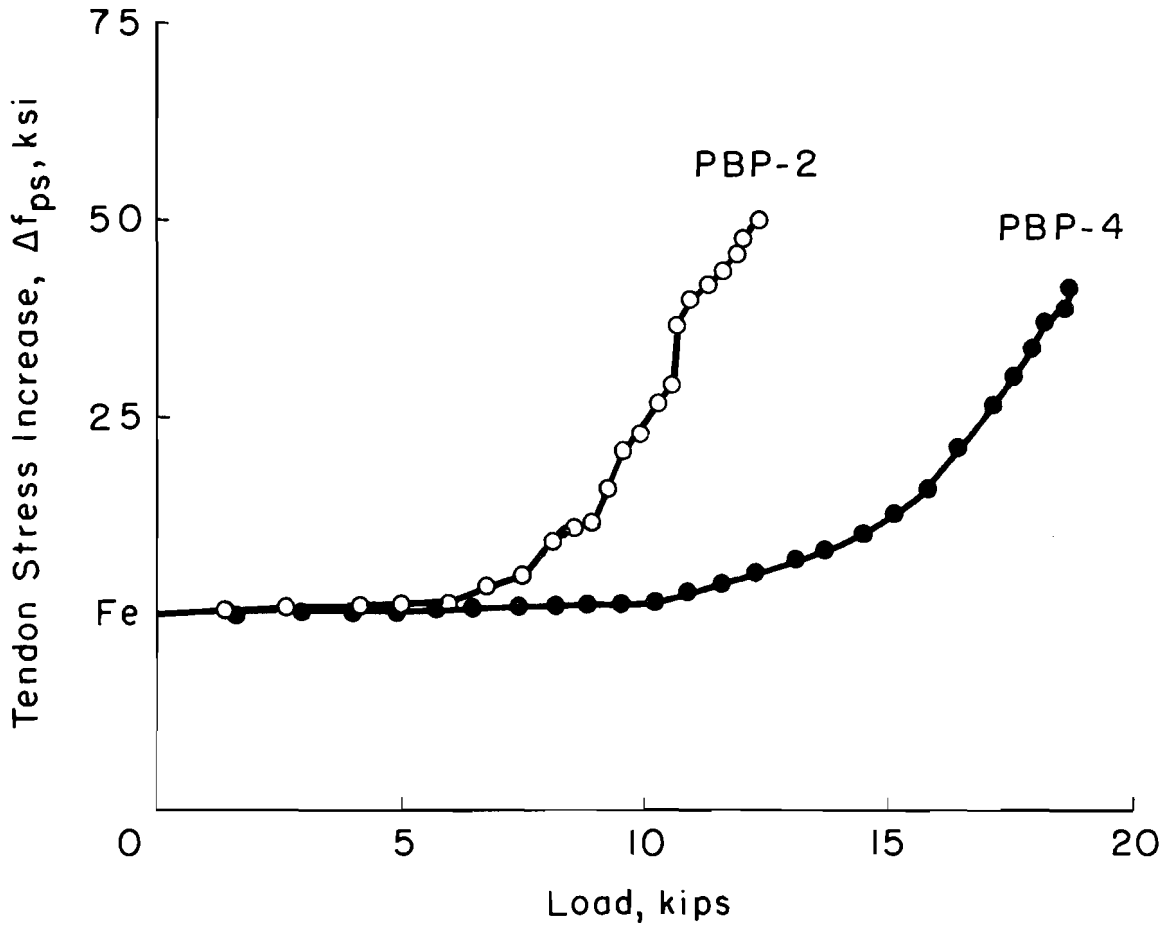

Fig. 5.8. Observed Tendon Stress Responses Under Loads for PBP-Series Beams.

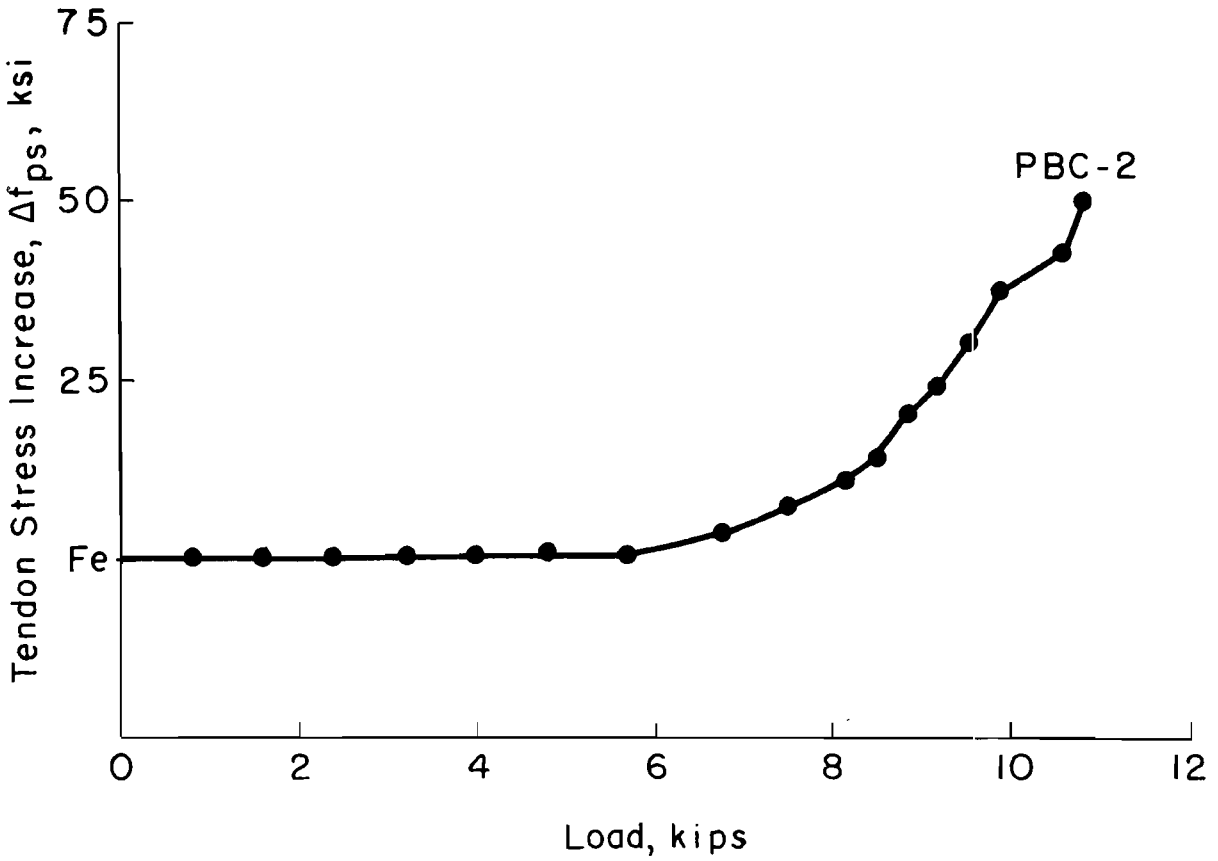

Fig. 5.9. Observed Tendon Stress Response Under Loads for Control Beam.

Actually, the final stresses shown were not the stresses at failure but they represent the final readings before failure occurred.

For some test beams, four strain gages were attached to the tendon to enable the tendon stresses to be determined. However, the gages were damaged during the impregnation process. The damage could have occurred during drying, monomer soaking, or curing. Tests to confirm the cause of damage were made by soaking the strain gage coating cement in the liquid monomer for 4 hours. The cement became soft and loose so that the monomer could penetrate through it, damaging the strain gages. Due to the loss of the strain gages, the tendon stresses for the beams containing bonded tendons could not be obtained.

(a) PBF-Series: Tendon stress responses for the beams containing a variable number of unbonded tendons are shown in Fig. 5.6. The curves indicate that the number of wires in the tendons affected the increment of the tendon stress; the higher the number of wires, the lower the tendon stress increment. The maximum increase in tendon stress varies from 68 ksi for PBF-2 to 38 ksi for PBF-8.

(b) PBM Series: Fig. 5.7 shows the tendon stress response for the PIC beams containing a 2-wire, unbonded tendon which was impregnated with the 25 percent BA monomer system for PBM-75 and the 50 percent BA monomer system for PBM-50. Both of them had essentially the same response under load. PBM-75 had a lower initial stress but developed a higher increase in tendon stresses. However, there was very little difference in final tendon stresses.

(c) PBB Series: As previously mentioned, the tendon stress along the tendon could not be measured due to the failure of the strain gages, but the tendon stress at the holding end of the tendon was measured during the testing in order to check the behavior of grouting materials. Both the polymer grouting material for PBB-4P and the conventional grouting material for PBB-4C performed adequately in bonding the tendons to the surrounding concrete. The wires were bonded so firmly that the tendons never slipped, as evidence by the fact that strain readings of the load cells at the anchoring ends indicated no measurable change for either beam.

(d) PBP Series: The tendon stress response for this test series is similar to one for PBF series. Beams with a larger number of tendons developed a smaller increase in tendon stress. Fig. 5.8 shows PBP-2, which contained a 2-wire, unbonded tendon, had a tendon stress increase of

50 ksi while PBP-4, which contained a 4-wire, unbonded tendon, had a stress increment of only 41.2 ksi. It should be noted that both beams are partially impregnated.

(e) PBC Series: The control beam, PBC-2, had a tendon stress response similar to those of the PIC beams. The response shown in Fig. 5.9 is linear up to 5.70 kips of load, when the first cracks occurred. From that point the tendon stress increased at a faster rate than the load. The total increment was about 50 ksi at the ultimate load of 10.80 kips.

5.2.4 Crack Patterns and Mode of Failure

(a) Crack Patterns: The first noticeable cracks generally appeared at midspan between the two load points. The cracks usually started from the bottom fiber of the beams and then propagated toward the top flange as the load increased. The cracks were marked while the loads were held constant. Figs. 5.10 to 5.14 show the major crack patterns for the beams tested for flexural behavior. The numbers located along the cracks are the loading stages corresponding to the deflection readings. The crack patterns for the beams were similar and generally typical of flexural cracking. The number of cracks varied for several reasons.

Number of Wires in Tendons. Beams with a higher number of wires in the tendons developed more cracks than those with a lower number of wires in the tendons because of the difference in initial stress in the concrete. Apparently, PBF-8, with an 8-wire, unbonded tendon, developed 12 cracks while PBF-2, with a 2-wire unbonded tendon, had only 10 cracks at the same deflection, 1.20 in.

Bonding Effect. The beams with bonded tendons had more uniform distribution of cracks than the ones with unbonded tendons. The PBB series beam which had been conventionally grouted had approximately 30 to 50 percent more cracks than those with the same number of tendons and no grouting. The beam which had been grouted with polymer concrete developed a more uniform crack distribution than the one with conventional grout. Beam PBB-4C developed 13 cracks while PBB-4P had 15 cracks, apparently because of its higher deflection or ductility.

Monomer Systems. The monomer systems had no apparent effect on distribution of cracks. All monomer systems used in this test program,

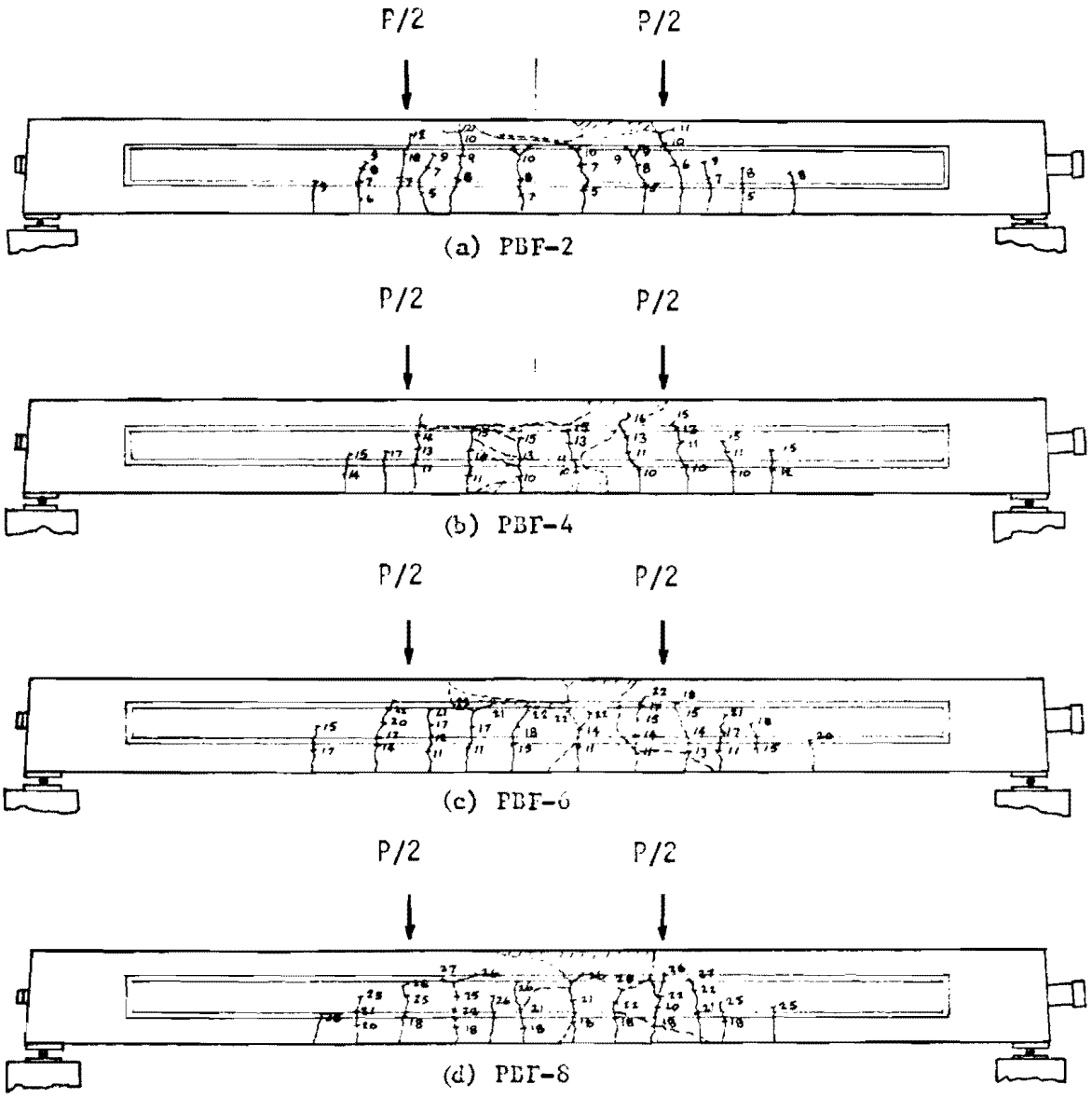

Fig. 5.10 Crack Patterns for PBF-Series Beams.

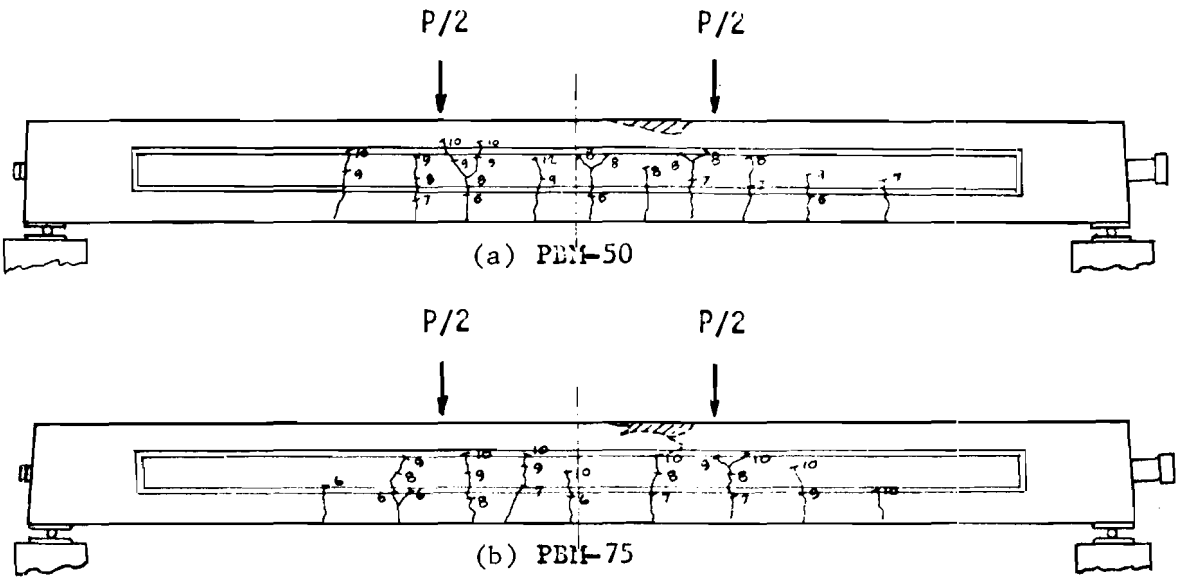

Fig. 5.11 Crack Patterns for PBM-Series Beams.

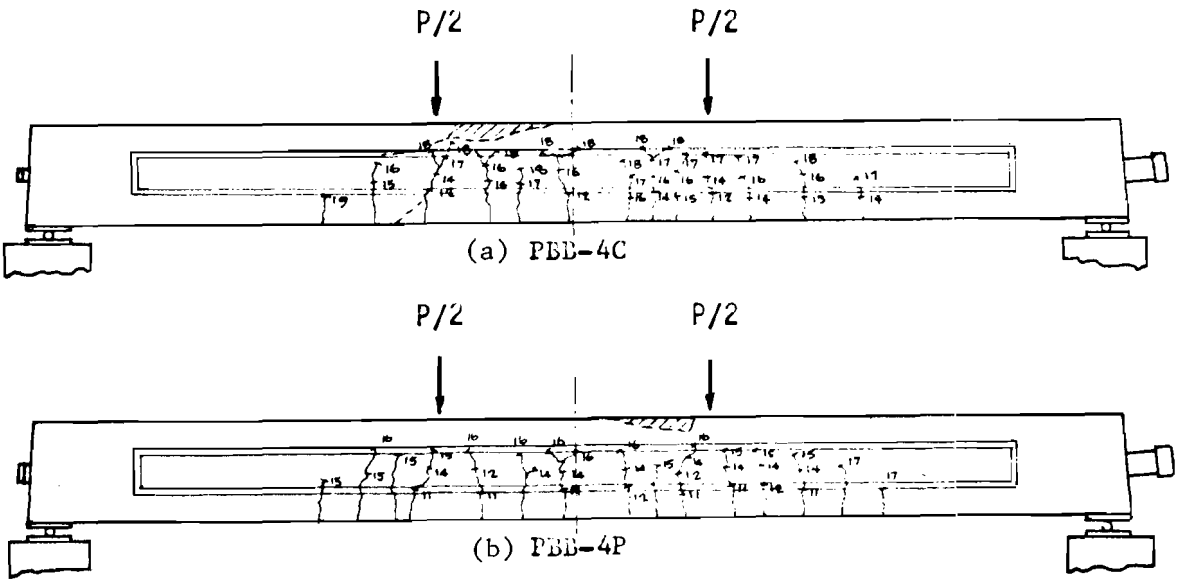

Fig. 5.12 Crack Patterns for PBB-Series Beams.

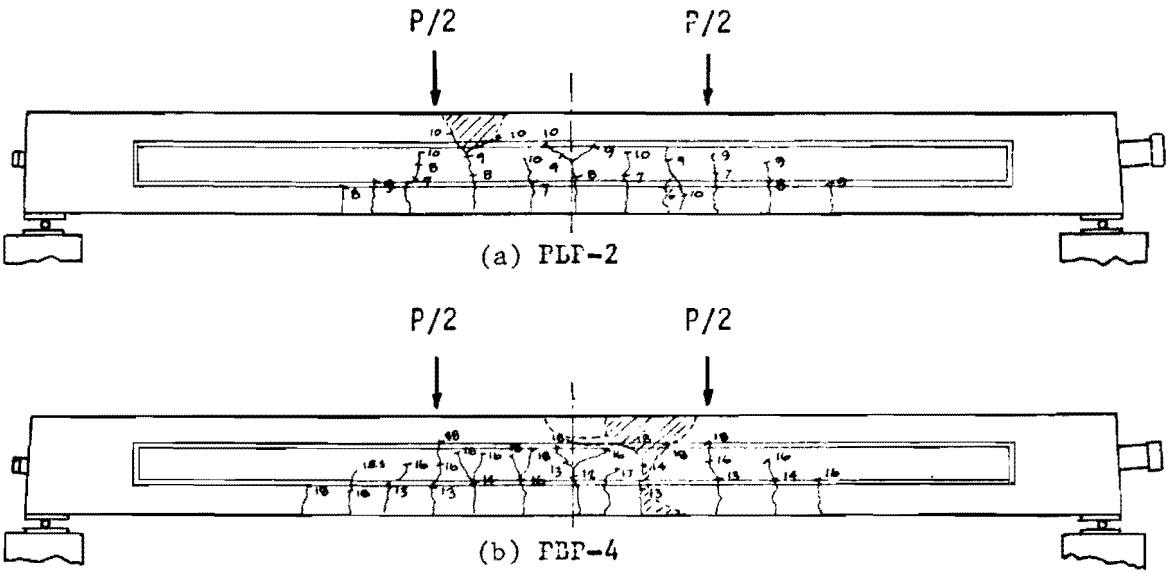

Fig. 5.13 Crack Patterns for PBP-Series Beams.

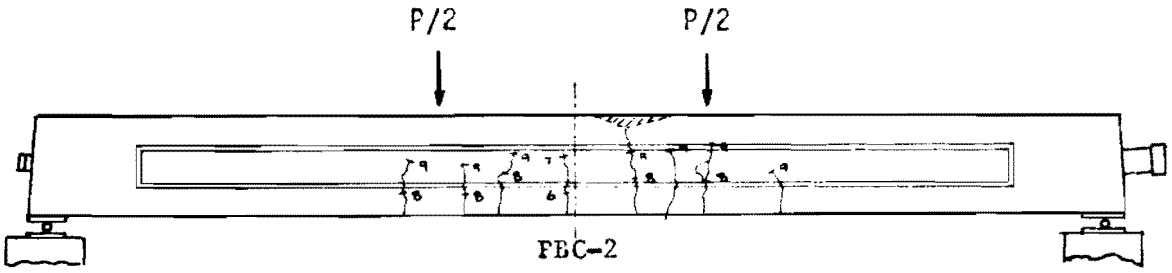

Fig. 5.14 Crack Patterns for Control Beam.

100 percent MMA (for PBF-2), 75 percent MMA + 25 percent BA (for PBM-75), and 50 percent MMA + 50 percent BA (for PBM-50), showed similar crack patterns and the number of visible cracks varied from 9 to 10, even though the beam had different maximum deflections.

PIC Depth. The control beam, without polymer impregnation had fewer cracks than the corresponding PIC beams. Fig. 5.14 shows that the control beam, PBC-2, developed only 8 cracks, and the fully-impregnated beam, PBF-2, shown in Fig. 5.10, had 10 cracks. In fact, the partially-impregnated beam, PBP-2, which had a polymer depth of 2.50 in., developed more cracks than the corresponding fully-impregnated one, PBF-2. It should be also noted that the crack patterns of the partially impregnated beams usually branched before propagating into the PIC zone, apparently due to the different mechanical properties of regular concrete and PIC.

(b) Modes of Failure: Two modes of failure were observed since the beams in this test were all under-reinforced. Initially, the beam failed by excessive elongation of the tendon, which is defined as tension failure. However, at this stage the beam was still able to carry the load but the deflections increased faster in comparison to the load. The flexural cracks progressed toward the top flange but they usually stopped at the neutral axis of the beam, and the cracks propagated until crushing of the compression zone occurred as a secondary failure, which will be classified as a flexural-compression failure. Shaded areas shown in Figs. 5.10 to 5.14 indicate the crushed concrete at failure. Crushing began at the extreme fiber in compression and progressed downward rapidly over the entire compression zone. The later failure occurred suddenly without warning and the failure was explosive, with a loud noise due to the energy release. The volume of crushed concrete and the behavior at final failure depended on several factors.

Number of Wires in Tendons. In the beams with the larger number of wires per tendon, the second failure occurred abruptly after the initial failure. The intensity of the explosive failure was greater due to higher prestressing forces and resisting moments, which caused greater depth of compression block, and to more stored energy. On the other hand, for the beams containing a lower number of wires in the tendon, the secondary failure occcurred with a slight warning after the first failure. Fig. 5.15 compares the modes of failure for the beams containing 2 and 8-wire, unbonded tendons (PBF-2 and

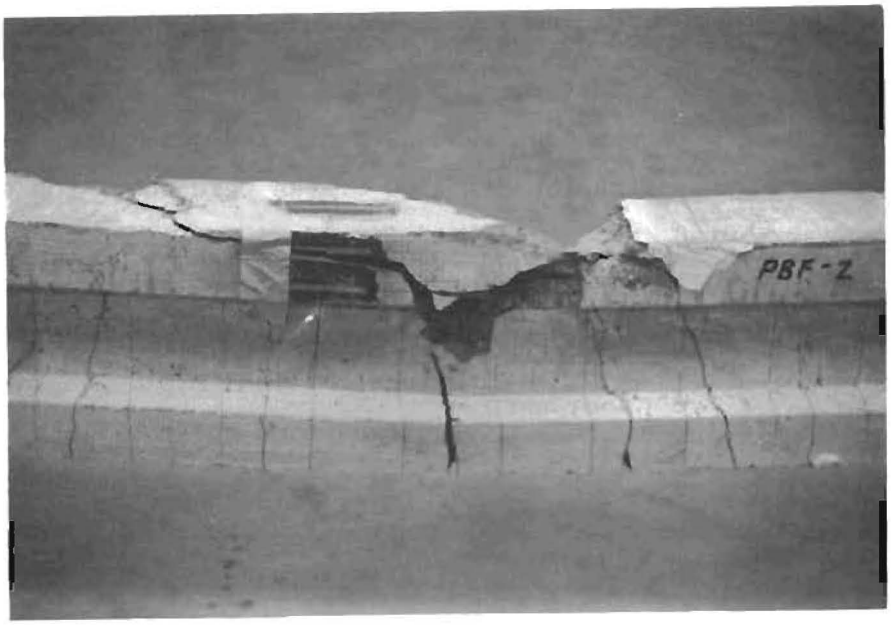

(a) PBF-2

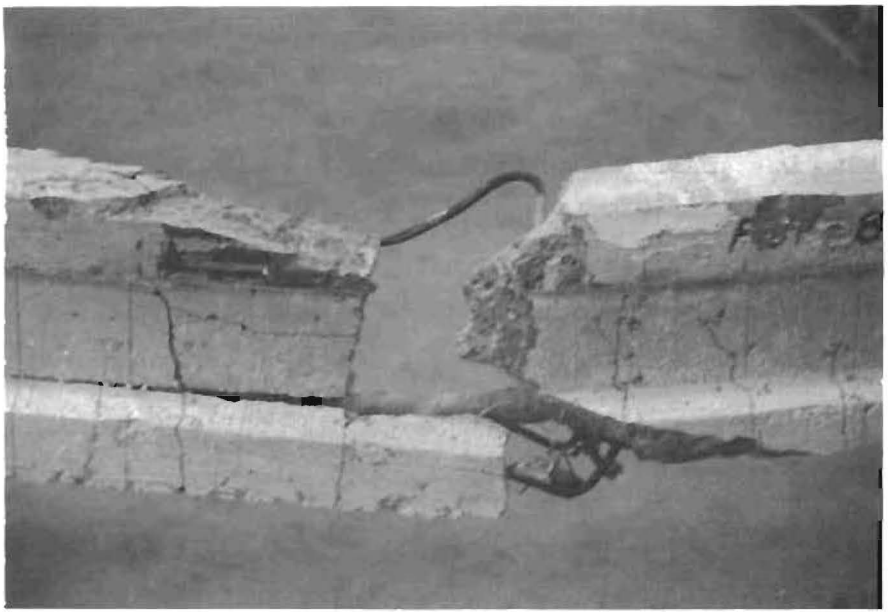

(b) PBF-8

Fig. 5.15 PBF-2 and PBF-8 After Failure.

PBF-8). PBF-2 had only a small amount of crushing on the compression side while PBF-8 totally collapsed as the web crushed.

Bonding Effect. Beams containing bonded tendons had better performance at failure than those with unbonded tendons since they distributed more cracks along the midspan of the beams. The cracks were about the same size and uniformly distributed, which resulted in reducing failure intensity. Fig. 5.16 shows two similar beams after failure: PBF-4 contained a 4-wire, unbonded tendon and PBB-4C contained the same number of wires in the tendon but they were grouted. Beam PBF-4 experienced a loud explosive failure while PBB-4C developed only a small amount of crushing at the top flange.

Monomer Systems. The beams impregnated with 100 percent MMA showed more crushing than the ones which were impregnated with the monomer system which contained BA. However, the test indicated no evidence of any difference in mode of failure between the beams impregnated with 75 percent MMA + 25 percent BA monomer system and the 50 percent MMA + 50 percent BA monomer system. Fig. 5.17 indicates the nearly identical appearances of PBM-75 and PBM-50 after failure. However, PBF-2 developed a greater amount of crushing at the top flange.

Polymer Depth. A comparison of the control beam to the corresponding partially and fully-impregnated PIC beams shows that the crushing volume of the control beam was smaller than both of the PIC beams, e.g., PBC-2 in Fig. 5.18 and PBF-2 in Fig. 5.15 and both in Fig. 5.17. If the comparison is made between the fully-impregnated beam and the partially-impregnated beam, the fully-impregnated beam developed a more violent failure than the partially-impregnated one, as PBP-4 in Fig. 5.18 and PBF-4 in Fig. 5.16.

5.2.5 Strain Distributions

The measured distributions of strain over the depth at midspan of the beams are presented in Figs. 5.19 through 5.21. The strain distributions were obtained by averaging the readings on individual gauge lines on opposite sides of the beam. The individual distributions are plotted with respect to the load level as labelled, and F indicates failure.

For all of the beams, the variation of strain with depth before cracking was linear. However, after cracking, the strain distributions became nonlinear, especially when the applied load approached the ultimate load.

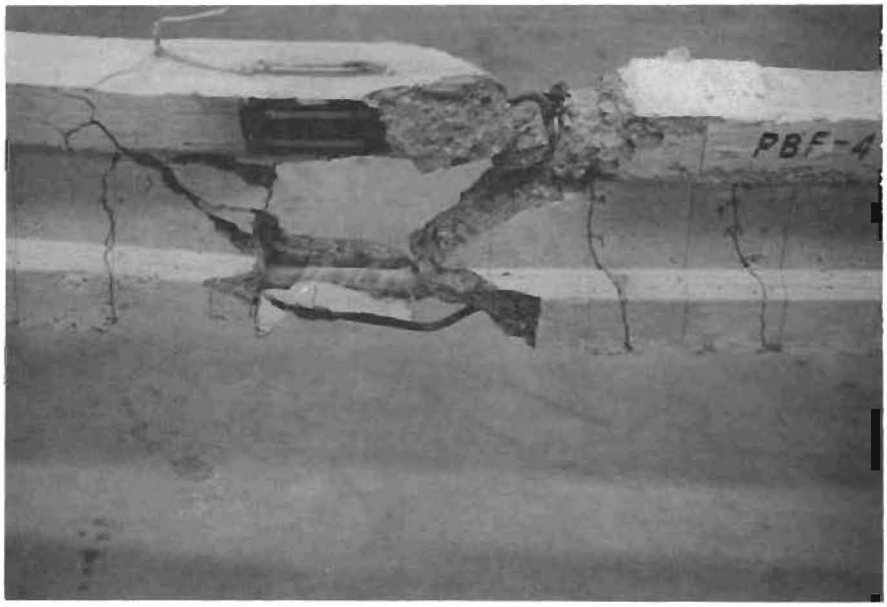

(a) PBF-4

(b) PBF-4C

Fig. 5.16 Bonded and Unbonded Beams After Failure.

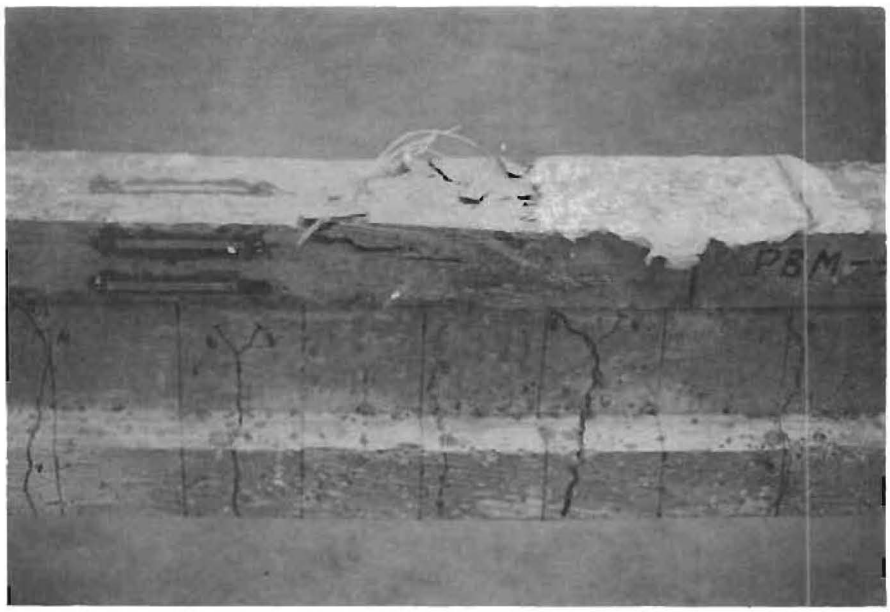

(a) PBM-50

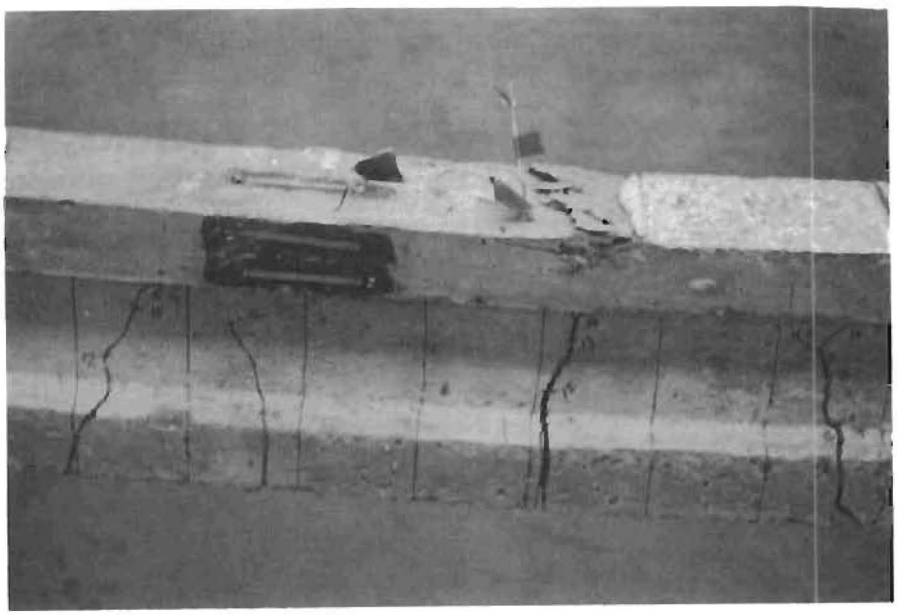

(b) PBM-75

Fig. 5.17 Beams with Different Monomer Systems After Failure.

(a) PBC-2

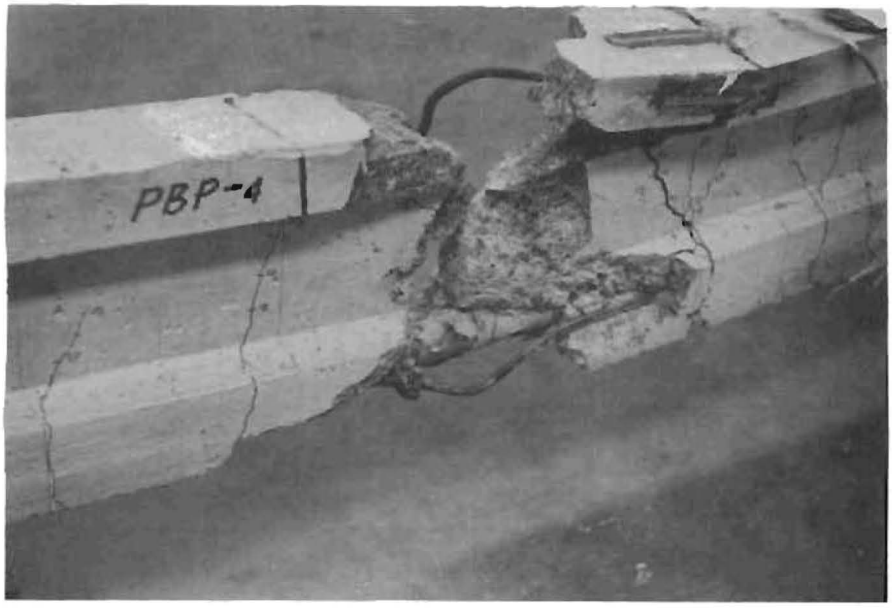

(b) PBP-4

Fig. 5.18 Control Beam and Partially Impregnated Beams After Failure.

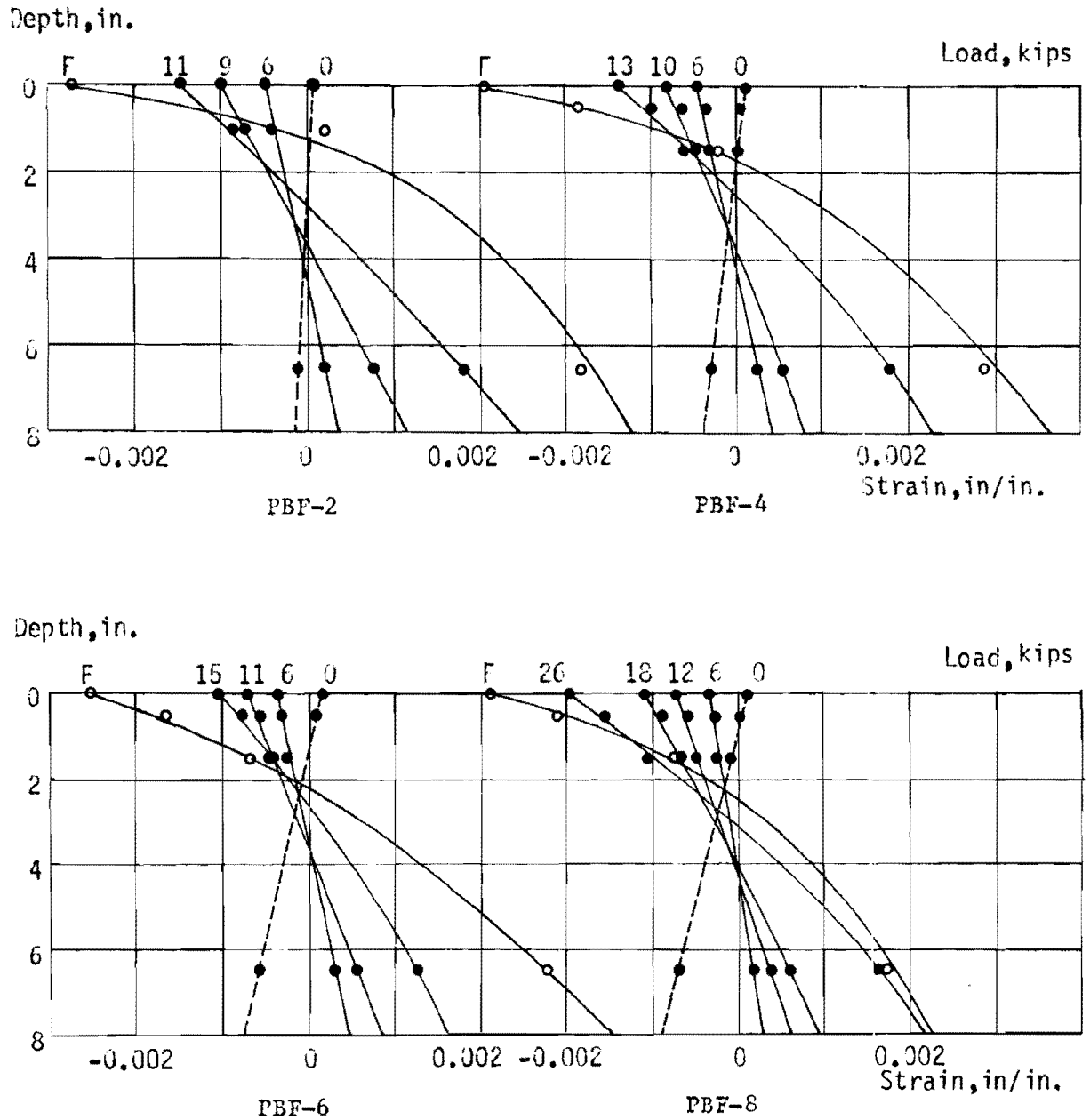

Fig. 5.19 Measured Strain Distributions for PBF-Series Beams.

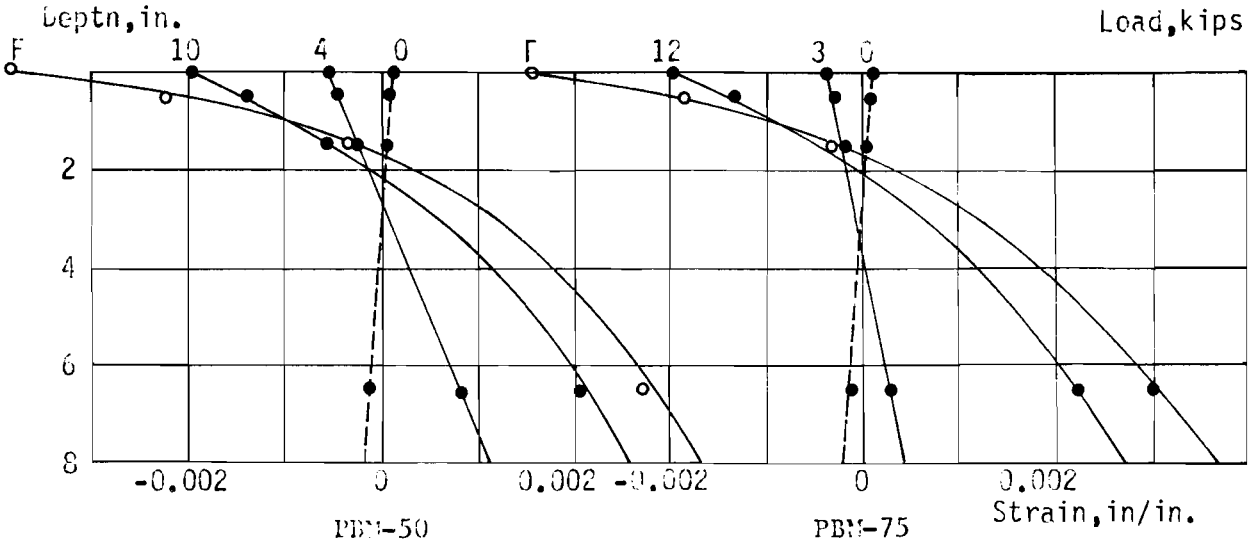

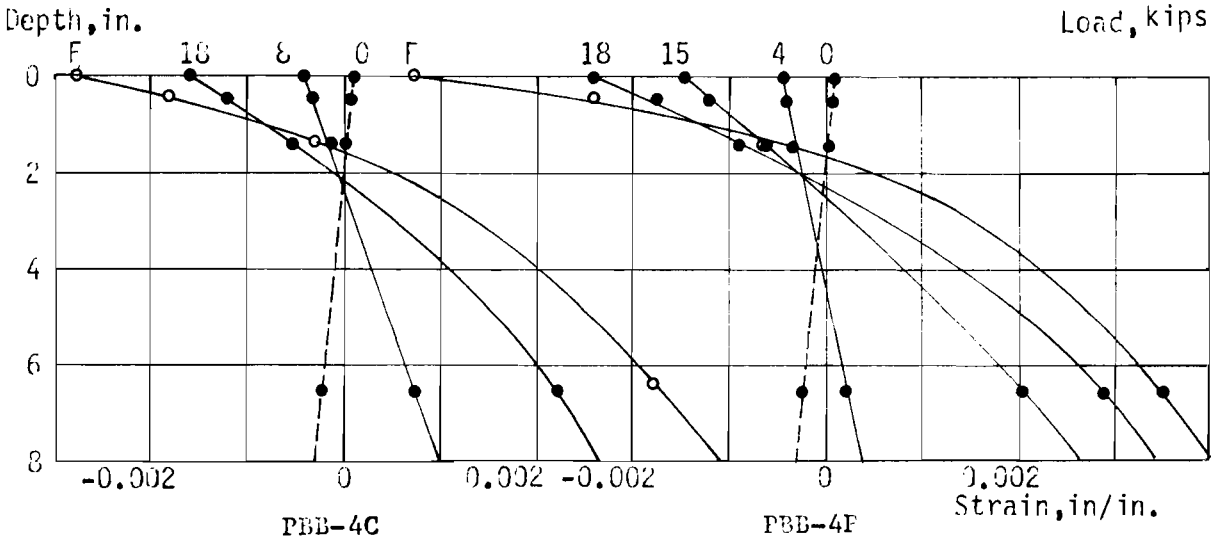

Fig. 5.20 Measured Strain Distributions for PBM and PBB Series Beams.

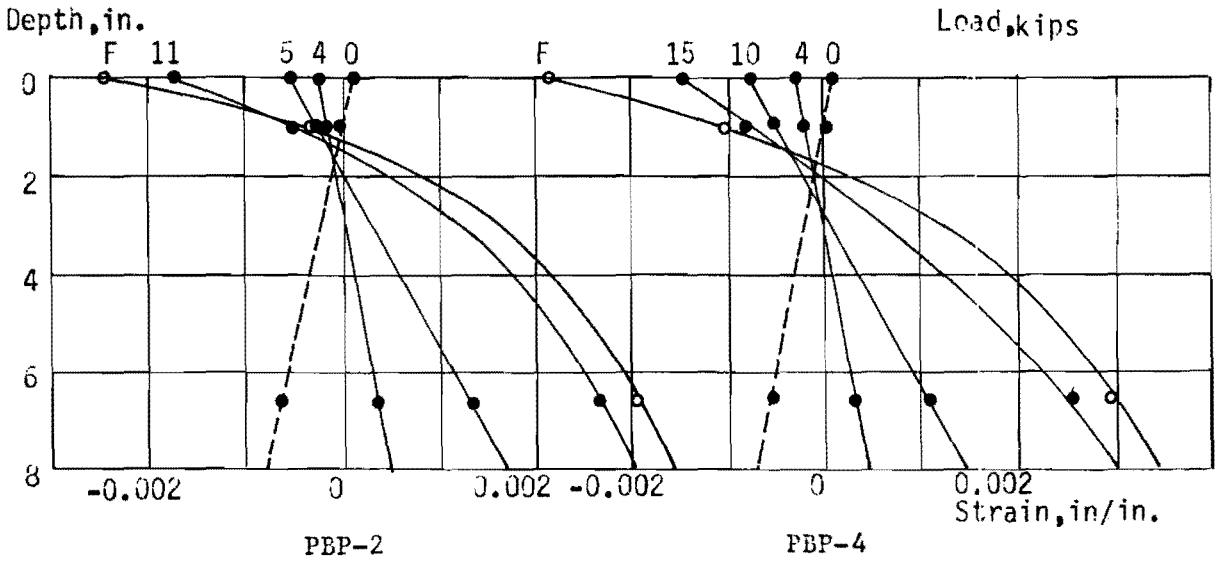

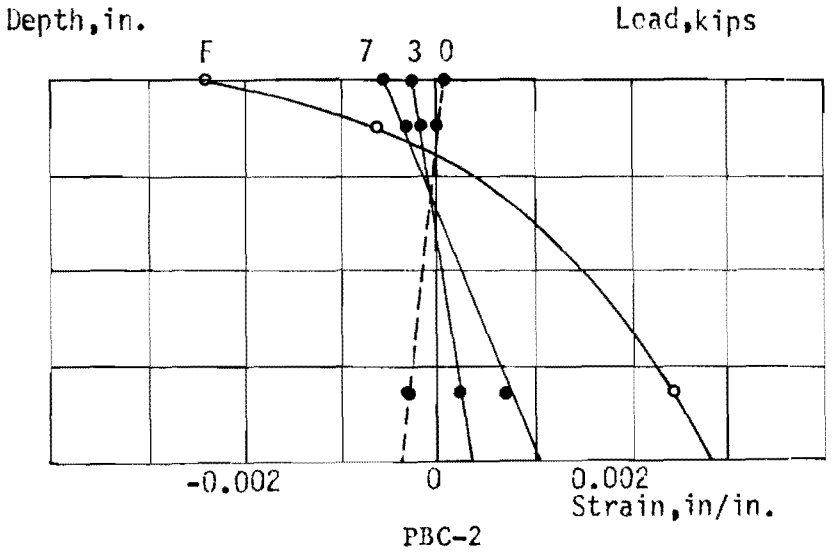

Fig. 5.21 Measured Strain Distributions for PBP and PBC Series Beams.

Cracks in the region of the flexural span would be considered to influence the strain distributions.

For unbonded beams, the strain distributions at failure for beams of the PBF series were similar; however the strain magnitudes differed. The strain at the tendon level for beams with higher percentages of steel was less than that for the one with a lower percentage of steel but the strains at the top extreme fiber for all the beams in this series were about the same. The top fiber strains for beams with 75 percent and 50 percent MMA-polymer impregnation were higher than the ones for the 100 percent MMA-polymer impregnated beams.

For bonded beams, in which cracks were more uniformly distributed over the flexural span, the strain distributions at failure were similar to those for unbonded beams but the strains were higher at both the top fiber and steel levels. The top fiber ultimate strain for the beam with polymer grouting was also higher than for the one with conventional grouting.

In the analysis of the bending stress, the assumption is usually made that the strains are distributed linearly over the depth of the beam. According to the measurement, some deviation from linearity existed due to inaccuracies in individual strain measurement or to small errors in locating the gauge lines. It is evident from the figures, however, that a reasonable agreement exists between the strains on the reinforcing steel and on the concrete surface. Hence it is assumed that Bernoulli's hypothesis is valid.

5.2.6 Deflection Curves

The deflections of all beams tested for flexure were observed by means of dial indicators which were attached to the top surfaces of the beams as described in Sect. 4.1.3. Figs. 5.20 through 5.24 show the deflection curves for each test beam corresponding to the load at first cracking, at 75 percent of ultimate load, and at ultimate load, respectively. The deflected shape of the beams is approximately a half sine wave. Some deviation from a sine wave, however, would be expected beyond the elastic range due to the wide cracks and slight inaccuracies in individual deflection measurements.

The deflected shapes of the beams were also calculated on the basis of the second integral of the M/EI diagram. They were found to agree with the test

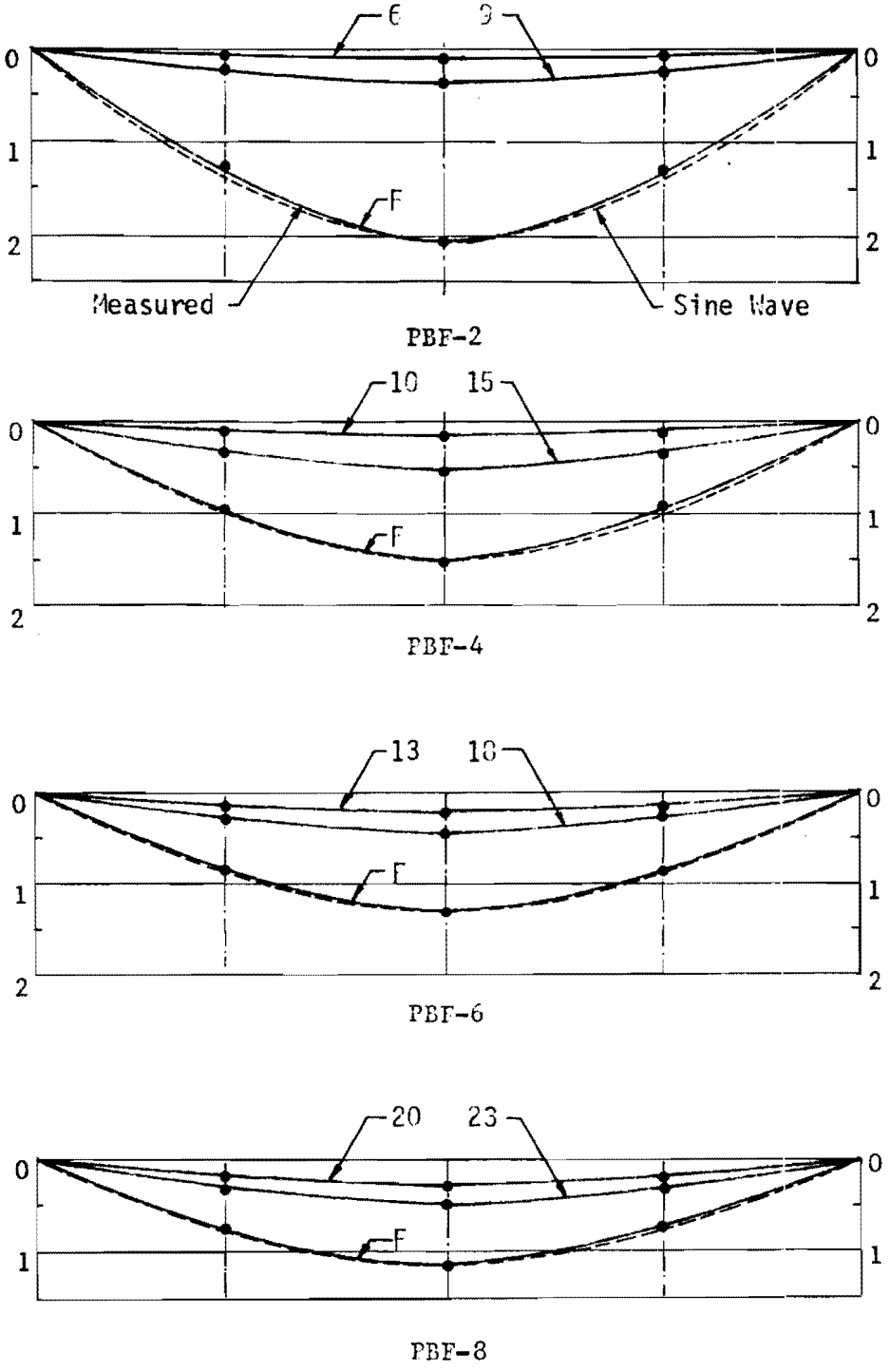

Fig. 5.22 Deflection Curves for PBF-Series Beams.

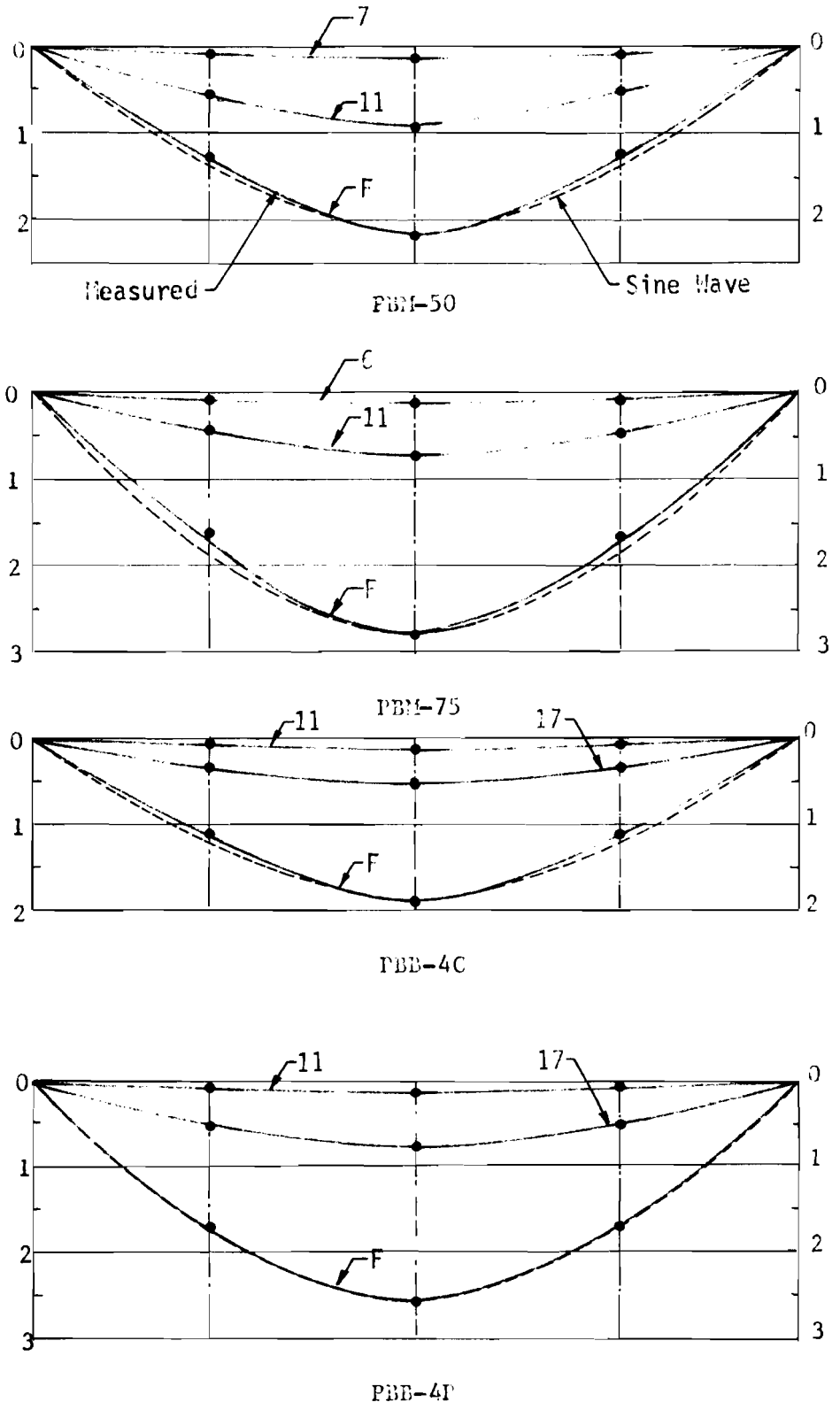

Fig. 5.23 Deflection Curves for PBM and PBB Series Beams.

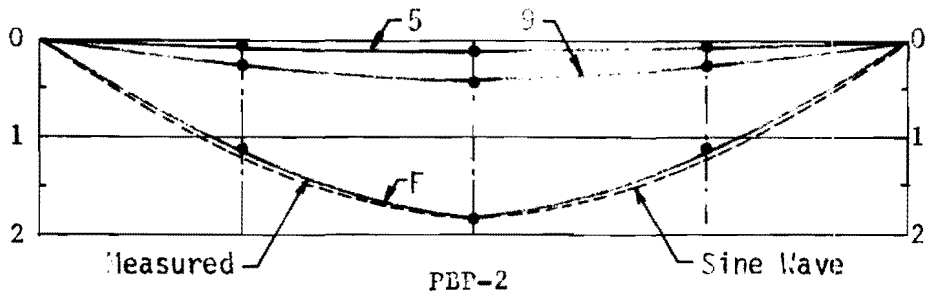

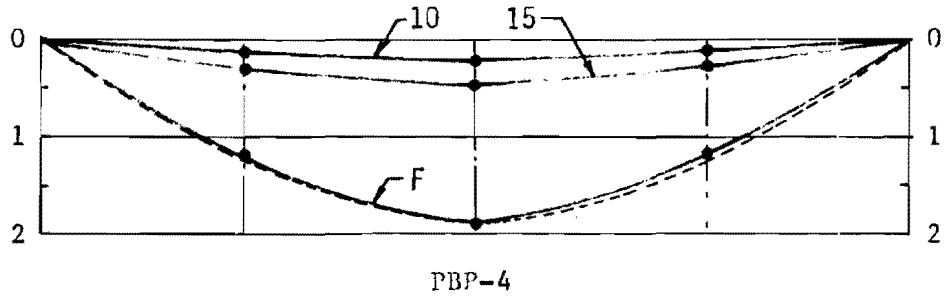

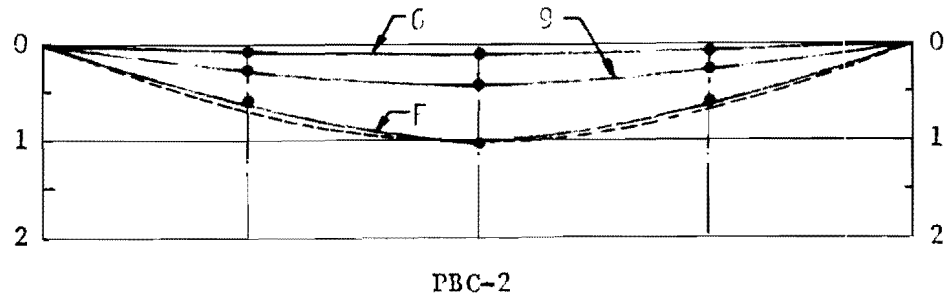

Fig. 5.24 Deflection Curves for PBP and PBC Series Beams.

results and with deflected shapes found from calculations based on an assumed half-sine wave shape for the curvature diagram.

5.3 Evaluation of Test Results

The evaluation of test results presented in this section will primarily concern the flexural behavior of post-tensioned PIC beams. Moment-curvature relationship, PIC stress distribution, friction loss, and some structural properties of PIC will be evaluated. Comparison of theoretical analysis to the test results will be made regarding tendon stress and load-deflection responses.

5.3.1. Friction Loss

Since tendon forces at both ends of the beams were measured during the stressing process, the frictional losses can be determined. Table 5.5 shows the maximum stressing force at one end and the holding force at the other end. Losses were determined as percentages of the stressing forces. The calculated holding forces presented in Table 5.5 were evaluated by Eq. 2.6, based on the coefficients $K = 0.002$, $\mu = 0.15$ for mastic-coated unbonded tendons and $K = 0.0015$, $\mu = 0.25$ for grouted tendons in metal sheathing. These coefficients are recommended in the ACI Building Code (43). Test results show very good agreement with predicted values for the control beam. However, they are slightly higher than the predicted values for PIC beams with mastic-coated and paper-wrapped tendons. On the other hand, the predicted values were less than the measured ones for the PIC beams with grouted tendons in metal sheathing conduit.

After the tests, the paper-wrapped conduits for unbonded beams were broken open to examine the tendons inside and it was found that the tendons were coated with the polymer. It is believed that the mastic-coated materials which were used for coating the tendons attacked or dissolved in the monomer during soaking, and the excess monomer may have been polymerized during the curing process. The polymer coating could have increased the friction coefficients between the tendons and surrounding materials.

Table 5.5

Friction Losses for Each Test Beam

Test Series	Beam No.	Maximum Stressing Forces F_1 (kips)	Measured Holding Forces F_2 (kips)	Calculated Holding Forces F_2 (kips)	Ratio $\frac{F_2 \text{test}}{F_2 \text{ cal.}}$	Measured Loss(%) $\frac{F_1-F_2}{F_1}$
PBF	PBF-2	17.50	15.00	16.67	0.90	14.30
	PBF-4	34.60	29.10	32.96	0.88	15.90
	PBF-6	51.40	44.60	48.97	0.91	13.20
	PBF-8	69.70	60.70	66.40	0.91	12.90
PBM	PBM-50	16.55	14.20	15.76	0.90	14.20
	PBM-75	16.55	14.00	15.76	0.89	15.40
PBB	PBB-4C	35.90	35.02	33.59	1.04	2.40
	PBB-4P	35.90	34.84	33.59	1.04	2.90
PBP	PBP-2	16.55	14.20	15.76	0.90	14.20
	PBP-4	35.25	31.00	33.58	0.92	12.00
Control	PBC-2	16.20	15.00	15.43	0.97	7.40

To evaluate the friction coefficients, Eq. 2.6 may be written as

$$\mu = \frac{\frac{F_1 - F_2}{F_1} - KL}{\theta} \qquad (5.1)$$

If the wobble friction coefficient, K, in Eq. 5.1 is known or assumed, then the curvature friction coefficient, μ, can be determined experimentally. Types of duct, tendon, and coating material are the essential factors affecting the wobble coefficient.

For the control beam, PBC-2, the wobble coefficient, K, was assumed to be 0.0015, based on the recommendation in the ACI Code 318-71 (43). The calculated value of friction coefficient, μ, was 0.30, which was in good agreement with the ACI recommendation. This value confirmed the test results reported in Refs. 20, 37, and 38.

For PIC beams in the PBB Series, tendons were in oversized metal sheathing ducts for the purpose of grouting. Since excess monomer in the conduits and around the tendons were blown out by means of 60-psi air source, wobble and friction coefficients would seem to be about the same as for unimpregnated beams. To find the actual friction coefficient, μ, the wobble coefficient, K, was assumed to be 0.0005, based on the ACI recommendation for grouted tendons. The calculated values were between 0.10 and 0.12, which are about 40 percent less than for test results by Guyon presented by Lin (37), but these values were in good agreement with the ACI Building Code.

For PIC beams with unbonded tendons, the losses as shown in Table 5.5 were averaged to be 14.0 percent. This indicated frictional loss can be divided into length and curvature effects. The curvature friction coefficient, μ, for drawn wires with roughly finished concrete surfaces as tested by Leonhardt (29) was in the range of 0.35 to 0.44. Similar tests for the Freyssinet system had been conducted in France by Guyon (44); the friction coefficients for paper-wrapped uncoated wires were in the range of 0.32 to 0.43. Since the lubrication around the tendons might have been destroyed and the polymer coating on the tendon could have increased the friction coefficient, the maximum value from these two tests was selected to evaluate the wobble coefficient, K. Substituting the values in Eq. 5.1, K will be 0.0059, corresponding to μ of 0.44 and average loss of 14 percent.

However, the wobble effect varies greatly with the amount of vibration used in placing the concrete and upon the spacing and stiffness of the support for the tendons. As an example, for Freyssinet cables in continuous plastic sheaths, the K values can be as high as 0.0040 if moderate vibration is applied to the concrete (38). It can be higher if heavy vibration is applied during concrete placing. It seems reasonable to assume a K value of 0.005 since the polymer coating on the tendon may be similar to the plastic sheath and heavy vibration was applied to the concrete.

The μ values as shown in Table 5.6 vary from 0.40 to 0.56. It should be noted that the number of tendons may have had some effect on friction coefficients, with the higher the number of tendons the lower the friction coefficients. The average value of μ was 0.49.

5.3.2 Useful Limit of Strain for Polymer-Impregnated Concrete

The useful limit of strain for concrete in flexure can be determined from measurements of compression strain in the extreme concrete fiber in the failure region of a beam. As shown in Figs. 5.19 through 5.21, the values of the maximum measured strains vary from 0.0026 to 0.0044. Several factors contribute to such a large range of values. Monomer system, polymer depth, type of tendon and grouting material would affect the maximum top fiber strains. Although shape of the cross section is not the independent variable in these tests, a comparison of the measured strain to those for inverted T-beams reported in Ref. 11 indicates shape to be another factor to influence the useful limit of strain.

Table 5.7 shows the average compressive strain and the range of strains for each test series, including the PBS-series which was designed to test beams for shear strengths. The shear strengths for the PBS-series will be presented in Chapter 6. Since the PBS-series beams failed in shear-compression, it is appropriate to discuss the maximum compressive strains in this section.

For post-tensioned PIC beams containing unbonded tendons and produced by a 100 percent MMA-monomer system, the measured strains were plotted with respect to the corresponding cylinder strength (Fig. 5.25) and the relationship can be written as

Table 5.6

Friction Coefficients Calculated From Test Results

Test Series	Beam No.	$\frac{F_1-F_2}{F_1}$	Assumed K	μ
PBF	PBF-2	0.1428	0.0050	0.48
	PBF-4	0.1589	0.0050	0.56
	PBF-6	0.1323	0.0050	0.44
	PBF-8	0.1291	0.0050	0.42
PBM	PBM-50	0.1420	0.0050	0.49
	PBM-75	0.1540	0.0050	0.54
PBB	PBB-4C	0.0245	0.0005	0.10
	PBB-4P	0.0295	0.0005	0.12
PBP	PBP-2	0.1420	0.0050	0.49
	PBP-4	0.1205	0.0050	0.40
Control	PBC-2	0.0740	0.0015	0.30

Table 5.7

Average Measured Values of Concrete Strain at Failure

Test Series		Description of Variables	Range of Strains	Average Measured Strain
PBF		100% MMA, full impregnation, unbonded	0.0026-0.0030	0.0028
PBS		100% MMA, full impregnation, unbonded	0.0027-0.0031	0.0029
PBP		100% MMA, partial impregnation, unbonded	0.0030-0.0031	0.0031
PBM	PBM-50	50% MMA + 50% BA, full impregnation, unbonded	-	0.0039
	PBM-75	75% MMA + 25% BA, full impregnation, unbonded	-	0.0034
PBB	PBB-4C	100% MMA, full impregnation, conventional cement grouting	-	0.0028
	PBB-4P	100% MMA, full impregnation, polymer grouting	-	0.0044
PBC		Unimpregnated control, unbonded	-	0.0027

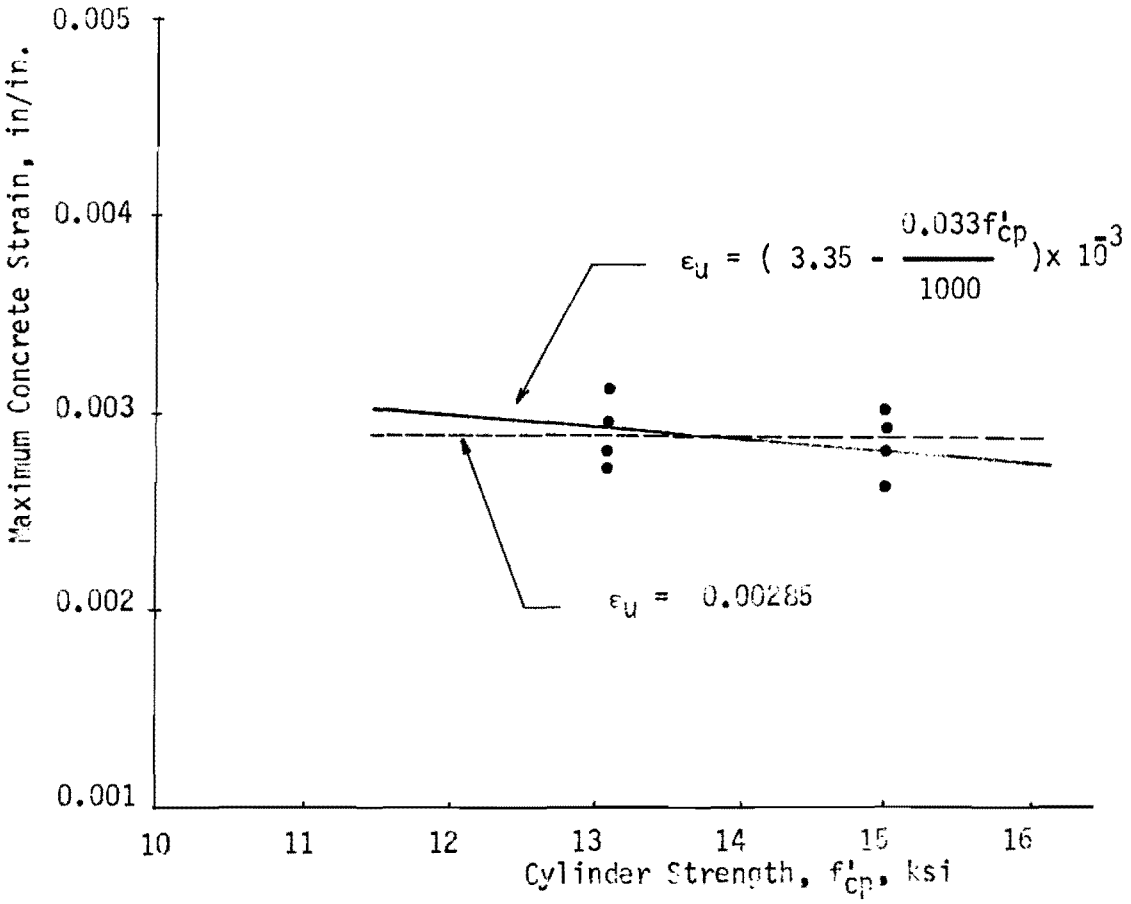

Fig. 5.25 Measured Values of Concrete Strain at Failure.

$$\varepsilon_u = \left(3.35 - 0.033 \frac{f'_{cp}}{1000} \right) 10^{-3} \qquad (5.2)$$

where ε_u = maximum compressive strain, in./in.

f'_{cp} = cylinder strength of PIC, psi.

However, the difference between the average strains for two test series, as shown in Fig. 5.25, is insignificant; the plots may be reasonably fitted by a horizontal line which represents a constant strain of 0.00285 for any strength of PIC.

It should be noted that the useful limits of strain considered in this section are for post-tensioned PIC beams containing unbonded tendons; for other kip parameters, the magnitude of useful limit of strain may be different.

5.3.3 Moment-Curvature Relationship

The moment-curvature diagrams shown in Figs. 5.26 through 5.28 were evaluated from the load-deflection response. Since the deflected shape of the beams has been confirmed by this test to be a half sine wave function of midspan deflection, the curvature at each load increment is the second derivative of the function. Similarly, the corresponding moments can be derived from the applied loads by means of the structural analysis. Actually, the moment-curvature relationship in this test program is similar in shape to the load-deflection response for each beam. However, the load-deflection relationship presented in Sect. 5.2 assumes zero deflection after the beam had been post-tensioned and the applied load was zero, while the moment-curvature relationship was considered to be zero prior to post-tensioning. Immediately after post-tensioning, the beam cambered upward due to the prestressing force; the curvature at this point was considered to be negative. As the external applied load or moment increased, the negative curvature decreased and the curvature became positive after the beam deflected through the reference level and moved downward. The curvature was linear up to the cracking moment and then became nonlinear up to the ultimate moment. Table 5.8 summarizes the curvature and moments at initial cracking and ultimate load for each test beam.

Rotation capacity, which is defined as a ratio of the curvature at ultimate to the corresponding curvature at the first cracks, could reasonably

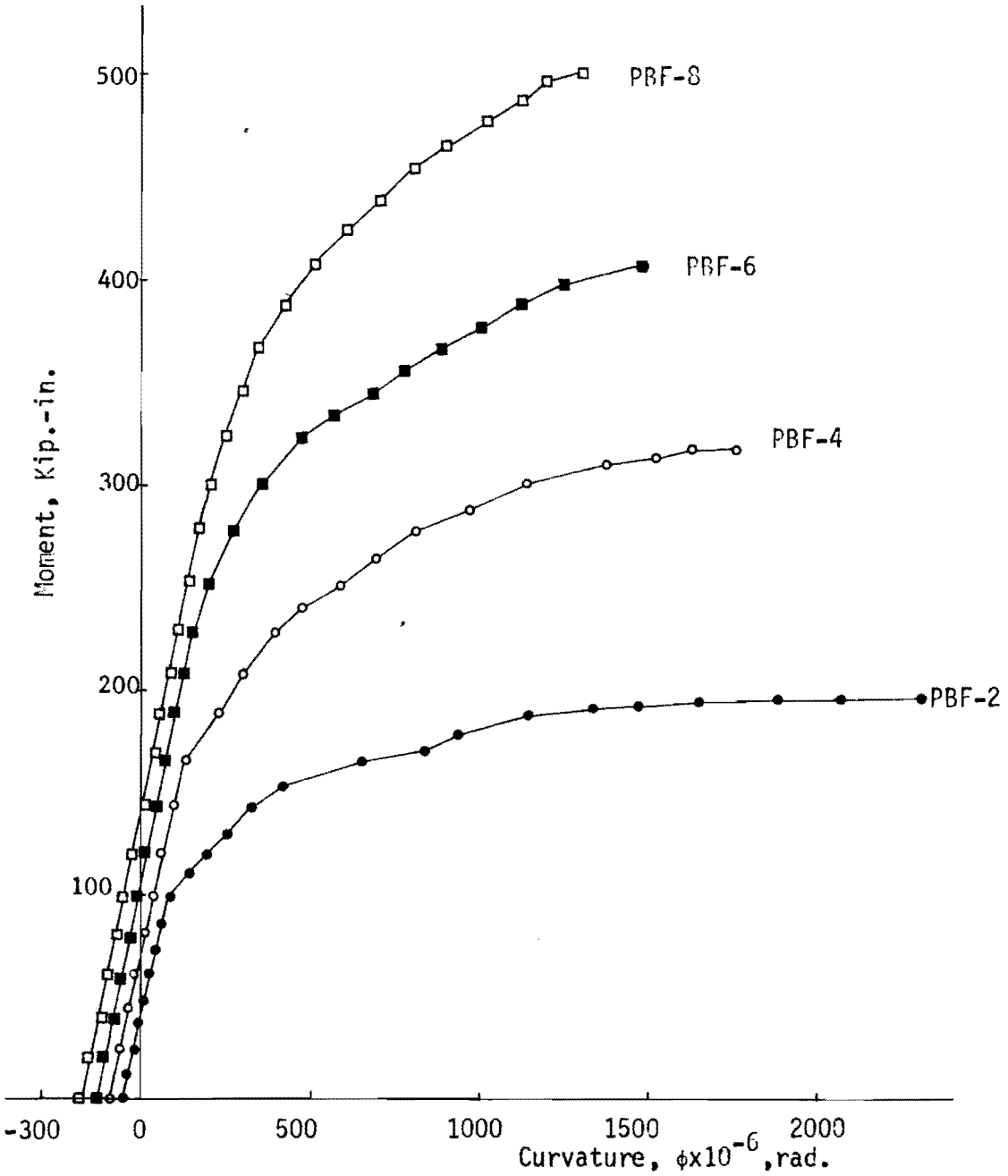

Fig. 5.26 Moment-Curvature Relationships for PBF-Series Beams.

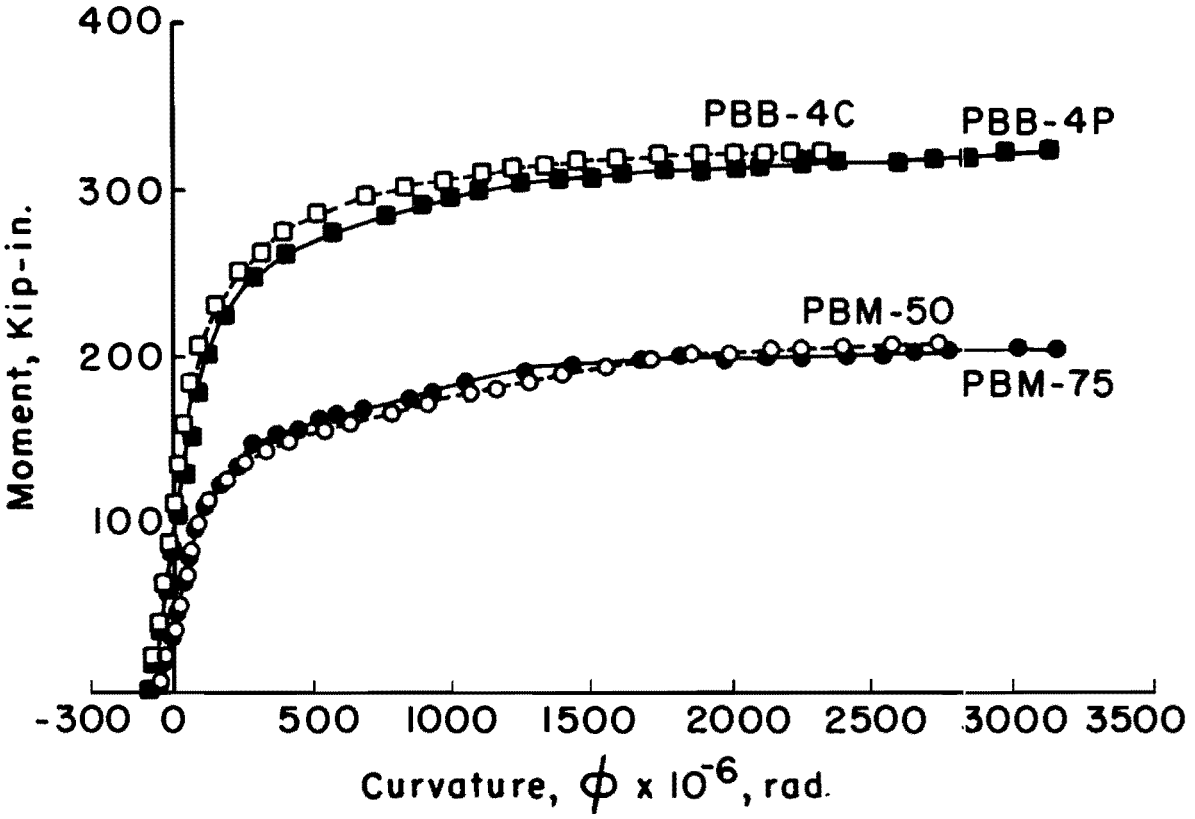

Fig. 5.27. Moment-Curvature Relationships for PBB and PBM-Series Beams.

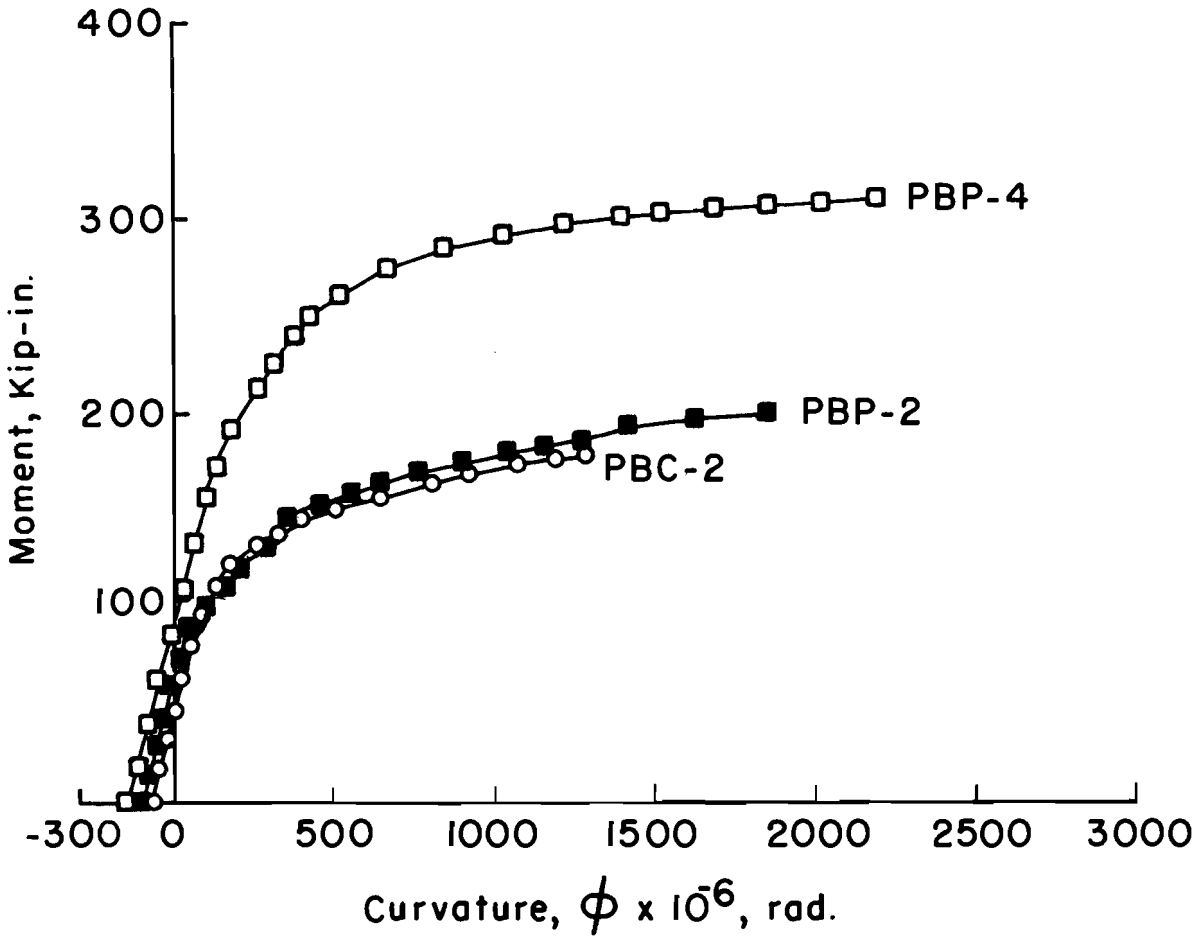

Fig. 5.28. Moment-Curvature Relationships for PBP and PBC-Series Beams.

Table 5.8

Moments and Curvatures at Initial Cracking and Ultimate for Flexural Test Beams

Test Series	Specimen No.	Cracking		Ultimate		Rotation Capacity ϕ_u/ϕ_{cr}
		Moment M_{cr} (lb-in)	Curvature ϕ_{cr} (rad x 10^{-3})	Moment M_u (lb-in)	Curvature ϕ_u (rad x 10^{-3})	
PBF	PBF-2	99,000	0.0930	196,000	2.550	27.5
	PBF-4	165,000	0.1340	318,000	1.770	13.2
	PBF-6	228,000	0.1580	408,000	1.500	9.5
	PBF-8	300,000	0.2000	503,000	1.310	6.6
PBM	PBM-50	99,800	0.1080	210,000	2.720	25.1
	PBM-75	99,800	0.0950	212,000	3.450	36.3
PBB	PBB-4C	181,000	0.0731	328,000	2.310	31.5
	PBB-4P	181,000	0.0914	325,000	3.120	34.1
PBP	PBP-2	88,300	0.0767	204,000	2.280	29.7
	PBP-4	158,000	0.1100	311,000	2.200	20.0
PBC	PBC-2	94,100	0.0914	178,000	1.290	14.1

represent the ductility of the post-tensioned PIC beams tested for flexure. Beams with high values of rotation capacity usually develop large deflections and have a warning before failure occurs. The test results summarized in Table 5.8 indicate the rotation capacity is affected by many factors, such as number of tendons or percentage of prestressing steel, tendon type, monomer system, and polymer depth. The effects of these independent variables can be described as follows:

Number of Tendons. Beams with a higher number of tendons developed less rotation capacity than those with a lower number of tendons; the PBF-series beams containing 2, 4, 6, or 8 unbonded wires have a rotation capacity of 27.46, 13.24, 9.46, and 6.55, respectively. It is evident that a beam with a low percentage of prestressing steel is more ductile than a beam with a higher percentage of steel.

Tendon Type. Beams containing bonded tendons developed higher rotation capacity than the one containing the same number of unbonded wires. The grouting materials slightly affect the rotation capacity of the beams; the bonded beams grouted with polymer developed about 10 percent higher rotation capacity than the one grouted with conventional cement and the bonded beams had more than twice the rotation capacity than unbonded beams.

Monomer System. The PIC beam produced with a 75 percent MMA + 25 percent BA monomer system seemed to develop the highest rotation capacity in comparison to the other two monomer systems (100 percent MMA and 50 percent MMA + 50 percent BA). The PBF-2 beam, which was impregnated with a 100 percent MMA monomer system, had a slightly higher rotation capacity than PBM-50, which was impregnated with a 50 percent MMA + 50 percent BA monomer system. However, the rotation capacities for both PBF-2 and PBM-50 were about 70 and 75 percent of that for PBM-75, respectively.

Polymer Depth. For unbonded beams, the rotation capacity for a fully impregnated beam was generally higher than for the unimpregnated control but it was less than for the corresponding partially impregnated concrete beams.

5.3.4 Structural Properties of Polymer-Impregnated Concrete for Flexural Members

There are many factors which affect the strength and modulus of PIC, such as monomer systems, polymer loadings, and impregnation techniques (1, 10). It has been found that the concrete mix design affects them only

slightly (3, 4). Four groups of concrete cylinders produced with different monomer systems and mix designs corresponding to the test beams were tested for compressive strength, modulus of elasticity, and splitting tensile strength and the test results are shown in Table 3.1.

(a) Stress-Strain Relationship: The stress-strain relationships for PIC cylinders subjected to repeated high intensity compressive loading are shown in Fig. 5.29. The stress-strain envelopes as shown were found to be almost identical to the curves obtained from a single continuous load application (40, 41).

For PIC produced with a 100 percent MMA monomer system, the curve was linear up to about 75 percent of the ultimate strength; at that point the curve deviated from a straight line to reach the maximum stress. The curve dropped abruptly after reaching the peak. The ultimate strain was about 0.0036 in./in.

PIC produced with a 75 percent MMA + 25 percent BA monomer system developed higher strength than that produced with a 50 percent MMA + 50 percent BA monomer system. The stress-strain curves for the 50 percent MMA + 50 percent BA PIC indicated higher ultimate strains and greater ductility than those for the 75 percent MMA + 25 percent PIC.

(b) Modulus of Elasticity: The modulus of elasticity, E_{cp}, of PIC can be estimated in terms of compressive strength, f'_{cp}, based on the plot in Fig. 5.30, by using Eq. 5.3. However, this expression is good for the PIC produced with the 100 percent MMA, 75 percent MMA + 25 percent BA, and 50 percent MMA + 50 percent BA monomer systems.

$$E_{cp} = 53{,}000 \sqrt{f'_{cp}} \qquad (5.3)$$

where f'_{cp} = compressive cylinder strength of PIC, psi

E_{cp} = modulus of elasticity of PIC, psi.

(c) Compressive Strength: The compressive strength, f'_{cp}, of PIC produced with the 100 percent MMA monomer system and percentage of polymer loading (PL) were plotted in Fig. 5.31. By linear regression an equation expressing the relation can be written as

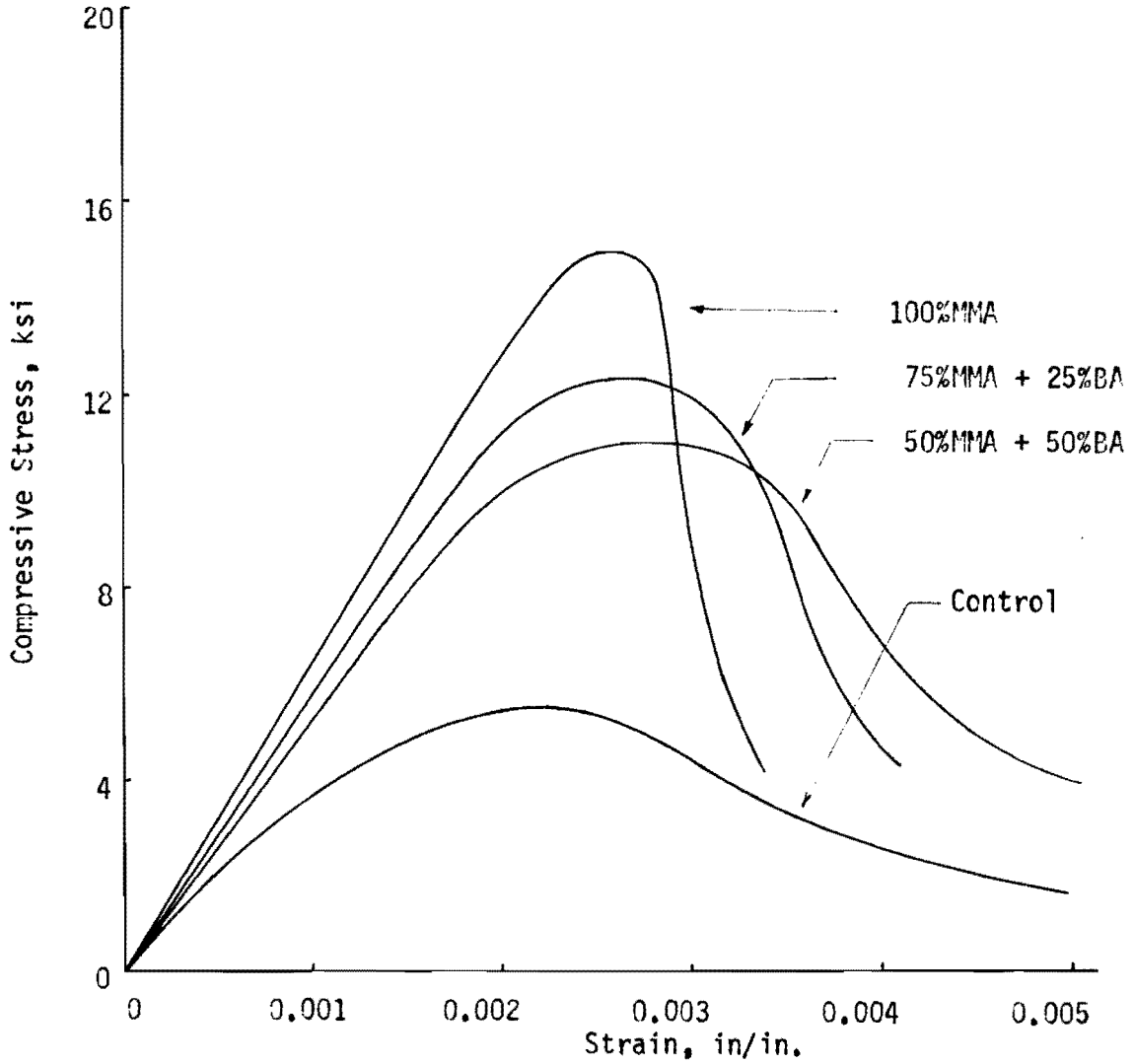

Fig. 5.29 Stress-Strain Relationship of Cylinders Subjected to Repeated High-Intensity Loading.

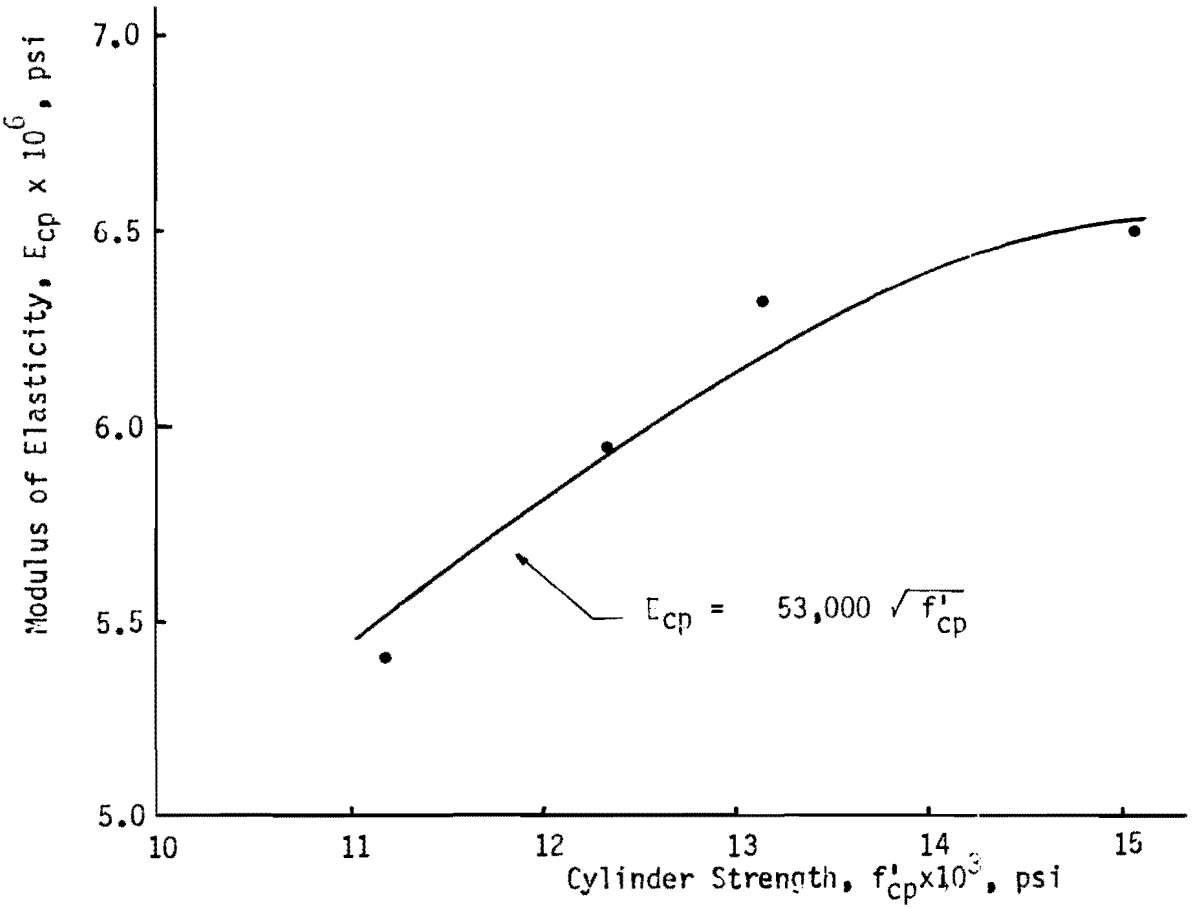

Fig. 5.30 Relationship Between Modulus of Elasticity and Cylinder Strength of Polymer-Impregnated Concrete.

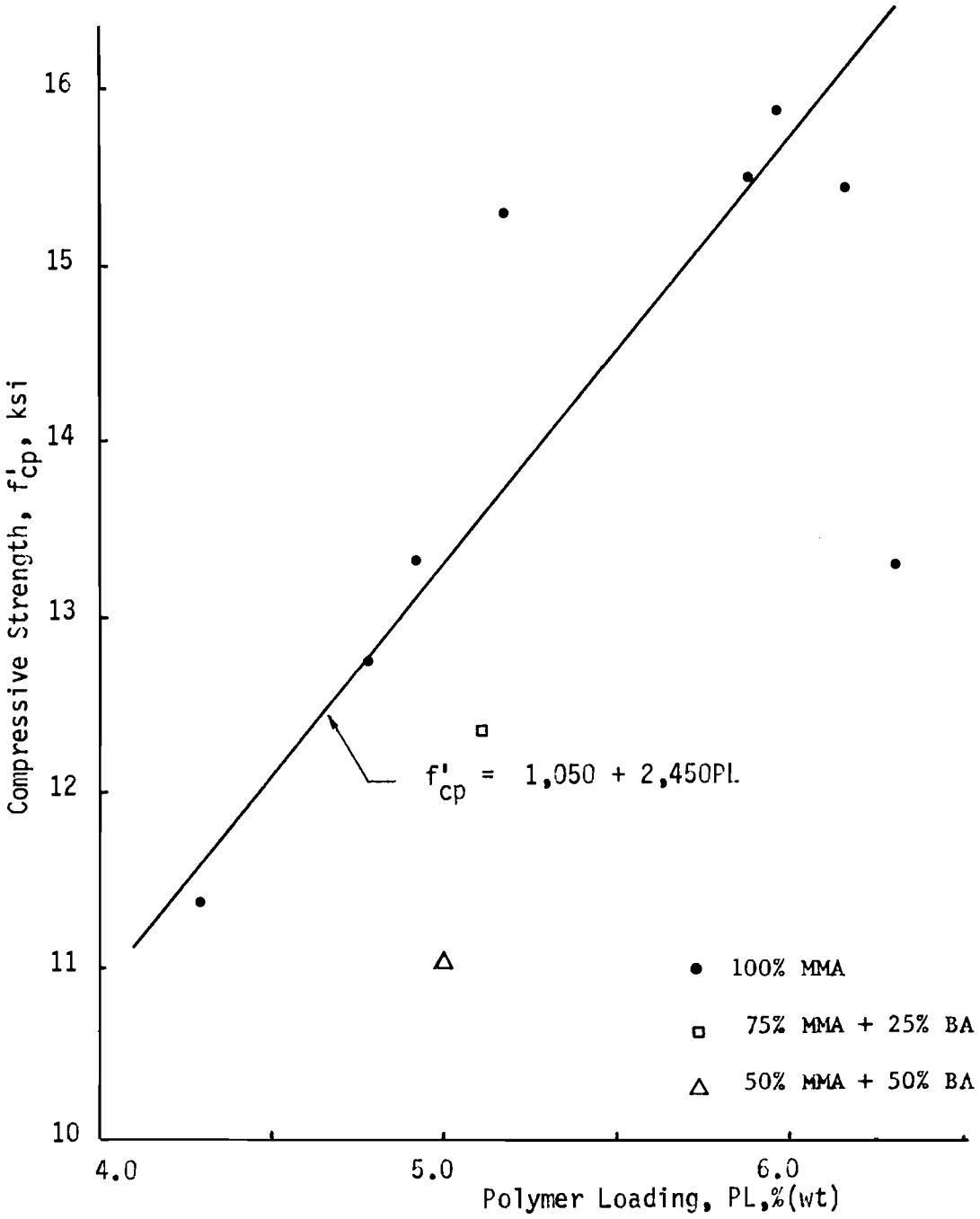

Fig. 5.31 Relationship Between Compressive Strength and Polymer Loading of 100% MMA Polymer-Impregnated Concrete.

$$f'_{cp} = 1{,}050 + 2{,}450\ (PL) \qquad (5.4)$$

where f'_{cp} = compressive cylinder strength of PIC, psi

PL = polymer loading (percent).

For the PIC produced with other monomer systems in this study, there are not sufficient points to determine a relationship. Test results for PIC produced with a 75 percent MMA + 25 percent BA monomer system and for PIC produced with a 50 percent MMA + 50 percent BA monomer system were also plotted in Fig. 5.31. It was found that the prediction using Eq. 5.4 was not applicable for PIC produced with these two monomer systems. In general, the compressive strength is determined by tests of cylinders.

(d) Splitting Tensile Strength: The splitting tensile strength may also be estimated in terms of the compressive strength as

$$f'_{tp} = C\sqrt{f'_{cp}} \qquad (5.5)$$

The value of C averaged about 11.25, as shown in Table 5.9. However, for a safe estimate for these test specimens C should be taken as 10.0. The expression then becomes

$$f'_{tp} = 10\sqrt{f'_{cp}} \qquad (5.6)$$

where f'_{tp} = splitting tensile strength of PIC, psi

f'_{cp} = compressive strength of PIC, psi

C = tensile strength coefficient, $f'_{tp}/\sqrt{f'_{cp}}$

(e) Modulus of Rupture: The modulus of rupture was calculated from the cracking moment of each test beam. When the first flexural crack in the bottom fiber of the beam occurs, the extreme fiber strength can be written as

Table 5.9

Tensile and Compressive Strengths for

Different Monomer Systems

Monomer System	Compressive Strength f'_{cp} (psi)	Tensile Strength f_{tp} (psi)	Tensile Strength Coefficient C*
100% MMA	13,100	1,280	11.40
100% MMA	15,100	1,520	12.40
75% MMA + 25% BA	12,300	1,200	10.80
50% MMA + 50% BA	11,200	1,100	10.40
		Average	11.25

$$*C = \frac{f'_{tp}}{\sqrt{f'_{cp}}}$$

$$f_b = \frac{M_{cr}\, y_b}{I} \qquad (5.7)$$

and

$$f_b = f_{rp} + f_{pc} - f_d \qquad (5.8)$$

where f_b = bottom fiber stress, psi

M_{cr} = observed cracking moment, lb-in.

y_b = distance from N.A. to extreme bottom fiber, in.

I = moment of inertia of beam cross section, $in.^4$

f_{rp} = modulus of rupture for PIC, psi

f_{pc} = bottom fiber stress due to an effective prestressing force, psi

f_d = bottom fiber stress due to beam weight, psi.

Eqs. 5.7 and 5.8 are used to calculate the modulus of rupture for PIC, as shown in Table 5.10. The PIC rupture modulus coefficient, K, is defined as a ratio of the rupture modulus, f_{rp}, to the square root of the compressive strength f'_{cp}. The average K-values for 100, 75, and 50 percent MMA-PIC are 6.58, 8.46, and 8.99, respectively. For a safe estimate, the rupture modulus for 100 percent MMA-PIC can be written as

$$f_{rp} = 6\sqrt{f'_{cp}} \qquad (5.9)$$

5.3.5 Stress Distribution of Polymer-Impregnated Concrete in Flexural Members

The distribution of stress in the compressive zone of reinforced or prestressed concrete members subjected to flexure is of fundamental importance in theories regarding the ultimate strength and behavior of such members. Many ultimate strength theories involving a variety of hypothetical stress blocks have been developed. The salient points of many of these theories were set out by Hognestad, and many different distributions of stress in concrete have been suggested (23). For PIC, the stress-strain distribution is slightly different from that for unimpregnated concrete in modulus, strength, and ultimate strain.

Table 5.10

Rupture Modulus for Different Monomer Systems

Beam No.	Monomer System	Compressive Strength f'_{cp} (psi)	Rupture Modulus f_{rp} (psi)	Rupture Modulus Coefficient K*
PBF-2	100% MMA	15,100	818	6.67
PBF-4			866	7.06
PBF-6			746	6.00
PBF-8			810	6.60
PBM-75	100% MMA + 25% BA	12,300	939	8.46
PBM-50	50% MMA + 50% BA	11,200	949	8.99

$$*K = \frac{f_{rp}}{\sqrt{f'_{cp}}}$$

Several concrete stress distributions proposed by others were modified in this study and used for input to generate load-deflection response of PIC beams utilizing the computer program PICB. Each calculated load-deflection response was compared to the corresponding observed response. Figs. 5.33 to 5.36 show the load-deflection responses for beams in PBF series generated by computer program PICB with the PIC stress distributions shown in Fig. 5.32. The parabolic and Hognestad's stress distributions were modified by specifying strain at maximum stress, ε_o, to be 0.0028 to conform to the test results presented in Sect. 5.3.2. The elastic stiffness from the calculated load-deflection responses based on these two assumed stress distributions were higher than the observed values. The load-deflection curves calculated by using Jensen's trapezoid and the triangular stress distributions are practically identical; these stress distributions produced the best agreement of load-deflection response with the test results, especially in the elastic range. The calculated ultimate load for each beam was always less than the observed.

It should be noted that the maximum compressive strain of the PIC beam calculated by Jensen's theory was also in good agreement with measured strain. Even the calculated modulus of elasticity, E_{cp}, was slightly less than that from the cylinder test, but the elastic stiffness of the load-deflection response was about the same as that in the test results.

5.3.6 Stress Distribution for Polymer-Impregnated Concrete Generated from Strain Readings

Strains at different distances from the extreme fiber of the test beams were monitored as described in Sect. 4.1.4. For each load, a linear strain distribution was found by the least squares method to evaluate the stress-strain curve of PIC in flexure. Based on the method proposed by Smith and Orangun (39), a computer program was developed by Phinyawat (11) for reinforced PIC beams and the program was adapted for prestressed PIC beams in this study. The method of analysis is based on the following assumptions:

(1) a plane section above the neutral axis remains plane after bending;

(2) the concrete below the neutral axis is cracked and offers no contribution to flexural strength; and

(3) the concrete stress is a function of strain only i.e., $f_{cp} = F(\varepsilon)$.

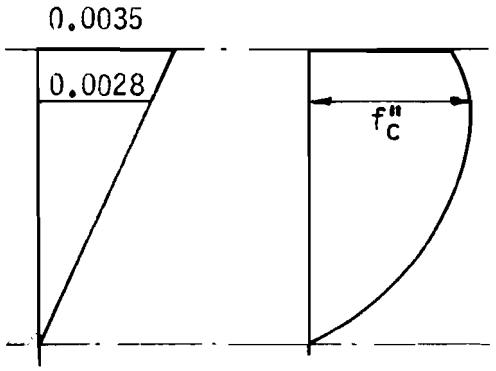

$$\varepsilon_o = 0.0028$$

$$f_c = f''_c \left[2\varepsilon/\varepsilon_o - (\varepsilon/\varepsilon_o)^2\right]$$

$$E_c = 2f''_c/\varepsilon_o$$

$$f''_c = f'_{cn}$$

(a) Parabolic Stress Distribution.

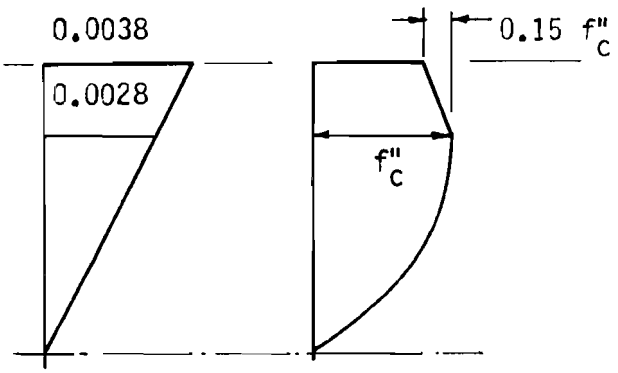

$$\varepsilon_o = 0.0028$$

$$f''_c = 0.85\, f'_{cp}$$

$$f_c = f''_c \left[2\varepsilon/\varepsilon_o - (\varepsilon/\varepsilon_o)^2\right]$$

$$E_c = 2f''_c/\varepsilon_o$$

(b) Hognestad's Stress Distribution.

(Continued)

Fig. 5.32 Modified Stress Distributions in Compression Zone of Polymer-Impregnated Concrete Beams.

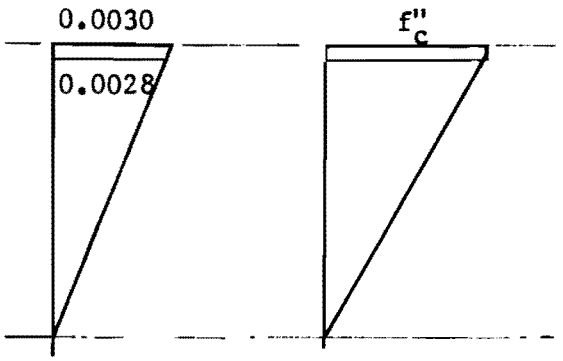

$$f''_c = f'_{cp}$$

$$\varepsilon_o = f''_c / E_c$$

$$\varepsilon_u = \varepsilon_o / (1-\beta)$$

$$\beta = 1 / \left[1 + (f'_{cp}/4000)^2\right]$$

$$E_c = \frac{30{,}000{,}000}{5 + \frac{10{,}000}{f'_{cp}}}$$

(c) Jensen's Stress Distribution.

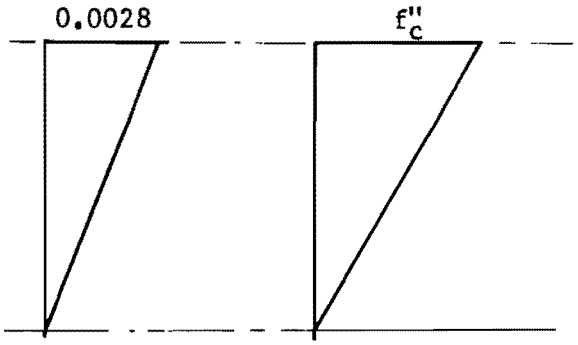

$$\varepsilon_u = \varepsilon_o = 0.0028$$

$$f''_c = f'_{cp}$$

$$E_c = f''_c / \varepsilon_o$$

(d) Triangular Stress Distribution.

Fig. 5.32 Modified Stress Distributions in Compression Zone of Polymer-Impregnated Concrete Beams (Cont.).

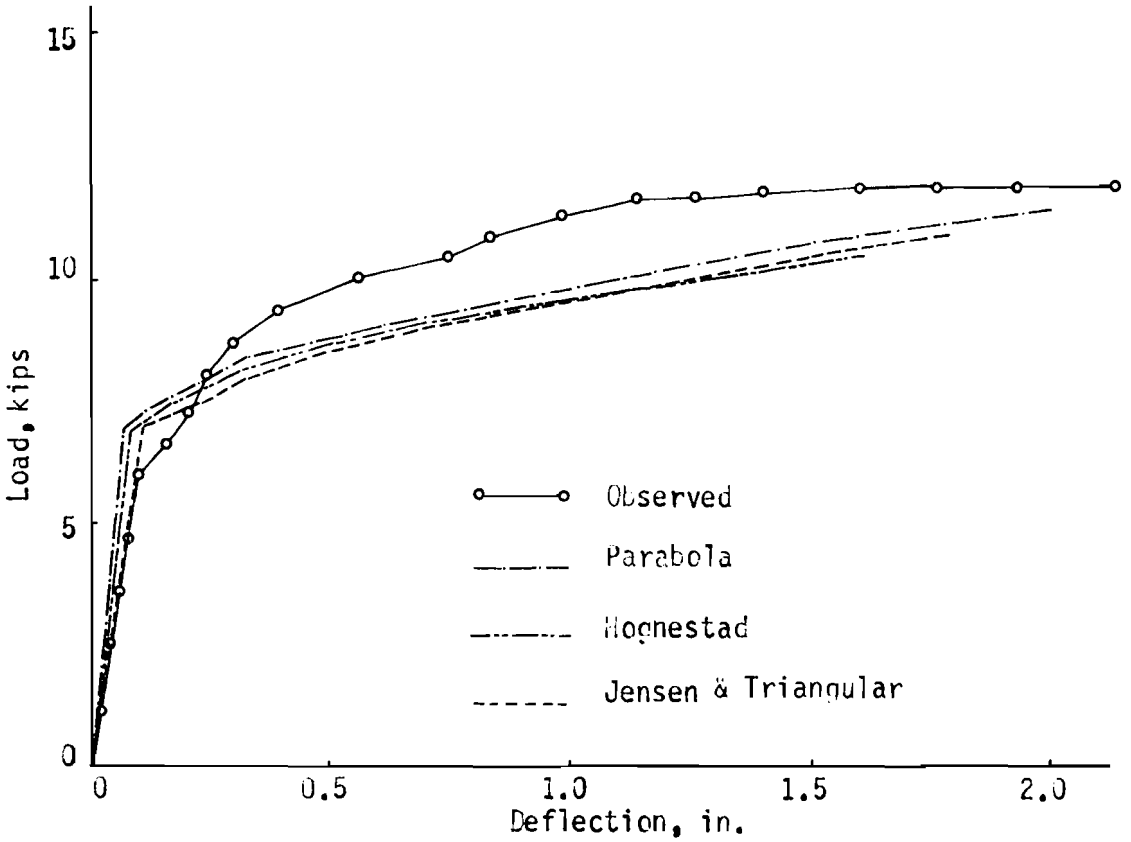

Fig. 5.33 Load-Deflection Responses for PBT-2 Generated from Modified Stress Distributions.

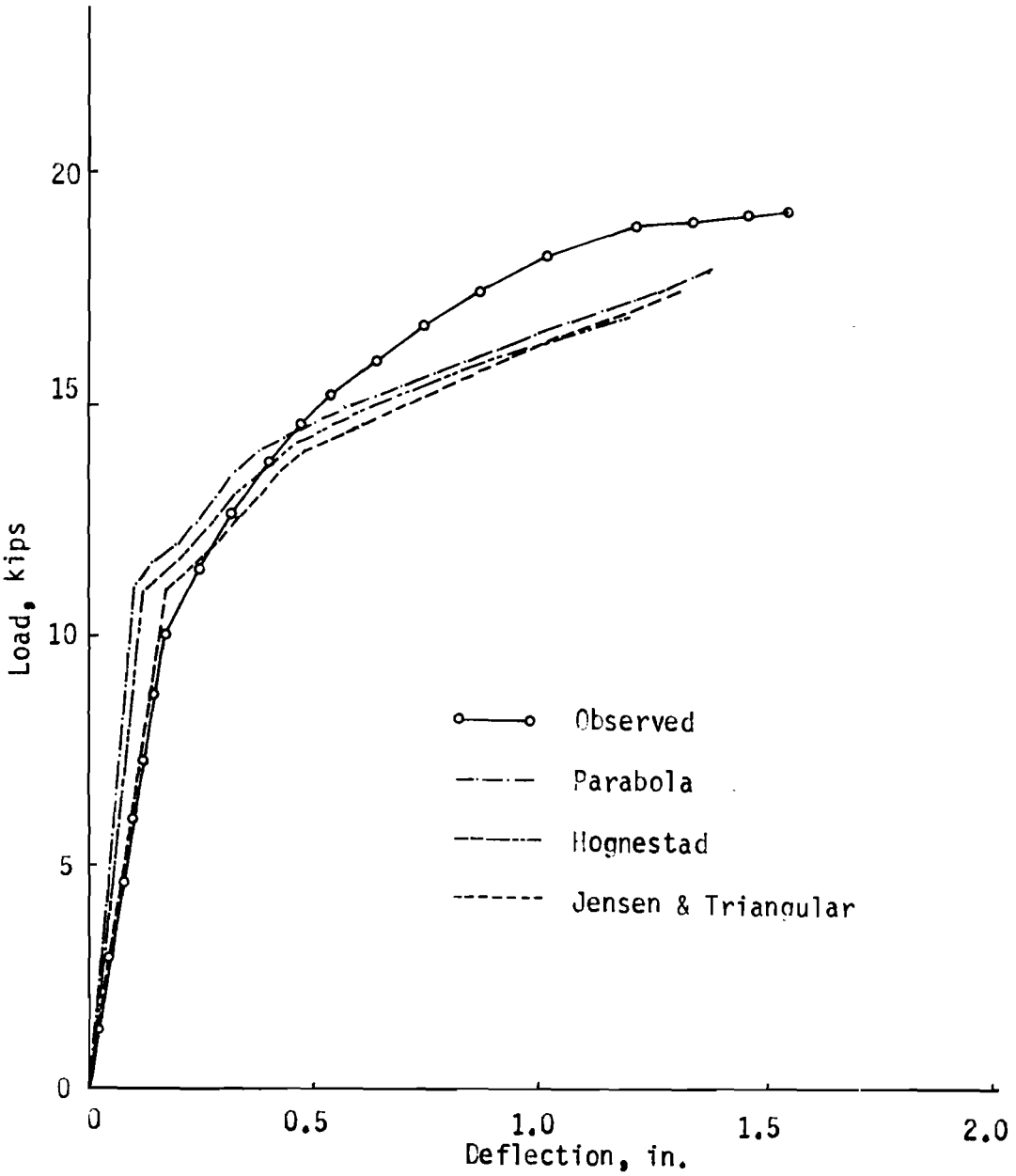

Fig. 5.34 Load-Deflection Responses for PBF-4 Generated from Modified Stress Distributions.

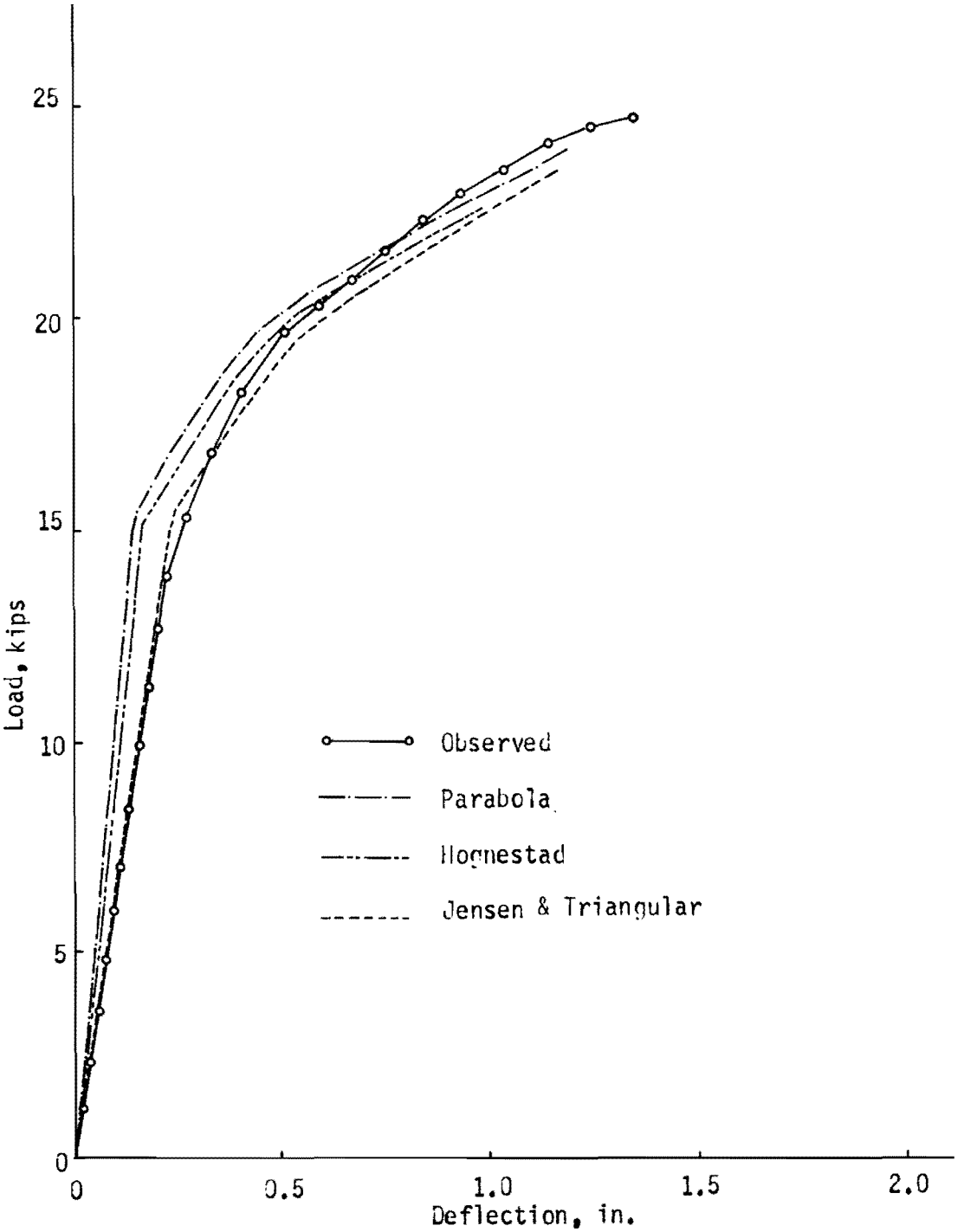

Fig. 5.35 Load-Deflection Responses for PBT-6 Generated from Modified Stress Distributions.

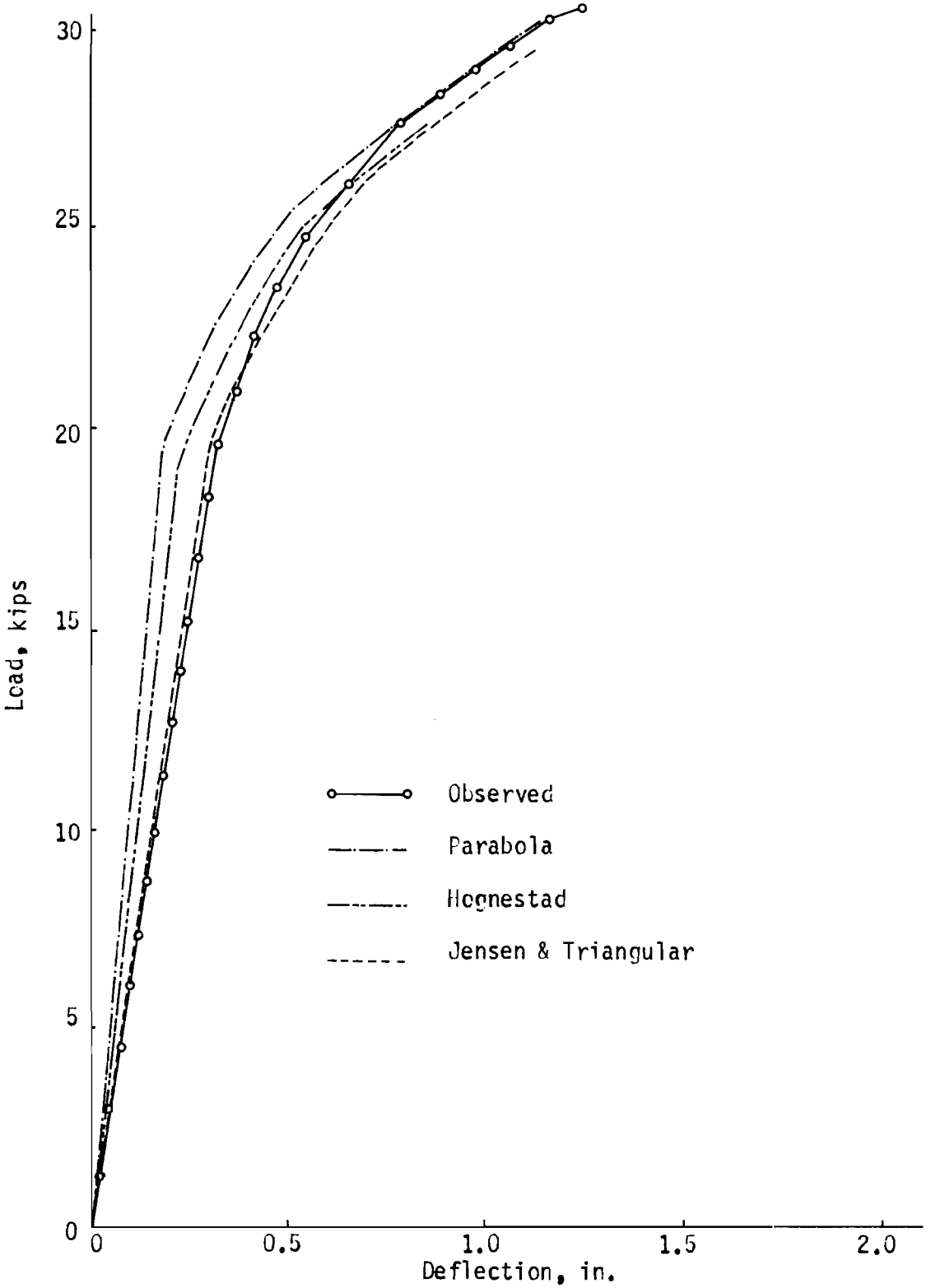

Fig. 5.36 Load-Deflection Responses for PBΓ-8 Generated from Modified Stress Distributions.

The experimental data needed to find $F(\varepsilon)$ are the bending moment, M, the compressive strains, ε, and the neutral axis depth, nd, where d is the effective depth. The neutral axis is generally located by linear fitting of the strains. The external bending moments are the results of the external applied loads while the internal bending moments are the product of the compressive force in terms of strain and the distance between the neutral axis and the centroid of the force. The prestressing moments are also included in the internal moments and the stress function $F(\varepsilon)$ can be solved by determining equilibrium between internal and external moments. For this study, the stress function is in the form of a fourth degree polynomial.

The compressive stress-strain curves shown in Fig. 5.37 were generated from the flexural tests of post-tensioned PIC beams. The curve for 100 percent MMA-PIC is from the test of PBF-2 while the curves for 75 percent and 50 percent MMA-PIC are from PBM-75 and PBM-50, respectively. It should be mentioned that these beams contain 2 unbonded tendons.

Comparing the computer stress-strain curves from beam tests to the curves from tests of cylinders shows slight differences in strength but significant differences in modulus of elasticity. The discrepancies might be the result of load reduction during the strain readings of the beams. The computed stress-strain curves are nonlinear even in the elastic range where the stress is less than 50 percent of the ultimate strength. The moduli of elasticity determined from the curves are not constant due to nonlinear behavior. The ultimate strengths of PIC calculated from measured strains appear to be higher than those observed from tests of cylinders.

5.3.7 Equivalent Rectangular Stress Distribution

The development of a rectangular stress distribution for 100 percent MMA-PIC in a flexural member is easily accomplished from the static equilibrium at failure of the test beams. Fig. 5.38 shows a strain distribution and a rectangular stress block of the beam at failure. The strain distribution in the compression zone of the beam is assumed to be linear. The neutral axis then can be located by linear fitting of the measured strains in PIC. The stress intensity of the equivalent stress distribution is $k_u f'_{cp}$, with depth a, where f'_{cp} is the compressive strength of PIC. The depth, a, is the depth of the equivalent stress block and can be

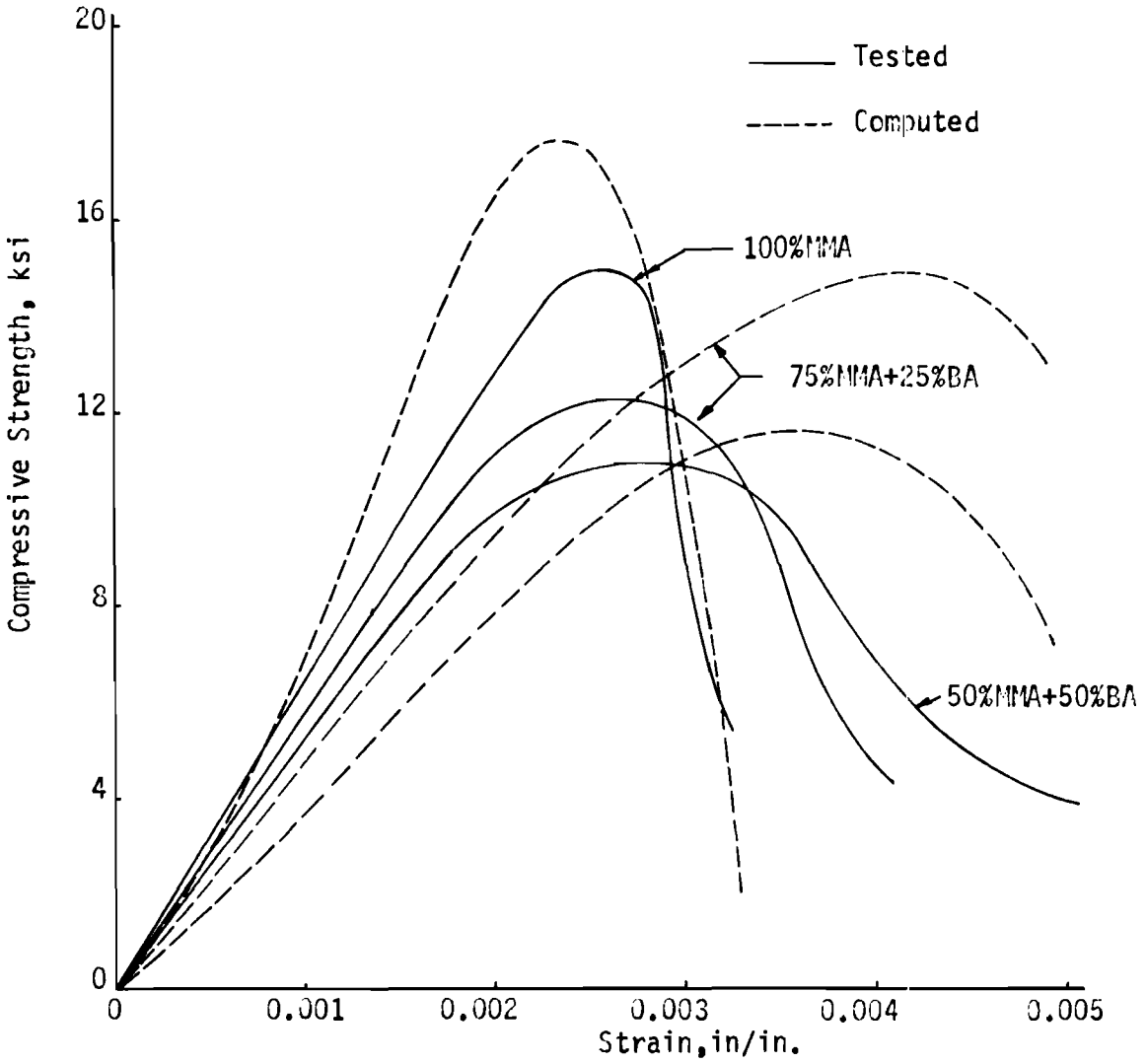

Fig. 5.37 Stress Distributions for Polymer-Impregnated Concrete Generated from Strain Readings.

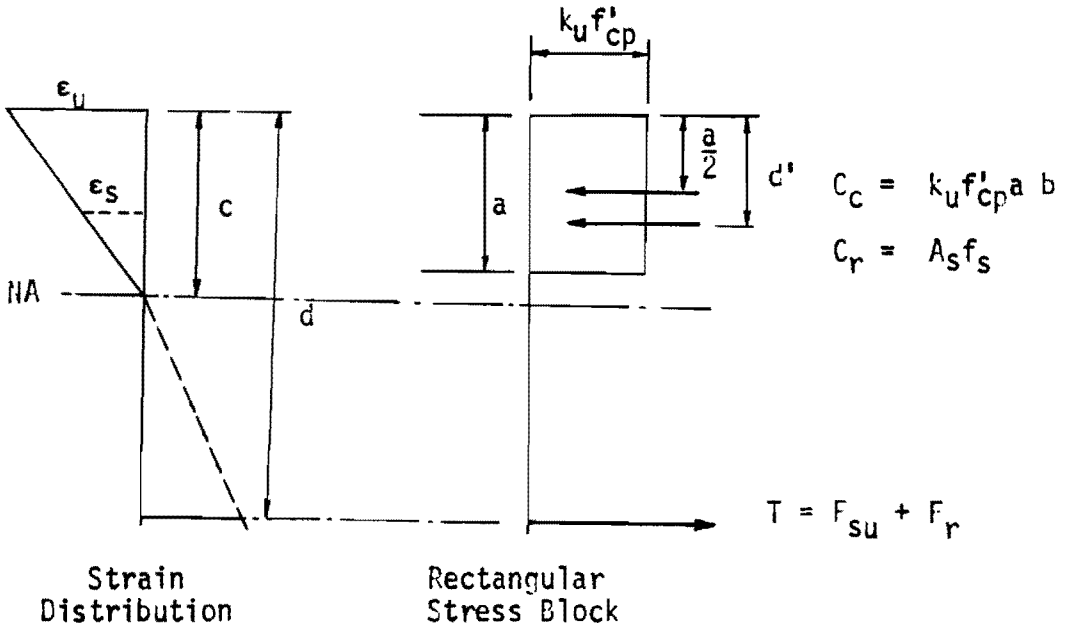

Fig. 5.38 Equivalent Rectangular Stress Distribution for Polymer-Impregnated Concrete Beams.

written as a fraction of c ($a = \beta c$) where c is the distance from the top fiber to the neutral axis. The total tension forces were contributed by the tendon force, F_{su}, as presented in Sect. 5.2.3 and by bonded reinforced steel, F_r, while the compression forces were carried by PIC (C_c) and by the supplementary reinforcing steel in the top flange (C_r). From the test results, the neutral axis at failure for each beam was located in the top flange; the PIC compressive force can be written as

$$C_c = k_u f'_{cp} a b \qquad (5.10)$$

where b is the flange width of the beam.

Both tension and compression forces due to reinforcing steel bars (C_r or F_r) were products of the steel area (A_s) and steel stress (f_s). The steel stress, of course, is usually converted from measured strain at steel level by means of the stress-strain relationship.

At failure the unknown variables k_u and a can be obtained by the strain equilibrium. The average values of k_u and a from 6 PIC beams were found to be 0.92 and 0.72, respectively (Table 5.11). A safe estimate for ultimate moment, the equivalent rectangular stress block with an intensity of 0.90 f'_{cp} and a depth, a, of 0.70 c could be used.

5.3.8 Comparison of Test Results to Theoretical Analysis

The theoretical analysis presented in this section is based on the numerical iteration method using computer program PICB as described in Chapter 2. Comparison of this analysis with the test results will be made considering only load-deflection response, tendon stress, and cracking moment. Some of those results will also be compared to predictions based on the present ACI Building Code (42).

The material properties as presented in Chapter 3 were the input for the numerical analysis. The complete compressive stress-strain relationship of PIC and unimpregnated concrete was assumed to be the same as the envelope curve from the tests of cylinders subjected to repeated high-intensity loading (Fig. 5.29). The predicted and observed results will be compared as follows.

Table 5.11

Development of Equivalent Rectangular Stress Block

Beam No.	c	a	$\beta = a/c$	k_u
PBF-2	0.75	0.54	0.72	0.91
PBF-4	1.20	0.86	0.71	0.97
PBF-6	1.90	1.30	0.68	0.89
PBF-8	2.00	1.36	0.69	1.04
PBB-4C	1.15	0.80	0.70	0.89
PBB-4P	1.10	0.88	0.80	0.81
		Average	0.72	0.92

(a) Load-Deflection Response: The calculated load-deflection responses presented in this study were generated by a numerical procedure using the computer program PICB. Each beam, when modeled for solution by PICB, was divided into thirty-two 3-in. increments. The friction coefficients used in this investigation were from tests, as presented in Sect. 5.3.1. The tendon stress at the holding end calculated by the computer program PICB at zero applied load was checked with measured tendon stress at the same end. If these two values were not in good agreement, the friction coefficients were adjusted to obtain a better result. Actually, only two trials are needed to match accurately an observed holding end tendon stress if none of the other parameters is changed.

Figs. 5.39 to 5.43 present the observed and calculated values for the load versus midspan deflection. The agreement is quite good in the elastic range of each beam; however, for larger loads the calculated deflections increase considerably faster than do the observed values. In all cases, the calculated initial stiffness of the beam is slightly higher than the observed, and the calculated ultimate load is usually less than the observed value.

The cracking loads calculated by the program PICB were also slightly higher than the test results except for the control beam (PBC-2), as shown in Fig. 5.43. The predicted ultimate deflections for both the fully impregnated PIC beams and the partially impregnated PIC beams are lower than the observed values but the opposite is true for the control beam.

The predicted curves for PBM-50 and PBM-75, as shown in Fig. 5.41, are identical in both elastic and inelastic ranges. It should be noted that the higher the number of wires in tendons of the PBF series (Figs. 5.39 and 5.40), the better the agreement between the predicted and the observed curves.

(b) Tendon Stress: An analysis of tendon stress was pursued by two different methods: a numerical analysis method for this study as discussed in Sect. 2.3 and an empirical method recommended by the ACI Building Code (42). The former method can generate the stress response in a tendon subjected to external loads while only the tendon stress at ultimate load can be calculated by the latter method.

Figs. 5.44 to 5.48 present the tendon stress responses under loads. The solid lines represent the observed responses and the dashed lines represent the predicted responses using the computer program. The predicted and the observed tendon stresses seem to increase linearly in the elastic range.

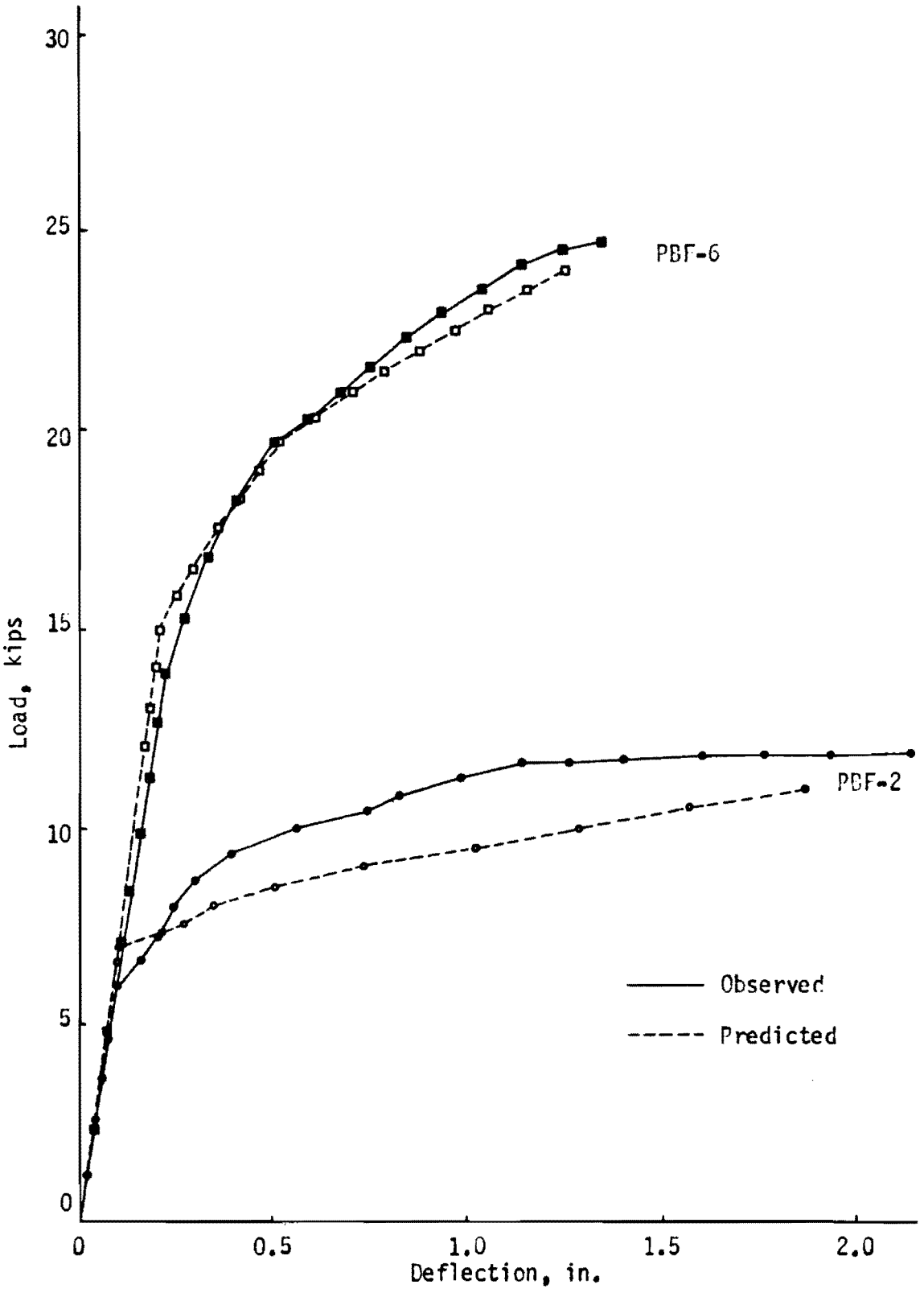

Fig. 5.39 Comparison of Load-Deflection Responses for PBF-2 and PBF-6.

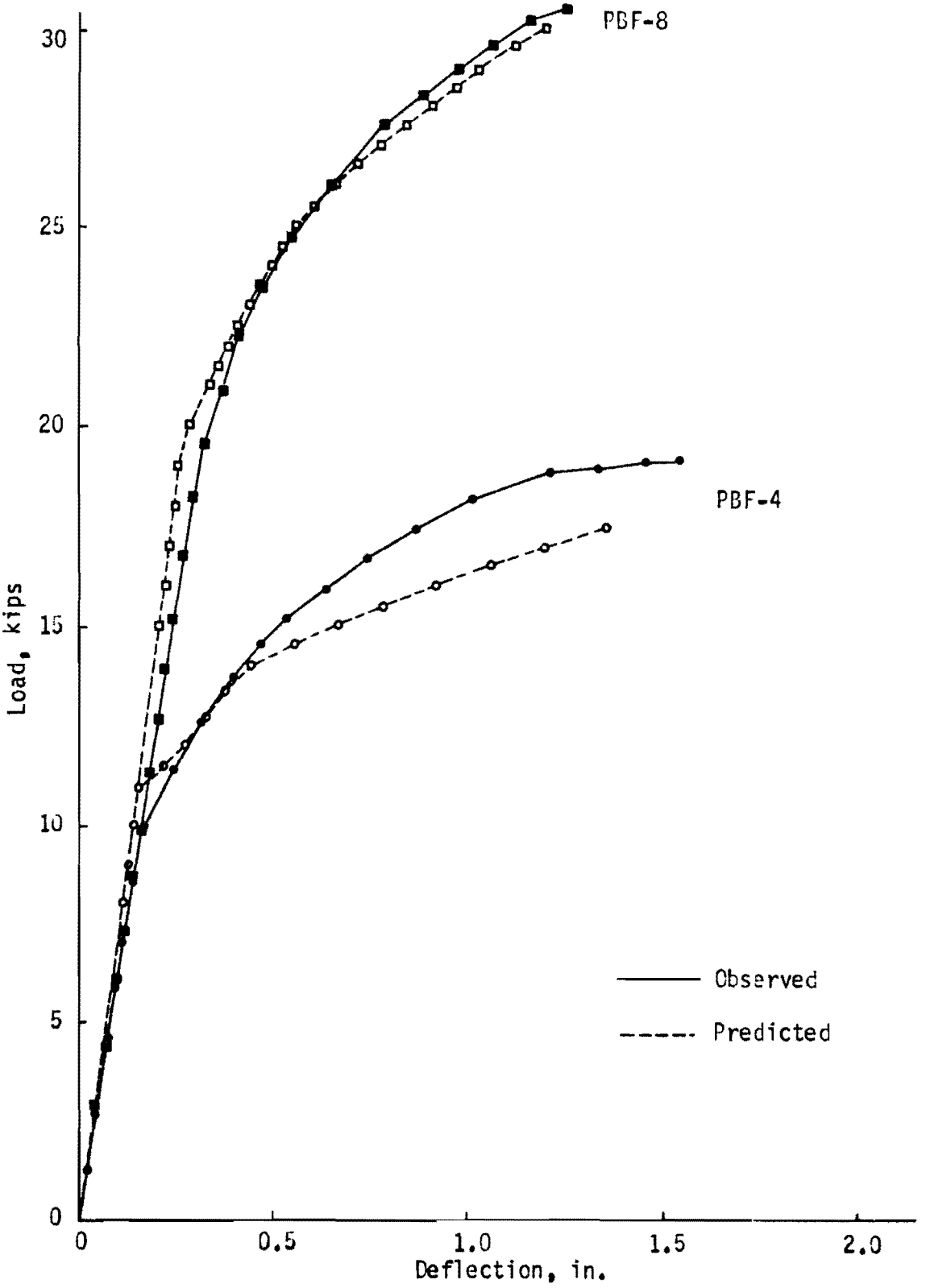

Fig. 5.40 Comparison of Load-Deflection Responses for PBF-4 and PBF-8.

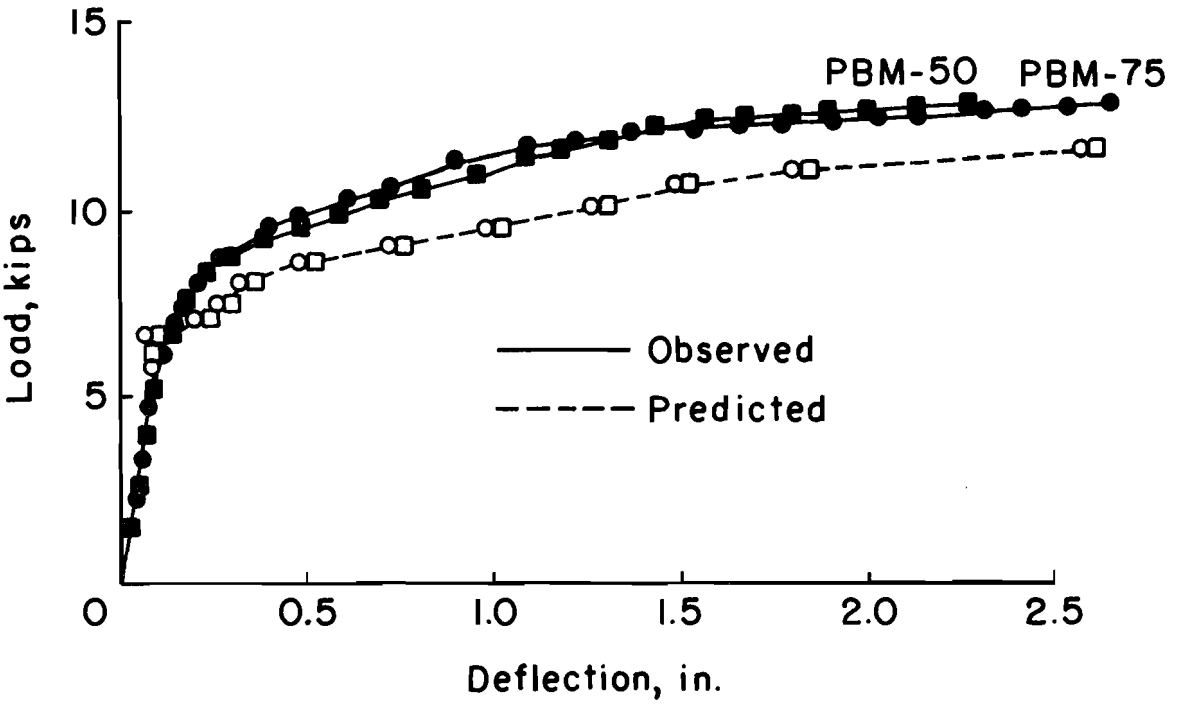

Fig. 5.41. Comparison of Load-Deflection Responses for PBM-50 and PBM-75.

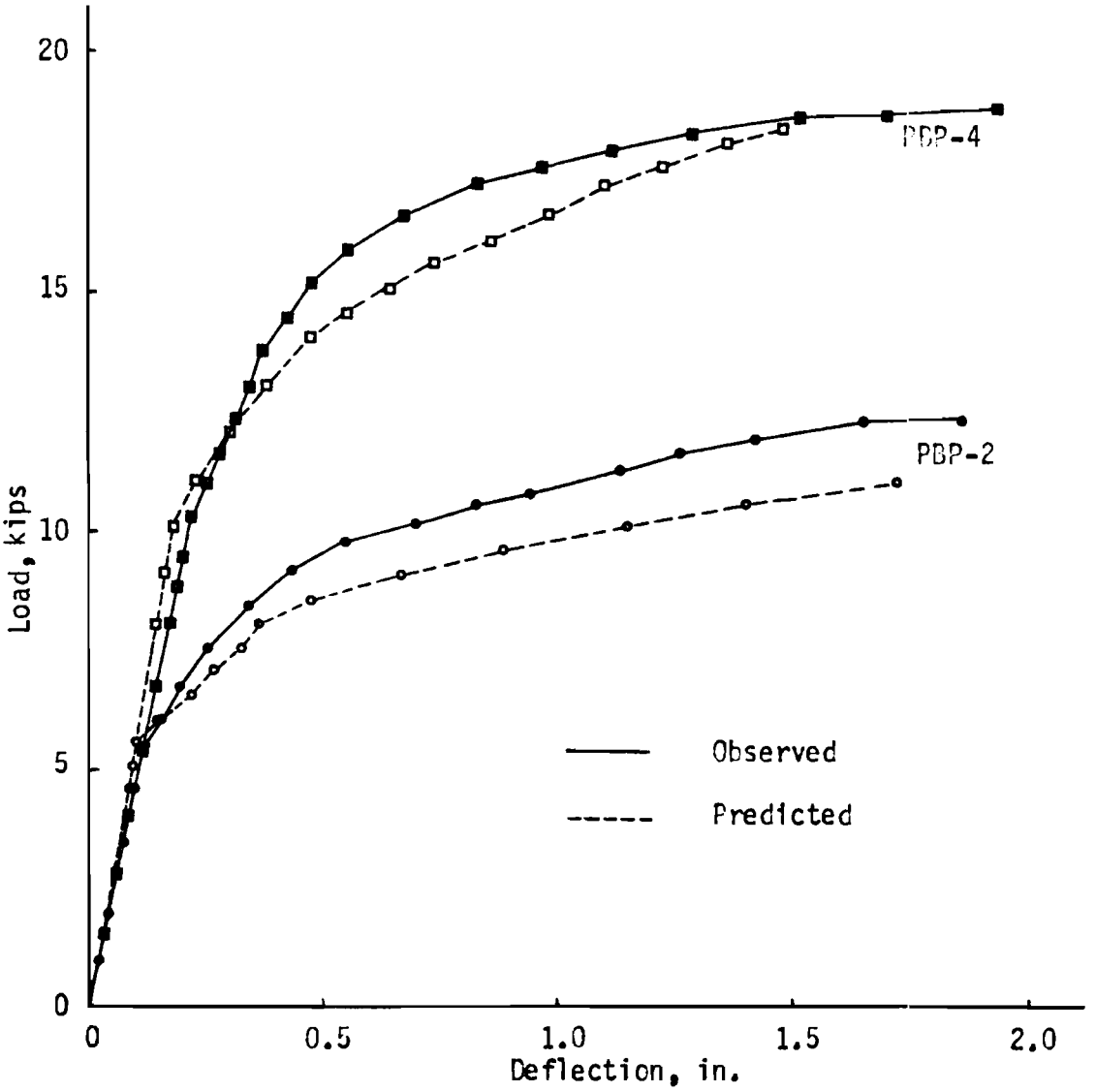

Fig. 5.42 Comparison of Load-Deflection Responses for PBP-2 and PBP-4.

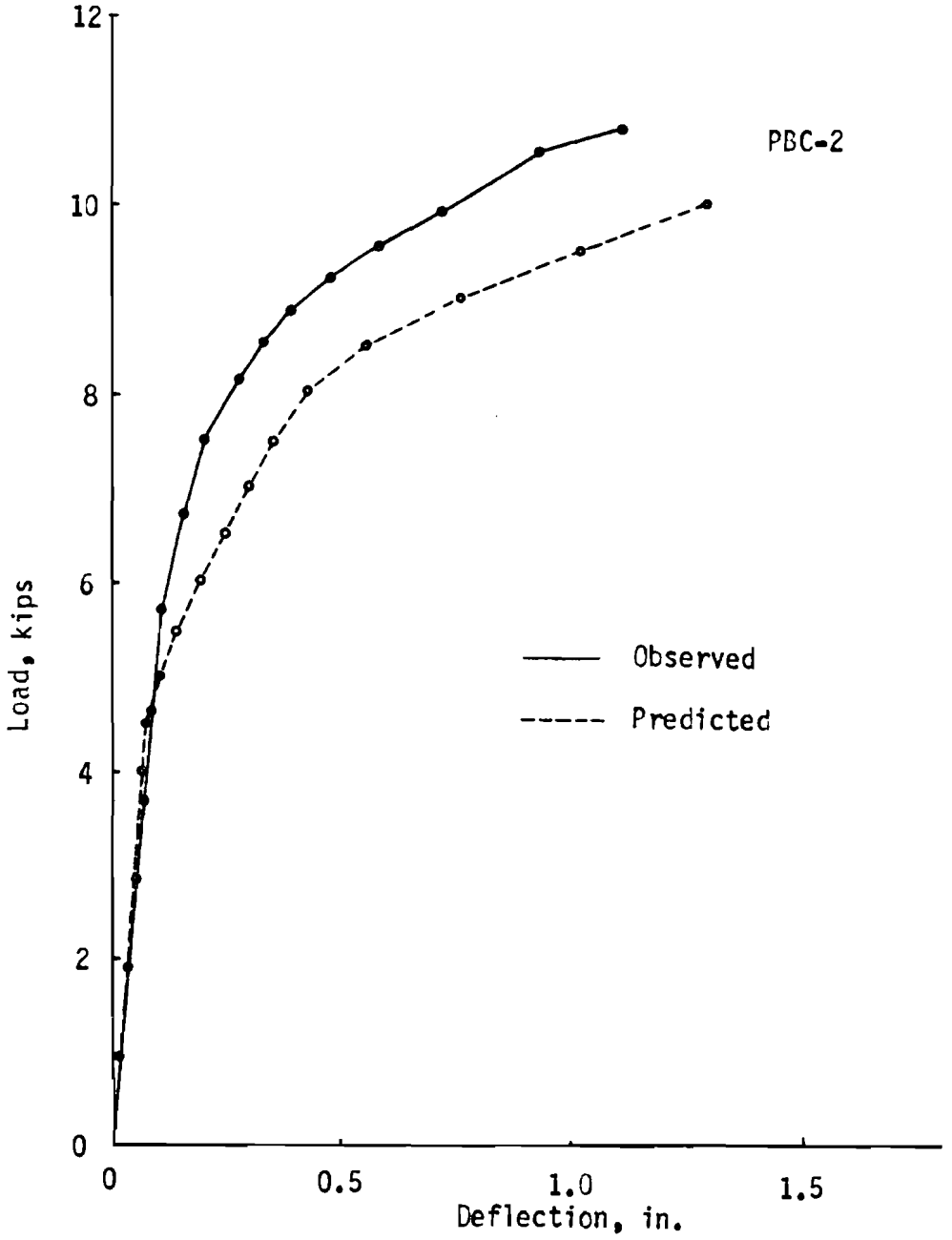

Fig. 5.43 Comparison of Load-Deflection Responses for PBC-2.

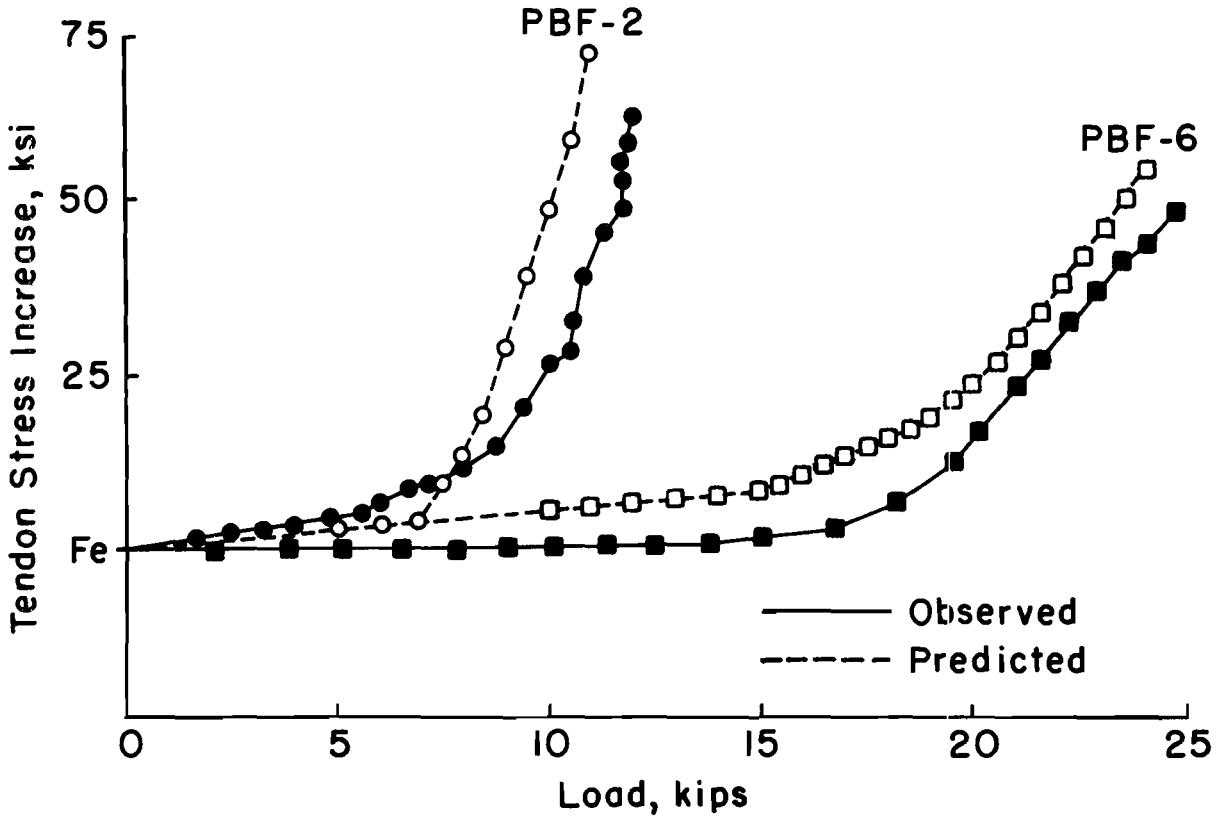

Fig. 5.44. Comparison of Tendon Stress Responses Under Load for PBF-2 and PBF-6.

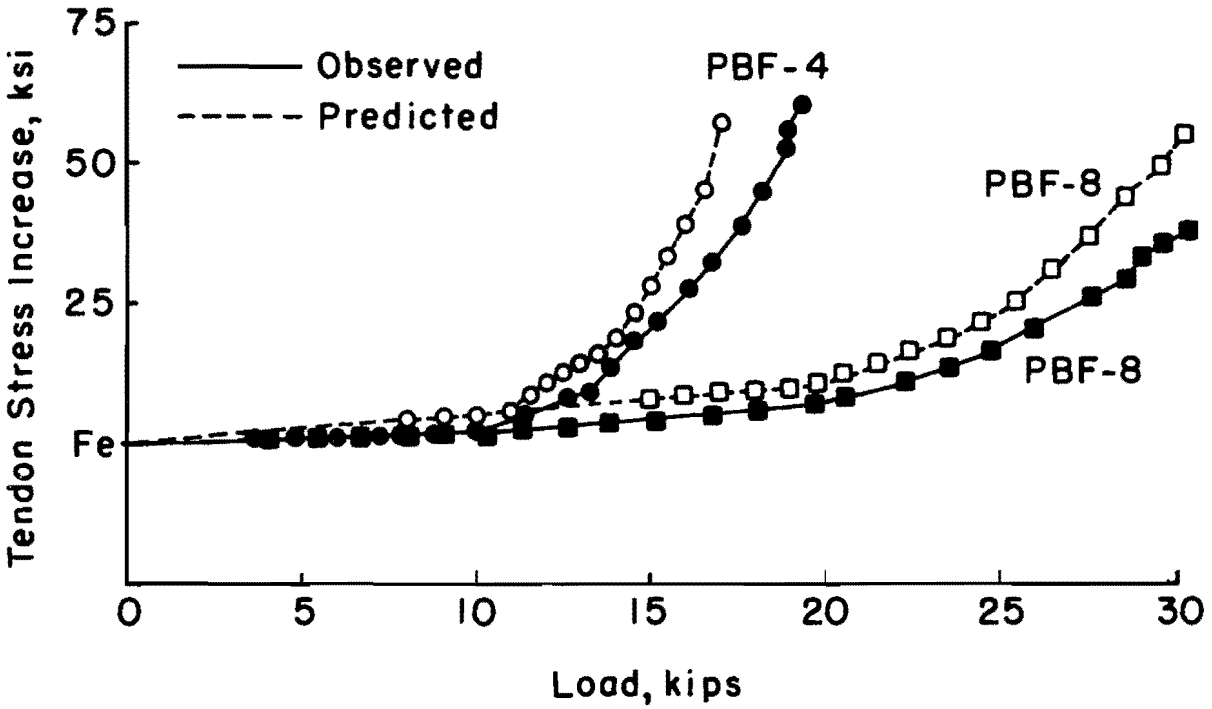

Fig. 5.45. Comparison of Tendon Stress Responses Under Loads for PBF-4 and PBF-8.

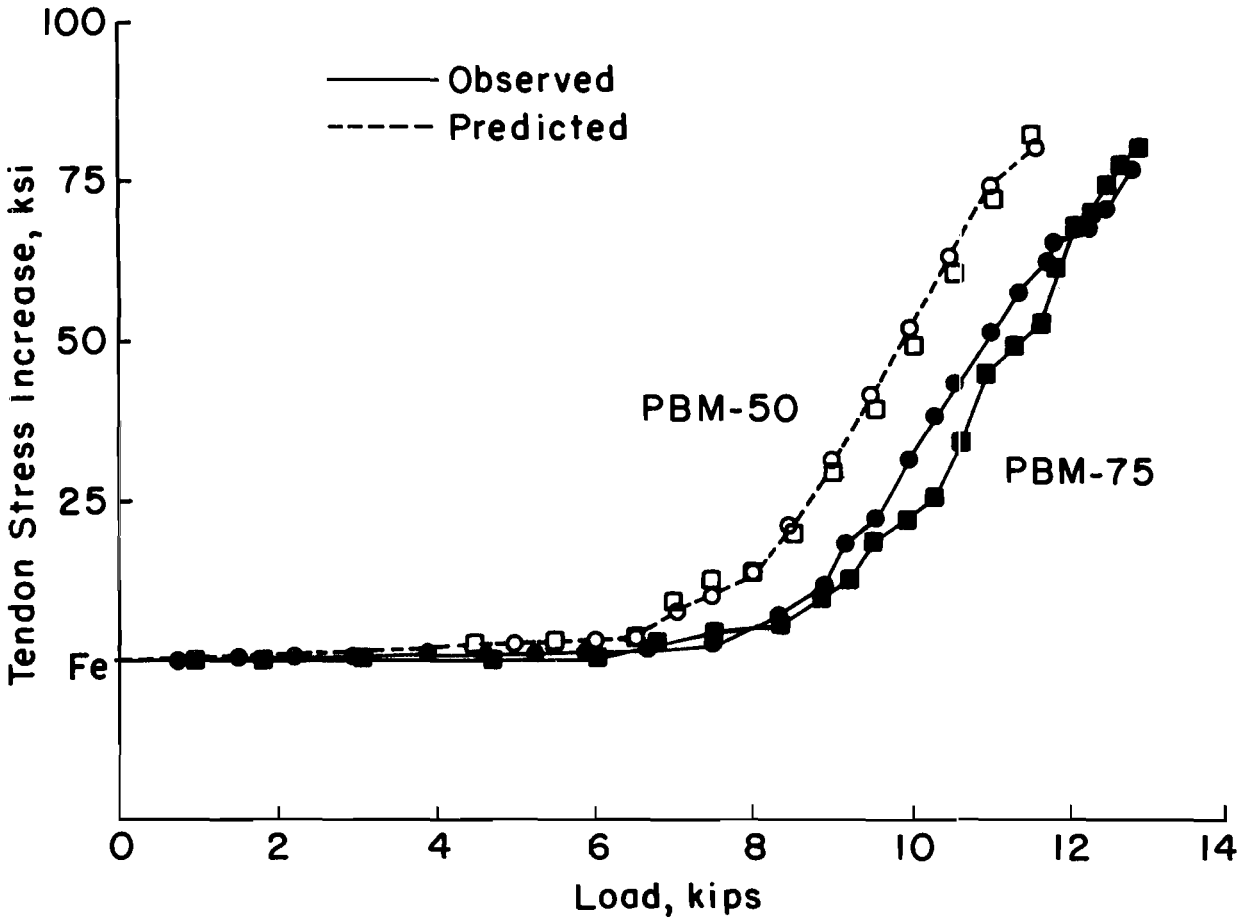

Fig. 5.46. Comparison of Tendon Stress Responses Under Loads for PBM-50 and PBM-75.

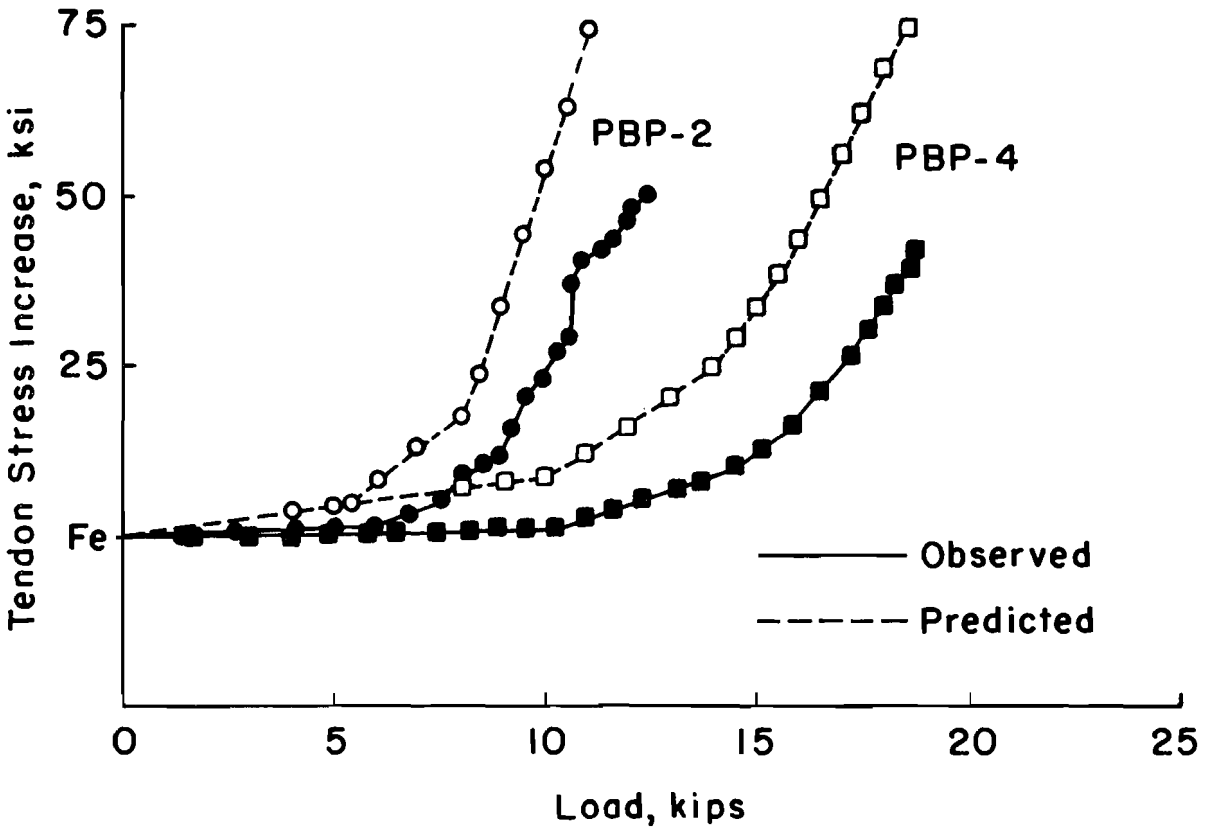

Fig. 5.47. Comparison of Tendon Stress Responses Under Loads for PBP-2 and PBP-4.

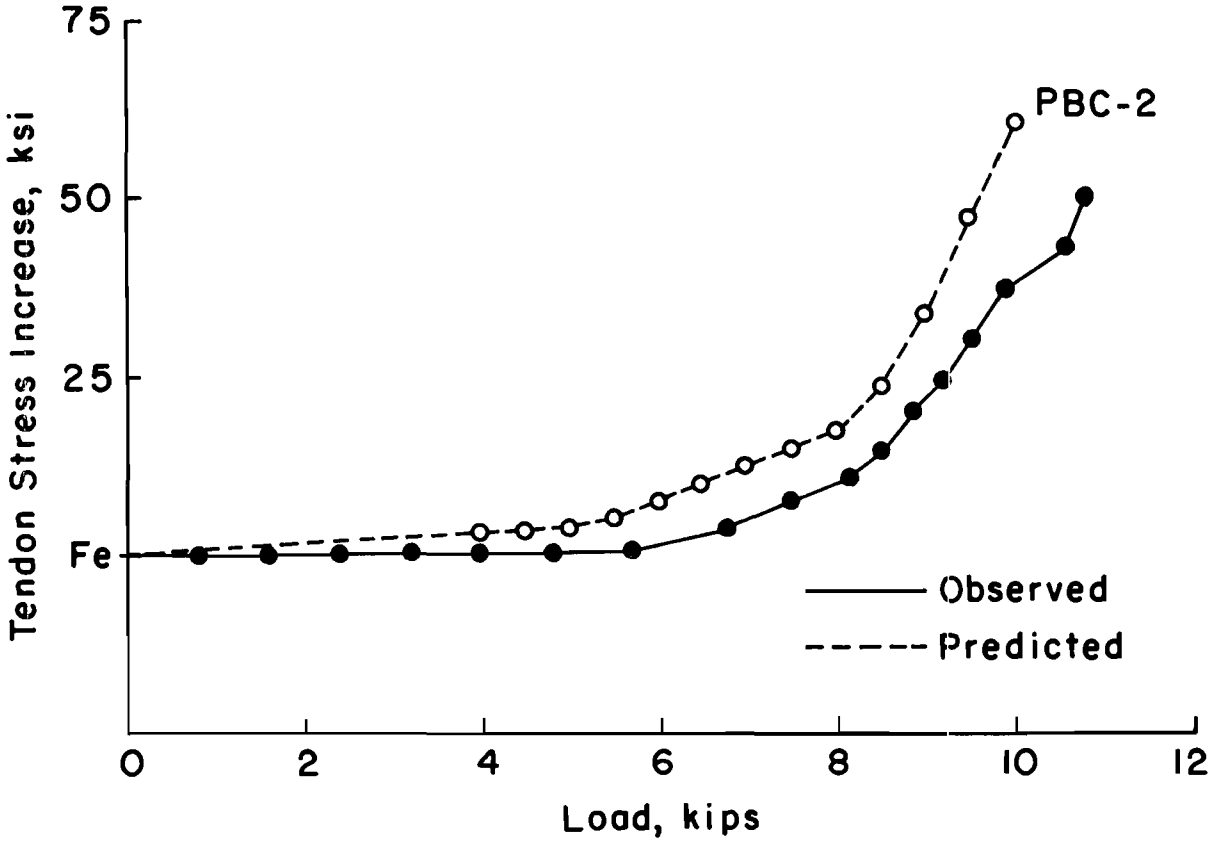

Fig. 5.48. Comparison of Tendon Stress Responses Under Loads for Control Beam.

For almost every case, the predicted curves indicate a stress increase greater than the observed rates before the development of cracks. As soon as the cracking occurs both seem to increase at approximately the same rate but the final stresses are slightly different.

The predicted response for tendon stress increase at midspan for each beam was practically identical to the curves plotted in Fig. 5.44 to 5.48 for the predicted stress increase at the anchorage end.

The predicted responses for PBM-50 and PBM-75 are almost identical, and they are in good agreement with test results (Fig. 5.46). The results for partially impregnated PIC beams and a control beam are shown in Figs. 5.47 and 5.48, respectively. They are similar to the other results, indicating a slight difference between the observed and the calculated results.

Tendon stress increases during loading calculated by ACI Eqs. 18.3 and 18.4 and presented in Table 5.12 are compared with the test values Δf_{ps} is the measured change in stress in this tendon; Δf_{ps}, is the change in stress calculated by ACI 318-71; and Δf_{ps_2} is the change in stress calculated by program PICB. For the control beam, the test value is about twice the values calculated from the ACI equations. For the PIC beams, the ratio of test values to predicted values is in the range from 1.35 to 2.16. Two values of predicted tendon stress increase are shown in the table for the partially impregnated beams because there are two types of concrete in the same beam; the first value assumes the strength of unimpregnated concrete while the second value assumes the strength of PIC. If the prediction is based on unimpregnated concrete, the ratios are 2.05 for PBP-2 and 2.34 for PBP-4. On the other hand, if the prediction is based on the PIC strength the ratios are 1.02 for PBP-2 and 1.36 for PBP-4. When the comparisons are made between the calculated tendon stress increase found by program PICB and the observed test results, they generally differ by less than 10 percent, except for PBF-8, which differs by about 30 percent, and the control beam, which is about 15 percent different.

(c) Cracking and Ultimate Moments: The rupture modulus of PIC was found to be $6\sqrt{f'_{cp}}$ as evaluated from the test results. The value confirmed the value recommended by the ACI Building Code for calculating a cracking moment for ordinary concrete. The cracking moments predicted by this rupture modulus are in good agreement with test results (Table 5.13). On the other hand, the cracking moments calculated by the numerical analysis

Table 5.12

Increased Tendon Stress

Beam No.	Δf_{ps} Observed (ksi)	Δf_{ps_1} Calculated by ACI-318-71 (ksi)	Δf_{ps_2} Calculated by PICB Program (ksi)	Ratio $\Delta f_{ps}/\Delta f_{ps_1}$	Ratio $\Delta f_{ps}/\Delta f_{ps_2}$
PBF-2	67.200	49.900	70.20	1.35	0.96
PBF-4	61.100	29.900	57.50	2.04	1.06
PBF-6	50.300	23.300	55.20	2.16	0.91
PBF-8	37.700	20.000	53.80	1.89	0.70
PBM-50	78.400	39.600	83.10	1.98	0.94
PBM-75	81.500	42.600	82.90	1.91	0.98
PBB-4C	-	47.500	-	-	-
PBB-4P	-	47.500	-	-	-
PBP-2	50.900	24.800[a] 49.900[b]	71.10	2.05, 1.02	0.72
PBP-4	40.800	17.400[a] 29.900[b]	74.60	2.34, 1.36	0.57
PBC-2	52.000	24.800	60.90	2.09	0.85

[a] assuming ordinary concrete throughout

[b] assuming PIC throughout

Table 5.13

Comparison of Cracking Moments

Beam No.	M_{cr} Observed (lb-in)	M_{cr1} * Predicted by $f_{rp} = 6\sqrt{f'_{cp}}$ (lb-in)	M_{cr2} Predicted by PICB Program (lb-in)	Ratio M_{cr}/M_{cr1}	Ratio M_{cr}/M_{cr2}
PBF-2	99,000	95,700	116,000	1.03	0.86
PBF-4	165,000	160,000	182,000	1.03	0.91
PBF-6	228,000	228,000	148,000	1.00	0.92
PBF-8	300,000	297,000	314,000	1.01	0.96
PBM-50	99,800	87,400	116,000	1.14	0.86
PBM-75	99,800	88,200	116,000	1.13	0.86

* $M_{cr1} = (f'_{rp} + f_{pe} - f_d)\ I/y_b$

(Continued)

Table 5.13

Comparison of Cracking Moments (cont.)

Beam No.	M_{cr} Observed (lb-in)	M_{cr1} * Predicted by $f_{rp} = 6\sqrt{f'_{cp}}$ (lb-in)	M_{cr2} Predicted by PICB Program (lb-in)	Ratio M_{cr}/M_{cr1}	Ratio M_{cr}/M_{cr2}
PBB-4C	181,000	177,000	-	1.02	-
PBB-4P	181,000	178,000	-	1.01	-
PBP-2	88,300	79,400	85,300	1.11	1.03
PBP-4	158,000	155,000	165,000	1.02	0.96
PBC-2	94,100	80,200	74,300	1.12	1.27

* $M_{cr1} = (f'_{rp} + f_{pe} - f_d)\ I/y_b$

method, program PICB, based on the splitting tensile strength of PIC, seem to be higher than the observed ones.

The ultimate moments, as shown in Table 5.14, were calculated by the ACI rectangular stress block, the equivalent rectangular stress distribution as presented in Sect. 5.3.7, and the computer program PICB. It should be noted that the calculated ultimate moments were based on the ACI rectangular stress block and the ultimate tendon stress from ACI Eqs. 18-13 and 18-14 while the calculation by the equivalent rectangular stress block was based on the ultimate tendon stress from the test results. The contribution of the bonded reinforcing steel in the bottom flange was considered.

The ultimate moments computed by the numerical procedure and by the equivalent stress block are in better agreement with the test results than the moments found from the ACI stress block. The maximum differences of those two methods from the observed values are 12 and 2 percent, respectively.

5.4 Effect on Independent Variables on Flexural Behavior

The variables which affect the flexural behavior are discussed in this section. They are percentage of steel, monomer system, polymer depth, and grouting effects. The effect on load-deflection response, tendon stress increase, tendon stress response, cracking moment, ultimate load, and ductility are considered.

5.4.1 Provision for Maximum Number of Wires in Tendon

In general practice, the initial prestress in steel should be about 60 to 70 percent of the specified ultimate strength; the number of tendons provided should be such that no cracking occurs in the concrete section during stressing of just after transfer. The ACI Code 318-71 (42) permits a maximum stress in steel due to jacking forces of up to 80 percent of the specified ultimate strength and to the initial prestress in steel immediately after transfer to be 70 percent of the ultimate strength. The permissible stress in concrete immediately after transfer, before losses, should not exceed 60 percent of the cylinder strength at the age of stressing, f'_{ci}, for compression and $3\sqrt{f'_{ci}}$ for tension. For the particular cross section used in these tests, a maximum of two 0.25-in. wires per tendon can be used in an unimpregnated beam; more tendon force could result in tension cracks on

Table 5.14

Comparison of Ultimate Moments

Beam No.	M_u Observed (lb-in)	M_{u1} Calculated by ACI-318-71 (lb-in)	M_{u2} Calculated by PICB Program (lb-in)	M_{u3} Calculated by Rect. Block (lb-in)	Ratio M_u/M_{u1}	Ratio M_u/M_{u2}	Ratio M_u/M_{u3}
PBF-2	191,000	173,000	182,000	191,000	1.11	1.05	1.00
PBF-4	318,000	269,000	289,000	317,000	1.18	1.10	1.00
PBF-6	408,000	363,000	396,000	408,000	1.12	1.03	1.00
PBF-8	503,000	455,000	495,000	493,000	1.11	1.02	1.02
PBM-50	210,000	158,000	190,000	-	1.32	1.10	-
PBM-75	212,000	160,000	190,000	-	1.33	1.12	-

(Continued)

Table 5.14

Comparison of Ultimate Moments (cont.)

Beam No.	M_u Observed (lb-in)	M_{u1} Calculated by ACI-318-71 (lb-in)	M_{u2} Calculated by PICB Program (lb-in)	M_{u3} Calculated by Rect. Block (lb-in)	Ratio M_u/M_{u1}	Ratio M_u/M_{u2}	Ratio M_u/M_{u3}
PBB-4C	328,000	309,000	-	327,000	1.06	-	1.00
PBB-4P	325,000	309,000	-	327,000	1.05	-	1.00
PBP-2	204,000	151,000[a]	182,000	191,000	1.35	1.12	1.06
		167,000[b]	-	-	1.22	-	-
PBP-4	311,000	262,000[a]	305,000	317,000	1.19	1.02	0.98
		276,000[b]	-	-	1.13	-	-
PBC-2		144,000	182,000	-	1.23	0.98	-

a tendon forces calculated by ordinary concrete strength
b tendon forces calculated by PIC strength

the top flange during stressing and immediately after anchoring. However, up to eight wires per tendon can be used in a fully impregnated PIC beam and five wires in a partially impregnated PIC beam, due to the higher tensile strength of PIC.

As mentioned earlier the tensile strength of PIC is about 3 times higher than of unimpregnated concrete. This permits the area of tendons to be increased by about the same ratio. The calculated compressive stresses immediately after anchoring were 1520 psi for the control beam (PBC-2) and 6550 psi for the PIC beams with the maximum number of tendons (PBF-8). For each case the stresses were less than 60 percent of their respective cylinder strengths. The tensile stresses were 276 and 1330 psi, respectively; both of them were higher than $3\sqrt{f'_{ci}}$ but less than the splitting tensile strengths. No cracks were observed during the stressing process so that the value of $3\sqrt{f'_{ci}}$ for permissible tensile stress in concrete after transfer is apparently conservative for PIC.

5.4.2. Effect of Percentage of Steel

(a) Toughness: The toughness of the PIC beams, which is represented by the area under the load-deflection curve, seems to be affected by the percentage of steel (ρ_p) or the number of tendons. Fig. 5.49 shows the relationship of toughness and percentage of steel (ρ_p). The relationship can be expressed as a polynomial which can be written as

$$T = 19.76 + 786\ \rho_p - 54880\ \rho_p^2 \qquad (5.11)$$

This equation can be used to predict the toughness of similar cross section PIC beams with a variation in percentage of steel.

(b) Ductility: The ductility of a prestressed concrete beam can be represented in terms of an inelastic rotation capacity or an inelastic displacement capacity. The inelastic rotation capacity is defined as the ratio of the curvature at ultimate to the curvature at first cracking. Similarly, the displacement capacity is the ratio of the displacements at ultimate and at first cracking. For a simply supported beam, these two values should be about the same, especially in the case of a reinforced concrete beam. In a prestressed concrete beam, the values may be slightly different due to the reference for zero deflection. Fig. 5.50 shows the relationship between the rotation capacity and the percentage of steel. The

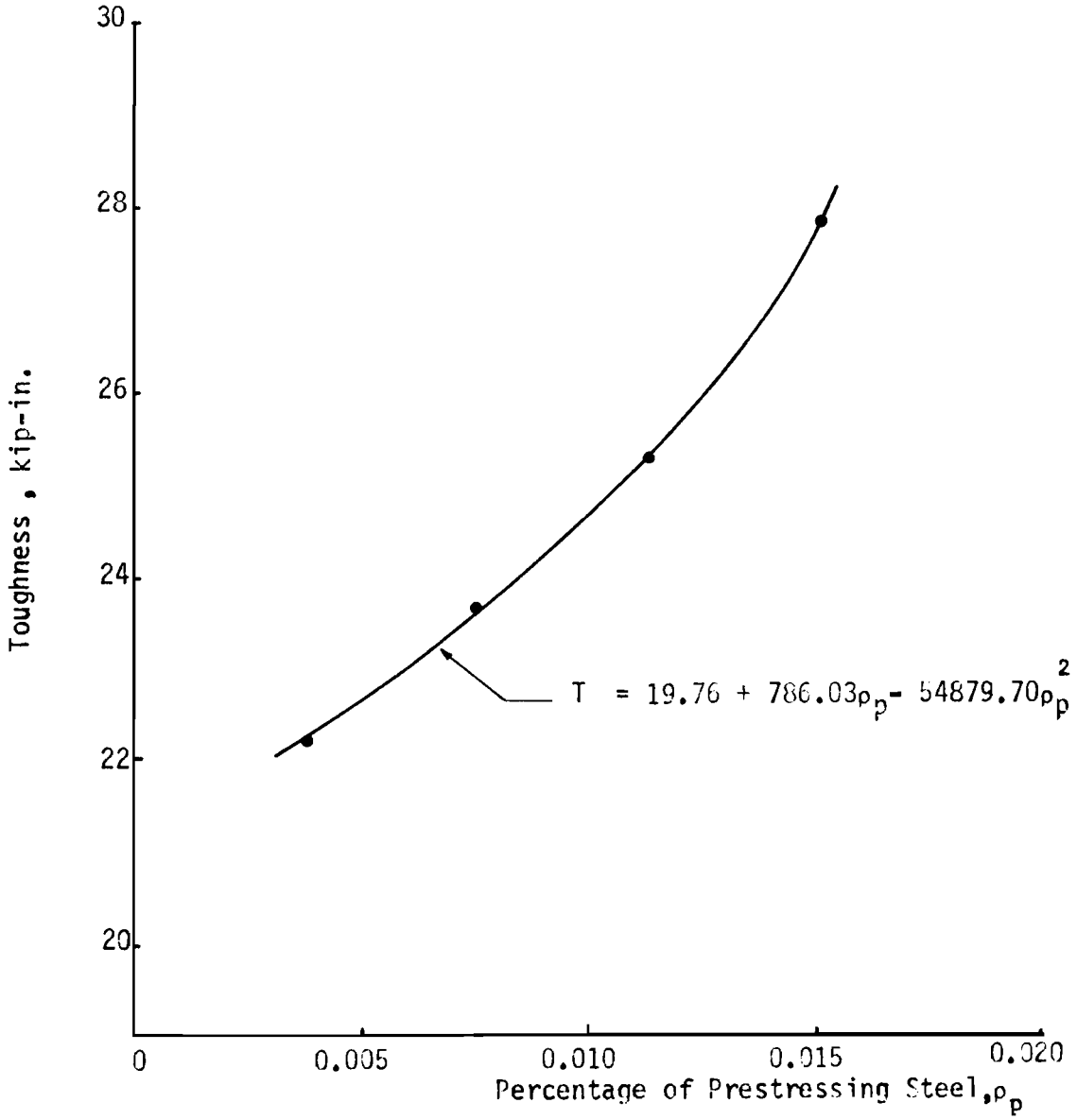

Fig. 5.49 Relationship Between Toughness and Percentage of Prestressing Steel.

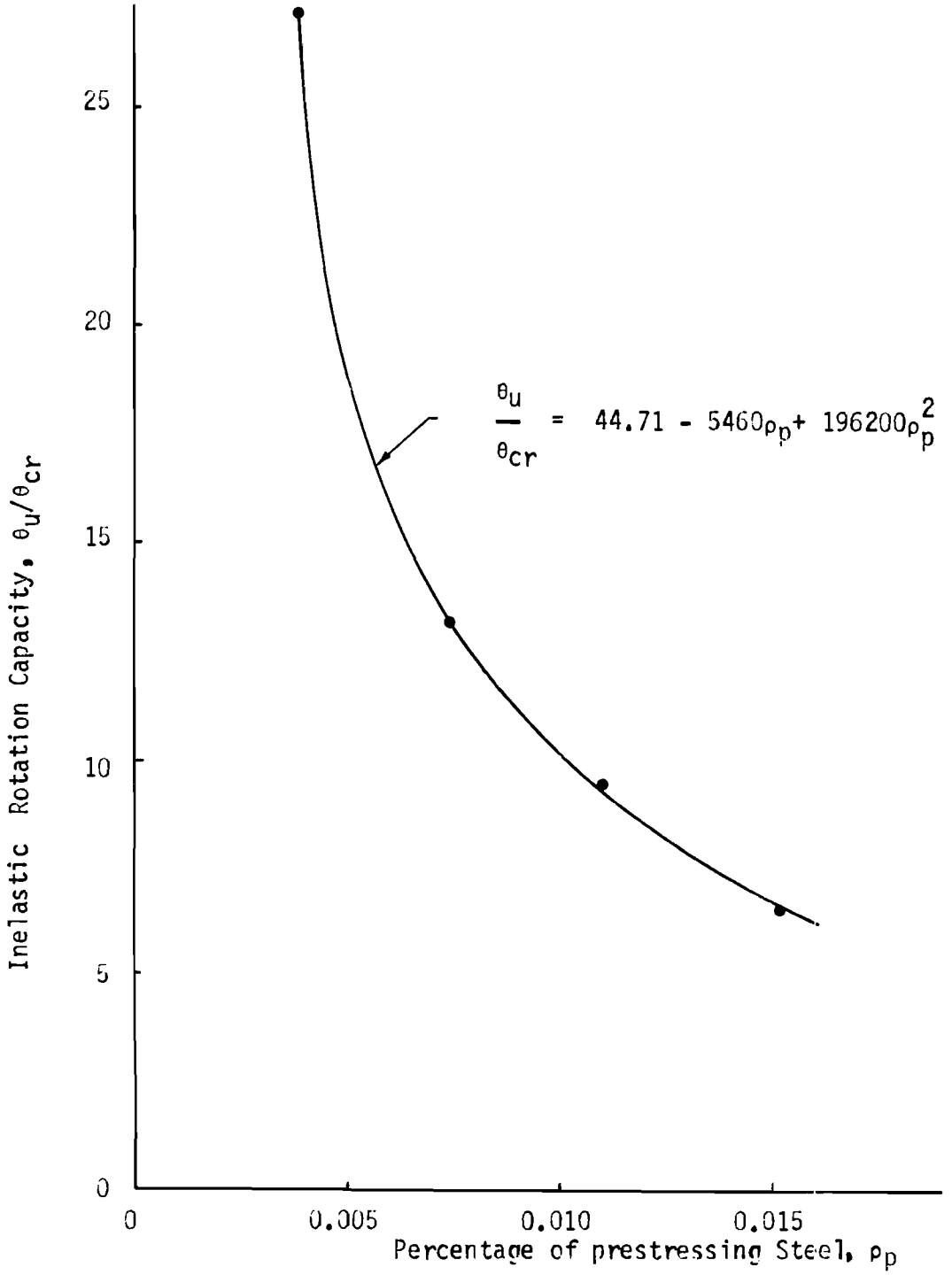

Fig. 5.50 Effect of Percentage of Steel on Inelastic Rotation Capacity for Polymer-Impregnated Concrete Beams.

percentage of steel or the number of wires in the tendon has a major effect on the ductility of PIC beams. The curve fittings was accomplished by the least squares method, and the equation is shown in the figure.

(c) Tendon Stress Increase: The tendon stress increase in a PIC beam containing a few wires is usually higher than in one containing more wires per tendon. Fig. 5.51 shows the relationship between percentage of steel and the tendon stress increase. The curve can be expressed as a linear or a nonlinear relationship, as written in Eq. 5.12 or 5.13, respectively; note that the tendon stress increase in these equations is in ksi:

$$\Delta f_{ps} = 75 - 2350\rho_p \qquad (5.12)$$

$$\Delta f_{ps} = 64 + 547\rho_p - 154000\rho_p^2 \qquad (5.13)$$

The first equation is similar to the last two terms of ACI Eq. 18-4. It can be modfied for general cases as follows:

$$f_{ps} = f_{se} + 75 - 2350\rho_p \quad \text{ksi} \qquad (5.14)$$

5.4.3 Effect on Monomer System

(a) Load-Deflection Responses: Fig. 5.52 compares the load-deflection responses of PIC beams containing two unbonded wires per tendon and impregnated with different monomer systems. The proportions of MMA used for PBF-2, PBM-75, and PBM-50, were 100, 75, and 50 percent, respectively. The response of the control beam (PBC-2) is shown in the same figure.

PBM-50 and PBM-75 developed slightly higher ultimate loads than PBF-2 (about 6 percent) and PBC-2 (about 15 percent). The elastic stiffness of PBF-2 was slightly higher than of the others, which were almost identical. The midspan deflections among all three PIC beams were slightly different but they were about twice as high as for the control beam. Similarly, the ductilities of PIC beams were about twice as great.

(b) Tendon Stress Responses: Tendon stress responses as shown in Fig. 5.53 are for the beams with two wires per tendon impregnated with different monomer systems. Up to a load of about 6 kips, the tendon stress remains constant except for PBF-2 for which it increases slightly. However, the tendon stress increases for PBM-50 and PBM-75 are about 20 percent higher than for PBF-2 and about 30 percent higher than for the control beam.

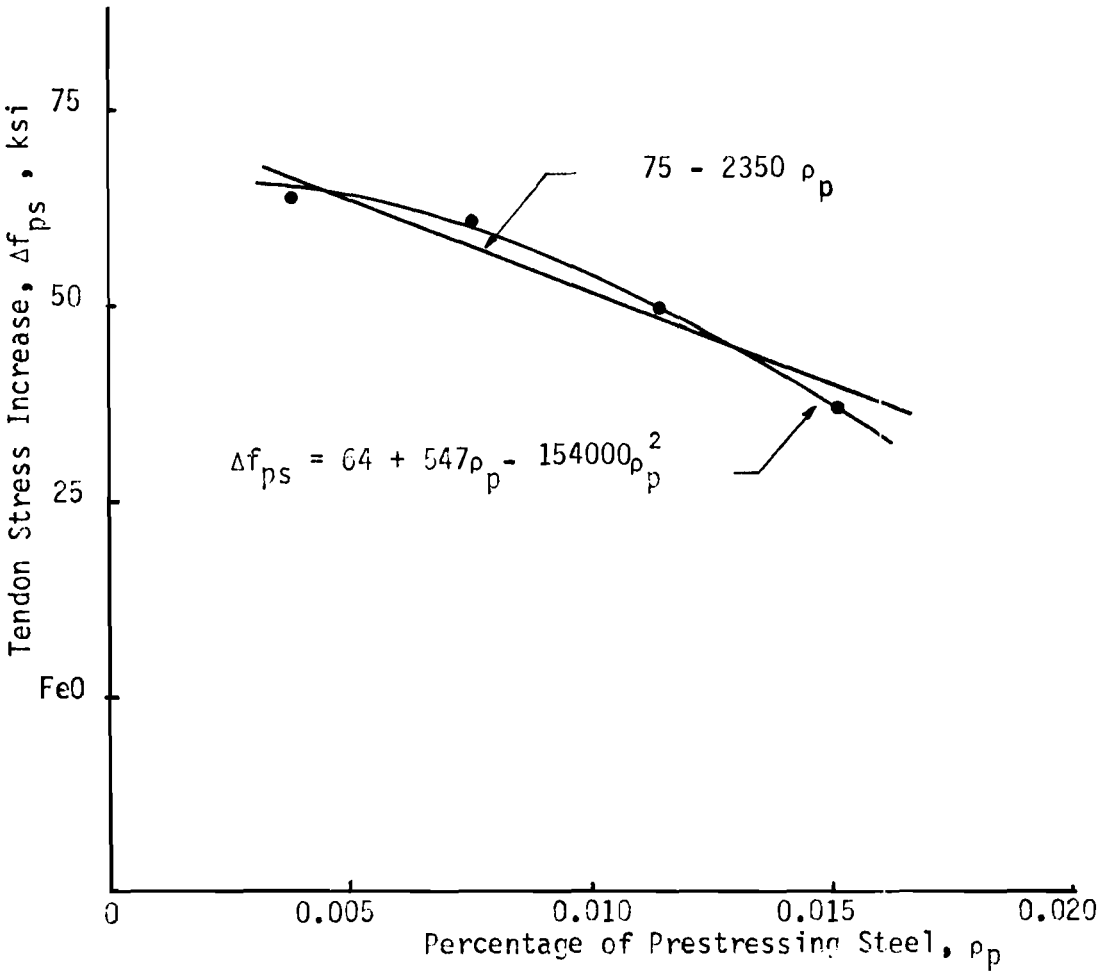

Fig. 5.51 Effect of Percentage of Steel on Tendon Stress Increase.

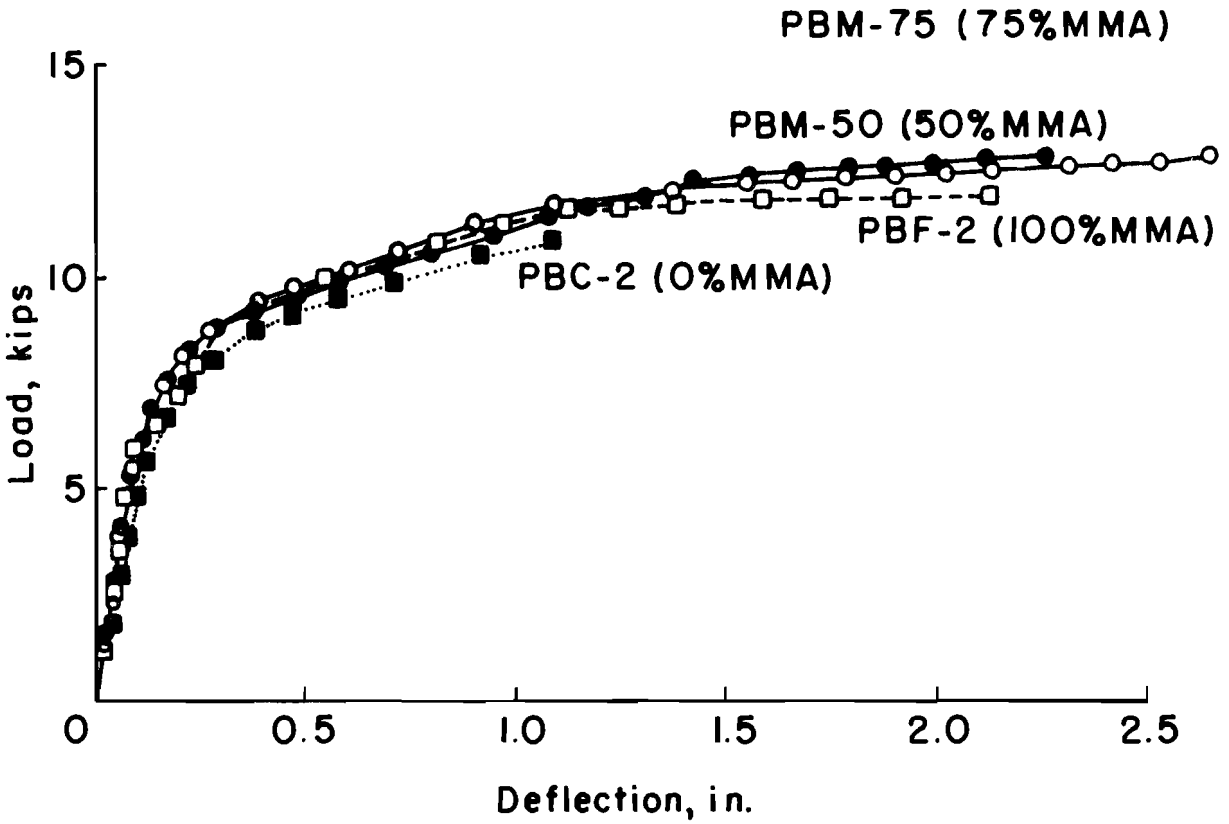

Fig. 5.52. Load-Deflection Responses for Beams with Different Monomer Systems.

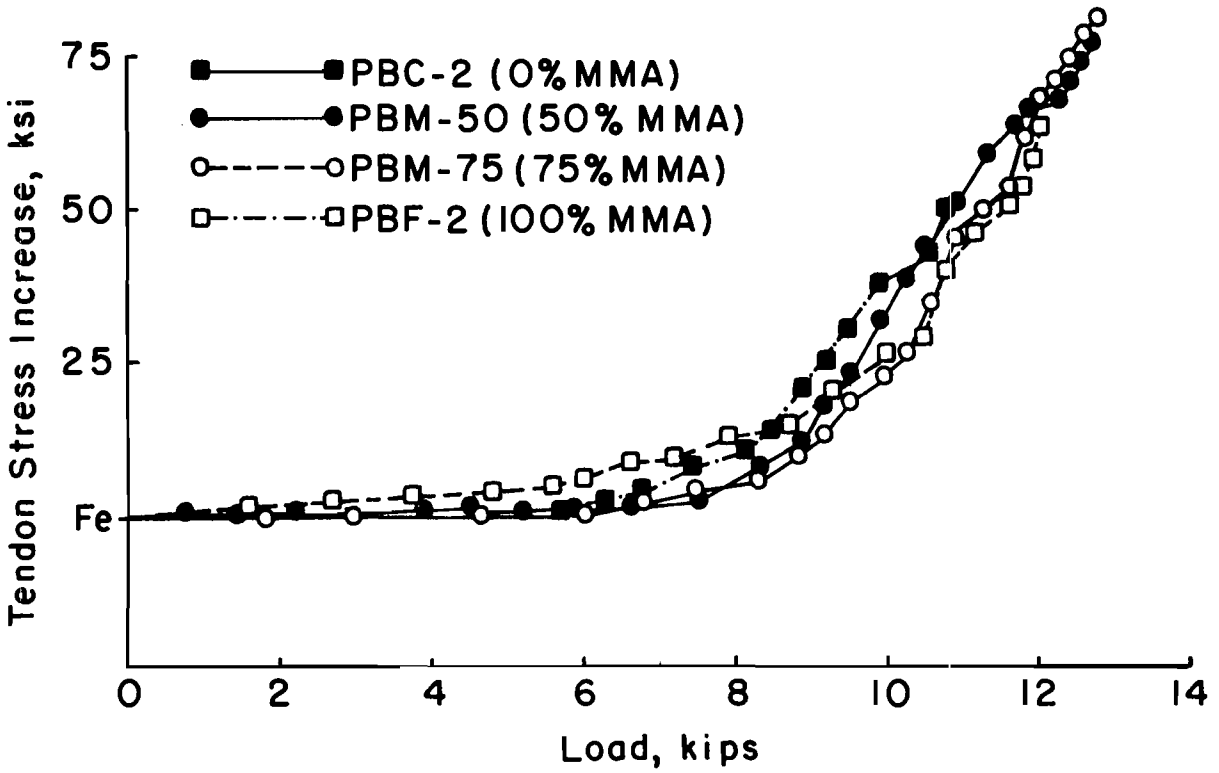

Fig. 5.53. Tendon Stress Responses for Beams with Different Monomer Systems.

Fig. 5.54 shows the relationship between the tendon stress increase and percentage of BA in the monomer system. The curve can be fitted by Eq. 5.15 as a linear relationship or by Eq. 5.16 as a parabolic relationship:

$$\Delta f_{ps} = 70.127 + 0.224\ P \qquad (5.15)$$

$$\Delta f_{ps} = 67.240 + 0.917\ P - 0.014\ P^2 \qquad (5.16)$$

where P = percentage of BA in monomer system, percent.

However, it can be observed that the monomer systems which consist of 25 and 50 percent BA for the post-tensioned PIC beams with two wire tendons only slightly affect the load-deflection response, the tendon stress response, or even the ultimate load, in comparison to the corresponding 100 percent MMA monomer system.

5.4.4 Effect of Polymer Depth

(a) Load-Deflection Response: Fig. 5.55 shows load-deflection responses for fully impregnated PIC beams, partially impregnated beams, and a control beam. The control beam, of course, has zero polymer depth, the partially impregnated beams have a 2.5-in. polymer depth, and the fully impregnated beams have a full polymer depth of 8.0 in. It can be observed that the fully impregnated beams have higher elastic stiffness than the partially impregnated beams and the control beam. Both partially and fully impregnated PIC beams with the same number of wires per tendon developed approximately the same ultimate load. For the beams containing 4-wire tendons, the partially impregnated beam (PBP-4) had about 25 percent larger deflection than the fully impregnated beams (PBF-4). However, for the beams containing 2-wire tendons, the partially impregnated beam (PBP-2) developed less ultimate deflection than the fully impregnated beam (PBF-2). The control beam developed only about 50 percent as much deflection as PBF-2. The cracking moment for PBF-2 was about 11 percent higher than for PBP-2; the cracking moment for PBF-4 was 4.5 percent higher than for PBP-4. The ductility of the fully impregnated beams was slightly different but it was about twice that for the corresponding control beam.

(b) Tendon Stress Response: Tendon stress increases in the elastic range for the fully impregnated beams were at a slightly greater rate than

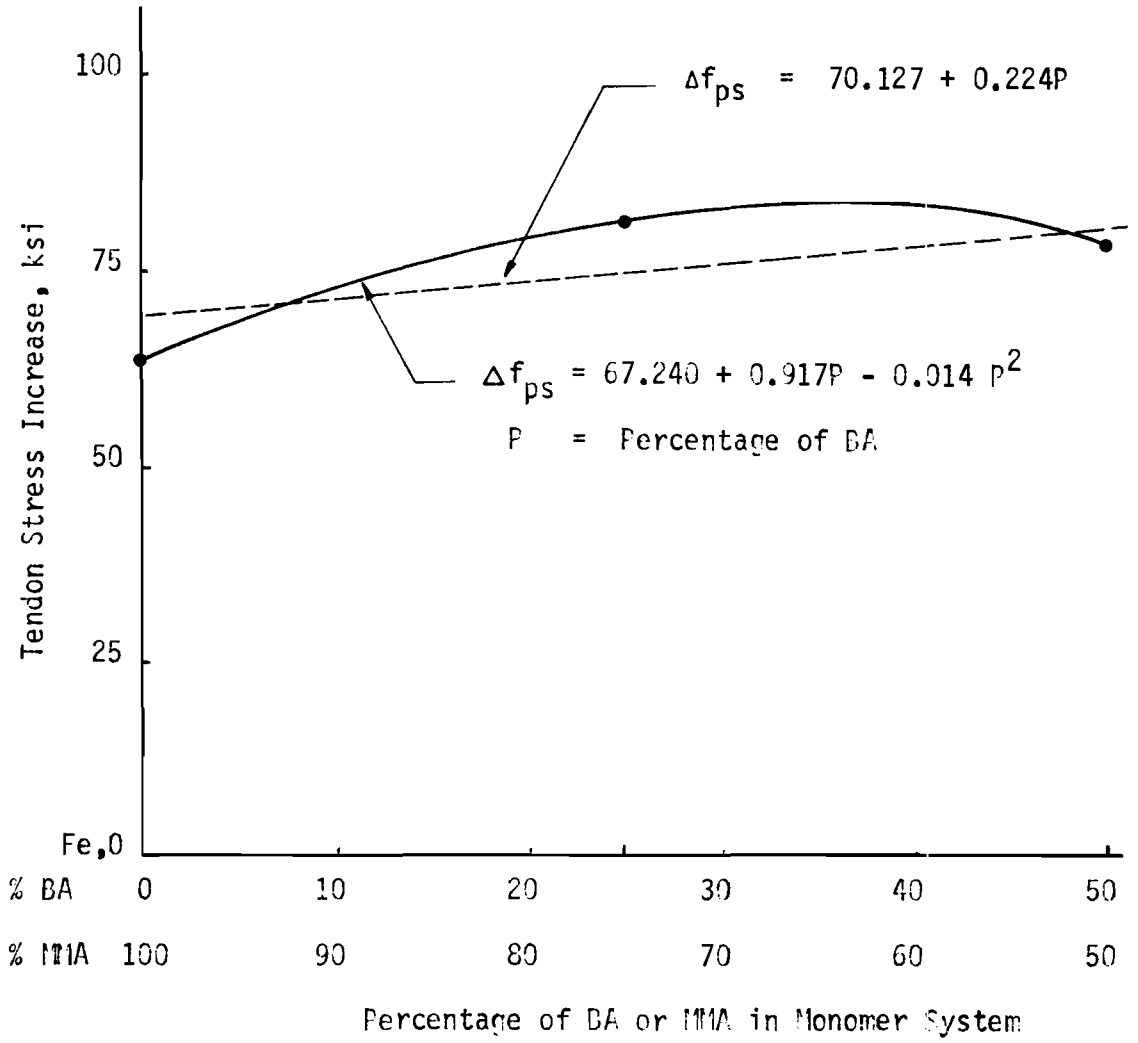

Fig. 5.54 Effect of Percentage of BA in Monomer System on Tendon Stress Increase.

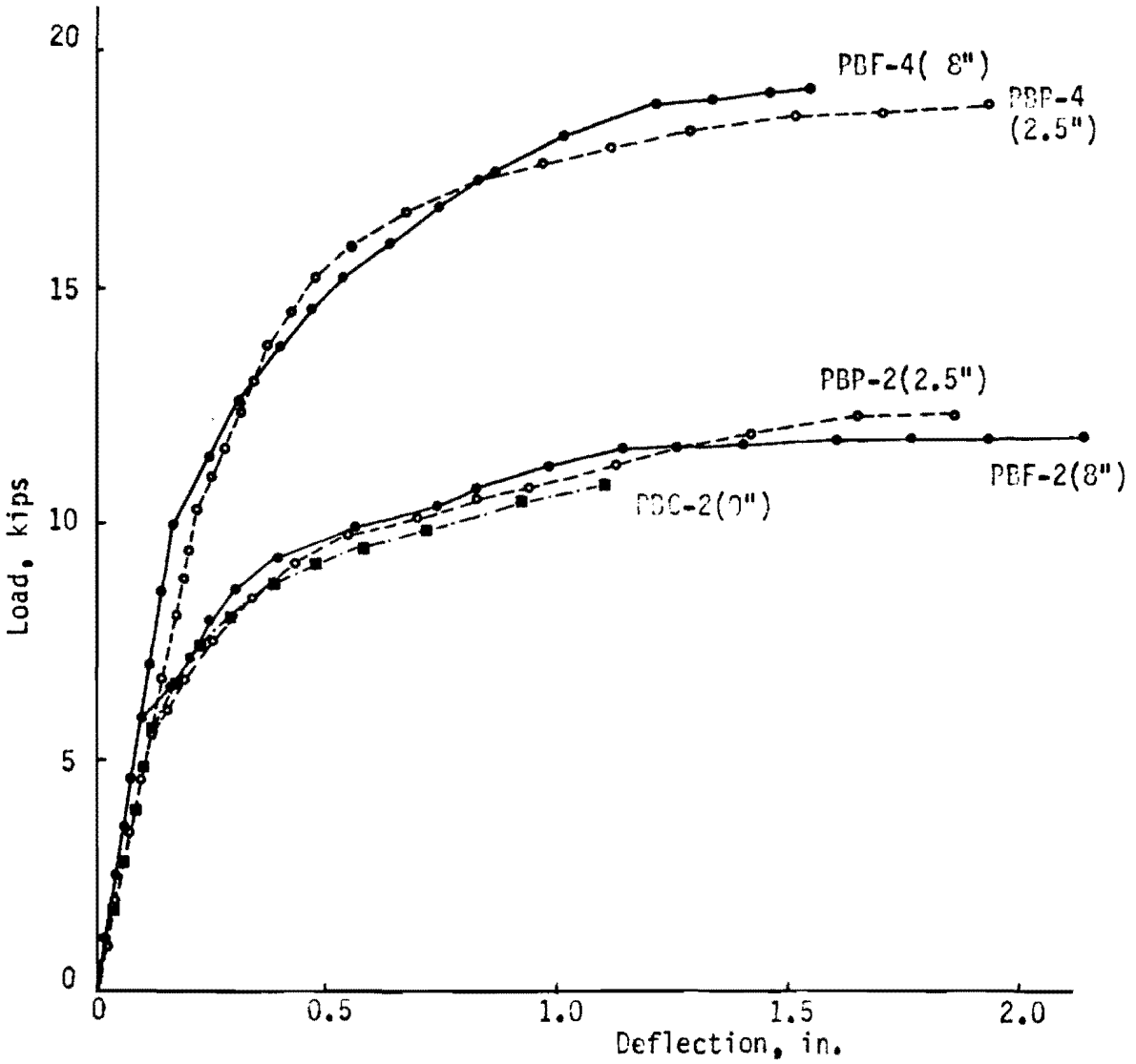

Fig. 5.55 Load-Deflection Responses for Beams with Different Polymer Depths.

for the corresponding partially impregnated beam and for the control, as shown in Fig. 5.56. The tendon stress increases for PBC-2 and PBP-2 were approximately the same and were about 20 percent less than for PBF-2. Similarly the stress increase for PBP-4 was about 30 percent less than for PBF-4.

5.4.5 Comparison of Bonded and Unbonded Tendon Members

The PIC beams with bonded tendons were 1 in. wider than the one with unbonded tendons so that they had higher elastic stiffness, as shown in Fig. 5.57. However, they developed approximately the same ultimate loads, with different midspan deflections. PBB-4P, which was grouted by the polymer material, showed the highest deflection while PBB-4C, which was grouted with conventional cement grout, was about 24 percent less and PBF-4, which contained unbonded tendons, was about 48 percent less. Both bonded tendon members had higher cracking moments than the unbonded tendon beam by about 8 percent. After the first cracks developed,the stiffnesses for PBB-4C and PBB-4P were still higher than for PBF-4 because the cracks in the bonded beams were distributed more uniformly along the length and no slip occurred between tendons and the surrounding concrete. In the test, the PIC beams containing bonded tendons developed higher rotation capacity or ductility than the beams containing unbonded tendons.

The two grouting materials used in this research seem to develop similar flexural behavior. The only differences are the application procedure and the relative costs. The cost of conventional grouting material was about 3 cents per pound but the application required a special grouting pump. The polymer materials cost about 65 cents per pound and no special mechanical device was required because the material is in a liquid state during application. The liquid monomer will polymerize within an hour and the grouted member can be placed in service at that time. The major advantages of the polymer grouting materials are ease in application, very short curing period, and equal or better ductility. However, before final conclusions can be drawn on the structural behavior, additional tests need to be performed. Some difficulty might be encountered in cases where the beams are very long and the tendon conduits are clogged so that the liquid monomer can not flow from one end to

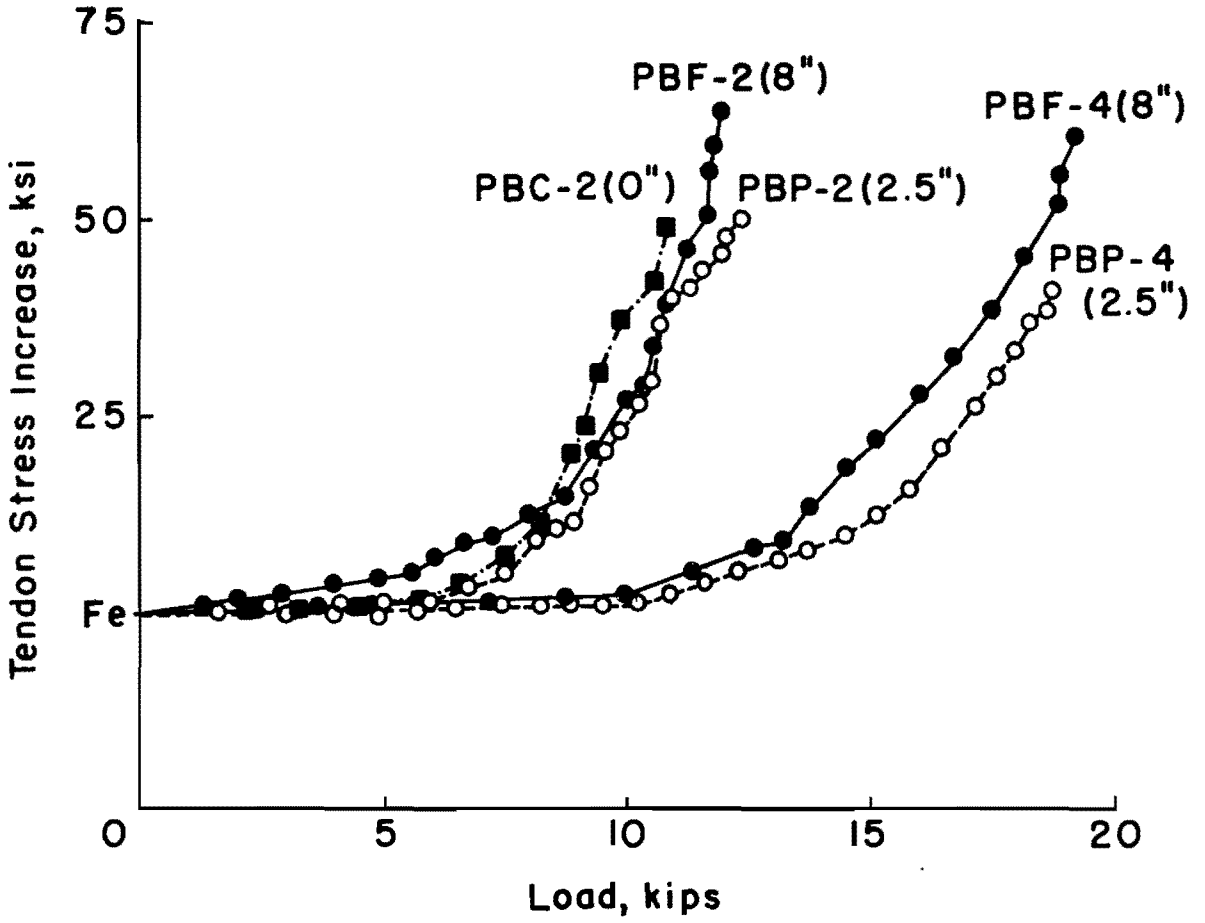

Fig. 5.56. Tendon Stress Responses for Beams with Different Polymer Depths.

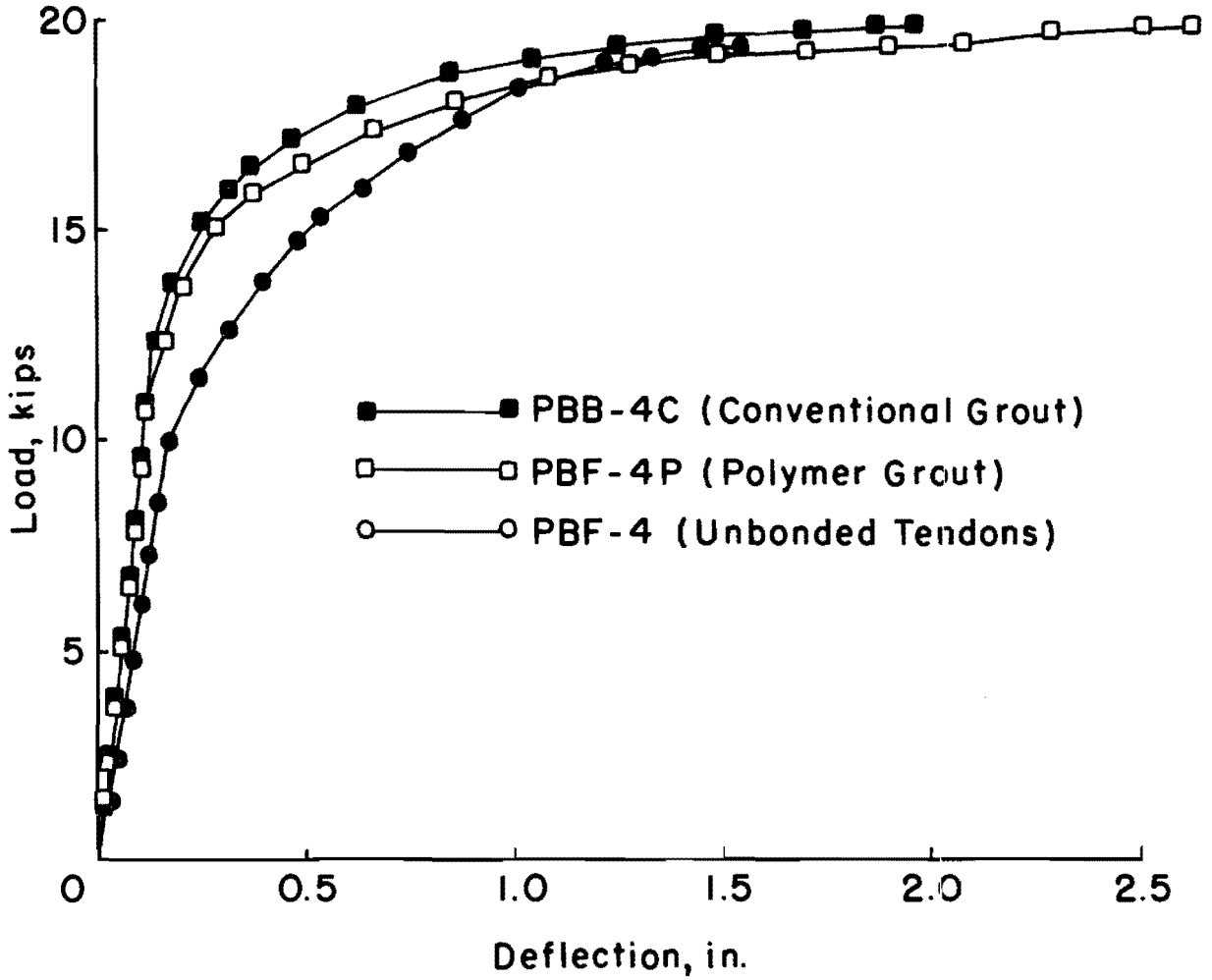

Fig. 5.57. Load-Deflection Responses for Beams Containing Bonded and Unbonded Tendons.

the other without additional pressure. It might be necessary to use a pump in those cases.

CHAPTER VI. TESTS FOR SHEAR STRENGTH

6.1 Description of Test Program

Six beams were tested in this study. All beams had the same symmetrical I-beam cross section (Fig. 3.3 (b)). Only two variable parameters were considered, the prestressing forces and the amount of web reinforcement. The beams were fully impregnated with a 100 percent MMA-monomer system, using the same technique as that described in Sect. 3.3. Two beams were unimpregnated and tested as the control beams.

The data for the test beams are given in Table 6.1. It should be noted that the shear spans and span lengths of the beams were constant, as shown in Fig. 4.1.

6.1.1 Fully Impregnated Beams

PBS-S Series: Three beams were tested in this series; PBS-4S, PBS-6S, and PBS-8S contained 4, 6, and 8 unbonded wire tendons, respectively. No. 2 grade 40 reinforcing bars were used for the web reinforcement. The amount of web reinforcement was about 50 percent less than for the beams tested to fail in flexure. The stirrup spacings are indicated in Table 6.1. The beams were prepared, impregnated, and tested using the procedures described in Chapters 3 and 4.

PBS-C Series: One fully impregnated beam was tested in this series. No stirrups were provided and the beam contained 6 unbonded tendons.

6.1.2 Control Beams

The beams were unimpregnated and were tested as the control beams. Two unbonded tendons were used, and they were post-tensioned to about 70 percent of the specified ultimate strength. The web reinforcement for beam PBC-2S was about 50 percent of that required for flexural failure. No web reinforcement was provided for the beam PBC-2C.

Table 6.1

Description of Beams for Shear Tests

Test Series	Specimen No.	Type of Concrete	No. of Wires in Tendon	$\rho_p = \frac{A_s}{bd}$	$\omega_p = \frac{\rho_p f_{ps}}{f'_c}$	Stirrups
S	PBC-2S	Control	2	0.0038	0.142	2#2@8" o.c.
	PBS-4S	PIC	4	0.0076	0.110	2#2@7" o.c.
	PBS-6S	PIC	6	0.0113	0.160	2#2@5" o.c.
	PBS-8S	PIC	8	0.0151	0.205	2#2@4" o.c.
C	PBC-2C	Control	2	0.0038	0.142	None
	PBS-6C	PIC	6	0.0113	0.110	None

6.2 Test Results

Beams tested for shear strength behavior were all subjected to essentially the same method of stressing and testing as described in Chapters 3 and 4. Tendon forces at the holding end and midspan deflections were monitored the same as in the tests for flexure. Load-deflection response as well as tendon stress response is presented.

Crack patterns, which are important in determining whether the mode of failure is diagonal shear or flexural shear, were observed and marked at each load increment until failure occurred. Strain readings in the concrete and in the steel were also taken at midspan of the beams.

6.2.1 Load-deflection Responses

Load-deflection responses shown in Fig. 6.1 and 6.2 are for the S-series beams in which some vertical stirrups were provided. They include both PIC and control beams. For the control beams, two wire unbonded tendons were used. Four, six, and eight wires per tendon were used for the fully impregnated PIC beams.

The curves seem to have generally the same elastic stiffness but the loads corresponding to first cracking and final failure were usually premature in comparison to the test for flexure. The ultimate deflections were dependent on the number of tendons.

Table 6.2 contains cracking moments and ultimate moments and their corresponding deflections for all test beams. The cracking loads were taken as the load at which the load-deflection response ceased to be linear. Both cracking and ultimate moments were calculated from the loads and shear spans. The deflections were also represented as a ratio of the span length.

6.2.2 Crack Patterns and Mode of Failure

(a) Crack Patterns: In general, cracking patterns at the beginning of the test were similar to the ones observed for the flexural tests. They were different in later stages of the loading due to the additional shear cracks. The first noticeable cracks usually appeared near the center line of the beam between the two load points and began from the tension face of the beams and extended into the web toward the top flange. The first crack

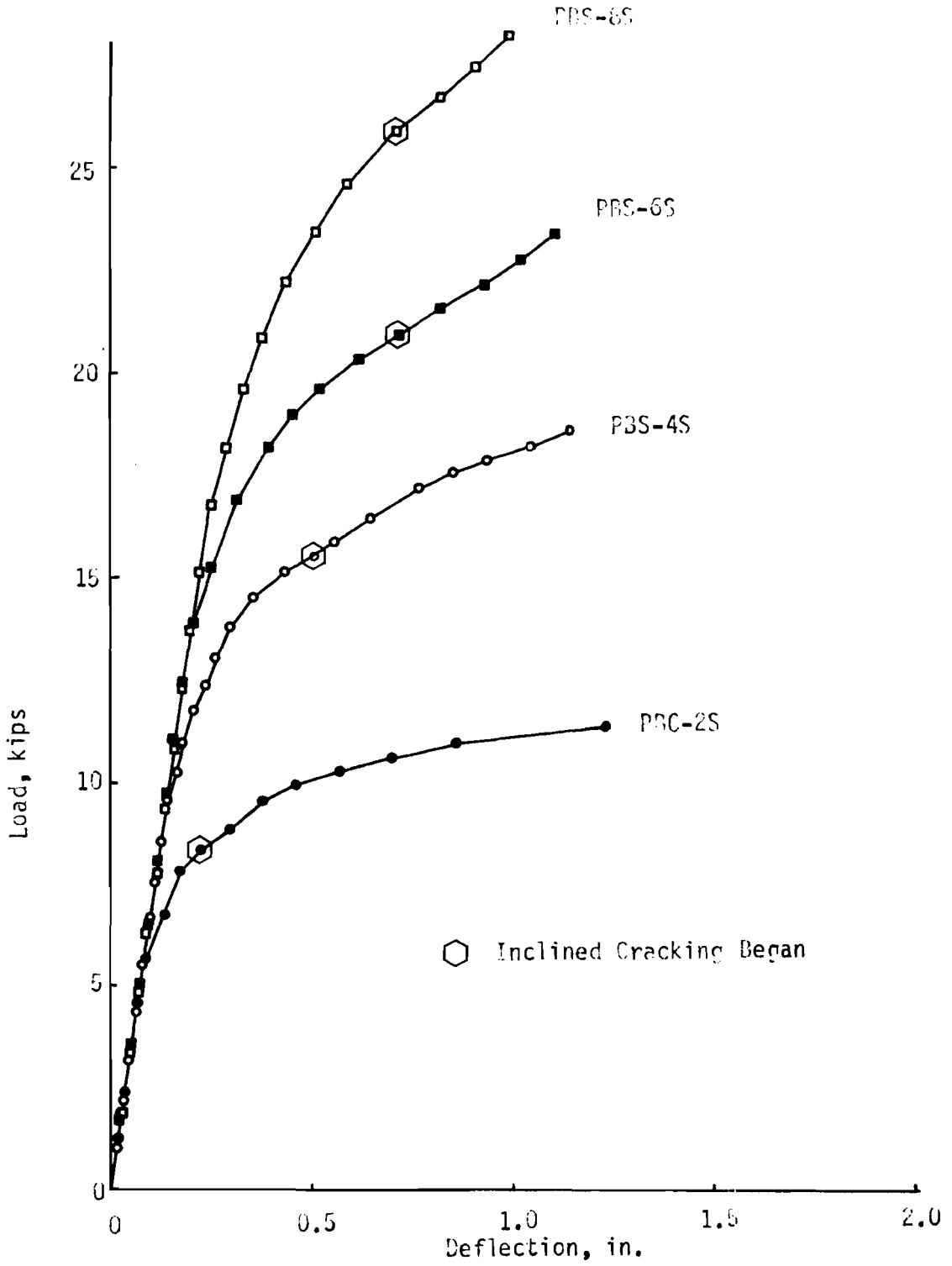

Fig. 6.1 Observed Load-Deflection Responses for S-Series Beams.

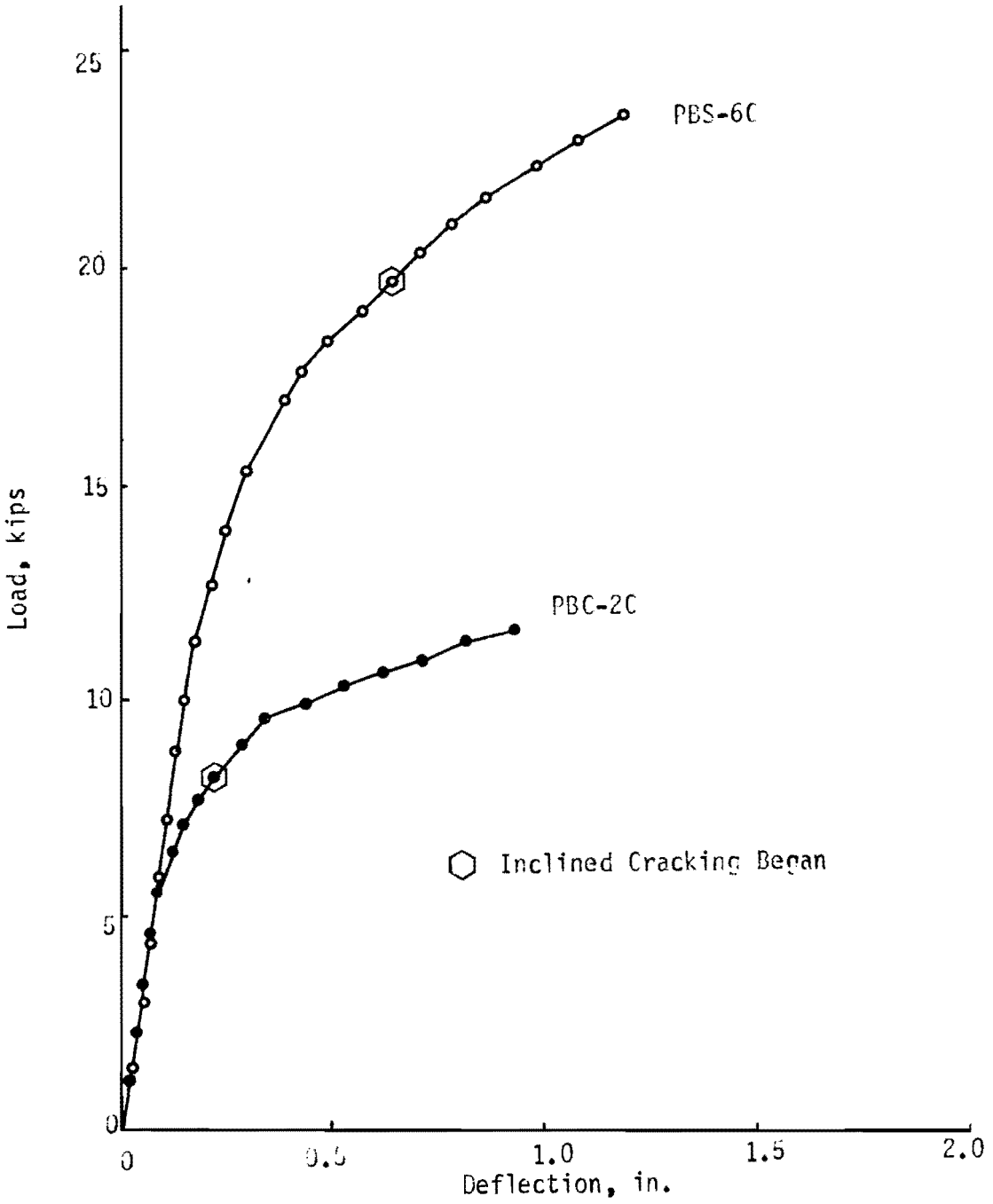

Fig. 6.2 Observed Load-Deflection Responses for C-Series Beams.

Table 6.2

Loads, Moments and Deflections at

Cracking and Ultimate for Shear Test Beams

Specimen No.	Cracking				Ultimate				Δ_u / Δ_{cr}
	Load P_{cr} (lb)	Moment M_{cr} (lb-in)	Deflection Δ_{cr} (in.)	Δ_{cr}/L	Load P_u (lb)	Moment M_u (lb-in.)	Deflection Δ_u (in.)	Δ_u/L	
PBC-2S	5,700	94,100	0.098	1/918	11,300	186,000	1.229	1/73	12.54
PBS-4S	9,550	158,000	0.150	1/600	18,600	307,000	1.147	1/79	7.65
PBS-6S	13,800	228,000	0.205	1/439	23,500	388,000	1.113	1/80	7.42
PBS-8S	16,800	287,000	0.263	1/342	28,300	466,000	0.988	1/91	3.76
PBC-2C	5,700	94,100	0.092	1/978	11,600	191,000	0.927	1/97	10.09
PBS-6C	11,400	188,000	0.183	1/492	23,500	388,000	1.193	1/75	6.52

patterns were typical of flexural cracking. Additional load caused new cracks in the shear span, outside the load points. The cracks in the shear span normally started from the tension face of the beams, extended vertically through the bottom flange, and, as soon as they reached the web, inclined toward the load point.

Fig. 6.3 shows the crack patterns for the S-series beams in which some stirrups were provided. Fig. 6.4 shows the crack patterns for the C-series beams in which no shear reinforcing was provided. The patterns along the beams were not quite symmetrically distributed, especially in the region outside the load point. More cracks were developed in the shear span next to the anchoring end than in the region of the stressing end. The number by each crack is the machine load when that crack occurred. The shaded areas and the dashed lines indicate the spalled areas and final cracks after failure.

(b) Mode of Failure: Modes of failure for the beams in the S series and in the C series are very similar. As the load increased, the existing cracks opened wider and shear cracks simply inclined toward the load point. When the inclined cracks reached the top flange, cracking became more severe and finally the top flange crushed immediately over the widest crack between the load points. This type of failure may be classified as a shear-compression failure.

Photographs shown in Figs. 6.5 and 6.6 illustrate the explosive failure, which normally depended on the number of wires in the beams. It should be mentioned that the crack patterns were marked from the beginning of the test until the load began to level off. Since the failures occurred very suddenly, without warning, the marking of cracks was discontinued after this point for the sake of safety. The unmarked cracking patterns are not very visible in the photos; however, the diagrams in Figs. 6.3 and 6.4 illustrate the cracking.

6.2.3 Tendon Stress Responses

Only the tendon forces at the holding ends were monitored during testing by means of load cells. Plots of loads versus increased tendon stresses are shown in Figs. 6.7 and 6.8. Fig. 6.7 illustrates beams in the S series, which included one control beam containing a 2-wire tendon (PBC-2S) and

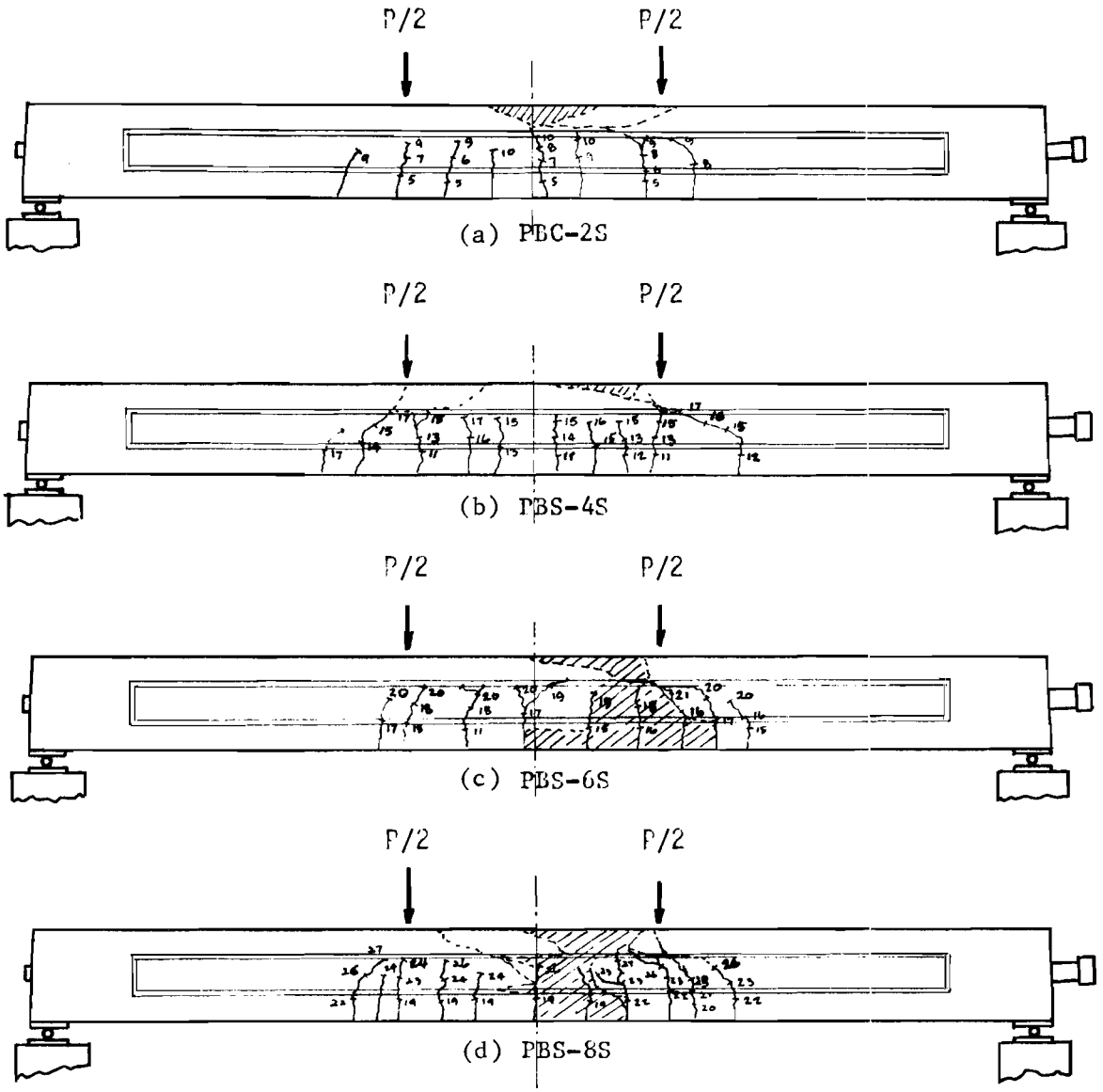

Fig. 6.3 Crack Patterns for S-Series Beams.

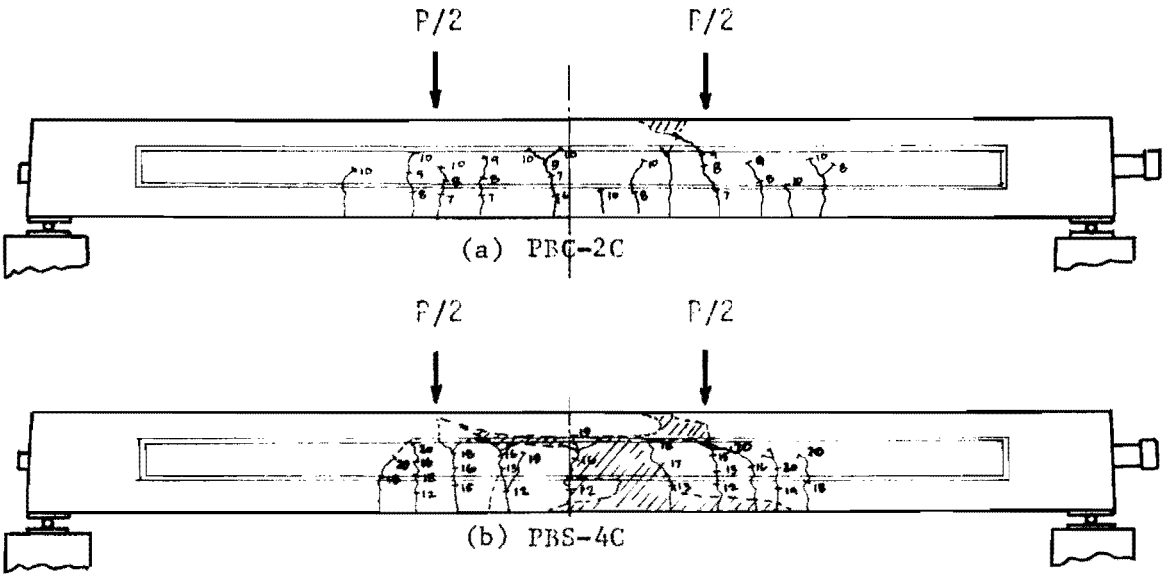

Fig. 6.4 Crack Patterns for C-Series Beams.

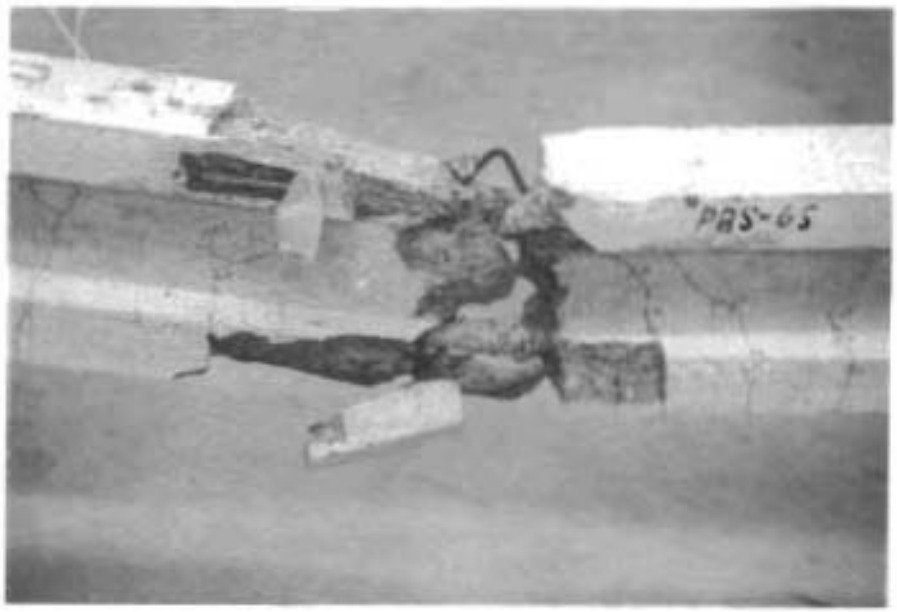

(a) PBS-6S

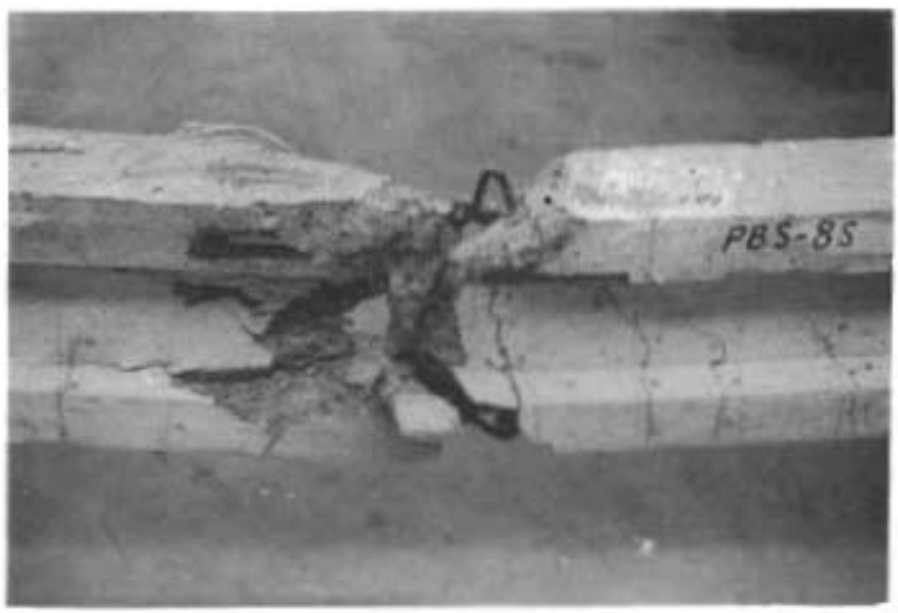

(b) PBS-8S

Fig. 6.5 PBS-6S and PBS-8S After Failure.

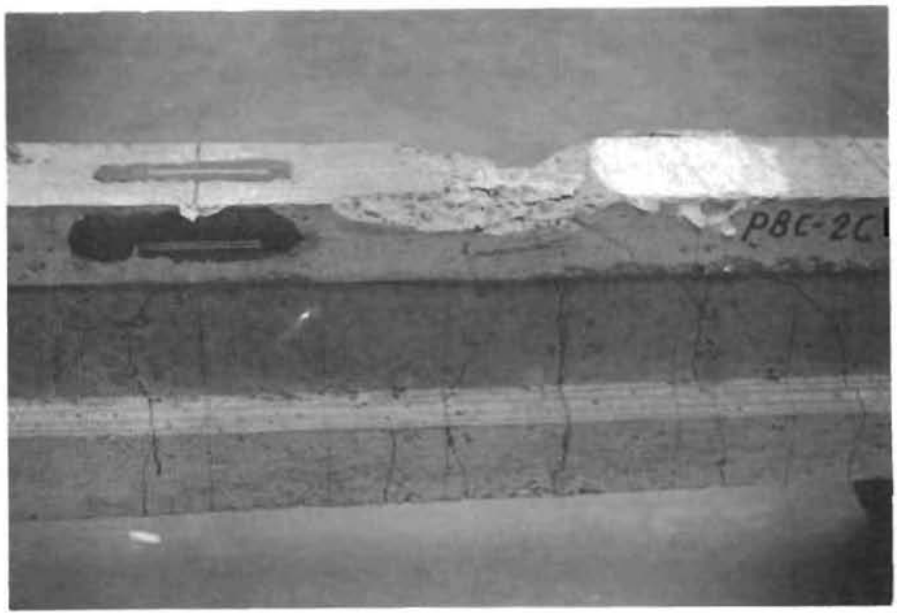

(a) PBC-2C

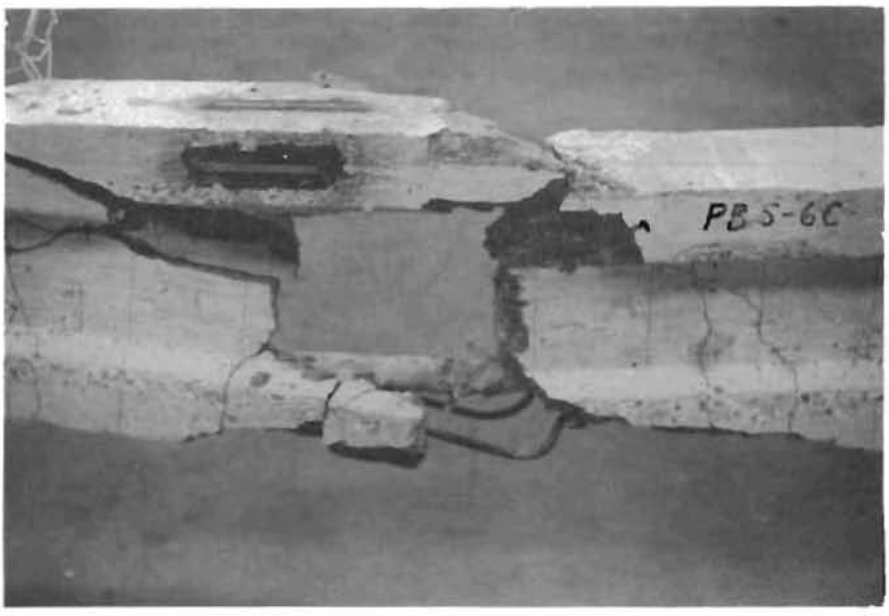

(b) PBS-6C

Fig. 6.6 PBC-2C and PBS-6S After Failure.

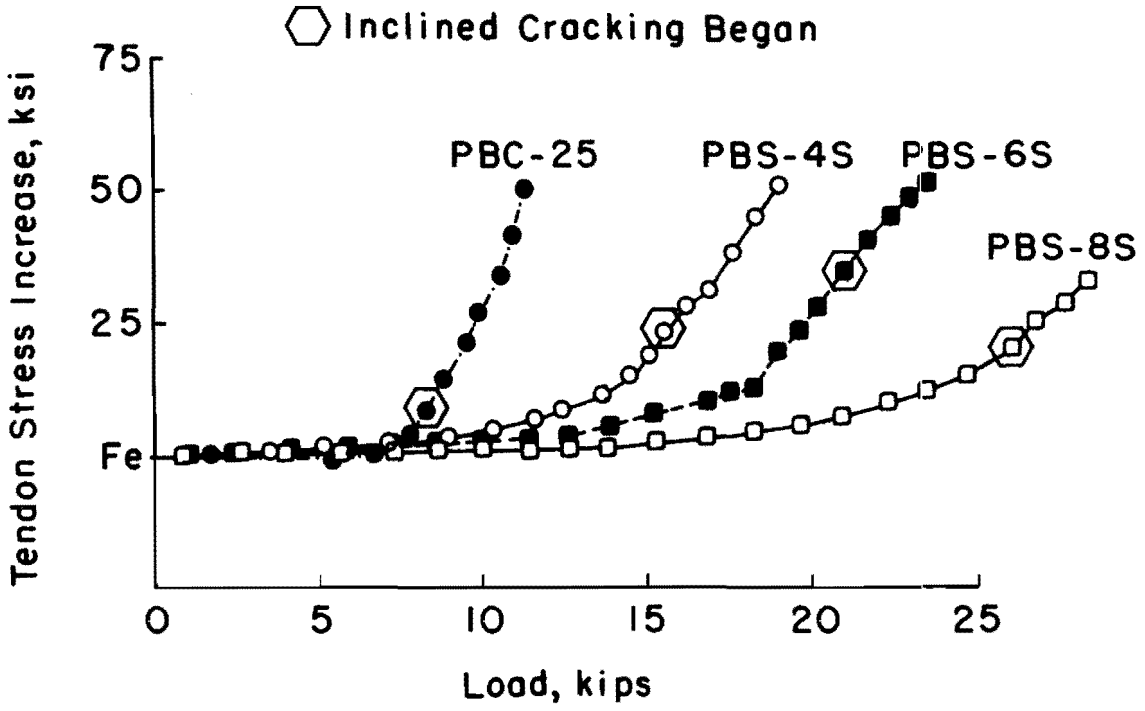

Fig. 6.7. Observed Tendon Stress Response Under Loads for S-Series Beams.

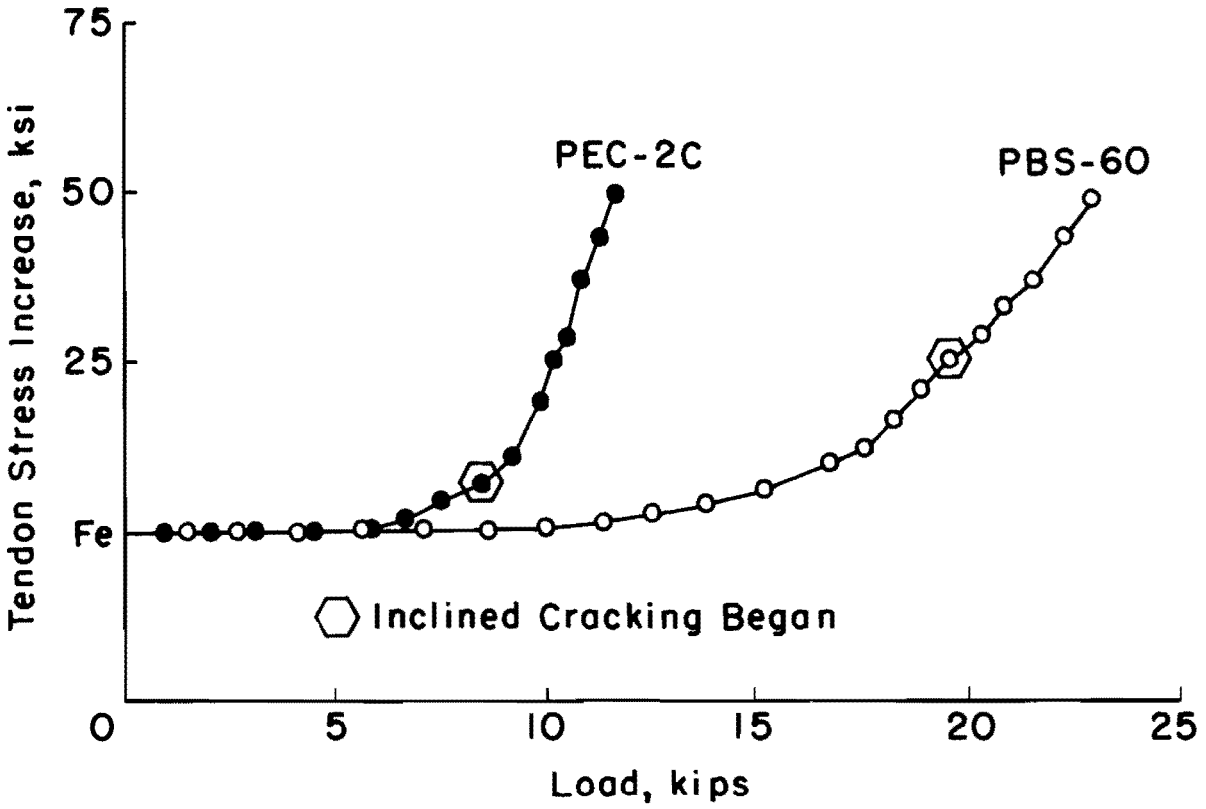

Fig. 6.8. Observed Tendon Stress Responses Under Loads for C-Series Beams.

three PIC beams (PBS-4S, PBS-6S, PBS-8S) containing 4, 6, and 8-wire tendons, respectively. Fig. 6.8 is for beams in the C series, which included one PIC beam (PBS-6C) with a 6-wire tendon and one control beam (PBC-2C) with a 2-wire tendon.

The curves are typical and indicate a linear response before the development of the first cracks. After the first cracking the response became nonlinear. The stresses at ultimate load did not consistently increase with the number of wires in the tendons as previously presented for the flexural test due to premature failure caused by shear associated with flexure. As shown in both figures, PBS-8S showed the lowest increased tendon stress. The rest of the beams had approximately the same 50-ksi increase in stresses.

6.2.4 Useful Limits of Strains

The useful limits of strains on the extreme fiber of the PIC beams, shown in Table 6.3, were measured by means of the strain gauges at midspan. The measured strains ranged from 0.0027 to 0.0031 in./in. and the average was about 0.0029 in./in. These values were plotted in Fig. 5.25 with the test results for the flexural tests, and the relationship between the maximum strain and the cylinder strength of PIC was presented by Eq. 5.2. It should be noted that this equation is appropriate for post-tensioned PIC beams impregnated with 100 percent MMA monomer system and the cross section used in this test.

The useful limits of strains for the control beams were 0.0027 and 0.0028 in./in. They were slightly less than those for PIC beams.

6.3 Evaluation of Test Results

The development of formulae to predict shear strength based on the test results is presented in this section. The shear strength at inclined cracking load and at ultimate load will be determined. The shear strength at inclined cracking may be classified into two categories: pure shear and flexural shear. The observed modes of failure are important to identify the shear failure modes and to analyze failure loads.

Table 6.3

Useful Limit of Strain for Beams Tested for Shear

Beam No.	Maximum Strain ε_u (in/in.)
PBC-2S	0.0028
PBS-4S	0.0028
PBS-6S	0.0027
PBS-8S	0.0031
PBC-2C	0.0027
PBS-6C	0.0029

6.3.1 Shear at Inclined Cracking

The inclined cracks in these test beams were observed in connection with flexural cracks developing between the load point and the support. The failure could have been flexural with some contribution of shear. The load at inclined cracking was greater than the load at which the critical flexural cracks formed. However, to determine the shear resistance for the PIC beams, the relationship of shear at flexural cracking and shear at inclined cracking must be evaluated.

(a) Shear at Critical Flexural Crack: Since the horizontal projections of the inclined cracks at failure were longer than the depth of the beam, flexural cracking at a distance d/2 in the direction of decreasing moment from the section considered was used as the point at which a vertical crack was assumed to initiate. For the test beams, the dead load was small compared with the applied load and the total shear at the formation of the critical flexural cracks may be expressed as follows:

$$V_{cr} = \frac{M_{cr}}{M/V - d/2} \qquad (6.1)$$

where M_{cr} = calculated flexural cracking moment

M, V = moment and shear due to applied loads at section considered

d = effective depth of the beam

For the particular case for the beam in these test, M/V represented the shear span of the beam. M_{cr} was calculated by Eq. 2.15, based on a modulus of rupture of PIC of $6\sqrt{f'_{cp}}$. Table 6.4 summarizes the shear necessary to form the flexural cracks at the critical section.

(b) Measured Shear at Inclined Cracking: Shear at the inclined cracking can be determined from the applied load by means of the structural analysis. The inclined cracking loads for the test beams were shown in the load-deflection response. Since the tendons were draped 2.5 in. at midspan, the shear carried by the tendons was considered. The dead weight of the beam was neglected in this computation. The net shear at inclined cracking can be written as follows:

Table 6.4

Shear to Form Flexural Cracks at Critical Section

Beam No.	Calculated M_{cr} (lb-in.)	$V_{cr} = \frac{M_{cr}}{M/V - d/2}$ (lb)
PBC-2S	81,600	2,740
PBS-4S	157,000	5,270
PBS-6S	230,000	7,730
PBS-8S	285,000	9,590
PBC-2C	78,700	2,650
PBS-6C	225,000	7,580

$$V_{cm} = V_m - V_T \tag{6.2}$$

where V_m = measured total shear at inclined cracking

V_T = shear carried by draped tendons

V_{cm} = net shear at inclined cracking.

Table 6.5 summarizes the net shear at inclined cracking. For the beams with web reinforcement, the inclined cracking loads are higher than for the beams without web reinforcement.

(c) Flexural Shear: The load at the flexural shear cracking is normally larger than the load which produces the critical flexural cracks. The additional shear required to form the inclined cracks can be evaluated from the test results. Fig. 6.9 shows the relationship between the shear at inclined cracking and the shear at the formation of the critical flexural crack. The test data were limited by the number of test beams. However, the expression for the flexural shear can be written as

$$V_{ci} = b_w d\sqrt{f'_{cp}} + \frac{M_{cr}}{M/V - d/2} \tag{6.3}$$

where V_{ci} = flexural shear, lb

b_w = web thickness, in.

d = effective depth, in.

f'_{cp} = compressive cylinder strength of PIC, psi

M_{cr} = calculated cracking moment (Eq. 2.15)

M, V = moments and shear at the considered section.

It should be noted that Eq. 6.3 is almost identical with Eq. 2.14, developed by Olesen for prestressed concrete beams (46). The data for unimpregnated beams were also plotted in Fig. 6.9. They are also in good agreement with the fitted curve.

Table 6.5

Measured Shear at Inclined Cracking

Beam No.	P_m (lb)	V_m (lb)	V_T (lb)	V_{cm} (lb)
PBC-2S	8,500	4,250	400	3,850
PBS-4S	15,500	7,750	850	6,900
PBS-6S	20,900	10,500	1,280	9,170
PBS-8S	26,000	13,000	1,630	11,400
PBC-2C	8,150	4,080	390	3,690
PBS-6C	19,600	9,800	1,260	8,540

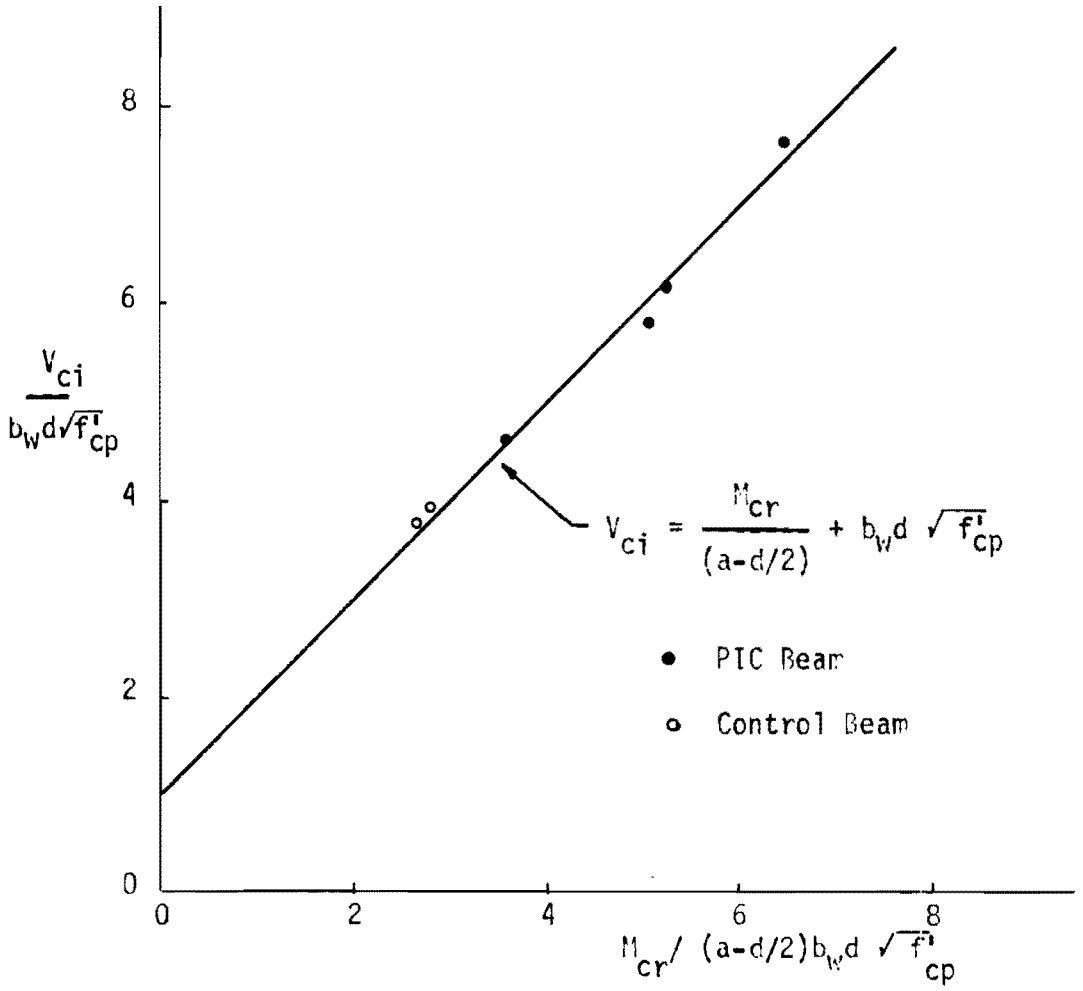

Fig. 6.9 Flexural Shear for Polymer-Impregnated Concrete Beams.

6.3.2 Ultimate Shear

The conditions at ultimate for a shear-compression failure are similar to those for a flexural failure (46). The analysis of the strength of beams failing in shear-compression could, therefore, be carried out in a manner similar to the analysis of flexural strength. For the flexural analysis, the equivalent rectangular stress distribution for PIC beams developed in the previous chapter is used. The measured tendon forces presented in Sect. 6.2 are considered in the computation.

On the other hand, a hypothesis for the mechanism of the action of web reinforcement after inclined cracking can be presented as follows:

$$V_{us} = V_c + V_{st} \qquad (6.4)$$

where V_{us} = ultimate shear, lb

V_c = shear at inclined cracking, lb

V_{st} = shear carried by web reinforcement, lb.

Shear carried by web reinforcement can be calculated by Eq. 2.17 rewritten as

$$V_{st} = \frac{A_v f_v s}{d} \qquad (6.5)$$

where A_v = area steel of each stirrup, $in.^2$

s = stirrup spacing, in.

f_v = effective strength of web reinforcement, psi

d = effective depth of the beam, in.

The values of V_c are calculated by Eq. 6.3 and, for draped tendon beams, the vertical component of tendon forces must be considered in the calculation. Since the strain in the web reinforcing steel had not been measured, it might be difficult to estimate the actual stress of the web reinforcement at ultimate. For the purpose of comparing the ultimate shear, the web reinforcement is assumed to reach the yield strength; then f_v can be replaced

by f_y. Table 6.6 summarizes the calculated and observed ultimate shears for the test beams. The calculated ultimate shear at flexural failure is smaller than the calculated values using Eq. 6.4. It is indicated that all beams could have failed by flexural or shear-compression failure.

6.4 Comparison of Test Results with Theoretical Analysis

The formula developed from the test data in the previous section is used to analyze the flexural shear for PIC beams. On the other hand, the flexural behavior regarding cracking moments, tendon stresses, and ultimate moments is calculated by the numerical procedure using computer program PICB and the equations developed in the previous chapter. Both flexural and shear behavior will be compared to the values calculated on the basis of the ACI equations. Since the test beams failed in flexure with a combination of shear, the comparison for flexural behavior in some cases might not be in good agreement with the analysis.

6.4.1 Cracking Moments

The modulus of rupture for the PIC was confirmed to be $6\sqrt{f'_{cp}}$ by the test results in the previous chapter. The calculated cracking moments (M_{cr_1}) based on this modulus of rupture are the same as the values calculated by the equation in the ACI Building Code. The cracking moments calculated by the computer program PICB for PIC beams are slightly higher than the test results because the computer program considered the tensile strength of PIC in computation. Cracking moments are compared in Table 6.7.

For control beams, the test results ranged from 17 percent higher for PBC-2S and 19 percent higher for PBC-2C than the predicted values using a modulus of rupture of $6\sqrt{f'_{cp}}$. For PIC beams, the test results were in good agreement with the prediction except one for PBS-6C. The cracking moments for the C-series beams were less than for the ones in the S series. The confinement provided by the web reinforcing might affect the initial cracking, which is usually caused by flexure (49).

Table 6.6

Computed and Measured Shear Capacities

Beam No.	Measured V_{um} (lb)	Calc. Shear at Flex. Failure V_{uf} (lb)	Calc. Shear (Eq.6.4) V_{us} (lb)	$\frac{V_{um}}{V_{uf}}$	$\frac{V_{um}}{V_{us}}$
PBC-2S	5,650	4,280	5,800	1.32	0.97
PBS-4S	9,300	9,470	11,400	0.98	0.82
PBS-6S	11,800	12,400	15,600	0.95	0.76
PBS-8S	14,100	15,400	19,300	0.92	0.73
PBC-2C	5,800	4,250	4,080	1.36	1.42
PBS-6C	11,800	12,000	9,800	0.98	0.97

Table 6.7

Comparison of Cracking Moments

Beam No.	Observed M_{cr} (lb-in)	Calculated M_{cr_1}* (lb-in)	Ratio M_{cr}/M_{cr_1}	Calculated M_{cr_2}** (lb-in)	Ratio M_{cr}/M_{cr_2}
PBC-2S	94,100	81,600	1.15	74,300	1.26
PBS-4S	158,000	157,000	1.00	182,000	0.87
PBS-6S	228,000	230,000	0.99	248,000	0.92
PBS-8S	277,000	285,000	0.97	314,000	0.88
PBC-2C	94,100	78,700	1.19	74,300	1.26
PBC-6C	188,000	225,000	0.83	248,000	0.76

* M_{cr_1} was calculated based on a modulus of rupture $6\sqrt{f'_{cp}}$.

** M_{cr_2} was calculated by the computer program PICB.

6.4.2 Tendon Stress Increase

Change in tendon stress for each test beam was calculated by ACI Eq. 18.4, which is generally used in design for post-tensioned concrete beams containing unbonded tendons, by the computer program PICB, which was developed for PIC beams failing in flexure, and by the equation developed in the previous chapter for PIC beams at flexural failure. The comparison of the observed and predicted values is summarized in Table 6.8. The test results are generally less than the prediction by the computer program PICB or by Eq. 5.12. It could have been the result of premature failure of shear associated with flexure. On the other hand, the predicted values by ACI Eq. 18.4 are about half of the observed values. This equation may represent a safe estimate for the tendon stress increase.

6.4.3. Ultimate Moments

The comparison of the observed and calculated ultimate moments is summarized in Table 6.9. The calculated moments were predicted analytically by (1) the computer program PICB, (2) the equivalent rectangular stress block for PIC developed in this study, and (3) the rectangular stress block recommended by the ACI Code. The tendon forces at ultimate used in the calculation with the equivalent rectangular stress block were assumed to be the same as for the test results given in Sect. 6.2, while the forces used in the computation by the ACI Building Code were assumed to be given by ACI Eq. 18.4.

Even for the beams failing in flexural shear, the values predicted by the ACI Building Code or by the computer program are less than the observed values. The ratio of the observed to the predicted ultimate moment for the control beams is higher than the ratio for the PIC beams.

The prediction based on the equivalent rectangular stress distribution developed in the previous chapter was used for the PIC beams only. The ultimate moments calculated by this method are higher than the test results, due to the premature failures.

Table 6.8

Comparison of Tendon Stress Increase

Beam No.	Observed Δf_{ps} (ksi)	Calculated Δf_{ps_1} (ksi) (ACI Eq. 18-4)	Ratio $\Delta f_{ps}/\Delta f_{ps_1}$	Calculated Δf_{ps_2} (ksi) (PICB)	Ratio $\Delta f_{ps}/\Delta f_{ps_2}$	Calculated Δf_{ps_3} (ksi) (Eq. 5.12)	Ratio $\Delta f_{ps}/\Delta f_{ps_3}$
PBC-2S	50.900	24.300	2.09	60.900	0.84	-	-
PBS-4S	50.900	27.400	1.86	57.500	0.89	57.300	0.89
PBS-6S	51.600	21.600	2.39	52.200	0.99	48.400	1.06
PBS-8S	31.400	18.600	1.70	53.800	0.58	39.700	0.80
PBC-2C	49.900	24.300	2.05	60.900	0.82	-	-
PBS-6C	47.900	21.600	2.22	52.200	0.92	48.400	0.99

Table 6.9

Comparison of Ultimate Moments

Beam No.	Observed M_u (lb-in.)	Calculated M_{u_1} (lb-in.) (ACI Eq. 18.4)	Ratio M_u/M_{u_1}	Calculated M_{u_2} (lb-in.) (PICB)	Ratio M_u/M_{u_2}	Calculated M_{u_3} (lb-in.) (Rect. Str. Blck.)	Ratio M_u/M_{u_3}
PBC-2S	186,000	141,000	1.32	144,000	1.29	-	-
PBS-4S	307,000	267,000	1.15	269,000	1.14	312,000	0.98
PBS-6S	388,000	361,000	1.08	363,000	1.06	409,000	0.95
PBS-8S	466,000	432,000	1.08	455,000	1.02	507,000	0.92
PBC-2C	191,000	140,000	1.36	144,000	1.32	-	-
PBC-6C	388,000	355,000	1.09	363,000	1.06	398,000	0.97

6.4.4 Shear Strength

Modes of failure for the beams in both the C series and the S series are considered to be a combination of flexure and shear. In Table 6.10 the observed shear strengths for each beam are much smaller than the diagonal shear strength calculated by the method presented in Sect. 2.2.2. This confirms that the test beams could have never failed in diagonal tension. On the other hand, the observed shear strength could be compared to the flexural shear only.

Table 6.11 is a comparison between the observed and predicted flexural shear strengths. ACI Eq. 11.11 is used to calculate V_{ci_1} for all beams while Eqs. 2.14 and 6.3 are used to calculate V_{ci_2} for the PIC beams and the control beams, respectively. The calculated values using the ACI equation indicate reserve strength in the range of 12 to 21 percent for the PIC beams and in the range of 23 to 25 percent for the control beams. The predictions by Eqs. 2.14 and 6.3 are in good agreement with the test results.

6.5 Effects of Independent Variables on Shear Strength

Actually, shear strength of post-tensioned PIC beams depends on many factors, such as shear span, shape of the cross section, percentage of steel or number of tendons, and vertical reinforcement. Only two variables were selected for this investigation: number of tendons and web reinforcement. The discussion includes the effect of percentage of steel as well as stirrup spacing. However, a comparison with corresponding beams in the flexural tests is also made.

6.5.1 Web Reinforcement

In general, web reinforcement for prestressed concrete beams will play an important role after the development of cracks. Web reinforcement will limit inclined cracking, which starts in the web and so does not result in gross distortion of the adjacent beam section and thus cause failure. This test program selected three different web reinforcements: the first is the PBF series, in which sufficient stirrups were used; the second is the S series, in which only half of the amount of calculated required stirrups in the PBF series was used; and the last is the C series, in which no stirrups were used. Plots in Figs. 6.10 through 6.12 show the load-deflection responses for

Table 6.10

Predicted Diagonal Shear Strength

Beam No.	Observed V_{cm} (lb)	Calculated V_{cw} (lb) (ACI Eq.11.12)	Calculated V_{cs} (lb) (Eq. 2.13)
PBC-2S	3,850	7,150	6,910
PBS-4S	6,900	13,300	12,100
PBS-6S	9,170	17,400	14,100
PBS-8S	11,400	20,700	15,500
PBC-2C	3,630	7,110	6,880
PBS-6C	8,540	17,200	14,000

Table 6.11

Observed and Predicted Flexural-Shear Strength

Beam No.	Observed V_{cm} (lb)	Calculated V_{ci_1} (lb) (ACI Eq. 11.11)	Ratio V_{ci}/V_{ci_1}	Calculated V_{ci_2}*(lb)	Ratio V_{cm}/V_{ci_2}
PBC-2S	3,850	3,070	1.25	3,710	1.03
PBS-4S	6,900	5,710	1.21	6,760	1.02
PBS-6S	9,170	7,740	1.19	9,220	0.99
PBS-8S	11,400	9,360	1.21	10,800	1.05
PBC-2C	3,690	3,000	1.23	3,610	1.02
PBS-6C	8,540	7,610	1.12	9,060	0.94

* V_{ci_2} calculated by Eq. 6.13.

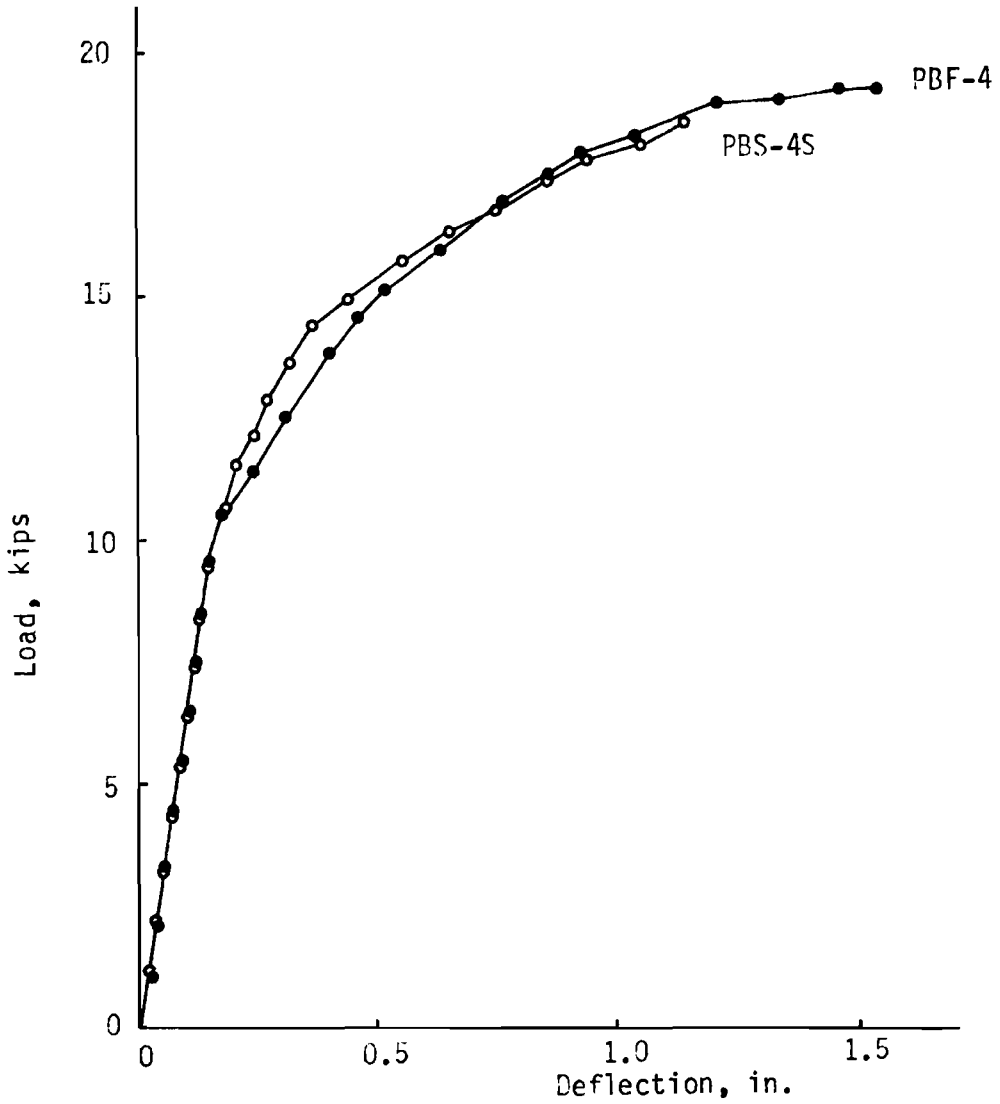

Fig. 6.10 Comparison of Load-Deflection Responses for PBF-4 and PBS-4S.

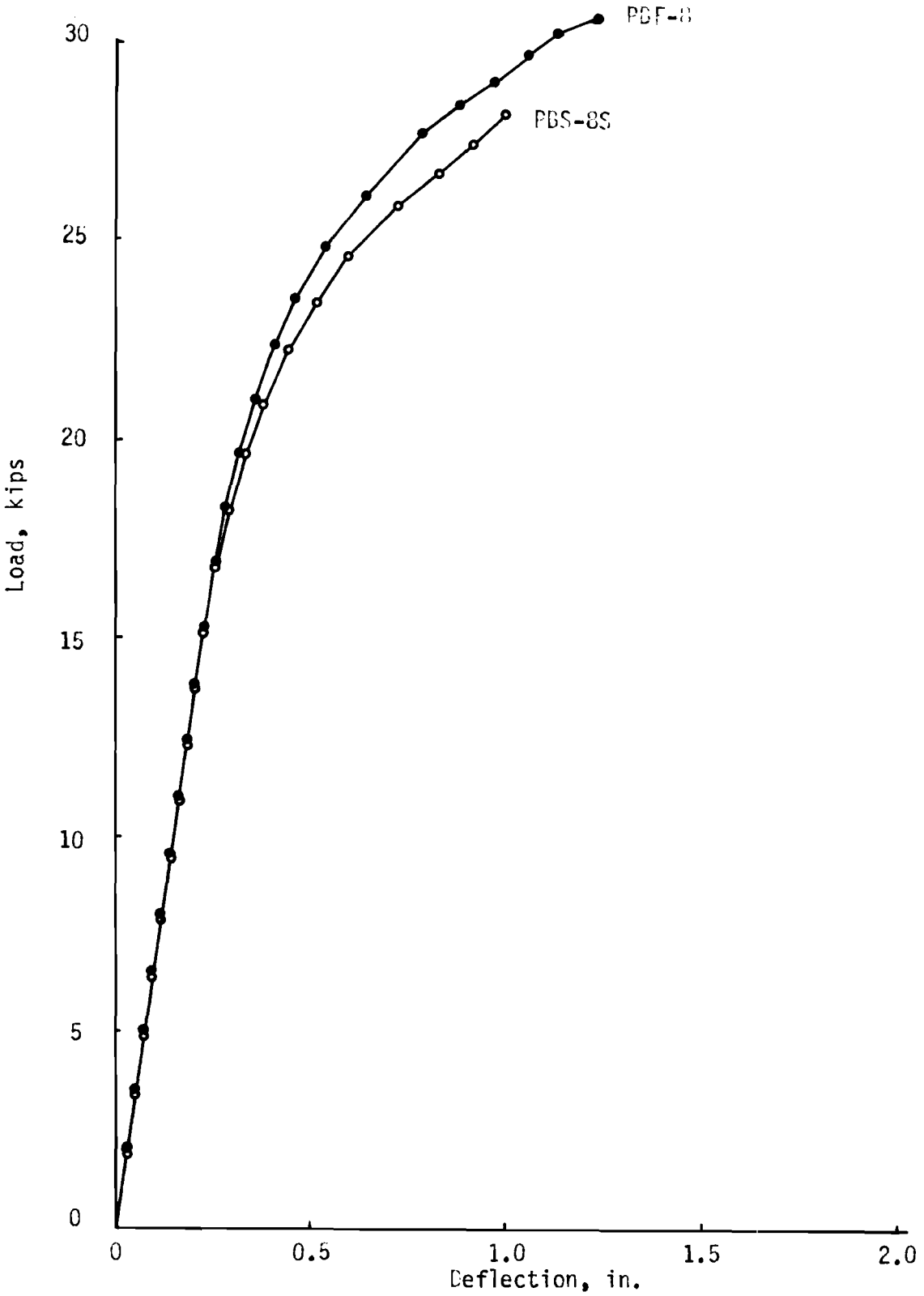

Fig. 6.11 Comparison of **Load-Deflection Responses for PBF-8 and PBS-8S.**

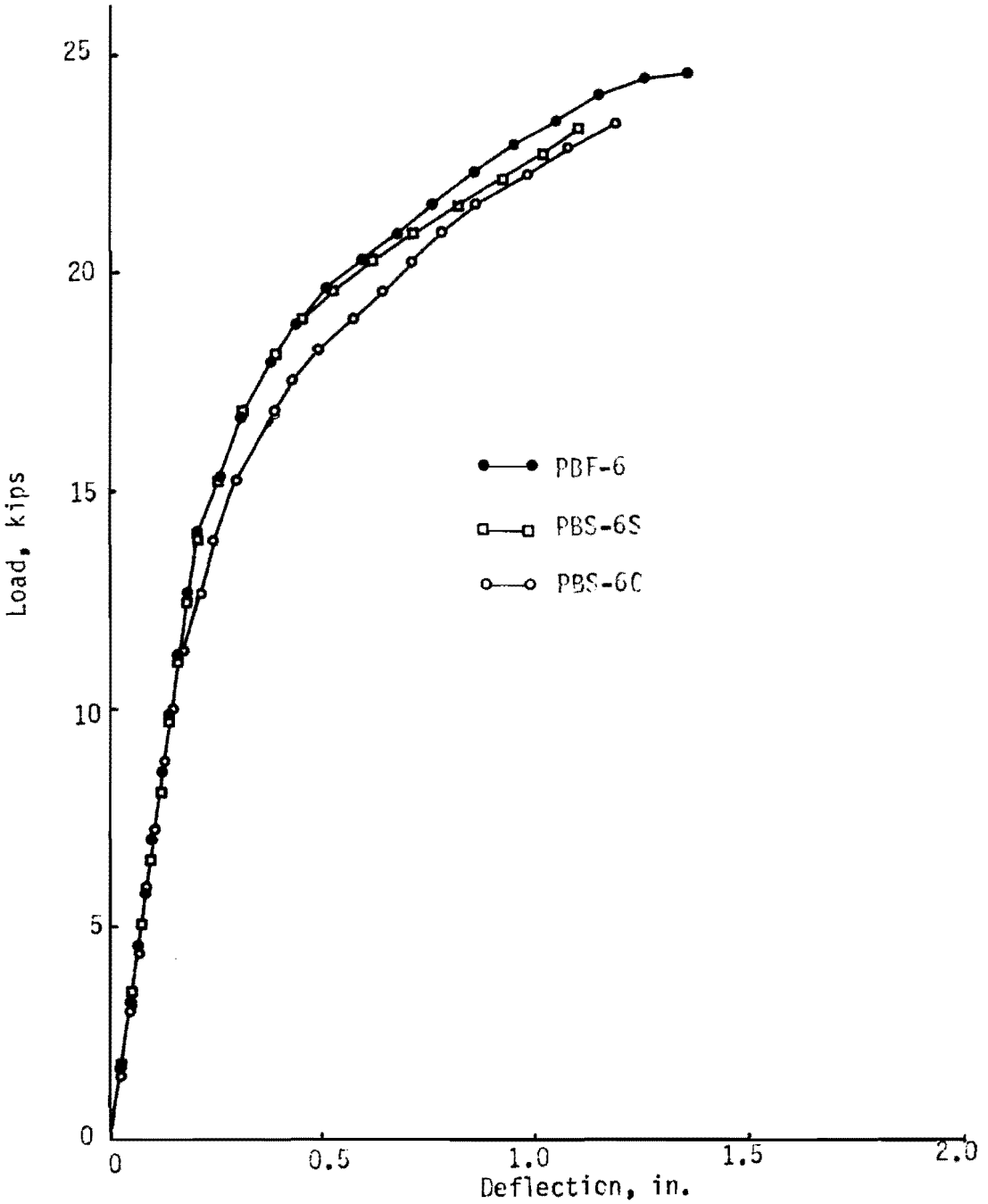

Fig. 6.12 Comparison of Load-Deflection Responses for PBF-6, PBS-6S, and PBS-6C.

beams in each series which contained the same number of wires per tendon. Even though the concrete mix used for the PBF series was different from the one for the S and the C series, the curves were considered to represent their principal behaviors.

Before cracking, beams in the PBF series show good agreement of responses with the corresponding beams in the S or C series but, soon after the first cracks were observed, the stiffnesses of the PBF-series beams were found to be higher than of the S-series beams in almost every case except the one for a 4-wire tendon (PBS-4S). The ultimate loads and the ultimate deflections for the beams in the flexural tests are higher than those for the beams in the shear tests. For the PIC beams containing 6 unbonded wires per tendon, the beam with some web reinforcement (PBS-6S) performed slightly better than the beam without the web reinforcement (PBS-6C). The stiffness after cracking and the ultimate load were found to be higher.

In summary, web reinforcement has a minor effect on the load-deflection response of the post-tensioned PIC beams tested; insufficient stirrups will result in lower ultimate loads and deflections. Even though the beams failed in a combination of flexure and shear, the flexural behavior seemed to predominate before final failure occurred.

6.5.2 Percentage of Prestressing Steel

Percentage of steel or number of wires per tendon normally affects flexural strength as well as shear strength. A higher number of wires per tendon means higher prestressing forces, which will lead to higher shear resistance. Fig. 6.13 shows the relationship between various kinds of shear strength and percentage of steel plotted from data in Tables 6.10 and 6.11. Only four points for each curve were plotted, corresponding to PBS-4S, PBS-6S, PBS-6C, and PBS-8S, which had percentages of steel equal to 0.0076, 0.0113, 0.0113, and 0.0151, respectively. The curves for both observed and calculated values have an approximately linear relationship with the number of wires per tendon. For the inclined cracking shear, the observed and calculated curves are in good agreement. On the other hand, the curve for the calculated ultimate shear is slightly higher than the curve for the observed values. However, they are in reasonable agreement.

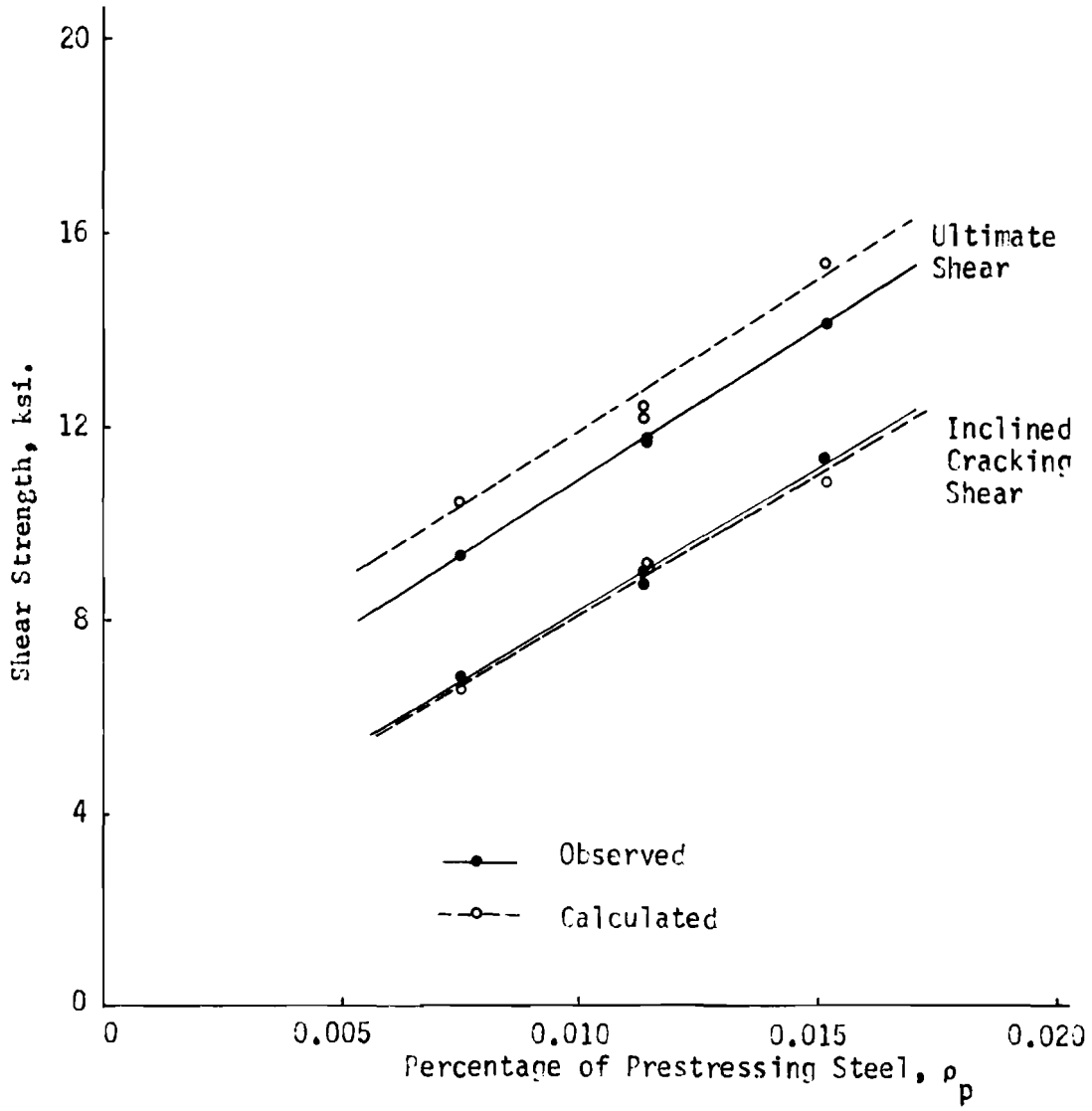

Fig. 6.13 Effect of Percentage of Steel on Shear Strength.

CHAPTER VII. TIME EFFECT ON FLEXURAL BEHAVIOR

7.1 Description of Test Program

Two post-tensioned PIC beams were subjected to sustained load for a period of 6 months. The beams were I-shaped in cross section, as described in Sect. 3.2, and had a clear span of 7 ft. 6 in. The beams were cast at the same time and with the same mix as the beams for the flexural tests. The beams contained 4 and 8-wire unbonded tendons, and sufficient web reinforcement was provided to prevent premature shear cracking.

The beams were impregnated with a 100 percent MMA monomer system by the procedure described in Chapter 3 before stressing. The tendons were tensioned to different levels, and the beams were subjected to different loads in order to produce different stress distributions over the cross section, as shown in Fig. 7.5.

7.1.1 Beam PBT-4

The beam had a four 0.25-in. wire, unbonded tendon that was stressed to 162 ksi at midspan, which is about 67.5 percent of the ultimate stress. After stressing, the time dependent deflections as well as the tendon stress were measured daily for two weeks under the beam's dead weight. The initial maximum concrete stresses were calculated to be 623 psi in tension at the top fiber and 3171 psi in compression at the bottom fiber.

After a period of 3 weeks, the beam was subjected to an average sustained load of 7.4 kips, which produced initial concrete compressive stresses of 2367 psi at the top fiber and 181 psi at the bottom fiber of the beam. The extreme fiber stresses were 15.7 percent and 1.2 percent of the PIC cylinder strength, respectively. The average compressive strength under the load was 1274 psi, which was about 8.5 percent of the cylinder strength.

7.1.2 Beam PBT-8

Eight unbonded wires were provided for PBT-8. The wires were the same size as used in PBT-4 and other beams in this test program. The maximum tension at stressing before insertion of the shims was 69.7 kips and the tendon force at the holding end was 60.7 kips, or about 69 percent of the specified tendon stress, which produced a midspan stress of 166 ksi in tension. The beam had been supporting its own weight for 3 weeks. Tendon forces at the anchoring end and midspan deflections were recorded every day during this relaxation period. The initial PIC stresses were estimated to be 1331 psi in tension at the top fiber and 6548 psi in compression at the bottom fiber.

Later, the beam was subjected to an average sustained load of 14.1 kips by the loading arrangement shown in Fig. 4.6. The load produced a top fiber stress of 4367 psi and a bottom fiber stress of 844 psi, both compression. The average compressive stress over the cross section of the beam was 2605 psi, which was about 17 percent of the PIC cylinder strength.

7.2 Test Results

The measurements of deflections, tendon forces, and strains were made daily during the first month, every second day during the next one and a half months, and weekly afterwards. The tendon forces were monitored only at the holding ends by the load cells.

7.2.1 Time-Dependent Deflections

Deflections at midspan and at supports were recorded with time. The support settlements were used for adjusting the midspan deflection. Figure 7.1 shows the deflections from the beginning of time after stressing under their own weight. The deflections were upwards; they increased very slowly during the first few days but at a faster rate later and during the second week. The curves show that the upward movement seemed to slow down during the third week. The camber of PBT-8 was slightly more than twice that for PBT-4 at the end of 2 to 3 days.

Fig. 7.2 shows midspan deflections subjected to the external sustained loads with variation of time. PBT-8, which was loaded with 14.1 kips, had a deflection force as high as PBT-4 with a sustained load of 7.4 kips. Both

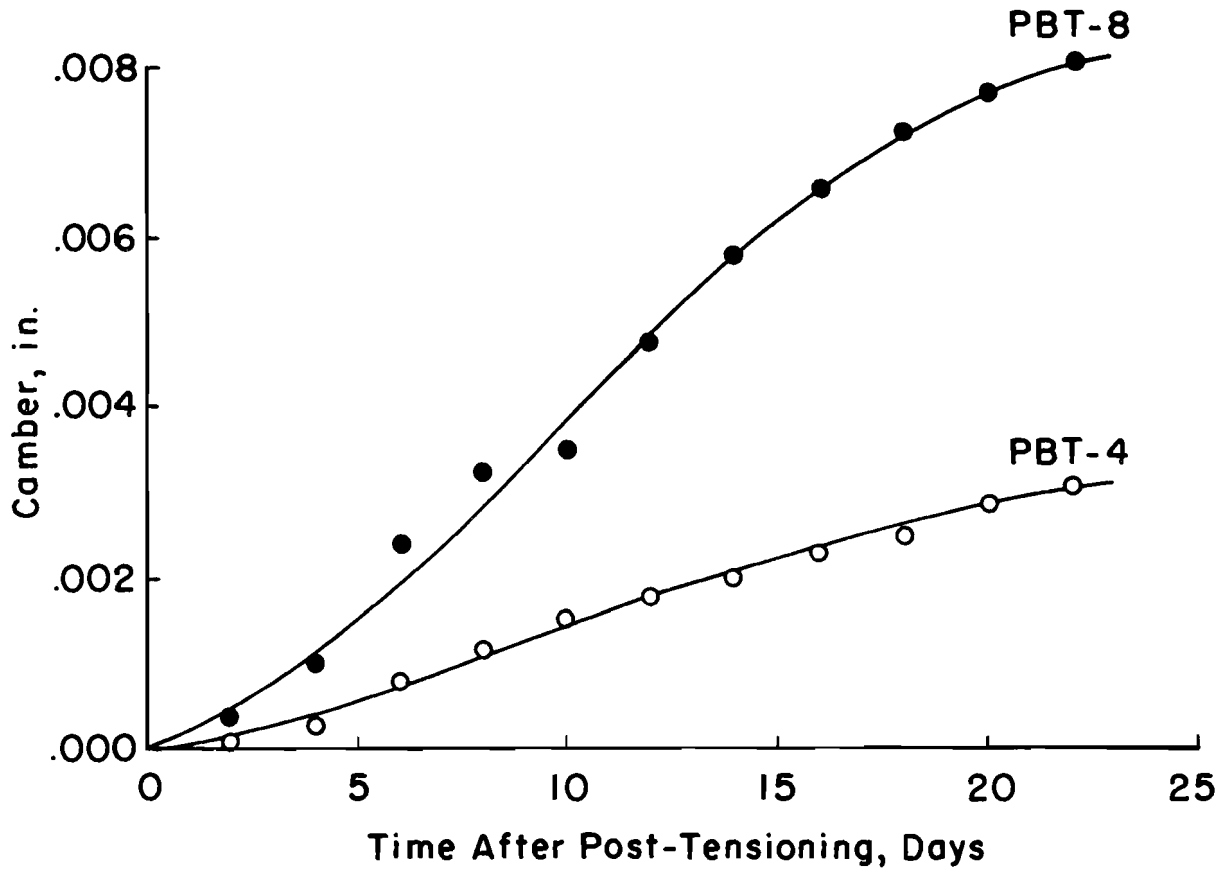

Fig. 7.1. Time Dependent Deflections Under Deadweight of the Beams.

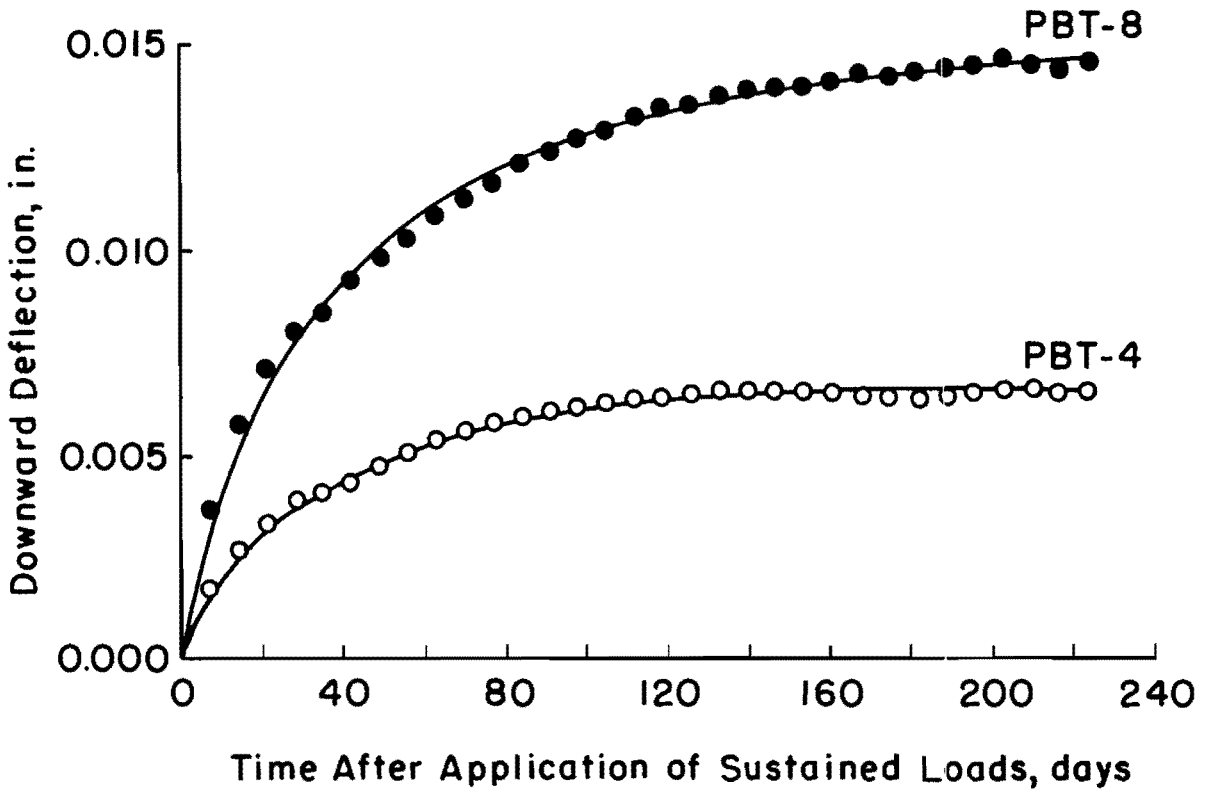

Fig. 7.2. Time Dependent Deflections Under Sustained Loads.

beams deflected downward after loading and their rates were higher during the first few weeks and became less after that. The time-dependent deflections present when the sustained load was applied were 0.012 in. for PBT-8, and 0.0059 in. for PBT-4 at the end of 3 months.

Creep was found to cease or become negligible after a sustained loading period of 4 months. The deflection due to creep for PIC beams was very small in comparison to the deflection due to the static loads. The ratio of creep deflection to static load deflection was about 1/19 for PBT-4 and 1/16 for PBT-8.

7.2.2 Tendon Stress

Change in tendon stresses with time was measured under dead load and under sustained loads. Tendon forces were monitored by load cells which were connected in a full bridge circuit. It should be noted that the error was found to be slightly high under long-term testing.

The tendon forces under dead load indicate loss of tension during that period (Fig. 7.3). Relaxation of steel was involved in these losses. The total loss was as high as 2.96 kips for PBT-8 and 1.29 for PBT-4. From these values, the relaxation was calculated to be about 4.05 percent for PBT-4 and 4.54 percent for PBT-8. The amount of relaxation was considered to be realistic for high strength steel wires. However, some error was probably involved in the load cell readings for the sustained load tests. Otherwise, the determination of relaxation by means of time-dependent deformation of the beams will be discussed later in this chapter.

Change in tendon stresses under sustained loads was relatively small in comparison to the initial post-tensioned stresses. Plots in Fig. 7.4 shows the change in tendon forces versus time. The curve for PBT-8 indicates the tension loss to be about 640 lb at the end of the 4-month period. The loss was high during the first month and increased slowly after that.

For the beam PBT-4, the change in tendon force was very small. However, the curve indicated a small gain in tension during the first month; then it was constant for a few weeks, and finally some loss in tension was detected. From the observed results, the maximum loss was about 160 lb at 4 months.

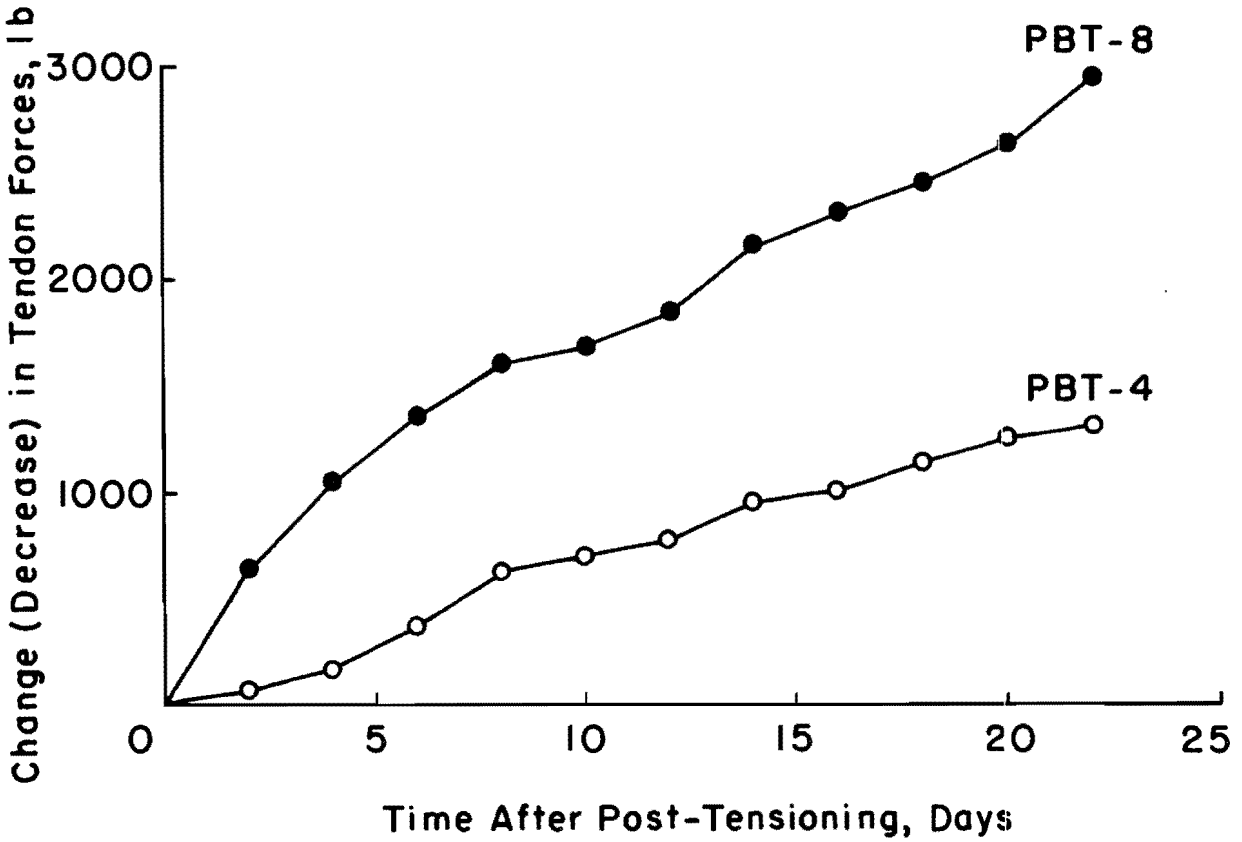

Fig. 7.3. Time Effect on Tendon Forces Under Deadweight of the Beams.

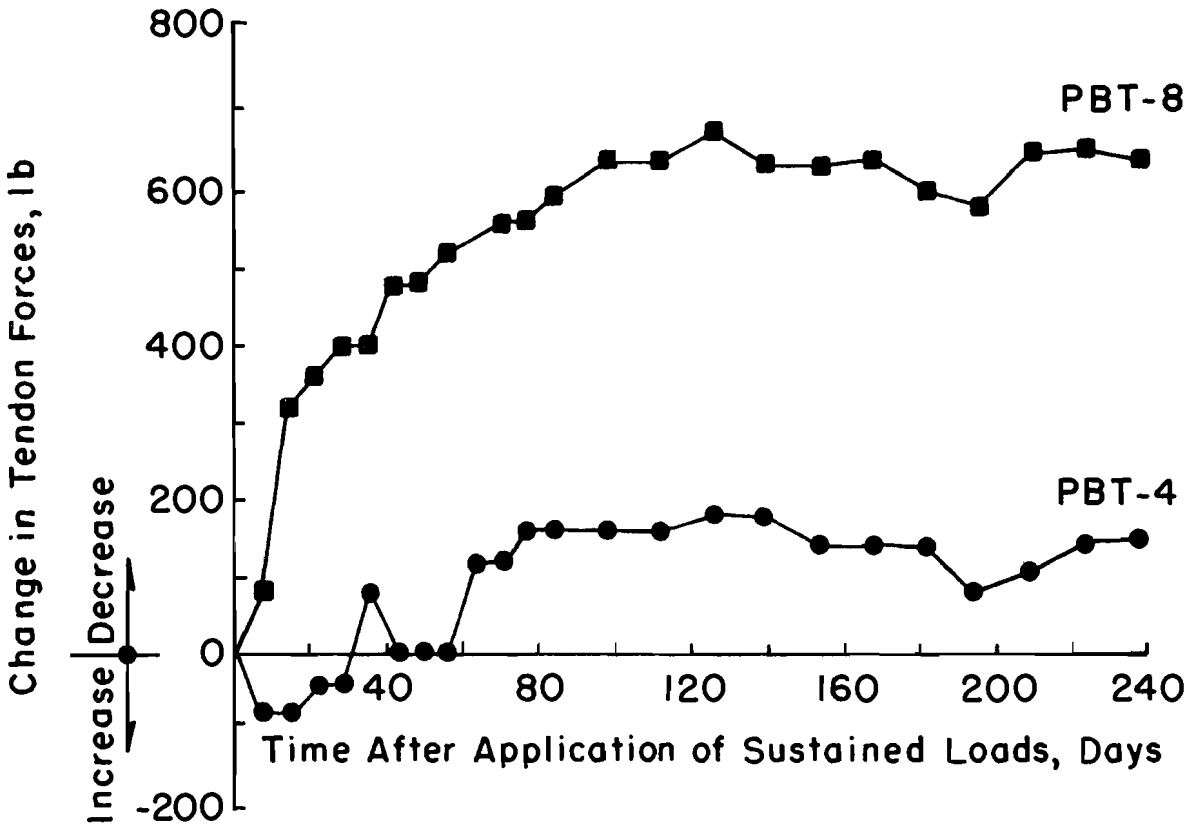

Fig. 7.4. Time Effect on Tendon Forces Under Sustained Loads.

7.2.3 Strain Distributions

Strains at various depths at midspan of the beams were monitored by two different devices: electrical resistance strain gauges and a Berry mechanical strain gauge. It was found that the electrical strain gauges with a quarter bridge circuit exhibited so much error for long-term testing that the results could not be used in the analysis.

Distribution of beam strains at given time intervals is shown in Fig. 7.5. The strains at each level represent readings made with the Berry gauge. Although some variation from a straight line was found at each time interval, a best-fit linear curve was used to represent the strain distributions throughout the depth of the cross section. Times shown in the figure are from the time that the sustained load was applied. The strains before post-tensioning are represented by the vertical zero strain line.

7.3 Evaluation of Test Results

The time-dependent deflections under sustained loads are used to compute the unit creep of PIC based on the assumption that relaxation does not occur during the test period. After the unit creep function is found, then the relaxation versus time relationship can be determined by working backward fromthe time-dependent deflections due to the beam weight. Another assumption made is that the unit creep strain during the test under dead load is the same as that during the test under the sustained loads. Actually, they may not be the same but the difference should not significantly affect the relaxation because the difference will be very small (19).

The unit creep of PIC is compared to the corresponding predicted creep of unimpregnated concrete, and the comparison of measured and computed tendon forces versus time is made.

7.3.1 Calculated Creep of Polymer-Impregnated Concrete

Time-dependent deflections under sustained loads were calculated on the basis of the following assumptions.

(1) The initial tendon forces are known for the members.

(2) The relaxation takes place during the first few days and ceases entirely after the end of three weeks prior to the sustained loads application.

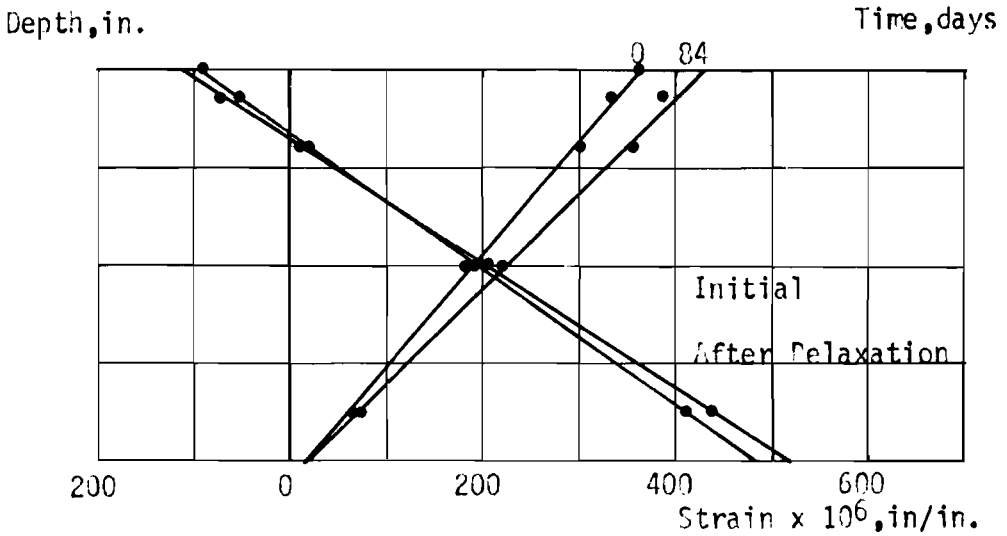

(a) Beam PBT-4.

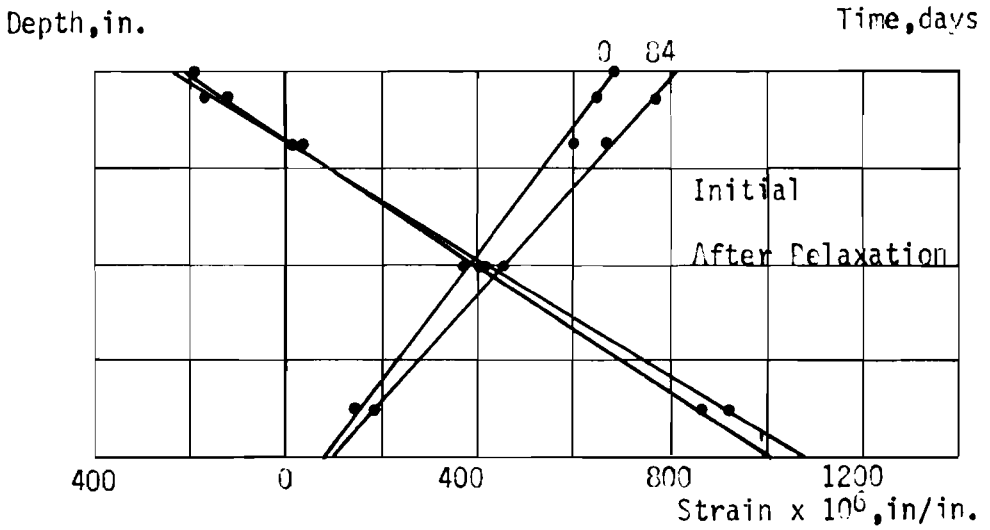

(b) Beam PBT-8.

Fig. 7.5 Strain Distribution over Beam Depth.

(3) The shrinkage of PIC is considered to be very small and can be neglected.

(4) Creep strain is proportional to stress up to 75 percent of the PIC strength under short-time loading.

(5) Strains are linear over the depth of the cross section.

(6) Steel has a linear stress-strain relationship under short-term loading.

The unit creep (creep strain per unit stress) versus time relationship for constant stress can be computed by the following steps.

(1) The stress distribution over the cross section is computed from the tendon forces, tendon eccentricity, external loads, and beam weight (Fig. 7.6).

(2) The unit creep at a particular time is assumed to be C micro in./in. per psi of stress.

(3) The creep strain at the extreme fibers is the product of the unit creep and the extreme fiber stress. Similarly, the creep strain at the steel level can be determined.

(4) The loss in steel stress caused by creep is the product of the change in strain at the level of steel (Step 3) and the modulus of elasticity of the steel.

(5) The change in stress in the extreme fibers is found by considering the loss of the steel stress as a load applied at the center of gravity of the steel and computing the corresponding elastic change in stress in the extreme fibers.

(6) The elastic change in strain at the extreme fibers is computed by dividing the change in stress (Step 5) by the instantaneous modulus of the PIC.

(7) The net change in strain at the extreme fibers is found by finding the algebraic difference between the gross change in strain found in Step 3 and the elastic change in strain found in Step 6.

(8) The change in member curvature is the algebraic difference between the extreme fiber strains divided by the beam thickness.

(9) The change in the deflection can be calculated from the curvature in Step 8 based on structural analysis.

(10) The unit creep, C, at any time can be solved by equating the deflection in Step 9 to an observed deflection from testing.

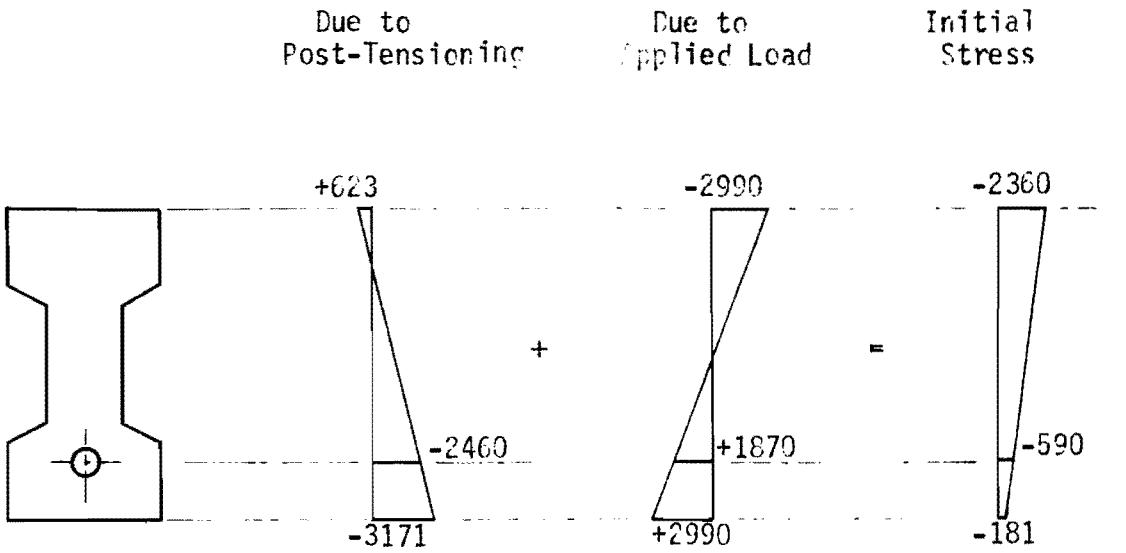

(a) Beam PBT-4.

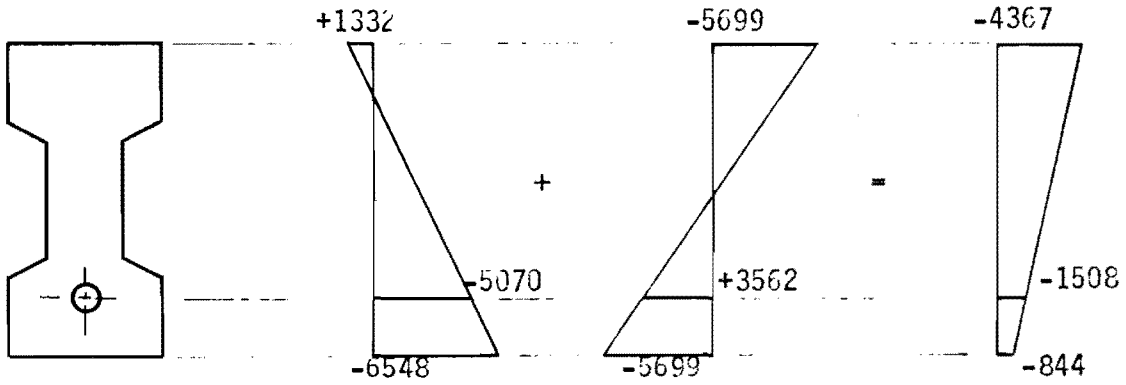

(b) Beam PBT-8.

Fig. 7.6 Initial Stress Distribution at Midspan.

Since the calculations are based on the initial stress, the unit creep might be slightly higher than predicted. However, after the relaxation had been determined, the unit creep was recalculated on the basis of tendon forces after losses. Fig. 7.7 shows the unit creep of PIC versus time. The solid lines are the values calculated from stress distributions in which relaxation was not considered; the dashed lines show the unit creep when the losses in the steel were taken into account.

It should be noted that the unit creep of PIC is also dependent on times and stress levels. The calculated unit creep from PBT-8, in which the average stress was 2605 psi, was found to be higher than the one from PBT-4, in which the average stress was 1274 psi. However, the unit creep represented by the dashed curves can be expressed by hyperbolic functions in terms of time:

(a) Average stress = 2605 psi ($0.17\ f'_{cp}$)

$$C = \frac{0.036\ T}{24 + T} \qquad (7.1)$$

(b) Average stress = 1274 psi ($0.08\ f'_{cp}$)

$$C = \frac{0.030\ T}{24 + T} \qquad (7.2)$$

where C = unit creep, micro in./in. psi

T = time, days.

7.3.2 Comparison of Creep in Polymer-Impregnated Concrete and Unimpregnated Concrete

The effects of creep and shrinkage strains in concrete are dependent on variables such as materials, stress level, and environment. A test program was conducted at Texas A & M University to determine creep and shrinkage strains for concrete from different geographical areas of Texas (22). For aggregate and the climate in central Texas (Austin area), the unit creep can be represented by a hyperbolic function:

$$C = \frac{385\ T}{25 + T} \qquad (7.3)$$

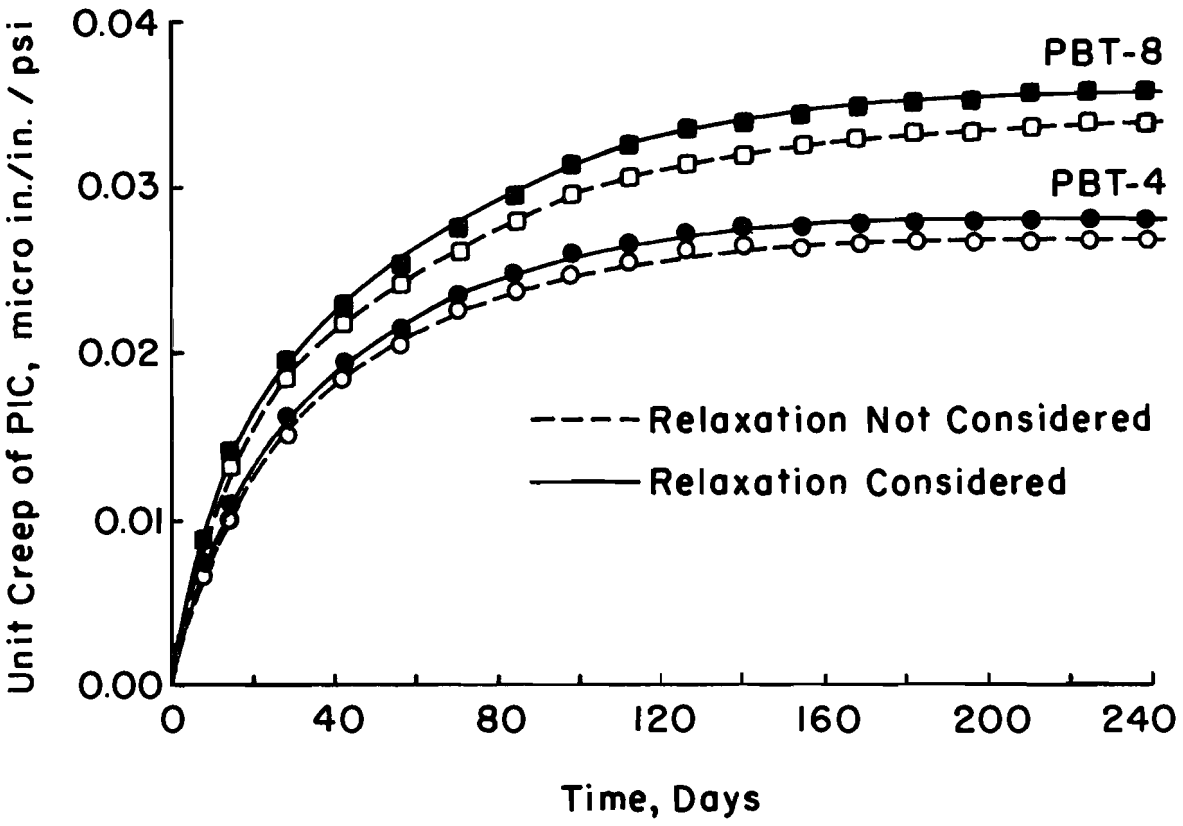

Fig. 7.7. Calculated Unit Creep of Polymer-Impregnated Concrete.

This expression was fitted on the basis of laboratory data, and the unit shrinkage was not included.

The unit creep of PIC in this investigation is tabulated in Table 7.1 in comparison with the unit creep of the unimpregnated concrete represented by Eq. 7.3 In a similar manner, the test results reported by Brookhaven National Laboratory (4.5) are also tabulated and compared for PIC and corresponding unimpregnated concrete. It should be noted that the unit creep of PIC is relatively small, about 1/12 to 1/13 of the creep in the control in this investigation. The BNL test results indicated creep of about 1/7 to 1/8 of the controls. Slight difference in unit creep of PIC is exhibited between these test results as far as the testing procedure, speciment series, types of aggregate, and impregnation technique. The maximum size of aggregate used at BNL was 3/4 in. while 3/8 in. aggregate was used in this test program. However, the low creep of PIC is a desirable property for the application to post-tensioned members.

7.3.3 Comparison of Measured and Computed Tendon Forces

Once the unit creep function of PIC is known, the loss in tendon forces due to creep strain can be determined. The unit creep, C, is substituted into step 4 of the computation procedure for creep as presented in Section 7.3.1, and the loss in steel stress can be obtained. The product of this stress and the total area of the steel will be the total loss in force in the tendons.

Fig. 7.8 shows the calculated and observed changes in tendon forces versus time under sustained loads. The calculated values are in reasonably good agreement with the measured values.

7.3.4 Relaxation of Steel

On the basis of the assumption that the relaxation of the steel tendons ceases entirely after the first three weeks and that unit creep function of PIC is the same for dead loads and sustained loads, then the relaxation can be determined from the time-dependent deflection under the beam weight. The other assumptions are the same as the ones for computation of creep. However, the computation procedure is similar to that for creep as follows.

Table 7.1

Comparison of Unit creep of PIC

and Unimpregnated Concrete

Time (days)	Central Texas Materials			BNL Materials		
	PIC[a]	Control	Control / PIC	PIC	Control	Control / PIC
7	0.0069	0.084	12.0	0.014	0.120	8.6
14	0.0100	0.138	13.8	0.018	0.160	8.9
28	0.0153	0.203	13.3	0.024	0.195	8.1
42	0.0186	0.241	12.9	0.028	0.220	7.9
84	0.0238	0.297	12.5	0.036	0.260	7.2
126	0.0263	0.321	12.2	0.038	0.275	7.2

[a] Test result from PBT-4

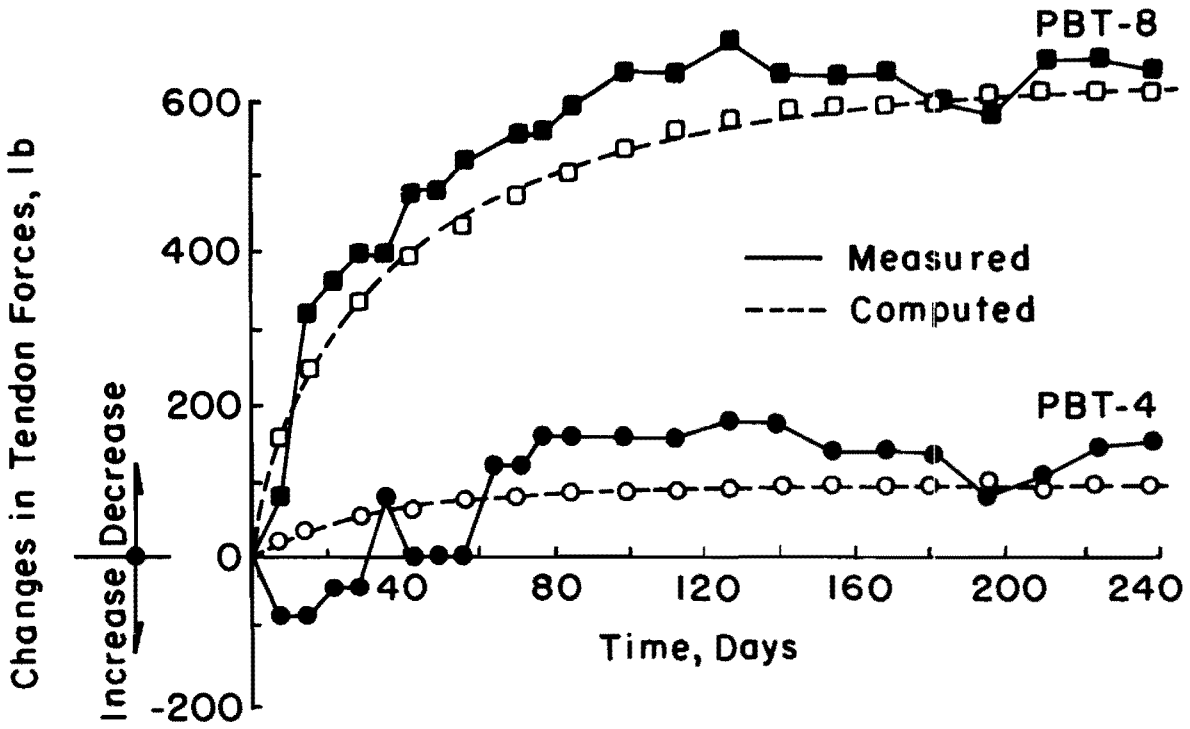

Fig. 7.8. Comparison of Measured and Computed Change in Tendon Force.

(1) The stress distribution over the cross section is computed from the tendon forces, tendon eccentricity, and beam weight.

(2) The unit creep at a particular time can be obtained from creep curves (Fig. 7.7) or from unit creep functions (Eq. 7.1 or 7.2).

(3) The creep strain at the extreme fibers is the product of the unit creep and the extreme fiber stress. Similarly, the creep strain at the steel level can be computed.

(4) The loss in steel stress caused by creep is determined by multiplying the change in strain at the steel level (Step 3) by the modulus of elasticity of steel, and then the loss of tendon force can be obtained by multiplying the stress loss by the area of steel.

(5) If the relaxation of steel is assumed to be R percent, then the loss of steel stress due to relaxation can be determined from the initial tendon forces.

(6) The change in stress in the extreme fiber is found by considering the loss of tendon force (Step 4 + Step 5) as a load applied at the centroid of the tendons and computing the corresponding elastic change in strain at the extreme fibers.

(7) The elastic change in strain at the extreme fibers is computed by dividing the change in stress (Step 6) by the instantaneous modulus of PIC.

(8) The net change in strain at the extreme fibers is the algebraic difference between the gross change in strain found in Step 3 and the elastic change in strain found in Step 7.

The change in member curvature can be determined from the change in Step 8 and by means of structural analysis, and the midspan deflection can be determined in terms of the unknown value of R. Since the deflection at a particular time is already known from time-dependent deflection tests, these to deflections can be equated and the relaxation, R, can be found.

Fig. 7.9 shows the computed time-dependent relaxation for both beams. They are in very good agreement with each other. The relaxation is high during the first few days, and it may be considered to cease entirely after two weeks. The curve for beam PBT-8 shows a slightly higher relaxation than the one for PBT-4 and the final relaxations for both of them are almost equal; they are 2.93 and 2.90 percent, respectively. The relaxation of steel from these tests is in good agreement with the test results conducted by Magnel as

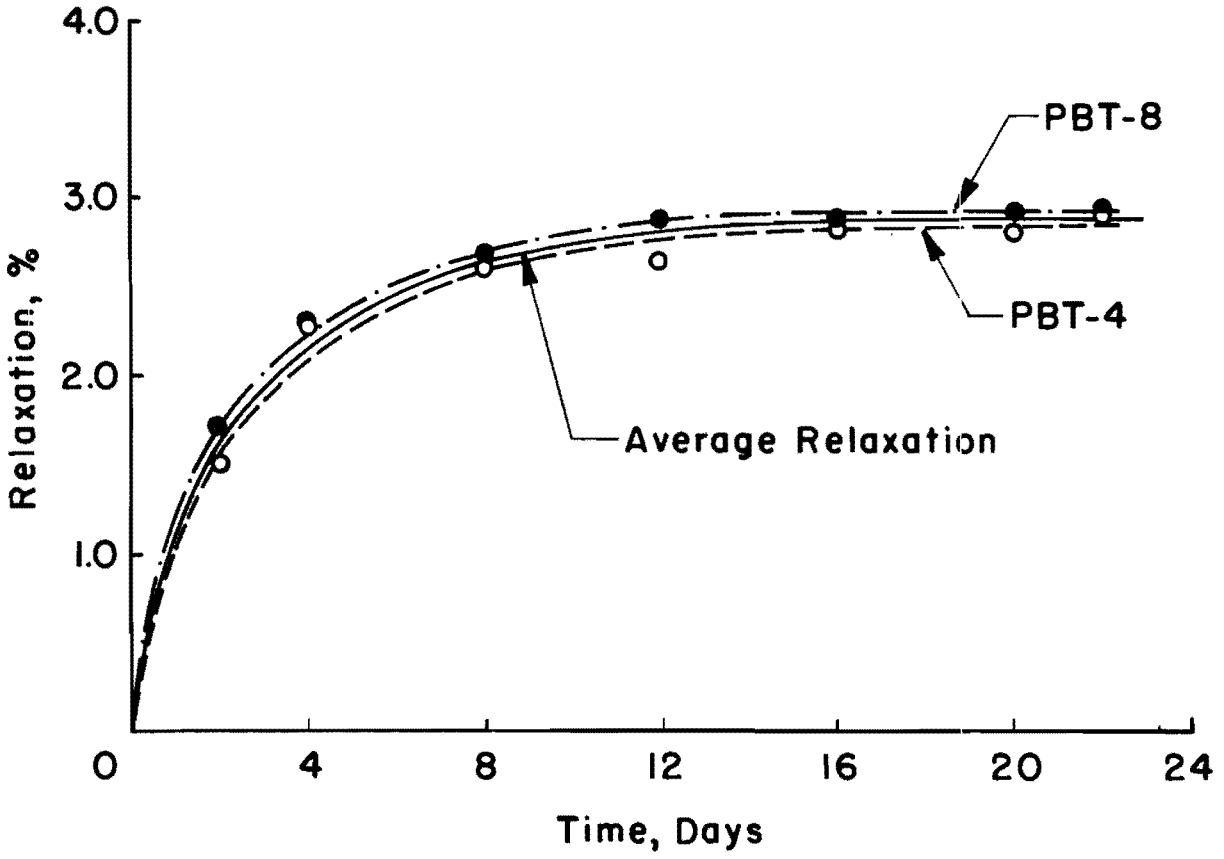

Fig. 7.9. Time-Dependent Relaxation of Prestressing Steel.

reported by Komendant (50) and with the values recommended by Lin (19), which are about 3 percent. It is slightly less than the values presented by Libby (51), which are about 4 percent.

A relaxation function can be represented on the basis of the average values of both curves versus time relationship. The predicted function can be written as

$$R = \frac{3.147\ T}{1.702 + T} \qquad (7.4)$$

where R = relaxation in percent

T = time in days.

CHAPTER VIII. DESIGN CRITERIA FOR POST-TENSIONED PIC BEAMS

For post-tensioned PIC beams investigated in this study, the computed results for flexure and shear based on the ACI Building Code were conservative estimates of the observed results. The numerical analysis procedure as well as the empirical method was developed or modified to predict the flexural and shear behaviors at various stages of loading. Loss of prestress due to the creep of PIC, relaxation of prestressing steel, and friction loss have been evaluated and compared to other reported values. The reasonable agreement among those results suggests that the proposed design criteria may be used with some degree of confidence for a post-tensioned PIC beam design problem. However, the criteria are only tentative because of the limited number of tests that have been made.

8.1 Structural Properties of Polymer-Impregnated Concrete

The structural properties of PIC for the mix design and monomer system used in this study can be estimated on the basis of empirical equations. The formulae are generally a function of cylinder strength of PIC, f'_{cp}, or percentage of polymer loading, PL.

8.1.1 Compressive Strength

In general, the compressive strength, f'_{cp}, is determined by direct compression tests of cylinders. However, the strength may also be estimated from the percentage of polymer loading. The equation for 100 percent MMA PIC can be written as

$$f'_{cp} = 1{,}050 + 2{,}450\ (PL) \qquad (8.1)$$

where the constants are in psi, and PL is the polymer loading in percent by weight.

8.1.2 Modulus of Elasticity

The compressive modulus of elasticity of PIC, E_{cp}, can be determined from the compressive strength, f'_{cp}. The relationship between these two properties can be expressed by

$$E_{cp} = 53{,}000 \sqrt{f'_{cp}} \tag{8.2}$$

where both E_{cp} and f'_{cp} are in psi. It should be noted that this equation can be used for 100 percent MMA, 75 percent MMA + 25 percent BA, and 50 percent MMA + 50 percent BA monomer systems.

8.1.3 Tensile Strength

The tensile strength of PIC is usually determined by the splitting tests. The equation presented herein shows very good agreement with the tests

$$f_{tp} = 10 \sqrt{f'_{cp}} \tag{8.3}$$

where f_{tp} = tensile strength of PIC, psi

f'_{cp} = compressive strength of PIC, psi.

8.1.4 Modulus of Rupture

The modulus of rupture for PIC beams has been evaluated from the cracking moments of the beams tested for flexure. It can be presented as a function of a cylinder strength, as follows:

$$f_{rp} = 6 \sqrt{f'_{cp}} \tag{8.4}$$

where f_{rp} = modulus of rupture of PIC, psi

f'_{cp} = cylinder strength of PIC, psi.

8.2 Loss of Prestress

Three major losses of prestress were considered in this investigation. They are friction loss, creep of PIC, and relaxation of prestressing steel.

These looses must be considered in determining the effective prestress or allowed for in design.

8.2.1 Friction Losses

The friction losses in post-tensioned tendons of PIC beams can be reasonably estimated by ACI Eq. 18.1 or 18.2. However, the wobble coefficient, K, and the friction coefficient, μ, depend on whether the conduits are for bonded or unbonded tendons. The following values are recommended.

(a) Unbonded Tendons: The tendons were wrapped with waterproof paper. The beams were soaked in the monomer and polymerized in hot water. The recommended values are

$$K = 0.0050$$

$$\mu = 0.500.$$

(b) Bonded Tendons: Sheathed metal conduits were used to protect the tendons. The beams were soaked in the monomer and the excess monomer was blown out by high pressure air before the beams were soaked in hot water for polymerization. The blowing operation was continued throughout the curing process to prevent the polymer from coating the tendon. The coefficients are recommended as follows:

$$K = 0.0005$$

$$\mu = 0.10.$$

8.2.2 Creep of Polymer-Impregnated Concrete

The unit creep of PIC can be approximately predicted by the following functions, which are based on the test results of two PIC beams with different prestressing forces and external sustained loads.

(a) When maximum fiber stress is less than or equal to 30 percent of the compressive strength of PIC ($f_{cp} \leq 0.3\ f'_{cp}$),

$$C = \frac{0.036\ T}{24 + T} \qquad (8.5)$$

(b) When maximum fiber stress is less than or equal to 15 percent of the compressive strength of PIC ($f_{cp} \leq 0.15\ f'_{cp}$),

$$C = \frac{0.030\ T}{24 + T} \qquad (8.6)$$

where C = unit creep of PIC, micro. in./in./psi

T = time, days.

8.2.3 Relaxation of Prestressing Steel

The relationship between relaxation of 0.25-in. wire grade 240 and time can be estimated as

$$R = \frac{3.147\ T}{1.702 + T} \qquad (8.7)$$

where R = relaxation, percent

T = time, days.

8.3 Flexural Strength

8.3.1 Stress Distribution of Polymer-Impregnated Concrete

The relationship between compressive stress and strain for PIC beams at ultimate may be considered satisfied by an equilibrium rectangular stress distribution such as Whitney's stress block. It can be defined as follows.

A PIC stress of $0.90\ f'_{cp}$ is assumed uniformly distributed over an equivalent compression zone bounded by the edges of the cross section and a straight line located parallel to the neutral axis at a distance $a = \beta_1 c$ from the fiber of the maximum compressive strain. The distance c from the fiber of the maximum strain to the neutral axis is measured in a direction perpendicular to that axis. A value of β_1 equal to 0.70 for any strength of PIC is recommended.

8.3.2 Tendon Stress

The tendon stress at ultimate for unbonded beams impregnated with a 100 percent MMA monomer system can be determined by the equation

$$f_{ps} = f_{se} + 75{,}000 - 2{,}354{,}000\ \rho_p \qquad (8.8)$$

where f_{ps} = tendon stress at ultimate, psi

f_{se} = effective stress in post-tensioned tendon, after losses, psi

ρ_p = ratio of prestressing steel, A_{ps}/bd.

When the BA is presented in the monomer system, the tendon stress at ultimate will be increased from Eq. 8.8 by

$$\Delta f_{ps} = 917\ P - 14.0\ P^2 \qquad (8.9)$$

where P = percentage of BA in the monomer system.

8.3.3 Cracking Moment

The cracking moment of post-tensioned PIC beams can be estimated by the following:

$$M_{cr} = \frac{I}{y}(f_{rp} + f_{pc} - f_d) \qquad (8.10)$$

This expression is similar to the M_{cr} used in ACI Eq. 11.11 for ordinary concrete beams. However, the modulus of rupture for PIC beams (f_{rp}) is recommended as $6\sqrt{f'_{cp}}$. The values of f_{pc}, f_d, y_t, and I are used as specified in the ACI Building Code.

8.3.4 Ultimate Moment

The ultimate moment can be computed by the strength design methods given in the ACI code. For PIC, the compressive force shall be determined by means of the stress distribution as defined in Sect. 8.3.1 and it shall be compatible to the tensile forces contributed by prestressing steel.

For prestressing steel, the tendon stress, f_{ps}, shall be determined by the equations presented in Sect. 8.3.2.

Nonprestressed bonded reinforcement when used in combination with prestressing steel can be considered to contribute to the tensile force in a member at ultimate an amount equal to its area times its yield strength.

8.4 Shear Strength

8.4.1 Web Shear

The test results did not provide sufficient data to establish an expression to estimate shear stress at diagonal cracking due to excessive principal tensile stress in the web. However, the comparison of the shear strength shown in Table 6.10 indicated that Eq. 2.13, which was proposed by Olesen (46) for prestressed concrete beams, might be reasonably used for post-tensioned PIC beams.

8.4.2 Flexural Shear

The flexural shear strength (V_{ci}) for post-tensioned PIC beams can be determined by

$$V_{ci} = b_w d \sqrt{f'_{cp}} + \frac{M_{cr}}{\frac{M}{V} - \frac{d}{2}} \qquad (8.11)$$

where f'_{pc} = compressive strength of PIC, psi

b_w = web thickness, in.

M_{cr} = cracking moment, lb-in. (See Eq. 8.10)

M = moment due to applied load at section considered, lb-in.

V = shear due to applied load at section considered, lb-in.

d = effective depth of the beam, in.

8.4.3 Ultimate Shear

The ultimate shear can be calculated in two ways depending on the modes of failure.

(a) Flexural Failure: The ultimate shear can be determined from the ultimate moment by means of the structural analysis. The ultimate moments can be computed by the method presented in Sect. 8.3.4.

(b) Shear Failure: If the beam failed in shear and the web reinforcing steel reached yield strength (f_y), the ultimate shear would be as follows:

$$V_u = V_{ci} + \frac{A_v f_y s}{d} \qquad (8.12)$$

where V_{ci} = inclined cracking shear calculated by Eq. 8.11, lb

A_v = area of vertical stirrup, in.

f_y = yield strength of the stirrups, psi

s = stirrup spacing, in.

d = effective depth, in.

V_u = ultimate shear, lb.

It should be noted that, if draped tendons are used, the vertical component of the tendon forces must be considered.

CHAPTER IX. CONCLUSIONS AND RECOMMENDATIONS

The behavior of post-tensioned PIC beams was investigated in this study. No previous research on post-tensioned PIC beams has been reported. Emphasis was placed on flexural strength, shear strength, and time-dependent deflections. Remarkable improvements in structural performance of post-tensioned concrete beams can be achieved by monomer impregnation and thermal catalytic polymerization before post-tensioning. Impregnation and polymerization processes have been developed which can be applied to produce full-scale PIC members; these methods are particularly appropriate for the precast concrete industry.

Nineteen simple span beams with an I-shaped cross section were tested using two symmetrically placed concentrated loads. The beams were 4 in. wide, 8 in. deep, and 8 ft. long. The web thickness was 2 in. while the flange thickness was 2 in. at the edge and 2 1/2 in. at the web. The span length was 7 ft. 9 in.,; the load points were located symmetrically, 2 ft. apart. Deflections, strains, tendon stresses, and load were measured. The tendons were stress-relieved wire with a 0.25-in. diameter. The specified ultimate strength was 240 ksi. No. 2 reinforcing steel grade 60 was also used as the supplementary reinforcement to prevent cracks during the drying process. On the basis of experimental and analytical results, the following conclusions and recommendations can be made. It should be emphasized, however, that the conclusions are based upon a limited number of beams and may not be applicable for beams with significantly different parameters.

9.1 Conclusions

9.1.1 Flexural Strength

Many variables affect the flexural behavior of post-tensioned PIC beams, such as the number of wires per tendon, monomer systems, type of tendons, and impregnation depths. Based on the results of this study, the following conclusions can be drawn regarding criteria presented in Chapter 5.

(1) The maximum tendon stress force provided for a post-tensioned concrete beam is generally controlled by the extreme fiber stress in concrete. The maximum tendon force that can be provided for a fully impregnated beam is about four times more than for an unimpregnated beam because the strength of PIC is about four times that of unimpregnated concrete. For the partial-depth impregnated beams, the maximum tendon force varies with the depth of impregnation.

(2) The percentage of prestressing steel or the number of 0.25-in. wires per tendon influences the load-deflection response of post-tensioned PIC beams. Higher percentages of steel result in higher strength, cracking moment, and toughness but lower deflection and inelastic rotation capacity.

(3) The monomer system which includes some butyl acrylate (BA) results in slight improvement in strength and ductility for post-tensioned PIC beams containing two 0.25-in. wires per tendon compared to corresponding beams with the 100 percent MMA-monomer system. The 25 percent BA-monomer system seems to be an optimum percentage of BA in this study.

(4) PIC beams with bonded tendons developed about 3 percent higher strength than beams with unbonded tendons, but they are significantly improved in ductility or inelastic rotation capacity. The polymer grouting provided higher failure deflection than the conventional cement grouting by 33 percent and than the unbonded beams by 48 percent.

(5) The partially impregnated beams had slightly less strength, stiffness, and inelastic rotation capacity than the corresponding fully impregnated ones.

(6) The control beam containing two 0.25-in. wires developed less strength and deflection than the fully impregnated PIC beams with two 0.25-in. wire tendons. The PIC beam with 2 wires per tendon developed 10 percent more strength and 100 percent more deflection than the control.

(7) The friction loss of PIC beams containing unbonded tendons which were wrapped with paper was higher than for unimpregnated beams because excess monomer polymerized and coated the tendons. The wobble and friction coefficients were determined to be about 0.005 and 0.50, respectively.

The friction loss of PIC beams containing bonded tendons in sheathed metal conduits was smaller than of the control beam because the excess monomer was blown out prior to curing. The wobble and friction coefficients

were found to be 0.0005 and 0.11, respectively, while those for control beams were 0.0015 and 0.30, respectively.

(8) The tendon stress response under externally applied loads was closely related to the load-deflection response. Higher deflections resulted in increased tendon stress.

(9) For the bonded beams, the cracks were more uniformly distributed along the beams than for the beams with unbonded tendons, and this resulted in higher stiffness and strength.

(10) Load-deflection and tendon stress predicted by numerical analysis using program PICB indicates good agreement with the test results in most cases.

(11) The strain distribution for either fully impregnated beams or partially impregnated beams was observed to be linear over the depth of the beam until the first crack occurred. Bernoulli's hypothesis was confirmed by the test results. A variation from a straight line was found when the load approached the ultimate load. More variation was noted for unbonded beams than for bonded beams.

(12) The deflected shape of each beam was approximately a half sine wave. Some deviation from a sine wave was observed beyond the elastic range due to the wide cracks.

(13) The useful limit of strain for polymer-impregnated concrete under compression of the extreme fiber of the beams varied from 0.0026 to 0.0044 in./in. For unbonded PIC beams produced with the 100 percent MMA monomer-system, the average value was 0.00285. The bonded beams developed a higher useful limit strain than the unbonded ones. Similarly, the beams produced with a monomer system containing butyl acrylate (BA) developed a higher useful limit strain than the ones produced with the 100 percent MMA-monomer system.

(14) The stress distribution for polymer-impregnated concrete generated from strain readings in beams indicated slight differences in strength and significant differences in modulus of elasticity in comparison to the results from cylinder tests.

(15) An equivalent rectangular stress block for 100 percent MMA-PIC developed in this study defined stress intensity to be $k_u f'_{cp}$, where f'_{cp} is the compressive strength of PIC Depth of the equivalent stress block, a, is a fraction of the distance from the top fiber to the neutral axis, c ($a = \beta c$).

The values of k_u and were found to be 0.90 and 0.70, respectively. The tensile strength of PIC is neglected in the computation of ultimate strength of the beams.

(16) Jensen's trapezoidal and triangular stress distributions may be used for PIC stress distribution to predict the load-deflection response of PIC beams using computer program PICB.

(17) Recommended design values for PIC beams for compressive strength, modulus of elasticity, tensile strength, modulus of rupture, tendon stress, cracking moments, and ultimate moments are as indicated in Chapter 8.

9.1.2 Shear Strength

The number of wires per tendon and the amount of web reinforcement were selected as the variables in this test series. Two unimpregnated beams were tested as companion control beams. The following conclusions can be made, based on the test results.

(1) The percentage of prestressing steel or the tendon force has a primary influence on the shear strength of the post-tensioned PIC beams; higher percentages of steel or prestress force resulted in increased shear strength.

(2) The web reinforcement affects the shear strength of the PIC beams; inadequate web reinforcement resulted in lower strength and deflection due to premature failure associated with shear cracking.

(3) For the I-shaped cross section and the shear span as used in this test, the flexural behavior seemed to predominate before final failure occurred. The mode of failure was classified as shear-compression.

(4) Prediction of flexural shear strength for PIC beams can be computed by equations shown in Sect. 8.4. The prediction using the ACI equation is about 20 percent less than the test results.

9.1.3 Time-Dependent Behavior

The primary variables were the prestressing forces and the external sustained loads. Both variables resulted in different stress distribution over the cross section of the beams. Two beams were tested for time-dependent behavior; one beam containing a 4-wire tendon was subjected to an average sustained load of 7.4 kips, which produced an initial compressive stress at

the top and bottom fibers of $0.16f'_{cp}$ and $0.012f'_{cp}$, respectively. The average compressive stress over the PIC cross section was about $0.08f'_{cp}$. The other beam contained 8 unbonded wires for tendon and was subjected to a sustained load of 14.1 kips, which produced a compressive stress at the top and bottom fibers of $0.30f'_{cp}$ and $0.06f'_{cp}$, respectively. The average compressive stress over the PIC cross section was about $0.17f'_{cp}$. Both beams were impregnated with 100 percent MMA-monomer system. The relationship between creep of PIC and time and between relaxation and time were determined. The following conclusions may be made.

(1) The unit creep of PIC obtained from time-dependent deflection tests of the post-tensioned PIC beams under sustained loads was considerably lower than that of corresponding unimpregnated concrete. It is about 1/10 to 1/13 of the average value for unimpregnated concrete.

(2) The creep functions determined from the test results of the two PIC beams were dependent upon the stress level; the higher the stress, the higher the creep (Sec. 8.2.2).

(3) The relaxation of the wire tendons used in this program was about 2.9 percent. The rate of relaxation was high during the first few days, and it ceased almost entirely after a period of two weeks.

(4) A variation from a straight line for the stress distribution was observed in the tests; however, a linear relationship was used to represent the successive strain distributions for purposes of analysis.

(5) The deflection due to creep for PIC beams was very small in comparison to the deflection due to the static load. The ratio of creep deflection to static load deflection was about 1/19 to 1/16.

9.2 Recommendations

The post-tensioned PIC beams were found in this study to perform very well in many respects. However, additional research is desirable to investigate other factors that may affect the behavior of post-tensioned PIC beams. The following studies are recommended.

(1) Development of equipment for impregnation on a commercial scale should be undertaken.

(2) Extensive studies in flexure, shear, and bond for post-tensioned PIC beams should be undertaken for a wide range of variables, including

cross-section shape, depth-to-span ratio, loading rate, and duration of loading.

(3) The use of polymer grouting should be further investigated for post-tensioned beams.

(4) Economic feasibility studies should be performed to determine under what conditions PIC is competitive with ordinary concrete.

APPENDIX A

COMPARISON OF LOAD DATA
FROM LOAD CELL AND HYDRAULIC JACK

(a) Load Data for PBC-2C in Post-Tensioning

Load No.	Hydraulic Jack		Load Cell	
	Press. Gauge (psi)	Load (kip)	Strain Rdg. (μin/in)	Load (kip)
1	150	0.80	23	0.90
2	300	1.85	46	1.90
3	440	2.80	72	2.85
4	560	3.70	100	3.90
5	700	4.65	130	4.90
6	850	5.70	155	5.85
7	1000	6.75	185	7.00
8	1120	7.50	205	7.80
9	1250	8.50	228	8.80
10	1400	9.55	252	9.80
11	1550	10.60	276	10.70
12	1700	11.65	302	11.70
13	1830	12.65	322	12.60
14	1960	13.50	344	13.50
15	2100	14.45	365	14.40
16	2250	15.50	388	15.30
17	2350	16.20	404	16.10

(b) Load Data for PBC-2C in Loading

Load No.	Hydraulic Jack		Load Cell	
	Press. Gauge (psi)	Load (kip)	Strain Rdg. (μin/in)	Load (kip)
1	150	0.80	16	0.80
2	300	1.85	32	1.60
3	440	2.80	70	2.80
4	560	3.70	97	3.80
5	700	4.65	121	4.80
6	850	5.70	156	6.00
7	1000	6.75	181	6.90
8	1120	7.50	203	7.80
9	1250	8.50	224	8.70
10	1400	9.55	248	9.50
11	1550	10.60	274	10.55
12	1700	11.65	298	11.65

APPENDIX B

CONCRETE MIX DATA

CONCRETE MIX DATA

Mix No. 1

Date: 12-23-75

Cement Factor: 6 sacks/cubic yard

Design W/C Ratio: 7 gallons/sack

Design Slump: 4 inches

Cement: Portland cement type III, high early strength

Mix Design: for a batch of 17 $ft.^3$

Cement	335	lb
Water	228	lb
Fine aggregate	688	lb
Coarse aggregate	1452	lb

Specimens: PBC-2S, PBC-2C

PBP-2, PBP-4

PBM-50, PBM-75

PBS-4S, PBS-6C, PBS-6S, PBS-8S.

Mix No. 2

Date: 1-22-76

Cement Factor: 6 sacks/cubic yard

Desgn W/C Ratio: 7 gallons/sack

Design Slump: 4 inches

Cement: Portland cement type III, high early strength

Mix Desgn: for a batch of 3.8 $ft.^3$

Cement	87.6	lb
Water	50.7	lb
Fine aggregate	216.6	lb
Coarse aggregate	158.7	lb

Specimens: PBF-2, PBF-4, PBF-6, PBF-8

PBT-4, PBT-8

PBC-2

PBB-4C, PBB-4P.

APPENDIX C

CYLINDER STRENGTH OF POLYMER IMPREGNATED CONCRETE AND UNIMPREGNATED CONTROL

CYLINDER STRENGTH OF PIC AND UNIMPREGNATED CONCRETE

(1) Compressive Strength of Concrete at 28 Days

Mix No. 1

Specimen No.	Spec. Type	Strength, psi
1	6 x 12	5670
2	6 x 12	5650
3	6 x 12	4670
4	6 x 12	5600
	Average	5400

Mix No. 2

Specimen No.	Spec. Type	Strength, psi
1	6 x 12	5240
2	6 x 12	5690
3	6 x 12	6180
4	6 x 12	5240
	Average	5580

(2) Splitting Tensile Strength of Concrete at 28 Days

Mix No. 1

Specimen No.	Spec. Type	Strength, psi
1	6 x 12	430
2	6 x 12	481
3	6 x 12	604
4	6 x 12	509
	Average	506

Mix No. 2

Specimen No.	Spec. Type	Strength, psi
1	6 x 12	458
2	6 x 12	487
3	6 x 12	568
4	6 x 12	536
	Average	512

(3) Compressive Strength of 100% MMA-PIC

Mix No. 1

Spec. No.	Cyl. Type	Polymer Loading, %	Strength, psi
1	3 x 6	5.16	15,400
2	3 x 6	4.28	11,400
3	3 x 6	4.91	13,300
4	3 x 6	4.78	12,700
	Average	4.78	13,100

Note: Average E = 6.320×10^6 psi.

Mix No. 2

Spec. No.	Cyl. Type	Polymer Loading, %	Strength, psi
1	3 x 6	6.31	13,300
2	3 x 6	5.95	15,900
3	3 x 6	5.88	15,500
4	3 x 6	6.14	15,500
	Average	6.07	15,100

Note: Average E = 6.50×10^6 psi.

(4) Splting Tensile Strength of 100% MMA-PIC

Mix No. 1

Spec. No.	Cyl. Type	Polymer Loading, %	Strength, psi
1	3 x 6	5.17	1,190
2	3 x 6	5.50	1,350
3	3 x 6	4.71	1,190
4	3 x 6	4.57	1,370
	Average	4.97	1,280

Mix No. 2

Spec. No.	Cyl. Type	Polymer Loading, %	Strength, psi
1	3 x 6	6.07	1,560
2	3 x 6	6.09	1,580
3	3 x 6	5.70	1,310
4	3 x 6	6.86	1,640
	Average	6.18	1,520

(5) Compressive Strength of 75% MMA + 25% BA-PIC

Spec. No.	Cyl. Type	Polymer Loading, %	Strength, psi
1	3 x 6	5.11	12,300
2	3 x 6	5.19	12,400
	Average	5.15	12,300

Note: Average E = 5.95×10^6 psi.

(6) Splitting Tensile Strength of 75% MMA + 25% BA-PIC

Spec. No.	Cyl. Type	Polymer Loading, %	Strength, psi
1	3 x 6	5.16	1,200
2	3 x 6	5.08	1,200
	Average	5.12	1,200

(7) Compressive Strength of 50% MMA + 50% BA-PIC

Spec. No.	Cyl. Type	Polymer Loading, %	Strength, psi
1	3 x 6	5.03	10,200
2	3 x 6	5.01	12,400
3	3 x 6	4.97	10,900
	Average	5.00	11,200

Note: Average E = 5.41×10^6 psi

(8) Splitting Tensile Strength of 50% MMA + 50% BA-PIC

Spec. No.	Cyl. Type	Polymer Loading, %	Strength, psi
1	3 x 6	5.10	1,200
2	3 x 6	4.99	1,000
	Average	5.05	1,100

APPENDIX D

PROPORTION OF GROUTING MATERIALS

PROPORTION OF GROUTING MATERIALS

(1) Cement Grouting Material for PBB-4C

Water	500	cc
Cement	2,500	cc

(2) Polymer Grouting Material for PBB-4P

MMA 90% (wt)	4,500	cc
BA 10%	500	cc
DMPT 2%	94	cc
LP 4%	188	gm.

APPENDIX E

CALIBRATION CURVE OF SPRINGS

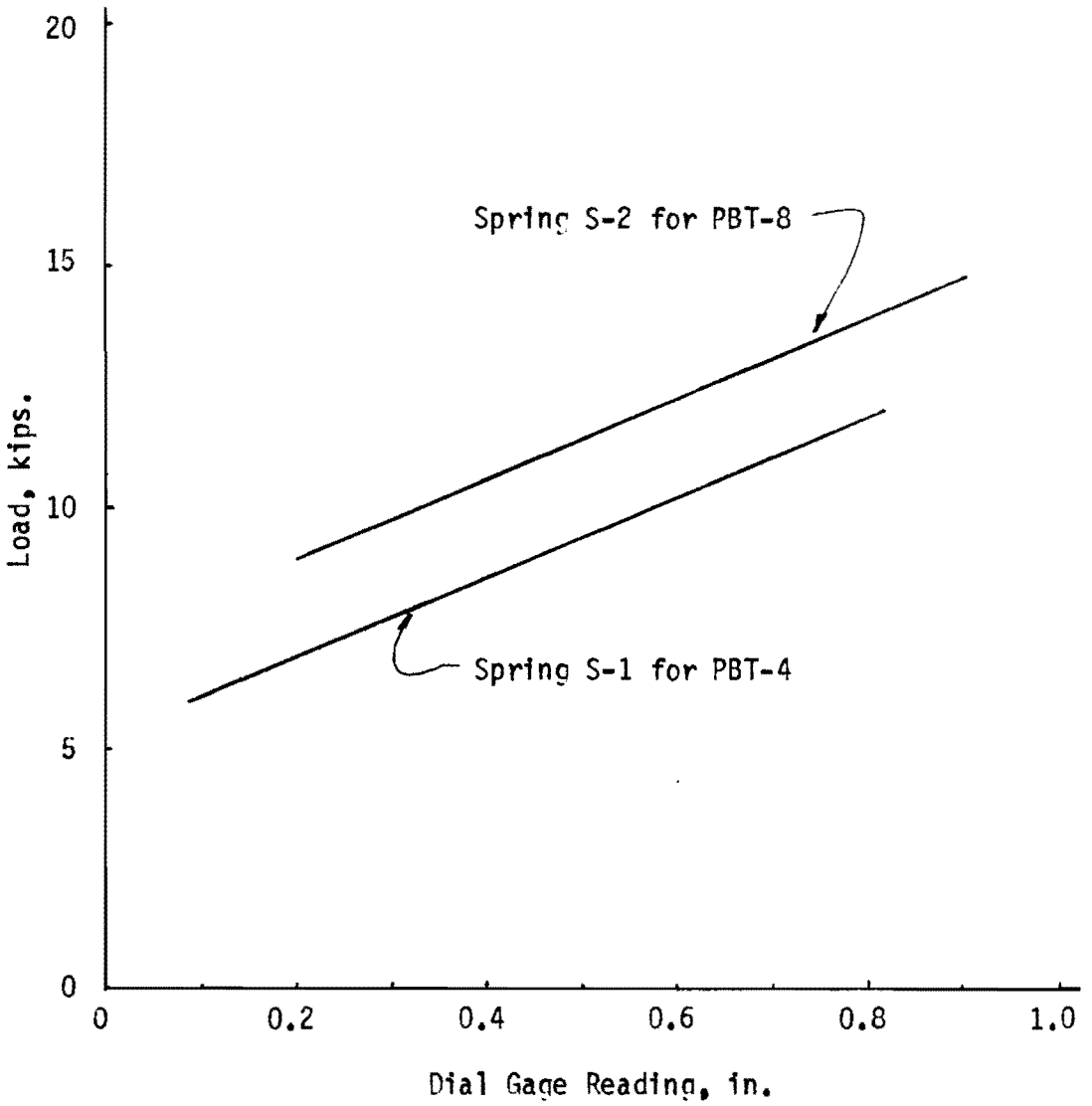

Fig. E-1 Calibration Curves of Springs

APPENDIX F

COMPARISON OF ELECTRICAL AND MECHANICAL STRAIN GAUGES FOR CONCRETE CYLINDER

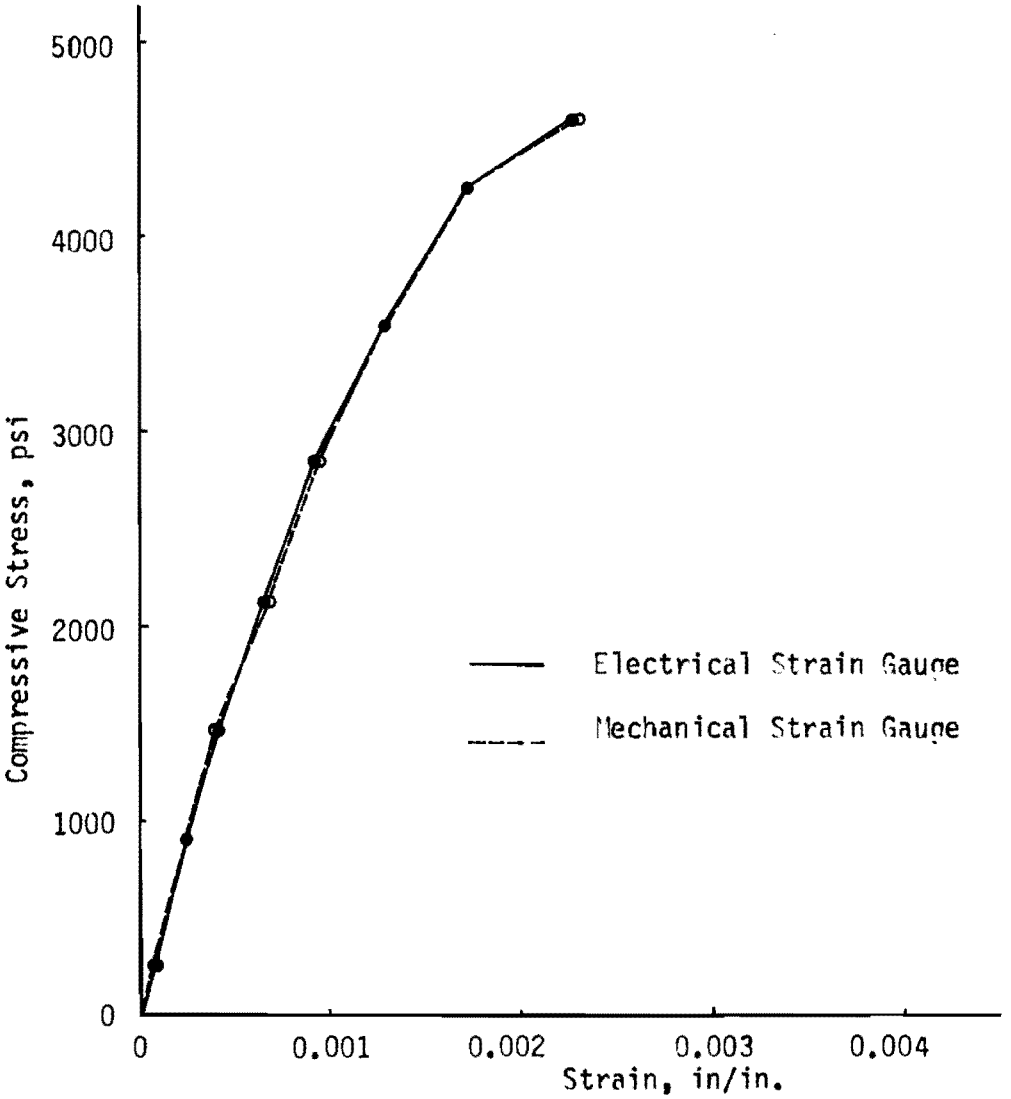

Fig. F-1 Comparision of Electrical and Mechanical Strain Gauges for Concrete Cylinder.

BIBLIOGRAPHY

1. Steinberg, M., Kukacka, L., Colombo, P., Kelsch, J., Monowitz, B., Dikeou, J., Backstrom, J., and Rubenstein, S. Concrete-Polymer Materials, First Topical Report, BNL 50134 (T-509) and USBR Gen. Rep. 41, 1968.

2. Dikeou, J., Backstrom, J., Hickey, K., Rubenstein, S., Jones, C., Steinberg, M., Kukacka, L., Colombo, P., Auskern, A., and Monowitz, B. Concrete-Polymer Materials, Second Topical Report, BNL 50128 (T-560) and REC-OCE 70-1, 1969.

3. Dikeou, J., Cowan, W., Depuy, G., Smoak, W., Wallace, G., Steinberg, M., Kukacka, L., Auskern, A., Colombo, P., Hendric, J., and Monowitz, B. Concrete Polymer Materials, Third Topical Report, REC-ERC 71-6 and BNL 50275 (T-602), 1971.

4. Dikeou, J., Cowan, W., Depuy, G., Smoak, W., Wallace, G., Steinberg, M., Kukacka, L., Auskern, A., Colombo, P., Hendric, J., and Monowitz, B. Concrete-Polymer Materials, Fourth Topical Report, BNL 50328 and REC-ERC 72-1, 1972.

5. Depuy, G.W., and Kukacka, L.E., editors. Concrete-Polymer Materials, Fifth Topical Report, REC-ERC 73012 and BNL 50390, 1973.

6. Fowler, D.W., Houston, J.T., and Paul, D.R. "Polymer-Impregnated Concrete for Highway Application," Research Report 114-1, Center for Highway Research, The University of Texas at Austin, 1973.

7. Fowler, D.W., Houston, J.T., and Paul, D.R. "Polymer-Impregnated Concrete Surface Treatments for Highway Bridge Decks," Polymer in Concrete, Publication SP-40, American Concrete Institute, Detroit, 1973.

8. Cowan, W.C., Carpenter, L., and Spencer, R.W. "Polymer-Impregnated Tunnel Support and Lining System," Procedings, North America Rapid Excavation and Tunneling Conference, Chicago, 1972. Vol. 1, Chapter 37, American Institute of Mining, Metallurgical and Petroleum Engineers, Port City Press, Baltimore, 1972.

9. Depuy, G.W., and Dikeou, J.T. "Development of Polymer-Impregnated Concrete as a Construction Material for Engineering Projects," Polymer in Concrete, Publication SP-40, American Concrete Institute, Detroit, 1973.

10. Yimprasert, P. "Durability, Strength, and Method of Application of Polymer-Impregnated Concrete for Slabs," unpublished Ph.D. dissertation, The University of Texas at Austin, Texas, Aug. 1975.

11. Phinyawat, P. "Flexural Behavior for Reinforced Polymer-Impregnated Concrete Beams," unpublished Ph.D. dissertation, The University of Texas at Austin, Texas, 1977.

12. Paul, D.R., and Fowler, D.W. "Surface Impregnation of Concrete Bridge Decks with Polymer," Journal of Applied Polymer Science, Vol. 19, pp 281-301, 1975.

13. Limsuwan, E., and Fowler, D.W. "Polymer Impregnation of Concrete Tiles," Research Report, The University of Texas at Austin, Texas, Jan. 1975.

14. Webster, R., Fowler, D.W., and Paul, D.R. "Partial Polymer Impregnation of Center Point Road Bridge,: Research Report 114-5, Center for Highway Research, The University of Texas at Austin, Texas, Jan. 1976.

15. Fowler, D.W., and Paul, D.R. "Polymer Impregnation of Concrete Walls," Research Report to U.S. Army District Engineers, Walla Walla, Corps of Engineers, Walla Walla, Washington, The University of Texas at Austin, May 1975.

16. Cowan, W.C., and Thurman, A.G. "Polymer-Impregnated Precast Prestressed Bridge Decks." Paper presented at American Concrete Institute Spring Meeting, San Francisco, April 1974.

17. Closner, J.J., De Bock, L.F., Legatos, N.D., Marchas, Y.T., and Gerwick, B.C., Jr. "Prestressed Concrete Proposed for LNG Carriers," Ocean Industry, Fb. 1974.

18. Fowler, D.W., Paul, D.R., and Yimprasert, P. "Corrosion Protection of Reinforcing Steel Provided by Polymer-Impregnated Concrete," Research Report 114-2, Center for Highway Research, The University of Texas at Austin, Texas, Dec. 1974.

19. Lin, T.Y. Design of Prestressed Concrete Structures, 3rd edition. John Wiley & Sons, Inc., New York, 1972.

20. Leonhardt, F. Prestressed Concrete Design and Construction, 2nd edition, Wilhelm Ernst and Sohn, Berlin-Munich, 1964.

21. Corley, W.G., Sozen, M.A., and Siess, C.P. "Time Dependent Deflections of Prestressed Concrete Beams," Highway Research Board Bulletin 307, National Academy of Sciences-National Research Council Washington D.C. 1962.

22. Ingram, L.L., and Furr, H.L. "Creep and Shrinkage of Concrete Based on Major Variables Encountered in the State of Texas," Research Report No. 170-1F, Texas Transportation Institute, Texas A & M Univ., College Station, Texas, Aug. 1973.

23. Billet, D.F., and Appleton, J.H. "Flexural Strength of Prestressed Concrete Beams," Journal ACI, June 1954 (Proc. Vol. 50).

24. Janney, J.R., Hognestad, E., and Mc Henry, D. "Ultimate Strength of Prestressed and Conventionally Reinforced Concrete Beams," Jounal ACI, Feb. 1956 (Proc. Vol. 52).

25. Warwaruk, J., Sozen, M.A., and Siess, C.P. "Strength and Behavior in Flexure of Prestressed Concrete Beams," Engineering Experiment Station, Bulletin No. 464, University of Illinois, 1962.

26. Hognestad, E., Hanson, H.W., and Mc Henry, D. "Concrete Stress Distribution in Ultimate Strength Design," Journal ACI, Dec. 1955 (Proc. Vol. 52).

27. Cooley, E.H., and Morice, P.B., Prestressed Concrete, Sir Issaac Pitman & Son, Ltd, London, 1958.

28. Hognestad, E., "A Study of Combined Bending and Axial Load in Reinforced Concrete Members," University of Illinois Engineering Experiment Station, Bulletin No. 399, 1951.

29. Leonhardt, F. "Continuous Prestressed Concrete Beams," Journal of ACI, Vol. 49, March 1953.

30. Pierce, D.M. "A Numerical Method of Analyzing Prestressed Concrete Members Containing Unbonded Tendons," unpublished Ph.D. Dissertation, The University of Texas at Austin, Texas, Jan. 1968.

31. Sozen, M.A. "Strength in Shear of Prestressed Concrete Beam without Web Reinforcement," Structural Research Series No. 139, University of Illinois, Aug. 1957.

32. MacGragor, J.G., Sozen, M.A., and Siess, C.P. "Strength and Behavior of Prestressed Concrete Beam with Web Reinforcememt," Structural Research Series No. 201, University of Illinois, Aug. 1960.

33. Bresler, B., and Pister, K.S. "Strength of Concrete under Combined Stresses," Journal ACI, Sept. 1958

34. Godden, W.G. Numerical Analysis of Beam Column Structures, Prestice-Hall, Inc., Englewood Cliffs, New Jersey, 1965.

35. Atkins, W.D. "Generalized Numerical Solution for Prestressed Concrete Beams," unpublished Master's thesis, The University of Texas at Austin, Texas, Aug. 1965.

36. Matlock, H., and Haliburton, T.A. "A Finite-Element Method of Solution for Linearly Elastic Beam-Columns," Research Report No. 56-1, Center for Highway Research, The University of Texas at Austin, Texas, Sept. 1966.

37. Lin, T.Y. "Cable Friction in Post-Tensioning," Journal of Strucutral Division, ASCE, Nov. 1956.

38. Cooley, E.H., "Friction in Post-Tensioning Prestressing System and Estimation of Friction in Prestressed Concrete," Cement and Concrete Association, London, 1953.

39. Smith, R.G., and Orangun, Co.O., "Evaluation of the Stress-Strain Curve of Concrete in Flexure Using Method of Least Squares, Journal ACI, July 1969.

40. Sinha, B.P., Gerstle, K.H., and Tulin, L.G., "Stress-Strain Relationship for Concrete Under Cyclic Loading," Journal ACI, Feb. 1964.

41. Korsan, I.D., and Jirsa, J.O., "Behavior of Concrete Under Compressive Loadings," Journal of Structural Division, ASCE, Dec. 1969.

42. ACI Committee 318, Building Code Requirements for Reinforced Concrete (ACI 318-71), American Concrete Institute, Detroit, 1971.

43. ACI Committee 318, Commentary on Building Code Requirements for Reinforced Concrete (ACI 318-71), American Concrete Institute, Detroit, 1971.

44. Guyon, T., Prestressed Concrete, John Wiley and Sons, N.Y. 1953.

45. Sozen, M.A., Zwoyer, E.M., and Seiss, C.P., "Investigation of Prestressed Concrete for Highway Bridges, Part I, Strength in Shear of Beams Without Web Reinforcement," Bulletin No. 452 Engineering Experiment Station, University of Illinois, 1959.

46. Olesen, S.O., Sozen, M.A., and Seiss, C.P., "Investigation of Prestressed Reinforced Concrete for Highway Bridges, Part IV, Strength in Shear of Beams with Web Reinforcement," Engineering Experiment Station, Bulletin No. 493, University of Illinois, 1967.

47. Mattock, A.H., Kriz, L.B., and Hognestad, E., "Rectangular Concrete Stress Distribution in Ultimate Strength Design," Journal ACI, Feb. 1961.

48. Nedderman, H., "Flexural Stress Distribution in Very High Strength Concrete," unpublished Master's Thesis, University of Texas at Arlington, Dec. 1973.

49. Park, R., and Paulay, T., Reinforced Concrete Structures, John Wiley and Sons, N.Y., 1975.

50. ASTM C-39-64, "Standard Method of Test for Compressive Strength of Molded Concrete Cylinders", ASTM, 1976.

51. Komendant, A.E., Prestressed Concrete Structures, MacGraw Hill, New York, 1952.

53. Libby, J.R., Prestressed Concrete, The Ranold Press Co., New York, 1963.